

Electrochemistry of gold-based alloys

By

Heinrich Möller

A dissertation submitted in partial fulfillment of the requirements for the degree of

Master of Engineering

in the Department of Materials Science and Metallurgical Engineering,
Faculty of Engineering, Built Environment and Information Technology,
University of Pretoria

2002

Electrochemistry of gold-based alloys

by

Heinrich Möller

Supervisor: Prof. P.C. Pistorius

Department of Materials Science and Metallurgical Engineering

Degree: Master of Engineering

ABSTRACT

The electro-oxidation of organic compounds at noble metal electrodes has been widely studied in the past. A bimetallic electrode is often more active than the respective pure metals. However, the effect of the microstructure of the alloys on their electrochemical properties has largely been ignored in the past.

The electro-oxidation of ethylene glycol at gold-platinum and gold-titanium electrodes in different heat treatment conditions was studied to determine how the different microstructures would influence the electrochemistry of these alloys.

Kirkendall porosity was produced by the solid solution heat treatment of the two-phased 60Au-40Pt electrodes. The extra surface area due to the porosity resulted in high apparent current densities at the porous electrodes in both acid and alkaline solutions without ethylene glycol. Only slightly higher apparent current densities were obtained at the porous gold-platinum electrodes compared to the non-porous electrodes when ethylene glycol was present in the solution. Kirkendall porosity was not produced by the solid solution heat treatment of the two-phased 50Au-50Pt electrodes.

The gold-platinum electrodes were more active for the electro-oxidation of ethylene glycol than both pure gold and platinum. The electrodes in the solid solution heat treatment condition were more active than the two-phased electrodes. This can be explained by the Third-body effect, which means that platinum atoms that are surrounded by gold atoms are less likely to become poisoned by intermediates than platinum atoms

that are surrounded by other platinum atoms. Poisoning of all the electrodes occurred during electrolysis of ethylene glycol at a fixed potential. The poisoning species at pure gold and pure platinum could be removed by potential pulsing and sustainable electrolysis of ethylene glycol was possible at these electrodes. Unfortunately, the same technique was not as successful with the gold-platinum alloys and their activities declined during the long-term electrolysis of ethylene glycol.

The electrochemical behaviour of the Gold 990 (Au-1wt% Ti) electrodes is similar to pure gold in acid and alkaline solutions. It is possible that the titanium content is too low to have a significant influence on the electrochemical behaviour of gold. The titanium may also be in the passive condition or it may have dissolved selectively from the Gold 990 alloy resulting in a pure gold surface.

Keywords: Gold, platinum, gold-platinum alloys, gold-titanium alloys, Gold 990, Kirkendall porosity, electrochemistry, electro-oxidation, ethylene glycol, cyclic voltammetry.

ACKNOWLEDGEMENTS

I would like to thank and herewith express my sincere appreciation to the following:

- Professor Chris Pistorius, my supervisor, for guidance and continuous support.
- Mintek for financial assistance.
- Doctor Elma van der Lingen and Stephen Roberts from Mintek for guidance and sample preparation.
- The Department of Materials Science and Metallurgical Engineering and IMMRI for facilities.
- Lida Roos, my fiancée, for her love, continuous support and patience.
- My father, mother, Robert, Danie and Johan for their prayers and support.
- The Roose: Lida's parents, Hannes and Marileen for their continuous support.
- Carel Coetzee for assistance with the SEM.
- Doctor Sabine Verryn of the Geology department for assistance with XRD.
- Sarah Havenga and Johann Borman for their assistance.
- My friend Heinrich Hutchison for his valuable contribution.
- The personnel and specially my fellow graduate students for their support and advice.
- The Lord, for the abilities He gave me and the opportunity to develop them.

CONTENTS

ABSTRACT.....	i
ACKNOWLEDGEMENTS.....	iii
CONTENTS.....	iv
CHAPTER 1: Introduction.....	1
CHAPTER 2: Theoretical background.....	2
2. Electrochemical behaviour of pure gold in aqueous media.....	2
2.1. Gold in acidic media.....	2
2.2. Gold in alkaline media.....	2
2.3. Premonolayer oxidation of gold.....	3
2.3.1. Premonolayer oxidation of gold in acid.....	4
2.3.2. Premonolayer oxidation of gold in base.....	6
2.4. The electro-oxidation of chemical compounds at gold electrodes in aqueous media..	6
2.4.1. Electro-oxidation by means of a submonolayer of adsorbed hydroxyl radicals....	8
2.5 Alloys of gold.....	8
2.5.1. Electrochemical behaviour of pure platinum.....	9
2.5.1.1. Mechanism of oxide formation.....	9
2.5.1.2. Electrochemical behaviour of platinum in alkaline solutions.....	11
2.5.1.3. Electrochemical behaviour of platinum in acid solutions.....	14
2.6 Gold-platinum alloys.....	15
2.6.1. Cold rolling of Au-Pt alloys.....	15
2.6.2. Precipitation in Au-Pt alloys.....	16
2.6.3. Electrochemical behaviour of Au-Pt alloys.....	17
2.6.3.1. Homogeneous alloys.....	17
2.6.3.2. Heterogeneous alloys.....	17
2.6.4. Electro-oxidation of chemical compounds at Au-Pt alloy electrodes	18
2.6.5. Possible explanations for synergism on Au-Pt alloys.....	18
2.6.5.1. The bifunctional theory.....	18

2.6.5.2. Changes in adsorption features.....	19
2.6.5.3. The Third-Body effect.....	20
2.6.5.4. The creation of surface Lewis acid sites on alloy electrodes.....	20
2.7. The 60Au-40Pt alloy electrode.....	21
2.8. The electro-oxidation of ethylene glycol at noble metal electrodes.....	22
2.8.1. The electro-oxidation of ethylene glycol at gold electrodes in acid.....	22
2.8.2. The electro-oxidation of ethylene glycol at gold electrodes in base.....	23
2.8.3. The electro-oxidation of ethylene glycol at platinum electrodes in acid.....	24
2.8.4. The electro-oxidation of ethylene glycol at platinum electrodes in base.....	25
2.8.5. The electro-oxidation of ethylene glycol at Au-Pt electrodes in base.....	27
2.9. The Au-1wt% Ti alloy (Gold 990)	28
2.9.1. Preparation of Gold 990.....	28
2.9.2. The electrochemical behaviour of pure titanium.....	29
2.10 Conclusions.....	32
CHAPTER 3: The heat treatment of Au-Pt alloys and the Gold 990 alloy.....	34
3.1. Introduction.....	34
3.2. The 60Au-40Pt alloy.....	34
3.2.1. The 60Au-40Pt alloy heat treated at 1300°C.....	34
3.2.2. The 60Au-40Pt alloy heat treated at 1200°C.....	37
3.2.2.1. The 60Au-40Pt alloy heat treated at 1200°C for 24 hours.....	38
3.2.2.2. Kirkendall porosity.....	40
3.2.2.3 The 60Au-40Pt alloy heat treated at 1200°C for 168 hours.....	41
3.2.3. The 60Au-40Pt alloy heat treated directly at 1200°C.....	42
3.2.4. The 60Au-40Pt miscibility gap heat treatments.....	44
3.2.4.1. The 60Au-40Pt alloy heat treated at 800°C for 50 hours.....	44
3.2.4.2. The 60Au-40Pt alloy heat treated at 600°C for 100 hours.....	47
3.3. The 50Au-50Pt alloy.....	49
3.3.1. The 50Au-50Pt alloy in the "ductile" condition.....	49
3.3.2 The 50Au-50Pt alloy in the solid solution condition.....	52

3.4. The Gold 990 alloy.....	53
3.4.1. The Gold 990 alloy in the solid solution condition.....	53
3.4.2. The Gold 990 alloy in the precipitation-hardened condition.....	54
3.5. Conclusions.....	55
CHAPTER 4: The electrochemical behaviour of gold-based alloys in acid solution without ethylene glycol.....	56
4.1. Introduction.....	56
4.2. Experimental.....	56
4.3. Results and discussion.....	57
4.3.1. Gold.....	57
4.3.2. Platinum.....	58
4.3.3. The 60Au-40Pt alloy.....	61
4.3.3.1. The 60Au-40Pt alloy in the 1300°C heat treatment condition.....	61
4.3.3.2. The 60Au-40Pt alloy in the 1200°C (24 hours) heat treatment condition.....	62
4.3.3.3. The 60Au-40Pt alloy in the 1200°C (168 hours) heat treatment condition.....	63
4.3.3.4. The 60Au-40Pt alloy in the 800°C heat treatment condition.....	67
4.3.3.5 The 60Au-40Pt alloy in the 600°C heat treatment condition.....	67
4.3.4. The 50Au-50Pt alloy.....	69
4.3.4.1 The 50Au-50Pt alloy in the "ductile" condition.....	69
4.3.4.2 The 50Au-50Pt alloy in the solid solution condition.....	70
4.3.5. The Gold 990 alloy.....	72
4.3.5.1. The Gold 990 alloy in the solid solution condition.....	72
4.3.5.2. The Gold 990 alloy in the precipitation-hardened condition.....	72
4.4. Conclusions.....	76
CHAPTER 5: The electrochemical behaviour of gold-based alloys in alkaline solution without ethylene glycol.....	77
5.1. Introduction.....	77
5.2. Experimental.....	77
5.3. Results and discussion.....	78

5.3.1. Gold.....	78
5.3.2. Platinum.....	79
5.3.3. The 60Au-40Pt alloy.....	81
5.3.3.1. The 60Au-40Pt alloy in the 1300°C heat treatment condition.....	81
5.3.3.2. The 60Au-40Pt alloy in the 1200°C (24 hours) heat treatment condition.....	82
5.3.3.3. The 60Au-40Pt alloy in the 1200°C (168 hours) heat treatment condition.....	83
5.3.3.4. The 60Au-40Pt alloy in the 800°C heat treatment condition.....	87
5.3.3.5 The 60Au-40Pt alloy in the 600°C heat treatment condition.....	88
5.3.4. The 50Au-50Pt alloy.....	89
5.3.4.1 The 50Au-50Pt alloy in the "ductile" condition.....	89
5.3.4.2 The 50Au-50Pt alloy in the solid solution condition.....	91
5.3.5. The Gold 990 alloy.....	94
5.3.5.1. The Gold 990 alloy in the solid solution condition.....	94
5.3.5.2. The Gold 990 alloy in the precipitation-hardened condition.....	94
5.4. Conclusions.....	96
CHAPTER 6: The electro-oxidation of ethylene glycol at gold-based alloys in an alkaline solution.....	98
6.1. Introduction.....	98
6.2. Experimental.....	98
6.3. Results and discussion.....	100
6.3.1. Gold.....	100
6.3.2. Platinum.....	102
6.3.3. The 60Au-40Pt alloy.....	106
6.3.3.1. The 60Au-40Pt alloy in the 1300°C heat treatment condition.....	106
6.3.3.2. The 60Au-40Pt alloy in the 1200°C (24 hours) heat treatment condition.....	108
6.3.3.3. The 60Au-40Pt alloy in the 1200°C (168 hours) heat treatment condition.....	111
6.3.3.4. The 60Au-40Pt alloy in the 800°C heat treatment condition.....	113
6.3.3.5 The 60Au-40Pt alloy in the 600°C heat treatment condition.....	116
6.3.4. The 50Au-50Pt alloy.....	118
6.3.4.1 The 50Au-50Pt alloy in the "ductile" condition.....	118

6.3.4.2 The 50Au-50Pt alloy in the solid solution condition.....	120
6.3.5. The Gold 990 alloy.....	122
6.3.5.1. The Gold 990 alloy in the solid solution condition.....	122
6.3.5.2. The Gold 990 alloy in the precipitation-hardened condition.....	124
6.3.6. Electrolysis of ethylene glycol at a fixed potential.....	128
6.3.6.1. Gold.....	129
6.3.6.2. Platinum.....	129
6.3.6.3. The 60Au-40Pt alloy in the 1300°C heat treatment condition.....	129
6.3.6.4. The 60Au-40Pt alloy in the 1200°C - 24 h heat treatment condition.....	130
6.3.6.5. The 50Au-50Pt alloy in the "ductile" heat treatment condition.....	130
6.3.6.6 The 50Au-50Pt alloy in the solid solution heat treatment condition.....	130
6.3.6.7. The Gold 990 alloy in the solid solution heat treatment condition.....	130
6.3.7. Electrolysis of ethylene glycol using potential pulsing.....	135
6.3.7.1. Gold.....	136
6.3.7.2. Platinum.....	140
6.3.7.3. The 60Au-40Pt alloy in the 1200°C - 24 h condition.....	143
6.3.7.4. The 50Au-50Pt alloy in the "ductile" condition.....	146
6.3.7.5 The 50Au-50Pt alloy in the solid solution condition.....	149
6.3.7.6. The Gold 990 alloy in the solid solution condition.....	152
6.4. Conclusions.....	158
CHAPTER 7: Conclusions and Recommendations.....	161
REFERENCES.....	164

Chapter 1

INTRODUCTION

The electro-oxidation of organic compounds at noble metal electrodes has been studied extensively for possible applications in electrochemical power sources (Parsons and VanderNoot, 1988) and electrochemical wastewater treatment (Comninellis, 1994). Gold is the noblest and most inert of all metals. It also possesses weak chemisorbing properties due to the absence of vacancies in its d-bands. Surprisingly, it still displays a wide range of electro-oxidation activity – especially in alkaline solutions (Burke and Nugent, 1998).

It is known that a bimetallic electrode is usually more active for the electro-oxidation of organics than the respective pure metals (Parsons and VanderNoot, 1988). The gold alloy containing 40% platinum has been identified (Stelmach et al., 1994) as being the most active for the oxidation of various organics in base. However, the effect of the microstructure of gold-platinum alloys on their electrochemical properties has largely been ignored in the past.

The Gold 990 alloy (Au-1wt% Ti) was developed originally for the jewellery industry (Gafner, 1989). The electrochemical properties of this alloy have not been investigated before. It is possible to heat treat Gold 990 to obtain two different heat treatment conditions: (a) with titanium in solid solution with the gold and (b) the precipitation-hardened condition, with small Au₄Ti precipitates.

This study has been subdivided into three main parts:

- In the first part, the heat treatments of the Au-Pt and the Au-Ti alloys are investigated. By employing different heat treatment temperatures and times, different microstructures are produced.
- In the second part, the electrochemical properties of the heat treated electrodes are studied in acid and alkaline solutions without an organic compound in the solution.
- In the third part, the electro-oxidation of ethylene glycol at Au-Pt and Gold 990 electrodes in different heat treatment conditions is investigated. Ethylene glycol was selected as a model organic compound due to the fact that its oxidation at noble metal electrodes has been studied extensively (Kadirgan et al., 1990; Hahn et al., 1987).

Chapter 2

THEORETICAL BACKGROUND

2. Electrochemical behaviour of pure gold in aqueous media

2.1. Gold in acidic media

A typical cyclic voltammogram recorded for a polycrystalline gold disc electrode in acid is shown in Figure 2.1 (Burke and Nugent, 1997). During the positive sweep, monolayer oxide (α -oxide) formation results in an increase in anodic current at 1.35 V versus the reversible hydrogen electrode (RHE). The charge associated with further monolayer oxidation for gold in acid tends to be distributed along a plateau with no major change until oxygen gas evolution commences at 2.0 V_{RHE} (not shown in Figure 2.1). During the negative sweep, the monolayer oxide reduction peak is observed at 1.1 V_{RHE} .

Birss and Xia (2001) formed α -oxide films at sputtered polycrystalline gold electrodes in 0.1 M H_2SO_4 solutions. The composition and properties of the film were established using potentiostatic, cyclic voltammetry, ellipsometric and in-situ mass measurement techniques. The α -oxide is proposed to be AuO at potentials below 1.5 V_{RHE} , and a mixture of AuO and Au_2O_3 above this, likely becoming primarily Au_2O_3 at still higher potentials. This is based on ellipsometric evidence and the measured mass to charge ratio of 8 g/mol electrons at all potentials.

2.2. Gold in alkaline media

Examples of cyclic voltammograms recorded for gold in base are shown in Figure 2.2 (Burke and Nugent, 1997). Monolayer oxide growth commences at 1.25 V_{RHE} . At more positive potentials, oxygen gas evolution occurs. Over the range of 1.6 to 2.0 V_{RHE} oxygen gas evolution is believed to be catalysed in a transient manner by some type of nascent hydrous gold oxide species formed at the monolayer oxide/aqueous solution interface (Burke and Nugent, 1997). Regular oxygen gas evolution on gold in base (as in acid) occurs only above 2.0 V_{RHE} .

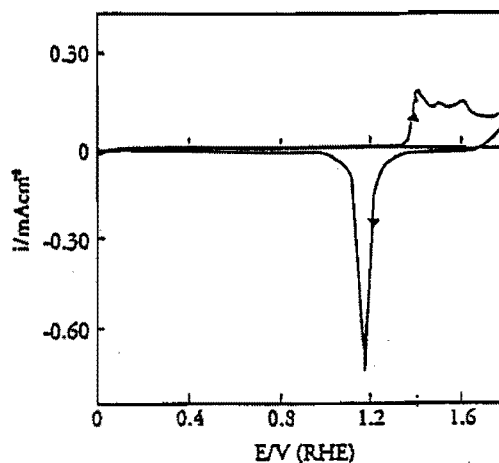


Figure 2.1. Typical cyclic voltammogram (0.0 to 1.80 V_{RHE} , 50mV/s, 25°C) recorded for a polycrystalline gold disc electrode in 1.0 mol/dm³ H_2SO_4 (Burke and Nugent, 1997).

An interesting feature of the negative sweep in Figure 2.2(b) is the appearance of a second cathodic peak at 0.85 V_{RHE} . The monolayer oxide reduction peak was observed in this case at 1.1 V_{RHE} and the subsequent peak is assumed to be due to the reduction of hydrous gold oxide species formed on the gold surface at the upper end of the cycle (Burke and Nugent, 1997).

2.3. Premonolayer oxidation of gold

Gold is frequently regarded as the ideal solid electrode system for fundamental investigations in electrochemistry. This is due to the fact that in the absence of redox active species in the aqueous phase, the system apparently exhibits only double layer (non-Faradaic) behaviour over the range of 0 to 1.3 V_{RHE} in acid and 0 to 1.2 V_{RHE} in base. However, there have been assertions that Faradaic behaviour due to the formation of oxy-species at the gold surface occurs within the double layer region. However, the extent of premonolayer oxidation (the coverage involved) is small. This makes it difficult to detect these species and the responses associated with them.

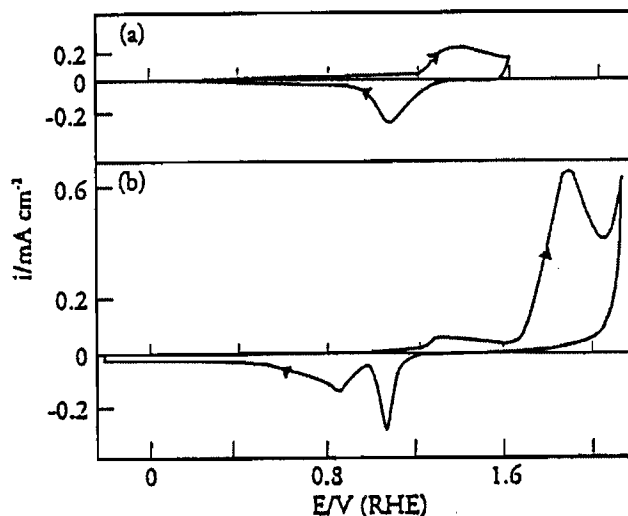


Figure 2.2. Typical cyclic voltammogram for a polycrystalline gold electrode in $1.0 \text{ mol/dm}^3 \text{ NaOH}$ at $25 \text{ }^\circ\text{C}$: (a) 0.0 to $1.60 \text{ V}_{\text{RHE}}$ at 50 mV/s ; (b) -0.2 to $2.1 \text{ V}_{\text{RHE}}$ at 10 mV/s (Burke and Nugent, 1997).

2.3.1. Premonolayer oxidation of gold in acid

Watanabe and Gerischer (1981) postulated on the basis of photoelectrochemical data that gold exhibited premonolayer oxidation extending over the potential range 0.85 to $1.35 \text{ V}_{\text{RHE}}$. They postulated that this incipient oxidation represented the formation of chemisorbed species (Au-OH and/or Au-O) with surface coverages up to 20%.

Hutton and Williams (1994), using Scanning Laser Microscopy, found that gold oxidised in the premonolayer region. They found that this incipient oxide was stable, only being removed by prolonged evolution of hydrogen gas.

Gordon and Johnson (1994) investigated gold electrodes in acid solution by means of an Electrochemical Quartz Crystal Microbalance (EQCM). They proposed that the species formed during premonolayer oxidation corresponded to adsorbed hydroxyl radicals, designated as AuOH . Figure 2.3(a) (Gordon and Johnson, 1994) shows a typical current-potential (I-E) curve obtained at a gold film electrode in 0.10 M HClO_4 . The very small anodic current observed during the positive potential scan in region A corresponds to charging of the electrical double layer. Region B during the positive scan corresponds to the premonolayer region and the slight increase in anodic current is concluded to result primarily from the formation of the submonolayer of hydrous oxide, designated as AuOH . The large wave in region C corresponds to the formation of the monolayer oxide. An electrochemical quartz crystal microbalance (EQCM) was

used to detect small surface mass changes during cyclic voltammetry. A decrease in frequency indicates an increase in mass. Figure 2.3(b) (Gordon and Johnson, 1994) shows the frequency-potential (f-E) curve recorded simultaneously with the I-E curve in Figure 2.3(a). During the positive scan there is no detectable change in frequency corresponding to double layer charging (region A). However, a rapid decrease in frequency (mass increase) by the amount Δf_B is observed in region B concomitantly with the formation of AuOH. Continuation of the positive scan through region C results in a further decrease in frequency by an amount Δf_C concomitantly with the formation of the monolayer oxide. Following scan reversal, the frequency remains constant until it increases very rapidly in the region corresponding to cathodic reduction of the monolayer oxide. Continuation of the negative scan back through the premonolayer region B results in further increase of frequency until the original value of f is attained in the double-layer region A.

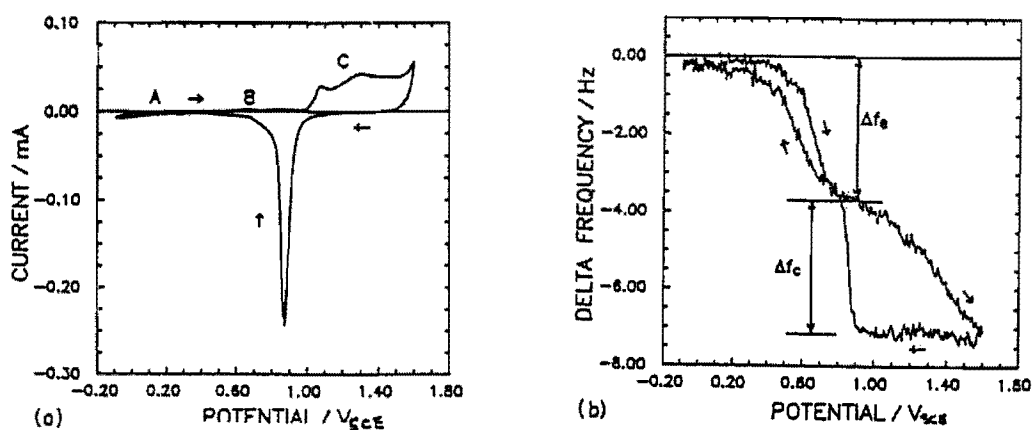


Figure 2.3. (a) Current-potential curve for Au EQCM film in 0.1 M HClO₄: scan rate 75 mV/s; no convective mixing. (b) Frequency-potential curve for Au EQCM film in 0.1 M HClO₄: scan rate 75 mV/s; no convective mixing. Obtained concomitant with I-E curve (Gordon and Johnson, 1994).

Gordon and Johnson (1994) proposed that the large values obtained for Δf_B and Δf_C in regions B and C respectively are the result of increased surface hydration as a consequence of the formation of AuOH (region B) and the monolayer oxide (region C). The magnitude of the increase was found to be independent of the nature of the acid. The mass increase in region B is consistent with an increase in surface hydration by about 32 H₂O molecules per AuOH site.

2.3.2. Premonolayer oxidation of gold in base

The electrochemical response due to premonolayer oxidation of gold in alkaline solutions tends to be of higher magnitude than in acid; the hydroxy species involved is more stable in solutions of high OH^- ion activity. Small peaks have been observed in the double layer region of cyclic voltammograms for gold in base (Burke and O'Leary, 1989).

Desilvestro and Weaver (1986) established, using Surface Enhanced Raman Spectroscopy (SERS), that the product of premonolayer oxidation was a hydroxy species, one that was of different character to the species involved in the regular monolayer oxidation reaction.

2.4. The electro-oxidation of chemical compounds at gold electrodes in aqueous media

Gold is the noblest and most inert of all metals. It is also a very weak chemisorber due to the absence of vacancies in its d-bands. It does, however, display a very wide range of electro-oxidation activity - especially in base (Vitt et al., 1990; Burke and Nugent, 1998).

Typical cyclic voltammograms for the electro-oxidation of formaldehyde, hydrazine, and ethylene glycol are shown in Figure 2.4 (Burke and Nugent, 1998). The following can be deduced from these cyclic voltammograms:

- i. The electro-oxidation of chemical compounds commences in the premonolayer region during the positive sweep. As soon as monolayer oxidation starts, oxidation of the compound is inhibited.
- ii. During the negative sweep, oxidation of the compound starts again as soon as the monolayer oxide has been reduced.
- iii. In general, chemical compounds are oxidised at gold before the formation of a surface oxide layer, while oxygen is evolved at a gold surface after the formation of the oxide layer.

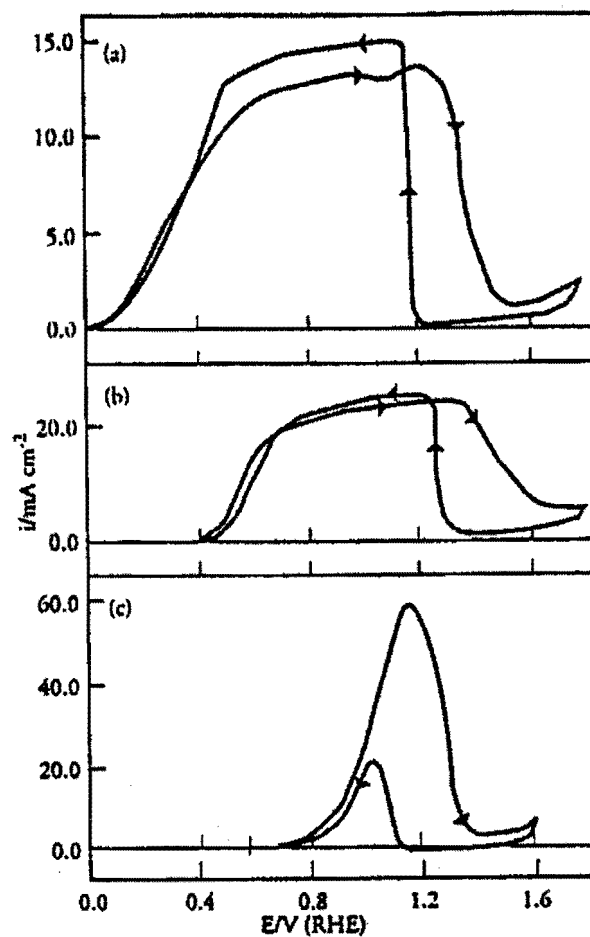


Figure 2.4. (a) Typical cyclic voltammogram (0 - 1.8 V, 5 mV/s) for a gold wire electrode in 1 mol/dm³ NaOH with HCHO, to a level of 0.1 mol/dm³, $T = 25\ ^\circ\text{C}$; (b) Typical cyclic voltammogram (0 - 1.8 V, 50 mV/s) for a smooth gold electrode in N₂-stirred 1 mol/dm³ NaOH with N₂H₄, to a level of 0.1 mol/dm³, $T = 25\ ^\circ\text{C}$; (c) Typical cyclic voltammogram (0 - 1.6 V, 50 mV/s) for a gold wire electrode in 1 mol/dm³ NaOH with 0.1 mol/dm³ ethylene glycol (CH₂OH)₂, $T = 25\ ^\circ\text{C}$ (Burke and Nugent, 1998).

2.4.1 Electro-oxidation by means of a submonolayer of adsorbed hydroxyl radicals

Electro-oxidation mechanisms have been proposed for oxidation at gold electrodes in acidic and alkaline solutions that involve adsorbed hydroxyl radicals (AuOH) (Vitt et al., 1990; Wen and Li, 1997). The adsorbed hydroxyl radicals are produced by means of the anodic discharge of H₂O in the premonolayer region (Vitt and Johnson, 1992).



The formation of the submonolayer of hydroxyl radicals is favoured in alkaline solutions, which explains the rather poor electro-oxidation properties of gold in acidic solutions. A mechanism has been proposed in which the adsorbed hydroxyl radicals participate in the oxygen-transfer step (Vitt et al., 1990). It has also been speculated that the AuOH species formed in the premonolayer region can assist in the adsorption of polar organic molecules. Oriented H₂O dipoles centred at catalytic AuOH sites may also influence the orientation of electro-active functional groups in reactants that must diffuse to these catalytic sites (Gordon and Johnson, 1994).

Vitt and co-workers (1990) proposed that adsorption is necessary for all compounds whose oxidation is accompanied by the transfer of oxygen via the electrode surface. A mechanism that involve three fundamental processes for the various adsorbed species has been devised for these anodic reactions:

- (1) oxygen transfer between the electrolyte and adsorbed hydroxyl radical (AuOH)
- (2) deprotonation and
- (3) electron transfer.

The mechanisms for various compounds seem to differ only in the order of these three reactions. For organic compounds (alcohols and aldehydes), deprotonation precedes electron transfer.

2.5. Alloys of gold

Noble metal alloys have been studied for the electro-oxidation of organic compounds, and some alloys display better activity than the pure metals. Most of the alloys that

have been studied are based on platinum (Parsons and VanderNoot, 1988; Stelmach et al., 1994).

2.5.1. Electrochemical behaviour of pure platinum

2.5.1.1. Mechanism of oxide formation

The early modelling of the initial stages of surface oxidation on platinum (Kozłowska et al., 1973) lead to the conclusion that two distinguishable and successive stages were involved:



followed by:



(potential range 1.1 to 1.4 V_{RHE}) also coupled with place-exchange, schematically represented by:



By using the electrochemical quartz-crystal nanobalance (EQCN) technique, Birss et al (1993) showed that the above two-step mechanism is inapplicable. The two-step mechanism would require a mass change of 17 g/mol electrons in step I and -1 g/mol electrons in step II. However, the anodic mass-response profile involves a continuous mass increase, contrary to the expectations according to mechanism I, II. It actually corresponds to the first stage (to 1.1 V_{RHE}) of oxide film development being formed as Pt/O, first to half-coverage by O-species up to 1.1 V_{RHE} . This is followed by completion of coverage by O-species up to 1.4 V_{RHE} coupled with place exchange between O and Pt (step III).

Thus, platinum surface oxide formation is believed to preferably involve discharge of water molecules directly forming 'PtO' species, process IV:



where the H_2O reagent is initially present at a platinum site in the inner region of the double-layer, i.e. residing at the metal surface. As the electrosorption of O species in process IV progresses, water molecules consumed in (IV) are replaced from the double-layer and appear on the surface of the developing oxide film, probably H-bonded to it.

The mechanism of platinum oxide formation is shown schematically in Figure 3.1 (Zolfaghari et al., 2002). The above mechanism has to include the anticipated participation of adsorbed H_2O molecules which, initially, are presumed to fully cover Pt sites (Fig. 2.5a). It is believed that the H_2O molecules are bridge-coordinated to two adjacent Pt atoms. The second step in the diagram (Fig. 2.5b) shows half coverage by O at 1.1 V_{RHE} . The third step in the diagram (Fig. 2.5c and 2.5d) illustrates how a nominally complete O monolayer on platinum eventually becomes developed through place-exchange between O and Pt over the two outer layers of the original platinum structure.

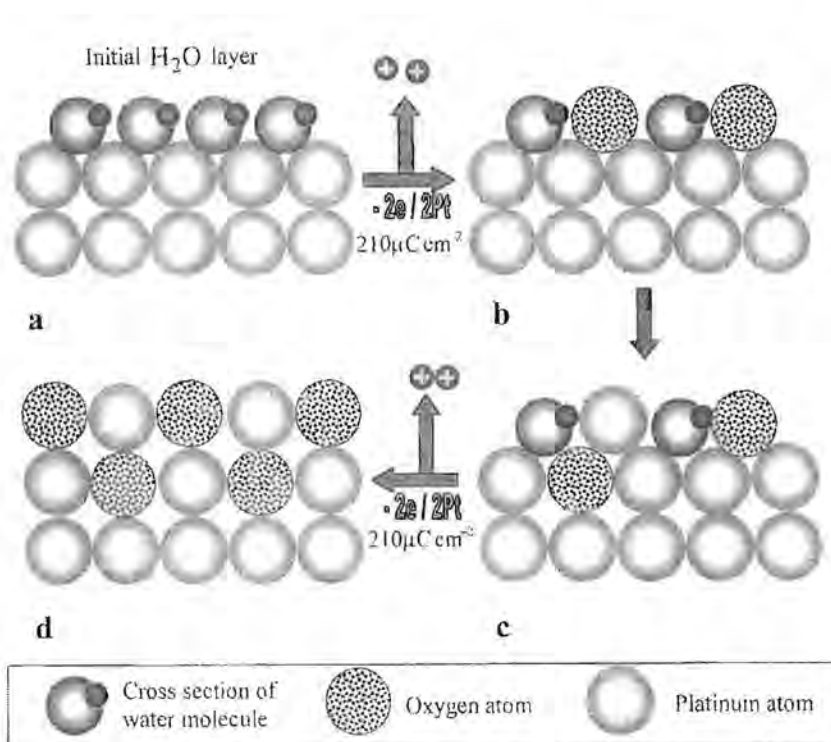


Figure 2.5. Cross-section of (a) initial water layer; (b) adsorbed O and H_2O ; (c) adsorbed H_2O and place-exchanged O; (d) surface oxide (Zolfaghari et al., 2002).

A similar model of initial, two-electron oxidation of the platinum surface has also been proposed by Harrington and co-workers (1997) in their simulation of ac voltammetry behaviour over the region of Pt oxide-film formation. It was found that the shape of the ac voltammograms does not change much with frequency, suggesting a single time constant for oxide growth. No features were seen in the early stages of growth that can be assigned to the fast OH electroadsorption, suggested previously to be the first step in oxide growth.

It was also suggested that although this mechanism is ruled out, some types of fast OH adsorption are still possible. Adsorption without charge transfer could be occurring. If OH electrosorption occurs in parallel with the slow oxide growth process, it might not be detectable by ac impedance. The admittances of the two processes would then be additive and a small admittance for OH electrosorption might contribute little to the total.

2.5.1.2. Electrochemical behaviour of platinum in alkaline solutions

Figure 2.6 (solid line) (Xia and Birss, 2000) shows a typical cyclic voltammogram of a Pt-coated quartz crystal in 0.1 M NaOH, as well as the associated frequency change (dashed line, inverse of mass change), measured during an oxidation/reduction scan between 0 and 1.6 V_{RHE} . In this range of potential the compact α -oxide film is formed (at ca. 0.6 V_{RHE}) and reduced, in peak C₁. The adsorption/desorption of a monolayer of hydrogen atoms is seen between 0.1 V and 0.4 V_{RHE} .

In Figure 2.6, a mass increase is seen, as expected, during Pt oxide formation, while oxide reduction is accompanied by an equivalent mass loss. From the integrated charge density during oxide reduction and the associated change in mass over the potential range of the cathodic peak, a ratio of 8.3g/mol e^- passed is obtained. A ratio of 8 g/mol electrons would be predicted for the formation of an anhydrous Pt oxide film, either PtO or PtO₂.

In the potential range of the hydrogen adsorption-desorption reaction it can be seen that as the potential is made more negative and hydrogen begins to adsorb, the electrode mass decreases, rather than increases, and vice versa during the positive scan. When hydrogen evolution commences in the negative scan, i.e. at 0.1 V_{RHE} , the frequency drops somewhat and then increases again in the positive scan. It is likely that the mass change between 0.15 and 0.4 V is due to the desorption of OH⁻ in the cathodic scan and its readsorption during the positive scan. The results of Figure 2.6 suggest that, during hydrogen atom adsorption on Pt (0.4-0.15 V_{RHE}), adsorbed hydroxide is concurrently being desorbed, then readsorbing again in the anodic sweep.

QCMB experiments involving α -oxide growth in 0.1 M NaOH with time at constant potentials were carried out by Xia and Birss (2000). Figure 2.7(a, b) (Xia and Birss, 2000) show both the oxide reduction charge density (per apparent area) and its g/mol e^-

ratio as a function of anodising time at two potentials: 1.3 and 1.6 V_{RHE} respectively. In both cases, the oxide reduction charge increases logarithmically with anodising time, reaching a near steady-state value after ca. 6 min (Fig. 2.7a) and 4 min (Fig. 2.8b).

Figure 2.7a shows that the mass to charge ratio for the oxide formed after very short times of anodising at 1.3 V_{RHE} is almost 9 g/mol electrons. While a ratio of 8 is expected for either PtO or PtO₂, this slightly higher value may indicate that the initial layer may have included some adsorbed OH⁻, or the formation of a small amount of PtOH or Pt(OH)₂ (expected ratio for both is 17g/mol e⁻). After 1 min of anodising at either 1.3 or 1.6 V, Figure 2.7(a,b) show similar ratios for the oxide film of 7.9 to 8.1 g/mol e⁻, the expected values for PtO or PtO₂. Unfortunately, the form of Pt oxide cannot be distinguished from the QCMB data.

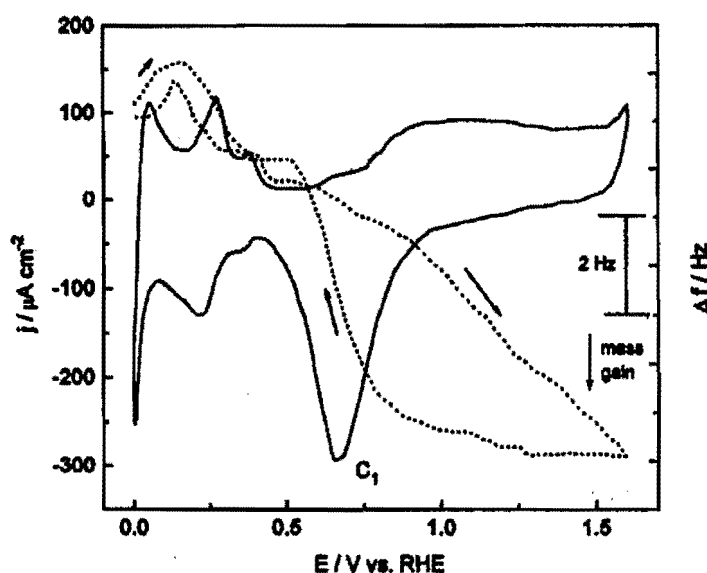


Figure 2.6. Cyclic voltammogram (solid line) and associated frequency change (dotted line) of a Pt-coated quartz crystal in 0.1 M NaOH between 0 and 1.6 V_{RHE} at 50mV/s (Xia and Birss, 2000).

Figure 2.8 (Xia and Birss, 2000) shows a plot of both the oxide reduction charge and the g/mol e⁻ ratios, monitored after 5 min at each of the anodising potentials between 1.2 and 1.9 V_{RHE} . The plot of the reduction charges appears to have two apparently linear segments, one for potentials less than 1.6 V, and one for potentials above this.

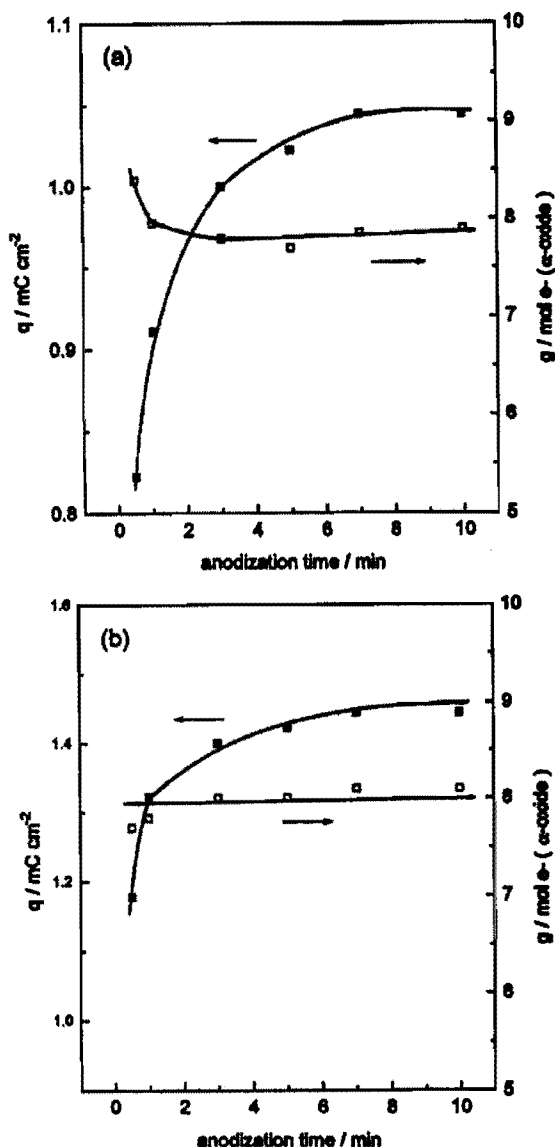


Figure 2.7: α -oxide reduction charge density (solid symbols) at 10 mV/s and its g/mol e^- ratio (open symbols) as a function of anodisation time of Pt-coated quartz crystal at (a) 1.3 V_{RHE} and (b) 1.6 V_{RHE} in 0.1 M NaOH (Xia and Birss, 2000).

Ellipsometric data (Xia and Birss, 2000) also indicates that the platinum oxide films, formed using potentials below 1.6 V_{RHE} , have different optical properties from those formed at potentials above 1.6 V_{RHE} . However, for all upper potential limits, except 1.2 V_{RHE} , the g/mol e^- ratio remains 8. These results has been interpreted as indicating that the oxide formed over the range 1.3 to 1.6 V_{RHE} is PtO, then changing to PtO₂ when the applied potential becomes higher than 1.6 V_{RHE} .

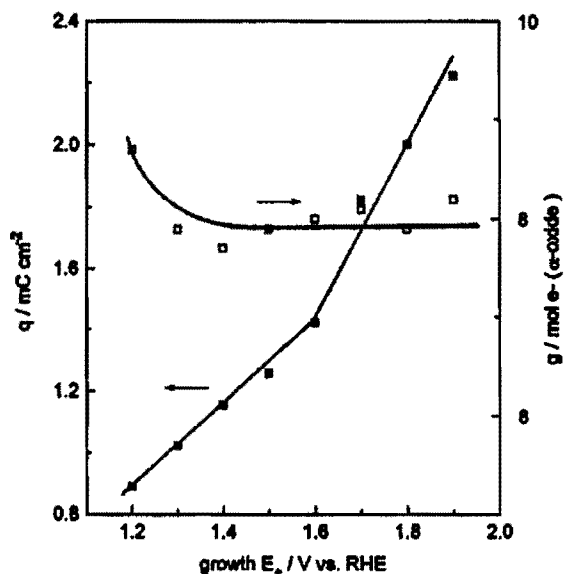


Figure 2.8. α -oxide reduction charge density (solid symbols) at 10 mV/s and its g/mol e^- ratio (open symbols) as a function of applied potential, after 5 minutes of anodisation of Pt-coated quartz crystal in 0.1 M NaOH (Xia and Birss, 2000).

2.5.1.3. Electrochemical behaviour of platinum in acid solutions

Figure 2.9 (solid curve) (Birss et al., 1993) shows a typical cyclic voltammogram of a Pt-coated quartz crystal in 0.1 M H_2SO_4 , as well as the associated mass changes (broken curve) measured during the experiment. A mass increase is seen, as expected, during Pt-oxide formation, while oxide reduction is marked by mass loss. From the integrated charge density during α -oxide reduction and the associated change in frequency over the potential range of the cathodic peak, a ratio of ca. 8 g/mol of electrons passed is obtained. This is similar to what was found for the oxide formed in alkaline solutions and suggests again that the α -oxide is anhydrous in nature (either PtO or PtO₂). However, ellipsometric data indicates that the platinum oxide film formed potentiostatically and by multicycling in 0.1 M H_2SO_4 has different optical properties than either of the two α -oxide films formed in base.

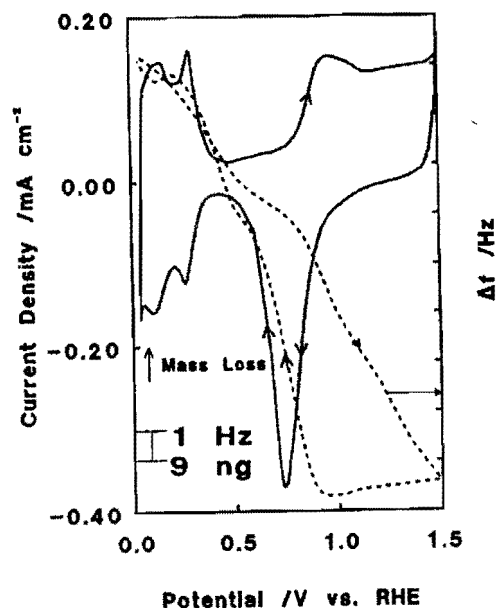


Figure 2.9. Cyclic voltammogram (solid line) and associated frequency change (dotted line) of a Pt coated quartz crystal in 0.1 M H₂SO₄; scanning rate 50 mV/s (Birss et al., 1993)

2.6. Gold-platinum alloys

The gold-platinum system has a miscibility gap (Figure 2.10) in the solid solution field (ASM Handbook, Volume 3: Alloy Phase Diagrams, 1992). The Pt-rich phase is frequently denoted as the α_1 phase and the Au-rich phase as α_2 .

There was interest in gold-platinum alloys during the 1950's and 1960's when they were used as spinning jets in the viscose rayon process (Darling, 1962).

2.6.1. Cold rolling of Au-Pt alloys

The whole range of alloys can be cold worked after quenching from temperatures not higher than 1000°C. The most ductile material is achieved by annealing at 1000°C, after which the temperature can be slowly dropped before water-quenching from 850°C (Darling, 1962).

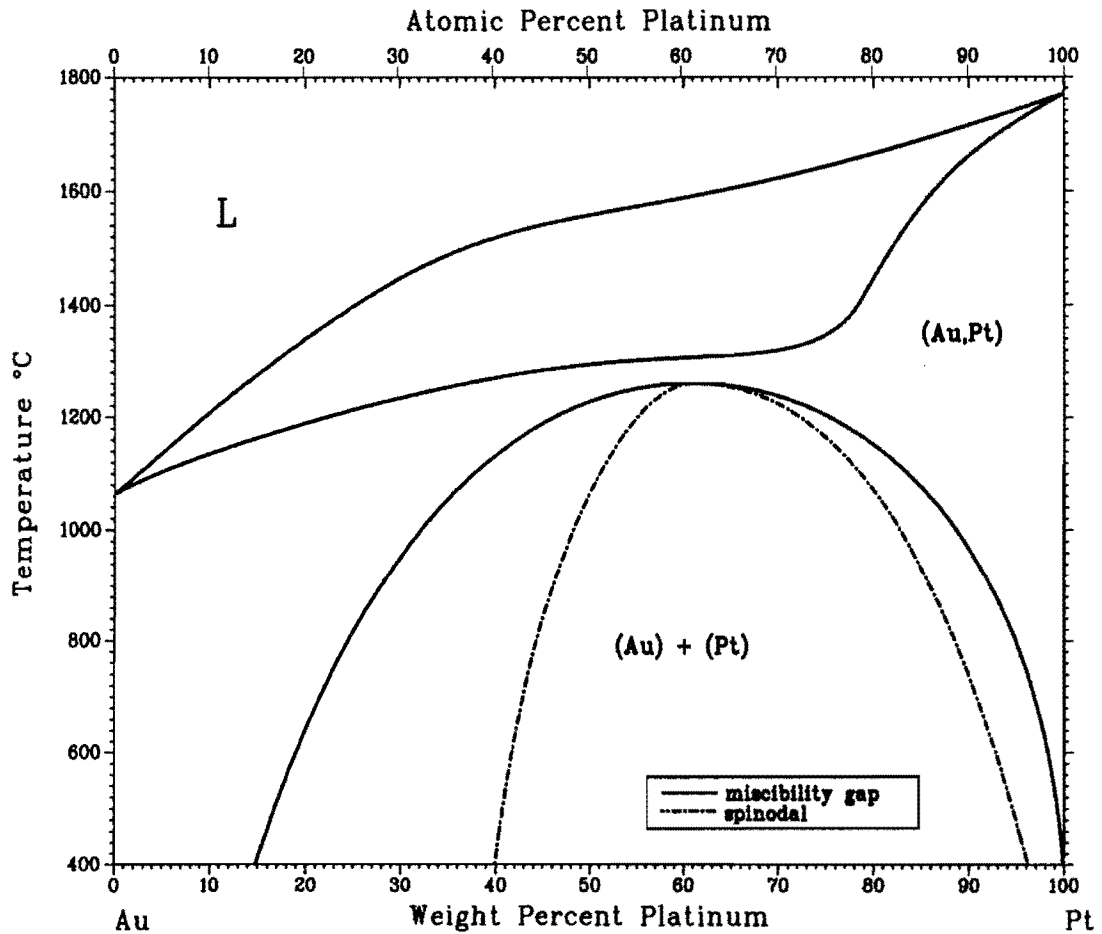


Figure 2.10. The Au-Pt phase diagram (ASM Handbook, Volume 3: Alloy Phase Diagrams, 1992)

2.6.2. Precipitation in Au-Pt alloys

The rate of precipitation depends upon the curvature of the free energy composition curves. The spinodal (Figure 2.10), being the locus of the inflexion points of the isothermal free energy composition curves, forms a lower limit of metastable equilibrium. Between the spinodal and the two-phase field exists a thermodynamic potential barrier that must be overcome before nucleation can occur, with the result that precipitation is retarded in this area (Darling, 1962).

2.6.3. Electrochemical behaviour of Au-Pt alloys

2.6.3.1. Homogeneous alloys

Woods (1971) studied the surface composition of Pt-Au alloys quenched from the region of continuous solid solution. Even though x-ray diffraction indicated that the alloys were homogeneous, the alloy electrodes gave current-potential curves (1 M H_2SO_4) that were equivalent to the sum of a pure platinum and a pure gold surface (Figure 2.11 (Woods, 1971)). It was suggested that this result can be explained if either:

1. Platinum and gold atoms in a homogeneous alloy have hydrogen and oxygen electroadsorption properties equal to that of platinum and gold atoms in the pure metals or
2. The surface of platinum/gold alloys always consists of the equilibrium phases even though the bulk is homogeneous.

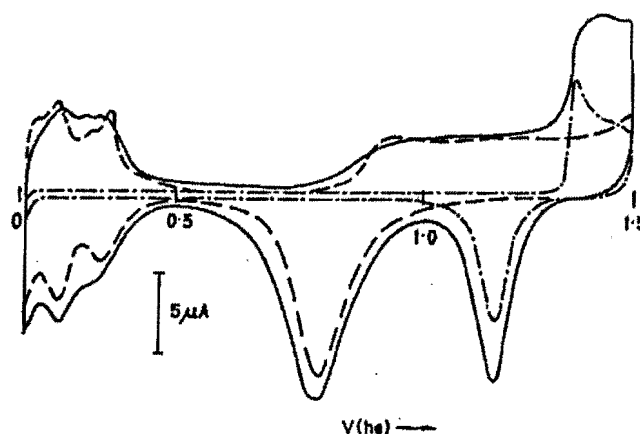


Figure 2.11. Current-potential curves showing hydrogen and oxygen adsorption in 1 M H_2SO_4 for a linear potential sweep of 40 mV/s. (----) Pt; (-.-.-) Au and (—) homogeneous 65%Pt-35%Au alloy (Woods, 1971).

2.6.3.2. Heterogeneous alloys

Breiter (1965) studied the anodic formation and cathodic reduction of oxygen layers on Au-Pt alloys in acid solutions. Platinum-gold alloys with gold contents ranging from 5 to 70 at% were studied. The alloys had to be annealed at 875°C before wires of 0.3 mm

diameter could be drawn. Heterogeneous (two-phased) Au-Pt alloys were produced with this heat treatment (Fig. 2.10). Current-potential curves were measured in 1 N H₂SO₄ at a sweep rate of 30 mV/s. The current-potential curves of the 20, 40 and 60at% Au alloys are shown in Figure 2.12 (Breiter, 1965). The most notable feature of Figure 2.12 is the fact that the alloys have two reduction waves. The first wave between 1.4 and 1.0 V_{SHE} is attributed to the reduction of the oxygen layer on “gold” and the second one between 1.0 V and 0.6 V_{SHE} to that of the layer on “platinum”. “Gold” is designated as being either gold atoms or the gold-rich phase of the heterogeneous alloys, while “platinum” is designated as being either platinum atoms or the platinum-rich phase of the alloys. The first reduction wave increased in height with increasing gold content while the second decreased (Fig. 2.12). The peaks of the two reduction waves appeared at slightly less anodic potentials on the alloys than on the respective pure metals. This indicates that the reduction of the oxygen layer on the two phases occurs with slightly larger hindrance than on the pure metals.

2.6.4. Electro-oxidation of chemical compounds at Au-Pt alloy electrodes

In alkaline media, the electro-oxidation activity of Au-Pt alloy electrodes is enhanced when compared with the respective metals (Stelmach et al., 1994; Beden et al., 1982). There are a few possible explanations for this synergistic effect of gold-platinum alloys.

2.6.5. Possible explanations for synergism on Au-Pt alloys

2.6.5.1. The bifunctional theory

The idea is that surface gold atoms adsorb oxygen-containing species, while surface platinum atoms adsorb the organic compound. The two different species interact leading to a final product. The two sites together give the complete reaction unit (Parsons and VanderNoot, 1988).

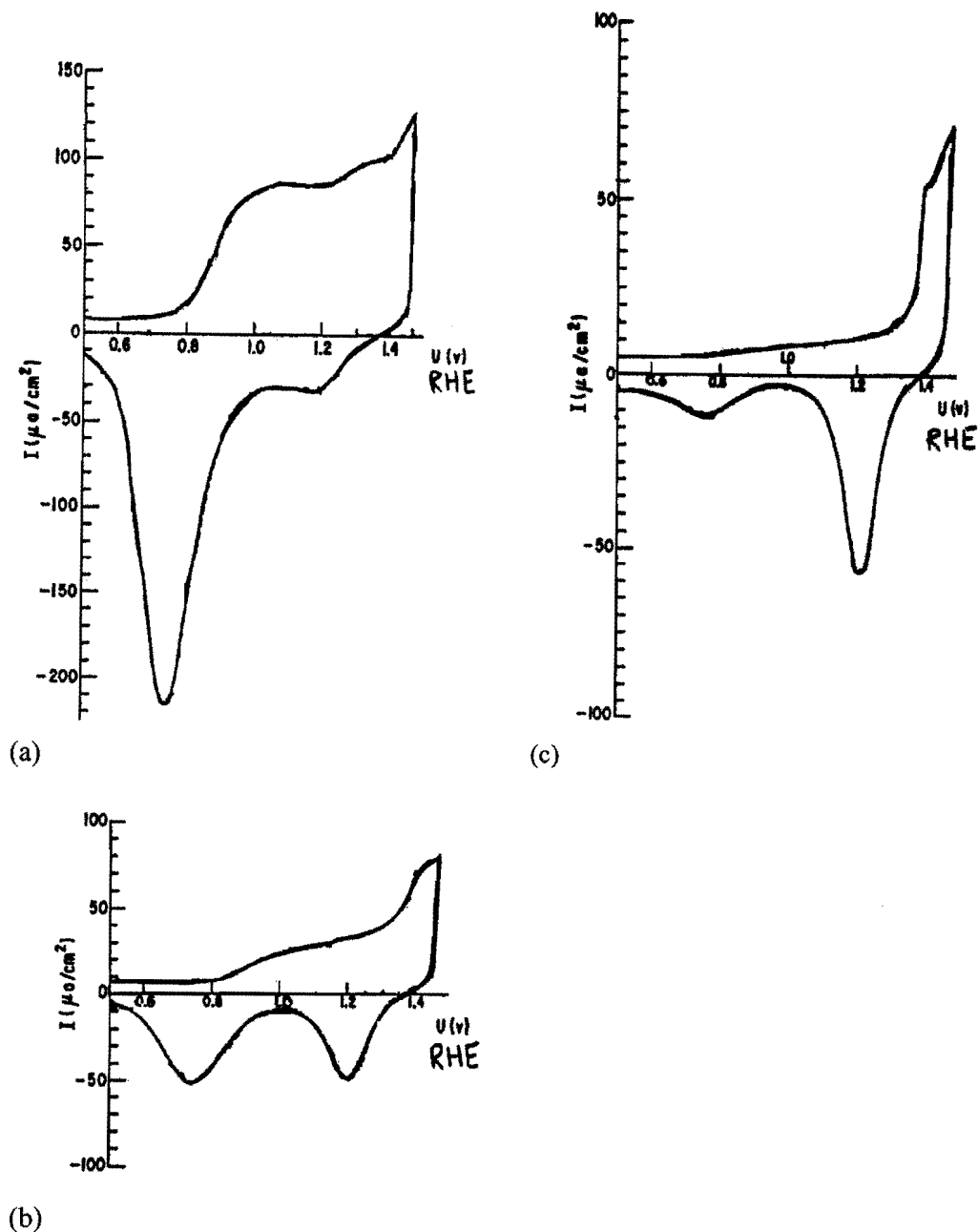


Figure 2.12. Current-potential curves for heterogeneous Au-Pt alloys containing (a) 20%, (b) 40% and (c) 60% Au in 1 N H_2SO_4 . Sweep rate 30 mV/s (Breiter, 1965).

2.6.5.2. Changes in adsorption features

Stelmach and co-workers (1994) found an increased rate of electro-oxidation of formaldehyde at alloy electrodes in comparison with the respective pure metals. They proposed that the energy of adsorption for the various forms of the substrate molecule is decreased sufficiently in order to facilitate further oxidative desorption of

intermediates and to suppress the adsorption of strongly bound intermediates. The adsorptivity of the surface remains high enough to support electro-oxidation.

2.6.5.3. The Third-Body effect

The formation of poisonous species adsorbed on more than one surface site is suppressed. For the electro-oxidation of formic acid, it was found that a platinum atom that is surrounded by gold atoms has the highest activity. A single platinum atom cannot be “poisoned” by the strongly bound intermediate since it needs adsorption sites that are only available on larger platinum clusters (Rach and Heitbaum, 1987).

2.6.5.4. The creation of Lewis acid surface sites on alloy electrodes

It is thought that the introduction of an alloying element that has a d-orbital occupancy less than that of the matrix will result in surface states at the alloy that function as Lewis acid sites. Furthermore, it is speculated that these surface sites enable adsorption of reactant species that are Lewis bases because of the existence of non-bonded electron pairs in these compounds e.g. the O-atoms in hydroxyl moieties of alcohols and carbohydrates, and N-atoms in amino acids (Mho and Johnson, 2001). This speculation is supported by successful modelling of the variations in the half-wave potential of the anodic voltammetric wave for dimethyl sulfoxide at β -PbO₂ film electrodes as a function of the variation in the level of doping by Bi (Popovic et al., 1998). The electrocatalytic benefit of reactant adsorption is explained on the basis of increase in residence time for the reactant species within the applied electric field at the electrode/solution interface.

Mho and Johnson (2001) studied the electrocatalytic response of carbohydrates at Cu-Mn alloy electrodes. The occupancy of the outermost d-orbital is lower for Mn (3d⁵) than that of Cu (3d¹⁰). The alloy composition of Cu:Mn = 95:5 was chosen to correspond to a homogeneous solid solution. The voltammetric responses observed for carbohydrates in 0.10 M NaOH were significantly larger at the preanodised CuMn electrodes as compared to preanodised pure Cu electrodes. It is speculated that the observed electrocatalytic effect comes as a beneficial consequence of the preadsorption of the carbohydrates at Mn sites (Lewis acid) in the preanodised CuMn surface.

Lewis acid surface sites will also be formed at gold-platinum alloys. The electron configuration of gold is $[\text{Xe}]4f^{14}5d^{10}6s^1$ and the electron configuration for platinum is $[\text{Xe}]4f^{14}5d^96s^1$.

2.7. The 60Au-40Pt alloy electrode

The Au-Pt alloy containing 60wt% Au has been identified previously (Stelmach et al., 1994) as the most active for the oxidation of aliphatic alcohols (Beltowska-Brzezinska, 1979), ethylene glycol (Eggert (Stelmach, 1994)) and formaldehyde (Beltowska-Brzezinska and Heitbaum, 1985) in alkaline media.

However, from the Au-Pt phase diagram (Fig. 2.10), it can be seen that different heat treatment temperatures can be used to produce different amounts of the α_1 and α_2 phases. The compositions of the two phases can also be changed by employing different heat treatment temperatures.

For the 60Au-40Pt alloy, annealing at 1100-1260°C will produce a homogeneous solid solution. Heat treatments at temperatures lower than 1100°C will produce a heterogeneous two-phased microstructure (Fig. 2.10). The different weight fractions of α_1 and α_2 , and their composition as a function of heat treatment temperature are shown in Table 2.1 for the 60Au-40Pt alloy. The lever rule was applied in order to calculate the various weight fractions.

Table 2.1: Equilibrium weight fractions and composition of phases in a 60wt% Au-40wt% Pt alloy as functions of temperature.

Temp. (°C)	Weight fraction of α_1	Composition of α_1		Weight fraction α_2	Composition of α_2	
		Wt%	Wt%		Wt%	Wt%
		Au	Pt		Au	Pt
1000	0.13	12	88	0.87	68	32
800	0.21	5	95	0.79	75	25
600	0.26	2	98	0.74	81	19
400	0.30	0	100	0.70	85	15

It will be interesting to study the electrochemical behaviour of the 60Au-40Pt alloy in different heat treatment conditions. The electro-oxidation of an organic compound, such as ethylene glycol, can be used to determine the effect of microstructure on the electrochemical properties of the alloy.

2.8. The electro-oxidation of ethylene glycol at noble metal electrodes

Ethylene glycol, $(\text{CH}_2\text{OH})_2$, is a non-toxic diol-alcohol. It has the advantage of involving a large number of electrons per molecule in its oxidation (the oxidation reaction needs 8 electrons per molecule when the final product is oxalate (Hauffe and Heitbaum, 1978)). The electro-oxidation of ethylene glycol at noble metal electrodes has been studied extensively, due to the interest of using it as a fuel for alcohol fuel cells (Christensen and Hamnett, 1989; Kadirgan et al., 1990; Beden et al., 1982, Hahn et al., 1987).

2.8.1. The electro-oxidation of ethylene glycol at gold electrodes in acid

The cyclic voltammogram for the electro-oxidation of ethylene glycol at a gold electrode in acid is shown in Figure 2.13 (Beden et al., 1987). It can clearly be seen from Figure 2.13 that nearly no oxidation of ethylene glycol occurs at gold in acid.

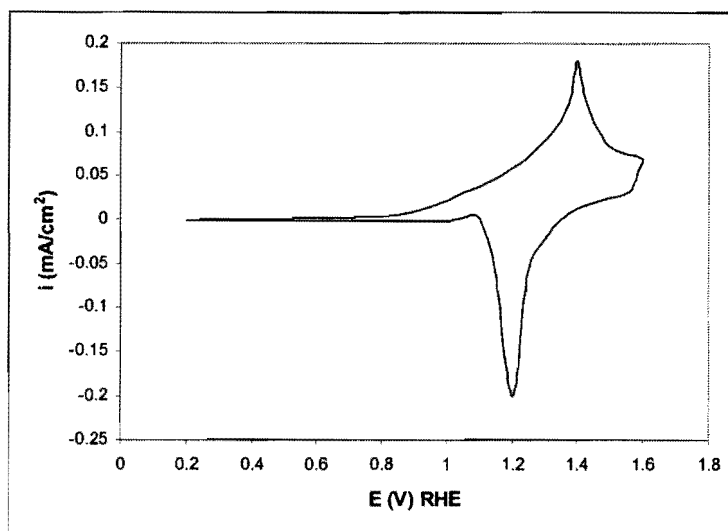


Figure 2.13. Oxidation of ethylene glycol at a gold electrode in acid medium. Conditions: 0.1 M HClO_4 , 0.1 M ethylene glycol, 25°C, 50 mV/s (After Beden et al., 1987).

2.8.2. The electro-oxidation of ethylene glycol at gold electrodes in base

A cyclic voltammogram for the electro-oxidation of ethylene glycol at a gold electrode in base is shown in Figure 2.14, together with the voltammogram of gold in the supporting electrolyte alone (Kadirgan et al., 1990). Ethylene glycol oxidation starts at $0.8 V_{\text{RHE}}$ during the positive sweep, giving a peak of 12 mA/cm^2 at approximately $1.2 V_{\text{RHE}}$ (peak A). The electro-oxidation of ethylene glycol is inhibited by the formation of the surface oxide on the gold electrode. During the negative sweep, oxidation of ethylene glycol commences only after the surface gold oxide has been reduced, reaching a current maximum of about 4 mA/cm^2 at $1 V_{\text{RHE}}$ (peak B). The positive and negative potential scans are almost superimposed in the potential range from 0.8 to $1 V_{\text{RHE}}$. Hauffe and Heitbaum (1978) found that the peak currents (peaks A and B) are somewhat smaller when the solution is stirred with argon gas. This can be explained by an accelerated transportation of intermediates into the solution.

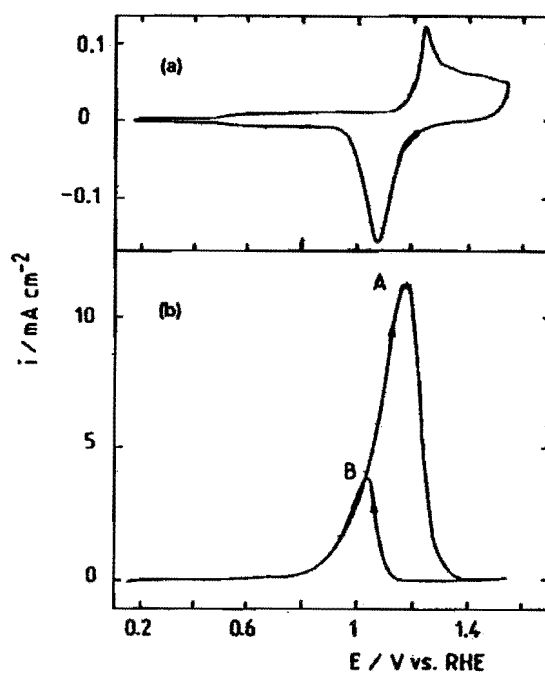


Figure 2.14. Cyclic voltammograms of a gold bead electrode (0.1 M NaOH , 25°C , 50 mV/s). (a) Without ethylene glycol; (b) with 0.1 M ethylene glycol (Kadirgan et al., 1990).

It is not possible to sustain long electrolysis of ethylene glycol at a fixed potential, because of poisoning phenomena that occurs at the electrode surface (Kadirgan et al., 1990). A cleaning procedure has to be used for sustainable electrolysis. The simplest technique is to use potential programs with potential plateaux separated repeatedly by a single cleaning potential sweep. The electrode surface and the poisons are oxidised at the upper potential limit. The surface oxides are reduced at the lower potential limit, before returning to the potential plateaux. The major product of electrolysis at 1.13 V_{RHE} is glycolate. Small quantities of oxalate, carbonate and formate are also formed (Kadirgan et al., 1990).

Kadirgan and co-workers (1990) used electromodulated infrared reflectance spectroscopy (EMIRS) to check for the presence of adsorbed CO-type poisons. These CO poisons would be formed by the rupture of the C-C bond during chemisorption at negative potentials. It was found the CO band is not present initially and that it grows during spectral accumulation performed to improve signal to noise ratio. However, the CO band is far from being the main infrared band observed. This implies that ethylene glycol does not dissociate immediately on gold at low potentials and that the CO poisoning species are formed only progressively. Glycolaldehyde and glyoxalate were found to be the main adsorbed species.

2.8.3. The electro-oxidation of ethylene glycol at platinum electrodes in acid

A cyclic voltammogram for the electro-oxidation of 0.1 M ethylene glycol in 0.1 M $HClO_4$ is shown in Figure 2.15 (Hahn et al., 1987). Several peaks and shoulders, labelled A to D are found.

Inhibition of hydrogen adsorption in the hydrogen region occurs due to adsorption of ethylene glycol. Electrochemically Modulated Infrared Reflectance Spectroscopy (EMIRS) was used by Hahn et al (1987) to study the adsorption of ethylene glycol. It was found that the adsorption is dissociative, leading to the formation of a poisoning linearly bonded CO species. Oxidation of the CO starts at 0.6 V_{RHE} , at the same potential where the overall oxidation process of ethylene glycol begins (Fig. 2.15).

By using in situ FTIR spectroscopy, Christensen and Hamnett (1989) identified the main products of ethylene glycol oxidation in acid as glycolic acid and CO_2 .

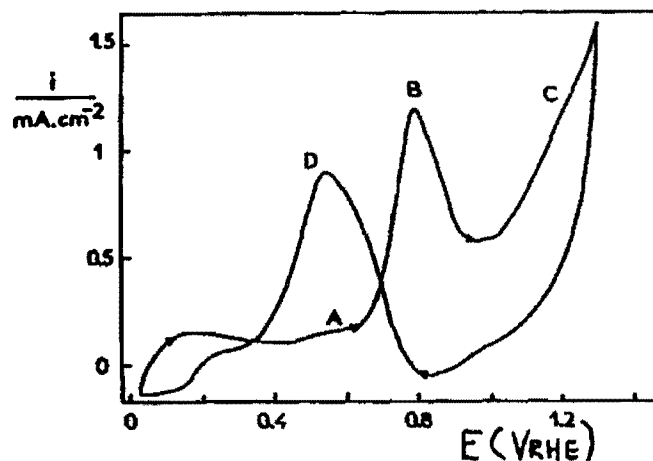


Figure 2.15. Cyclic voltammogram for the oxidation of 0.1 M ethylene glycol in 0.1 M HClO_4 , on platinum. Conditions: 100 mV/s, 25°C (Hahn et al., 1987).

2.8.4. The electro-oxidation of ethylene glycol at platinum electrodes in base

Cyclic voltammograms of a platinum electrode in 1 M NaOH in the absence and in the presence of 0.1 M ethylene glycol are shown in Figure 2.16 (Kadirgan et al., 1983). Ethylene glycol oxidation begins at 0.35 V_{RHE} during the positive sweep, giving a steep rise A at 0.65 V_{RHE} , then a peak B of 6.6 mA/cm^2 at 0.73 V_{RHE} and a small peak C at 1.05 V_{RHE} . The decrease of current after peak B is related to the formation of surface oxides on the platinum electrode. Ethylene glycol oxidation takes place during the negative sweep after the reduction of the surface oxides, reaching a maximum rate of 2 mA/cm^2 at 0.63 V_{RHE} (peak D). The current densities obtained in alkaline solution are much higher than in acid solution (Figure 2.15). The oxidation process also appears to be less irreversible in alkaline than in acid medium, in which the main oxidation peaks of ethylene glycol are separated by more than 250 mV during the positive and negative sweeps (Fig. 2.15).

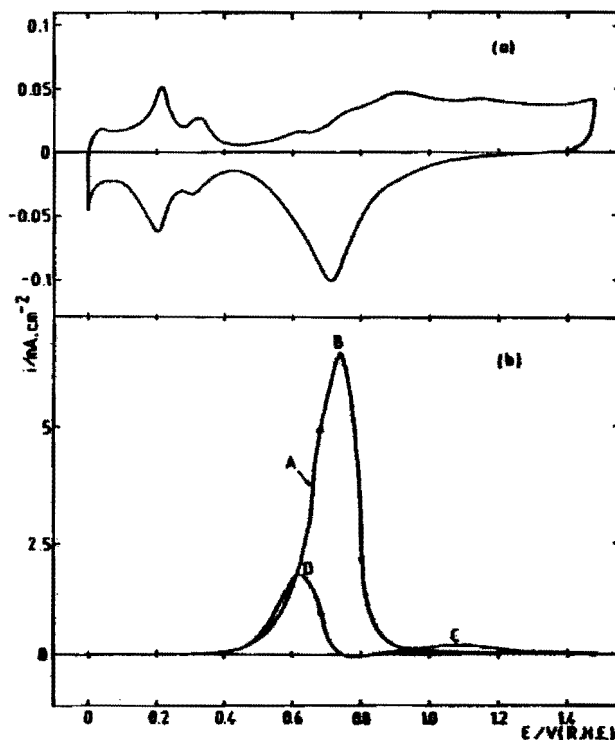


Figure 2.16. Cyclic voltammograms of a Pt bead electrode (1 M NaOH, 25°C, 50 mV/s): (a) without ethylene glycol; (b) with 0.1 M ethylene glycol (Kadirgan et al., 1983).

Electrochemically Modulated Infrared Reflectance Spectroscopy (EMIRS) was used by Hahn et al (1987) to study the adsorption of ethylene glycol at platinum in alkaline solutions. The adsorption was found to be dissociative. However, almost equal amounts of bridge-bonded and linearly bonded CO species were found in alkaline solutions. This is in contrast to acidic solutions, where only linearly bonded CO species were found (Hahn et al., 1987). An important shift towards lower wavenumbers of the linearly-bonded CO band centre was observed when the pH was increased. This might be due to interactions with the solvent or with adsorbed OH species, and a decrease of the CO coverage. The adsorption of molecular ethylene glycol may also play a role. The drastic change in the CO coverage as a function of pH is most probably related to a change in the electrocatalytic activity of platinum towards the oxidation of ethylene glycol when changing from acid to alkaline solutions.

The main products of ethylene glycol oxidation in base at platinum are glycolate, oxalate and CO_3^{2-} , determined by in situ FTIR (Christensen and Hamnett, 1989).

2.8.5. The electro-oxidation of ethylene glycol at Au-Pt electrodes in base

The cyclic voltammograms for ethylene glycol oxidation in base at Au, Pt and a 50Au-50Pt alloy electrode are shown in Figure 2.17 (Beden et al., 1982). The Au-Pt alloy electrode was prepared by electrolytic codeposition of the two metals on a platinum bead. The alloy electrode was then annealed by warming it to red heat in a hydrogen flame. For the alloy electrode it can be seen that during the positive sweep, electro-oxidation of ethylene glycol occurs in two main peaks. The first peak is in the same potential range as pure platinum and the second peak corresponds to oxidation on pure gold. However, the current densities obtained with the alloy electrode are much higher than those on the pure metals. At the Pt-region, the electro-oxidation activity is enhanced eight times and at the Au-region two times.

The 60Au-40Pt alloy electrode has been found to be the most active for ethylene glycol oxidation (Eggert (Stelmach, 1994)). However, the effect of the heat treatment condition of this alloy (Table 3.1) on the electro-oxidation of ethylene glycol needs to be considered.

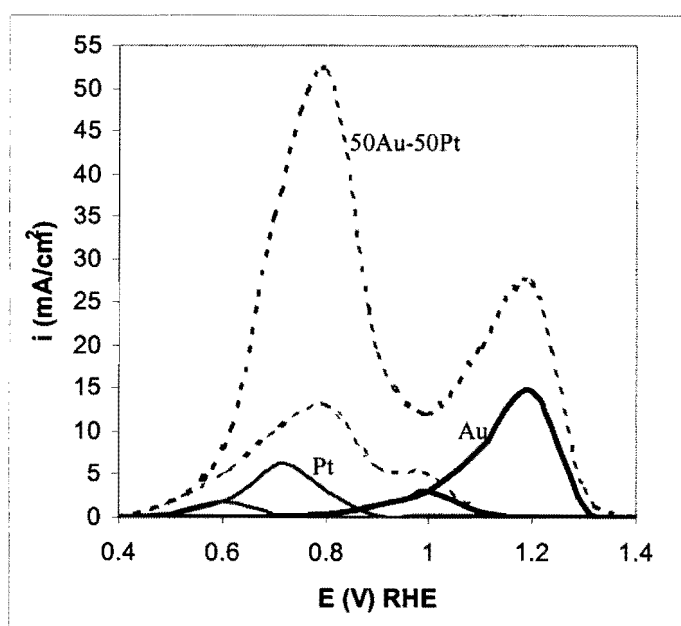


Figure 2.17. Cyclic voltammograms for ethylene glycol electro-oxidation in 1 M NaOH (0.1 M ethylene glycol, 25 °C, 50 mV/s) on a platinum bead electrode, a gold bead electrode and a 50Au-50Pt alloy electrode (After Beden et al., 1982).

2.9. The Au-1wt% Ti alloy (Gold 990)

The Au-1wt% Ti alloy was originally developed to produce an alloy with at least 990 fineness, with colour close to that of pure gold and with durability as good as that of standard jewellery alloys (Gafner, 1989).

The addition of 1 wt% (4 at%) of titanium to gold substantially hardens the precious metal and enhances its wear resistance. The enhanced hardening is due to the formation of fine Au_4Ti precipitates under the appropriate thermo-mechanical treatments (The Au-Ti phase diagram (ASM Handbook, Volume 3: Alloy Phase Diagrams, 1992) is shown in Figure. 2.18). The addition of titanium to gold satisfies two important criteria for achieving optimum precipitation hardening:

- 1) It has a high solubility in gold at elevated temperature, which maximises its dissolution into gold.
- 2) The gold-titanium system has a shallow solvus curve towards pure gold, which enables a significant proportion of titanium to be retained in supersaturated solid solution on quenching. The Au_4Ti compound, which constitutes the strengthening precipitate, is substantially harder than the gold matrix and so gives rise to a substantial reinforcement.

2.9.1. Preparation of Gold 990

The alloy is prepared (Gafner, 1989) by melting together the constituents in a vacuum induction furnace, and casting the alloy into a suitable ingot. It is then precipitation hardened in two stages by first carrying out a solution heat-treatment, involving a heating stage at 800°C in air, or a vacuum or inert atmosphere, followed by quenching the ingot in water. Tests have shown that no significant loss of titanium occurs when solutionising is in air, because a protective surface layer forms. This brown layer can subsequently be removed mechanically or by dipping the alloy in a 10% $K_2S_2O_7$ solution in water. Precipitation hardening is accomplished by heating the alloy at a lower temperature, typically at 400-500°C, with or without an intermediate cold working stage.

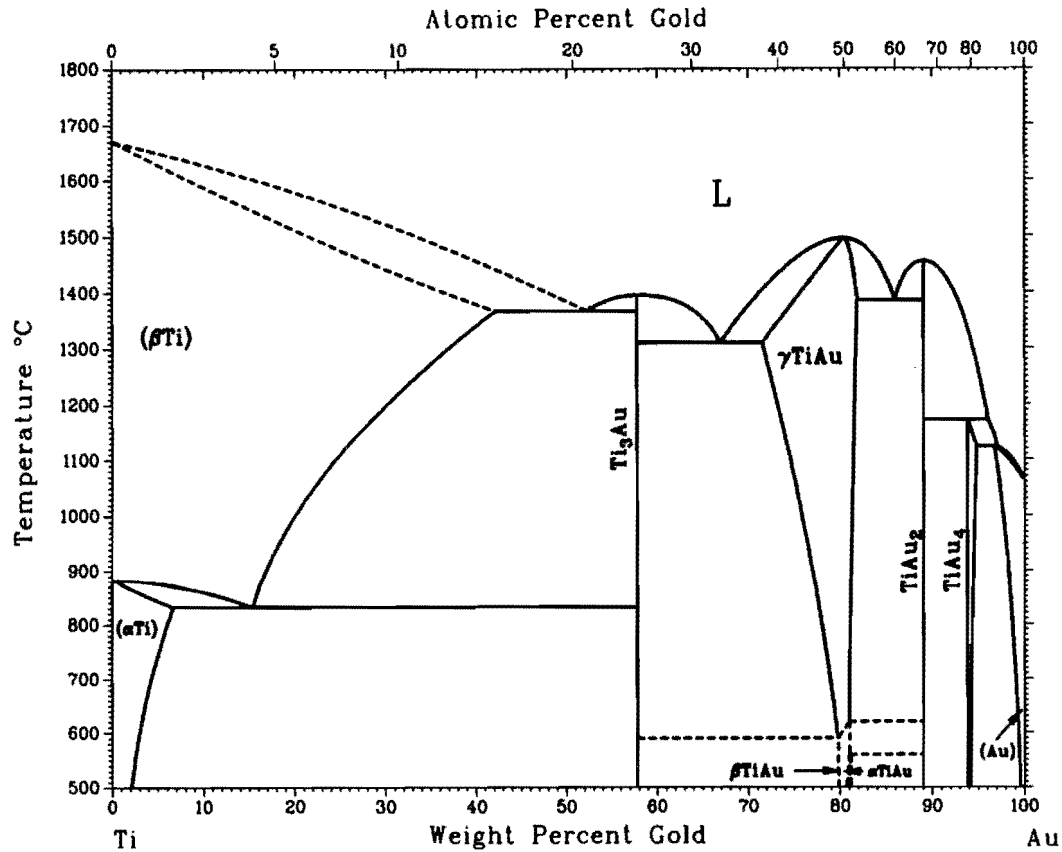


Figure 2.18. The Au-Ti phase diagram (ASM Handbook, Volume 3: Alloy Phase Diagrams, 1992).

It would be of interest to investigate the electrochemical properties of the alloy in two different heat treatment conditions (Fig. 2.18):

- 1) With titanium in solid solution.
- 2) In the precipitation-hardened condition (with Au₄Ti precipitates).

2.9.2. The electrochemical behaviour of pure titanium

Potentiodynamic polarisation curves for titanium in 0.5 M H₂SO₄ were measured at 303, 313 and 323 K by Shibata and Zhu (1995) and are shown in Figure 2.19.

An active-passive transition is found at around -0.49 V_{Ag/AgCl}. The critical current for passivation and the passive current increase with temperature. It is interesting that a second peak appears around 2.1 V_{Ag/AgCl}, which decreases with increase in temperature. The origin of this peak is still uncertain. According to Armstrong (1977) it could be due to a phase transformation of the originally formed oxide. The steady passive current was again reached beyond this second peak. A rapid current increase then

follows due to oxygen evolution. The oxygen evolution potential shifted in the negative direction with increase in temperature.

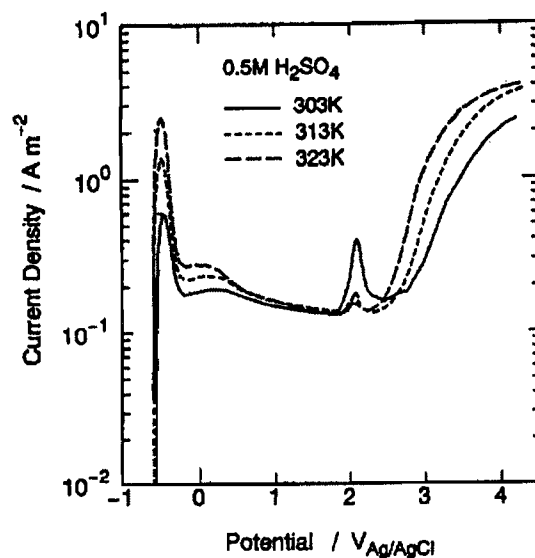


Figure 2.19. Anodic polarisation curves of Ti in 0.5 M H_2SO_4 solution at 303, 313 and 323 K (Shibata and Zhu, 1995).

The frequency and current responses as a function of the potential for titanium in 5 M H_2SO_4 are shown in Figure 2.20 (Herranen and Carlsson, 2001). As expected, the anodic current corresponding to dissolution of titanium is first accompanied by an increase in frequency (this corresponds to a decrease in mass). After reaching the passivation potential at -470 mV_{SCE} , with the corresponding critical current density (i_c), the current decreases as a result of oxide formation. However, the mass continues to decrease in the active-passive region. This indicates that the passive layer is not intact until a passive potential of about -150 mV_{SCE} is reached. An increase in mass is observed in the passive region. A second current density peak at 1.72 V_{SCE} was only found in 0.1 M H_2SO_4 - proposed to be due to a phase transformation of the oxide (Armstrong, 1977).

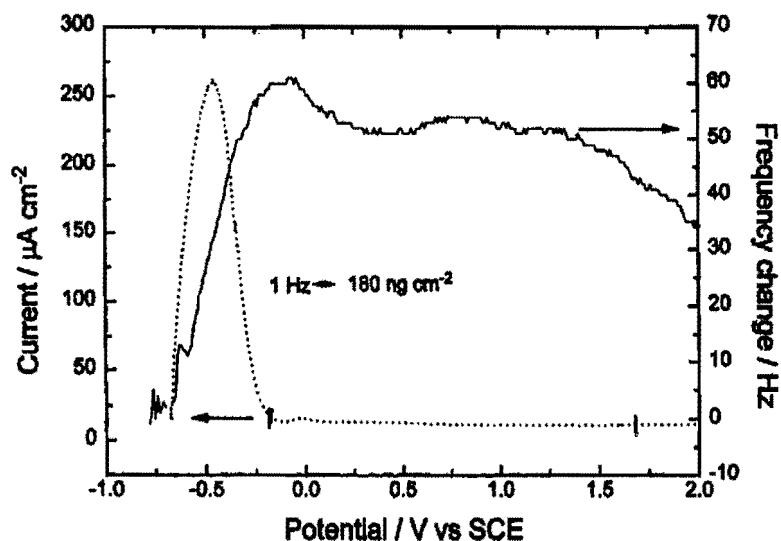


Figure 2.20. Current and frequency changes as functions of the potential of Ti in 5 M H_2SO_4 (Herranen and Carlsson, 2001).

A number of studies of the structure and composition of passive films on titanium have been reported. Armstrong (1977) studied the electrochemical behaviour of titanium films in 1 M HClO_4 and 0.5 M H_2SO_4 and characterised the surface oxide by XPS and AES. This indicated a mixture of metal oxides (TiO_2 , Ti_2O_3 and TiO). Electrodes prepared at a larger anodic charge (potentials up to 2 V_{SCE}) showed more TiO_2 character.

Pure titanium is expected to be in the passive condition at the potentials applied for cyclic voltammetry of gold electrodes (0 – 1.8 V_{RHE} in acid and 0 – 1.6 V_{RHE} in base, Figures 2.1 and 2.2). This fact is also supported by the Pourbaix diagram for titanium shown in Figure 2.21 (Pourbaix, 1974).

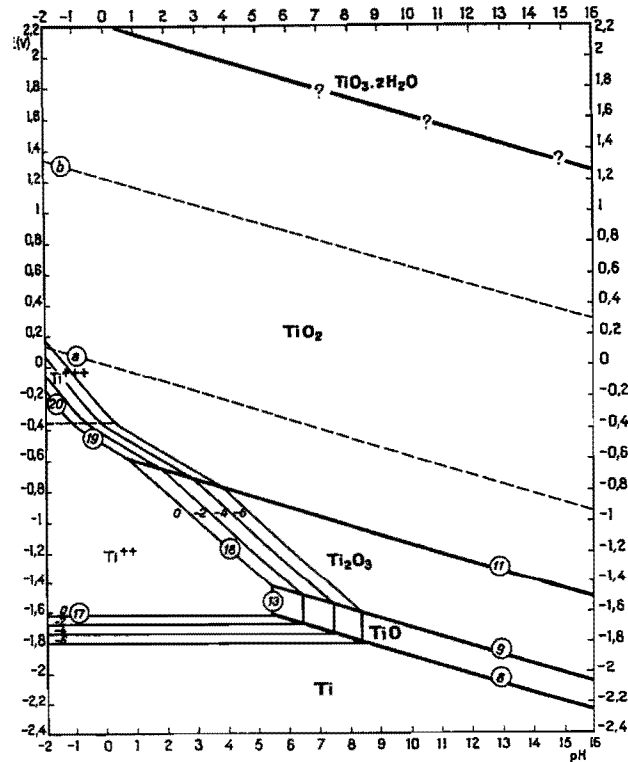


Figure 2.21: Potential – pH equilibrium diagram for the system titanium – water, at 25°C (Pourbaix, 1974).

2.10. Conclusions

- Even though gold is a weak chemisorber, it displays a wide range of electro-oxidation activity, especially in alkaline solutions.
- It is believed that organic compounds are oxidised at gold anodes in the presence of a submonolayer of adsorbed hydroxyl radicals (AuOH) before monolayer oxide formation.
- A bimetallic electrode is usually more active for the electro-oxidation of organics than the respective pure metals.
- The 60Au-40Pt alloy electrode has been identified in the literature as being the most active for the electro-oxidation of various organics in base. However, the effect of the microstructure of the alloy on its electrochemical properties has largely been ignored in the past.
- The electro-oxidation of ethylene glycol at noble metal electrodes has been studied extensively. This organic compound can therefore be used as a model compound to study the effect of heat treatment condition on the electrochemical properties of the gold alloys.

- The Gold 990 alloy was developed originally for the jewellery industry. The electrochemical properties of this alloy have not been studied before.

Chapter 3

THE HEAT TREATMENT OF Au-Pt ALLOYS AND THE GOLD 990 ALLOY

3.1. Introduction

The gold alloy containing 40% platinum has been identified (Stelmach et al., 1994) as being the most active for the oxidation of various organic compounds in alkaline solutions. However, the effect of the microstructure of gold-platinum alloys on their electrochemical properties has largely been ignored in the past. The purpose of this chapter is to discuss the microstructures of the 60Au-40Pt alloy obtained after different heat treatments. The spinodal decomposition reaction in the 50Au-50Pt alloy is also discussed.

The Gold 990 alloy (Au-1wt%Ti) is a precipitation-hardenable alloy. The different heat treatments of the Gold 990 alloy will also be reviewed in this chapter.

3.2. The 60Au-40Pt alloy

Gold and platinum (both 99.99%) were melted together (in the required ratio) in an arc-furnace with a water-cooled copper hearth under a protective argon atmosphere. The sample (approximately 10 g) was turned around after each melt and re-melted three times to ensure homogeneity.

3.2.1. The 60Au-40Pt alloy heat treated at 1300°C

The 1300°C heat treatment of the 60Au-40Pt alloy is shown schematically in Figure 3.1. Partial melting of the sample will occur at 1300°C. The liquid phase will be gold-rich with a composition of approximately 85Au-15Pt. The solid phase will be platinum-rich. The composition of this phase is difficult to estimate, due to the fact that the solidus line is almost horizontal at these temperatures. A small deviation from 1300°C will result in

large deviations in the composition of this phase. For the same reason, the lever rule cannot be used to accurately predict the amount of each phase that will be formed. However, the Pt-rich phase obtained by this heat treatment will have a higher gold content than the Pt-rich phases formed in the miscibility gap (Figure 3.1).

The sample was kept at 1300°C for 1 hour before quenching in water. After quenching, the sample was cold-rolled to a thickness of approximately 2 mm. A disk with a diameter of 6 mm was subsequently punched. The sample was mounted in a resin by using a black phenolic thermosetting powder. It was polished using diamond paste (6, 5 and finally 1 μm). The microstructure was studied by means of optical microscopy and scanning electron microscopy (SEM).

The microstructure of the 60Au-40Pt alloy after the 1300°C heat treatment is shown in Figure 3.2. Etching was not required to produce the microstructure shown in Figure 3.2. It can be seen that the Pt-rich areas formed by this heat treatment are relatively large, with typical diameters of 30 –50 μm (Figure 3.2).

Back-scattered electron imaging cannot be used to study the Au-rich and Pt-rich areas, because the atomic weights of gold and platinum are similar (196.97 and 195.08 g/mol respectively). However, the Au-rich and Pt-rich phases can be distinguished by elemental mapping using energy dispersive X-ray analysis in a scanning electron microscope.

An elemental map (using energy-dispersive X-ray analysis based on the L lines of the two metals) of the 60Au-40Pt alloy heat treated at 1300°C is shown in Figure 3.3. The elemental map confirms that optical microscopy without etching of the sample can be employed to study the microstructures of Au-Pt alloys (Compare Figures 3.2 and 3.3).

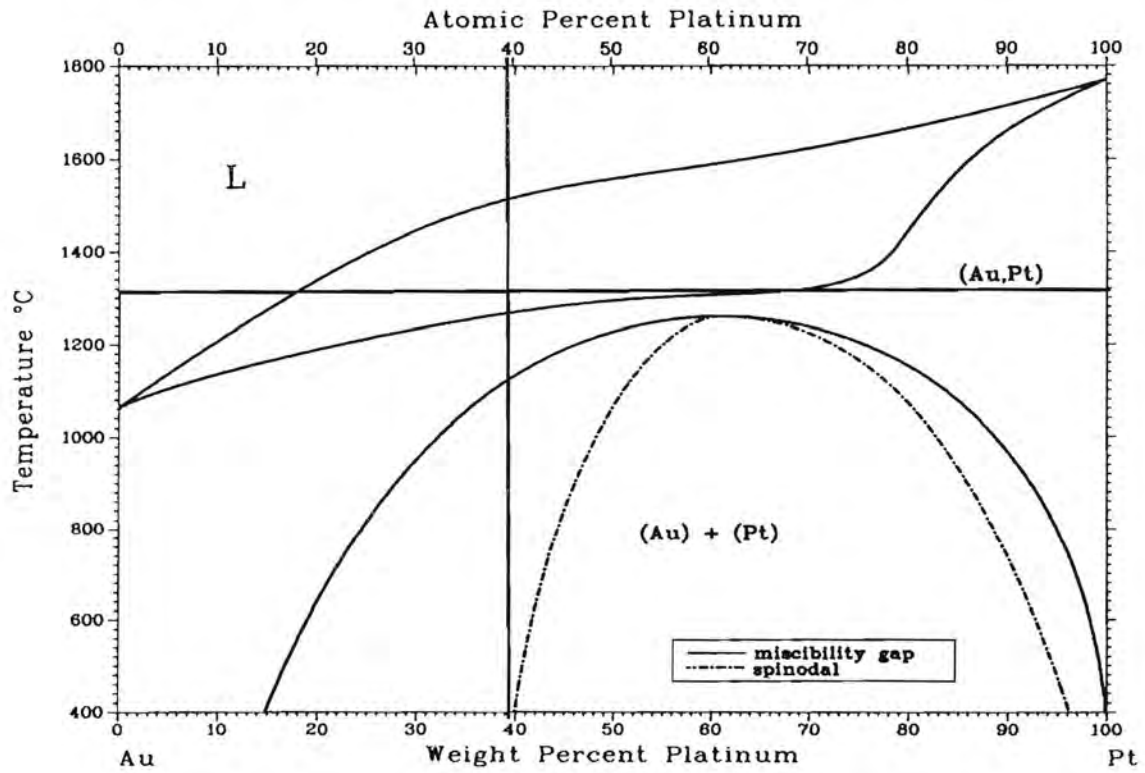


Figure 3.1. The 1300°C heat treatment of the 60Au-40Pt alloy (*ASM Handbook, Volume 3: Alloy Phase Diagrams, 1992*)

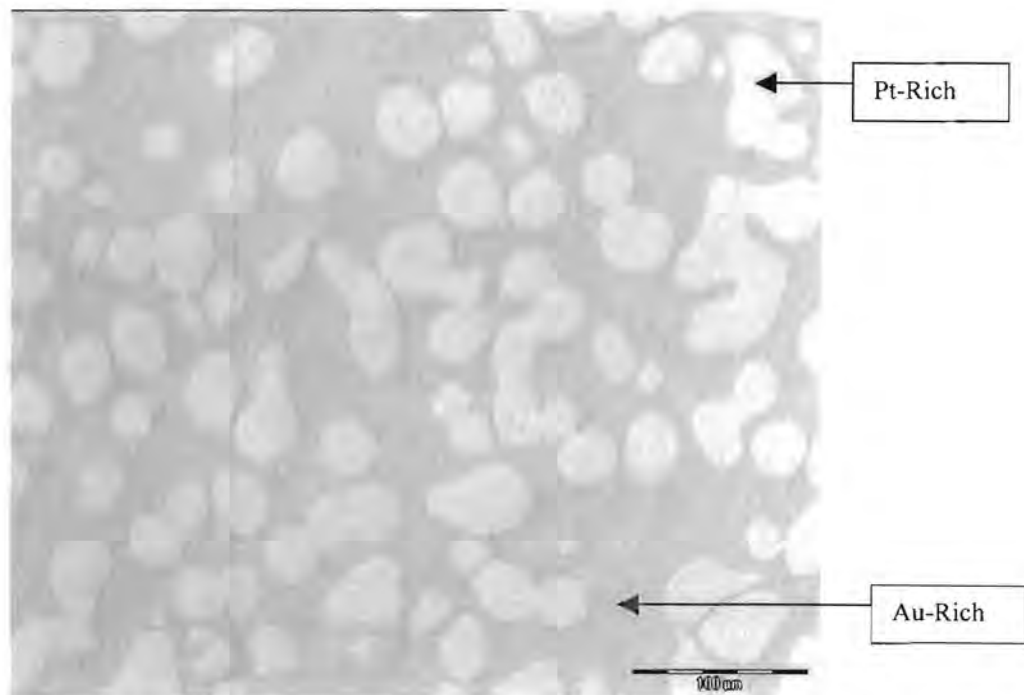


Figure 3.2. Optical photomicrograph of the 60Au-40Pt alloy after heat treatment at 1300°C for 1 hour (No etching).

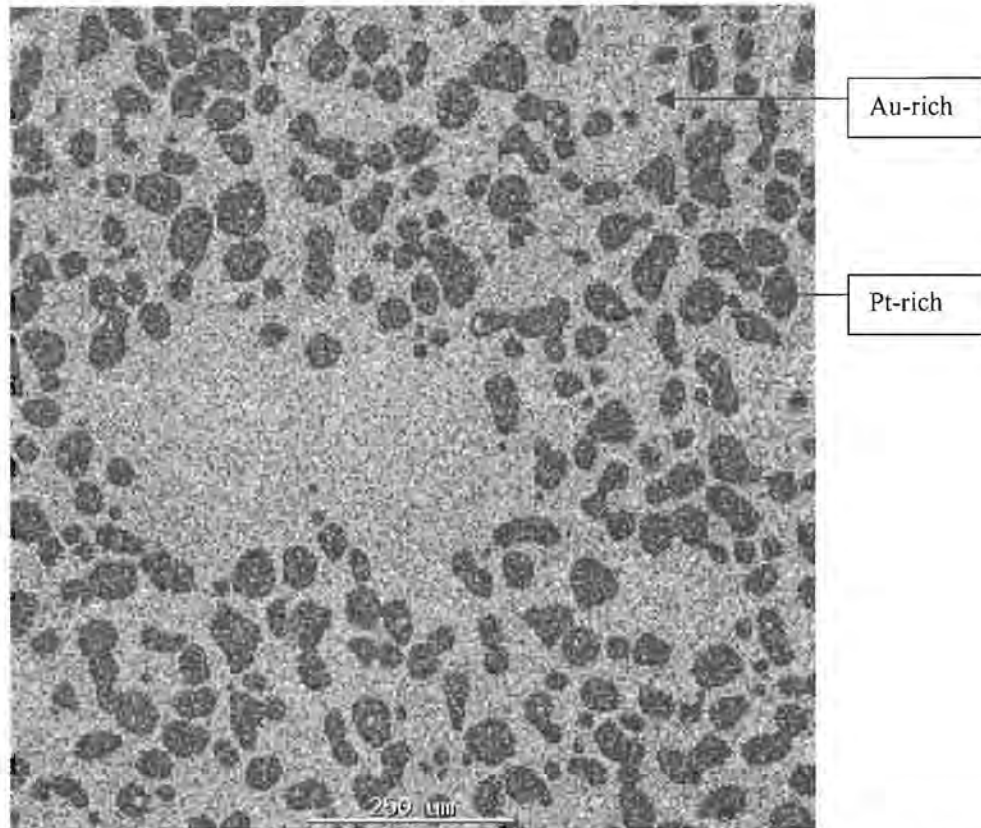


Figure 3.3: Elemental map (based on L lines of energy-dispersive X-ray analysis) of the 60Au-40Pt alloy heat treated at 1300°C.

3.2.2. The 60Au-40Pt alloy heat treated at 1200°C

Samples of the 60Au-40Pt alloy in the 1300°C heat treatment condition were heat treated at 1200°C, followed by water quenching. The 1200°C heat treatment of the 60Au-40Pt alloy is shown schematically in Figure 3.4. This heat treatment is designed to produce a homogeneous solid solution of platinum in gold. Due to the fact that the Pt-rich areas are relatively large in the 1300°C condition (Fig. 3.2), the influence of time at 1200°C was investigated by heat treating two samples for different times. The first sample was treated at 1200°C for 24 hours and the second sample for 168 hours (1 week).

The samples were polished using diamond paste (6, 5 and finally 1 μm). The microstructures were studied by means of optical microscopy and scanning electron microscopy (SEM). X-ray diffraction (XRD) was used to confirm whether a solid solution was produced after the solutionising heat treatment.

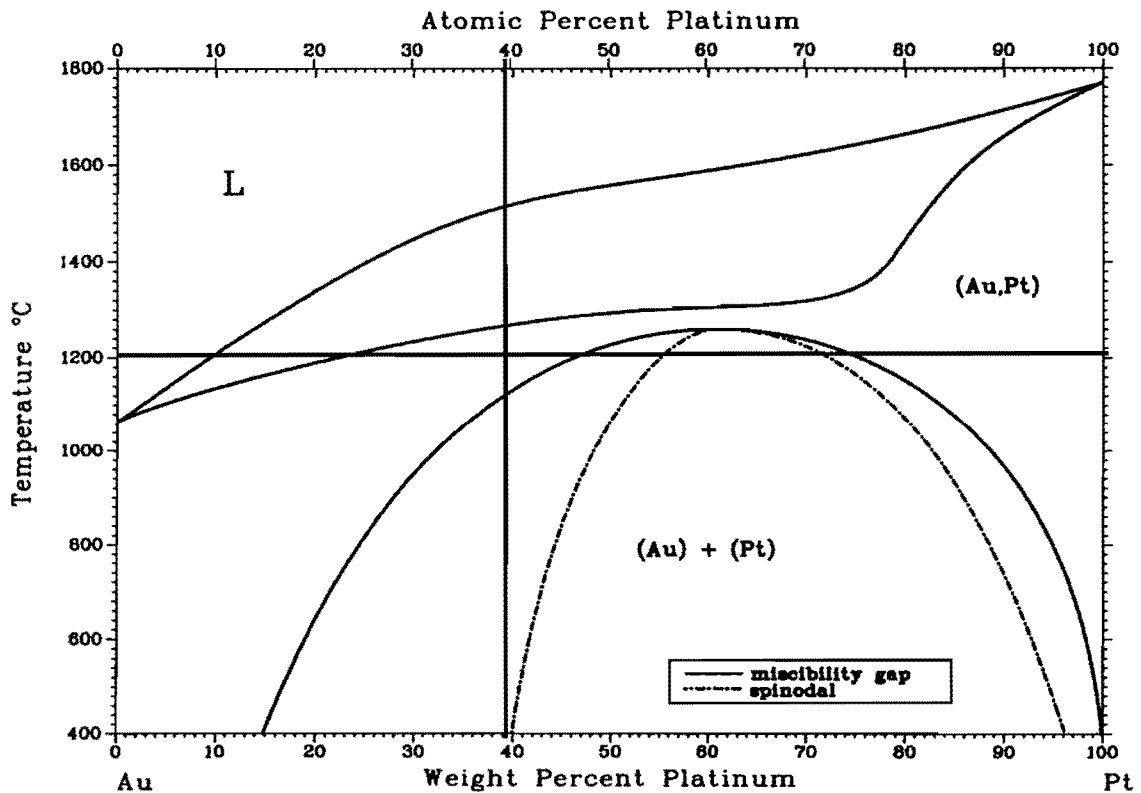


Figure 3.4. The 1200°C heat treatment of the 60Au-40Pt alloy (ASM Handbook, Volume 3: Alloy Phase Diagrams, 1992)

3.2.2.1. The 60Au-40Pt alloy heat treated at 1200°C for 24 hours

The X-ray diffraction patterns for the 1300°C and the 1200°C heat treated samples are shown in Figure 3.5. The 1300°C treated sample has two peaks, corresponding to the Au-rich and Pt-rich phases. Two peaks are observed because of the difference in lattice parameters of the two phases. Both phases are face-centered cubic (fcc). The 1200°C treated sample only has one peak, showing that the solutionising heat treatment was successful. The “prestik” peaks in Figure 3.5 are due to the sample holder that was used during XRD.

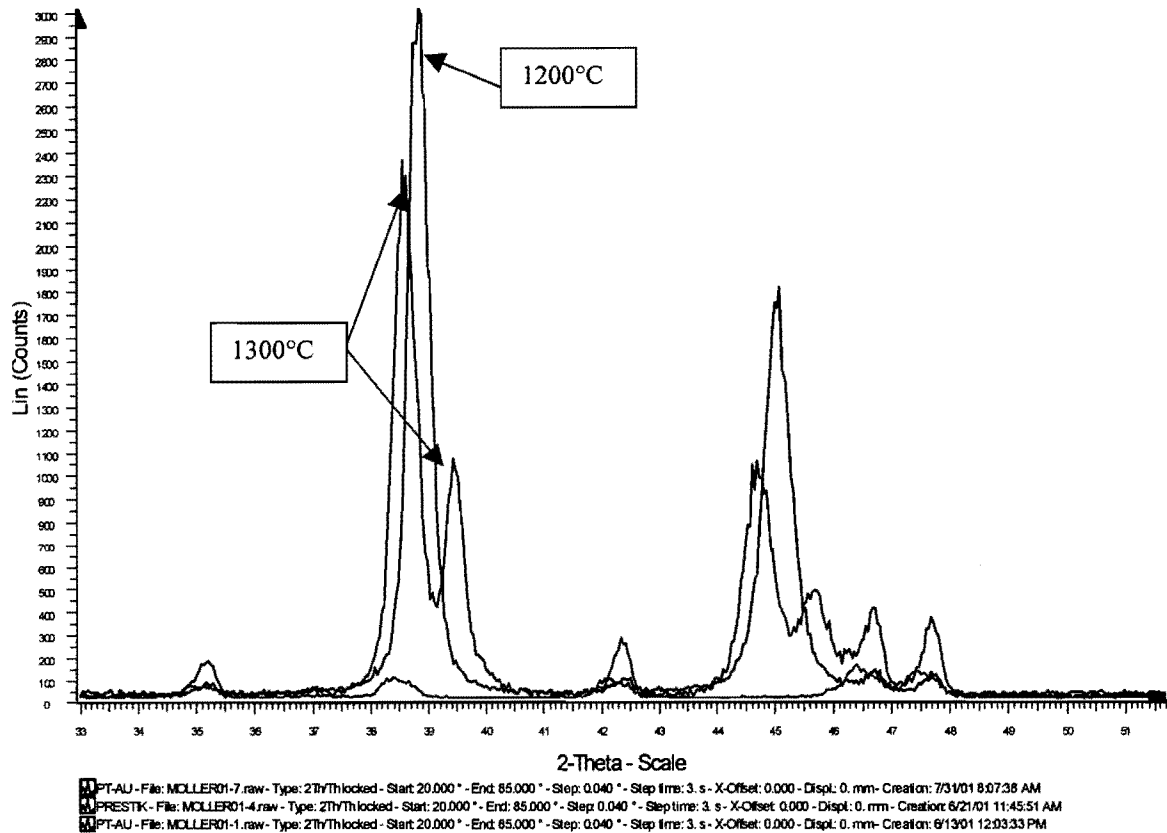


Figure 3.5. X-ray diffraction patterns of the samples heat treated at 1300°C and at 1200°C.

The microstructure of the 60Au-40Pt alloy after heat treatment at 1200°C for 24 hours is shown in Figure 3.6. The microstructure confirms that a single-phase solid solution was produced. However, it can be seen that porosity resulted during this heat treatment.

The porosity is not due to shrinkage during solidification, because at 1200°C no liquid is formed. It can, however, be explained by the Kirkendall effect.

Electrochemistry of gold-based alloys

By

Heinrich Möller

A dissertation submitted in partial fulfillment of the requirements for the degree of

Master of Engineering

in the Department of Materials Science and Metallurgical Engineering,
Faculty of Engineering, Built Environment and Information Technology,
University of Pretoria

2002

Electrochemistry of gold-based alloys

by

Heinrich Möller

Supervisor: Prof. P.C. Pistorius

Department of Materials Science and Metallurgical Engineering

Degree: Master of Engineering

ABSTRACT

The electro-oxidation of organic compounds at noble metal electrodes has been widely studied in the past. A bimetallic electrode is often more active than the respective pure metals. However, the effect of the microstructure of the alloys on their electrochemical properties has largely been ignored in the past.

The electro-oxidation of ethylene glycol at gold-platinum and gold-titanium electrodes in different heat treatment conditions was studied to determine how the different microstructures would influence the electrochemistry of these alloys.

Kirkendall porosity was produced by the solid solution heat treatment of the two-phased 60Au-40Pt electrodes. The extra surface area due to the porosity resulted in high apparent current densities at the porous electrodes in both acid and alkaline solutions without ethylene glycol. Only slightly higher apparent current densities were obtained at the porous gold-platinum electrodes compared to the non-porous electrodes when ethylene glycol was present in the solution. Kirkendall porosity was not produced by the solid solution heat treatment of the two-phased 50Au-50Pt electrodes.

The gold-platinum electrodes were more active for the electro-oxidation of ethylene glycol than both pure gold and platinum. The electrodes in the solid solution heat treatment condition were more active than the two-phased electrodes. This can be explained by the Third-body effect, which means that platinum atoms that are surrounded by gold atoms are less likely to become poisoned by intermediates than platinum atoms

that are surrounded by other platinum atoms. Poisoning of all the electrodes occurred during electrolysis of ethylene glycol at a fixed potential. The poisoning species at pure gold and pure platinum could be removed by potential pulsing and sustainable electrolysis of ethylene glycol was possible at these electrodes. Unfortunately, the same technique was not as successful with the gold-platinum alloys and their activities declined during the long-term electrolysis of ethylene glycol.

The electrochemical behaviour of the Gold 990 (Au-1wt% Ti) electrodes is similar to pure gold in acid and alkaline solutions. It is possible that the titanium content is too low to have a significant influence on the electrochemical behaviour of gold. The titanium may also be in the passive condition or it may have dissolved selectively from the Gold 990 alloy resulting in a pure gold surface.

Keywords: Gold, platinum, gold-platinum alloys, gold-titanium alloys, Gold 990, Kirkendall porosity, electrochemistry, electro-oxidation, ethylene glycol, cyclic voltammetry.

ACKNOWLEDGEMENTS

I would like to thank and herewith express my sincere appreciation to the following:

- Professor Chris Pistorius, my supervisor, for guidance and continuous support.
- Mintek for financial assistance.
- Doctor Elma van der Lingen and Stephen Roberts from Mintek for guidance and sample preparation.
- The Department of Materials Science and Metallurgical Engineering and IMMRI for facilities.
- Lida Roos, my fiancée, for her love, continuous support and patience.
- My father, mother, Robert, Danie and Johan for their prayers and support.
- The Roose: Lida's parents, Hannes and Marileen for their continuous support.
- Carel Coetzee for assistance with the SEM.
- Doctor Sabine Verryn of the Geology department for assistance with XRD.
- Sarah Havenga and Johann Borman for their assistance.
- My friend Heinrich Hutchison for his valuable contribution.
- The personnel and specially my fellow graduate students for their support and advice.
- The Lord, for the abilities He gave me and the opportunity to develop them.

CONTENTS

ABSTRACT.....	i
ACKNOWLEDGEMENTS.....	iii
CONTENTS.....	iv
CHAPTER 1: Introduction.....	1
CHAPTER 2: Theoretical background.....	2
2. Electrochemical behaviour of pure gold in aqueous media.....	2
2.1. Gold in acidic media.....	2
2.2. Gold in alkaline media.....	2
2.3. Premonolayer oxidation of gold.....	3
2.3.1. Premonolayer oxidation of gold in acid.....	4
2.3.2. Premonolayer oxidation of gold in base.....	6
2.4. The electro-oxidation of chemical compounds at gold electrodes in aqueous media..	6
2.4.1. Electro-oxidation by means of a submonolayer of adsorbed hydroxyl radicals....	8
2.5 Alloys of gold.....	8
2.5.1. Electrochemical behaviour of pure platinum.....	9
2.5.1.1. Mechanism of oxide formation.....	9
2.5.1.2. Electrochemical behaviour of platinum in alkaline solutions.....	11
2.5.1.3. Electrochemical behaviour of platinum in acid solutions.....	14
2.6 Gold-platinum alloys.....	15
2.6.1. Cold rolling of Au-Pt alloys.....	15
2.6.2. Precipitation in Au-Pt alloys.....	16
2.6.3. Electrochemical behaviour of Au-Pt alloys.....	17
2.6.3.1. Homogeneous alloys.....	17
2.6.3.2. Heterogeneous alloys.....	17
2.6.4. Electro-oxidation of chemical compounds at Au-Pt alloy electrodes	18
2.6.5. Possible explanations for synergism on Au-Pt alloys.....	18
2.6.5.1. The bifunctional theory.....	18

2.6.5.2. Changes in adsorption features.....	19
2.6.5.3. The Third-Body effect.....	20
2.6.5.4. The creation of surface Lewis acid sites on alloy electrodes.....	20
2.7. The 60Au-40Pt alloy electrode.....	21
2.8. The electro-oxidation of ethylene glycol at noble metal electrodes.....	22
2.8.1. The electro-oxidation of ethylene glycol at gold electrodes in acid.....	22
2.8.2. The electro-oxidation of ethylene glycol at gold electrodes in base.....	23
2.8.3. The electro-oxidation of ethylene glycol at platinum electrodes in acid.....	24
2.8.4. The electro-oxidation of ethylene glycol at platinum electrodes in base.....	25
2.8.5. The electro-oxidation of ethylene glycol at Au-Pt electrodes in base.....	27
2.9. The Au-1wt% Ti alloy (Gold 990)	28
2.9.1. Preparation of Gold 990.....	28
2.9.2. The electrochemical behaviour of pure titanium.....	29
2.10 Conclusions.....	32
CHAPTER 3: The heat treatment of Au-Pt alloys and the Gold 990 alloy.....	34
3.1. Introduction.....	34
3.2. The 60Au-40Pt alloy.....	34
3.2.1. The 60Au-40Pt alloy heat treated at 1300°C.....	34
3.2.2. The 60Au-40Pt alloy heat treated at 1200°C.....	37
3.2.2.1. The 60Au-40Pt alloy heat treated at 1200°C for 24 hours.....	38
3.2.2.2. Kirkendall porosity.....	40
3.2.2.3 The 60Au-40Pt alloy heat treated at 1200°C for 168 hours.....	41
3.2.3. The 60Au-40Pt alloy heat treated directly at 1200°C.....	42
3.2.4. The 60Au-40Pt miscibility gap heat treatments.....	44
3.2.4.1. The 60Au-40Pt alloy heat treated at 800°C for 50 hours.....	44
3.2.4.2. The 60Au-40Pt alloy heat treated at 600°C for 100 hours.....	47
3.3. The 50Au-50Pt alloy.....	49
3.3.1. The 50Au-50Pt alloy in the "ductile" condition.....	49
3.3.2 The 50Au-50Pt alloy in the solid solution condition.....	52

3.4. The Gold 990 alloy.....	53
3.4.1. The Gold 990 alloy in the solid solution condition.....	53
3.4.2. The Gold 990 alloy in the precipitation-hardened condition.....	54
3.5. Conclusions.....	55
CHAPTER 4: The electrochemical behaviour of gold-based alloys in acid solution without ethylene glycol.....	56
4.1. Introduction.....	56
4.2. Experimental.....	56
4.3. Results and discussion.....	57
4.3.1. Gold.....	57
4.3.2. Platinum.....	58
4.3.3. The 60Au-40Pt alloy.....	61
4.3.3.1. The 60Au-40Pt alloy in the 1300°C heat treatment condition.....	61
4.3.3.2. The 60Au-40Pt alloy in the 1200°C (24 hours) heat treatment condition.....	62
4.3.3.3. The 60Au-40Pt alloy in the 1200°C (168 hours) heat treatment condition.....	63
4.3.3.4. The 60Au-40Pt alloy in the 800°C heat treatment condition.....	67
4.3.3.5 The 60Au-40Pt alloy in the 600°C heat treatment condition.....	67
4.3.4. The 50Au-50Pt alloy.....	69
4.3.4.1 The 50Au-50Pt alloy in the "ductile" condition.....	69
4.3.4.2 The 50Au-50Pt alloy in the solid solution condition.....	70
4.3.5. The Gold 990 alloy.....	72
4.3.5.1. The Gold 990 alloy in the solid solution condition.....	72
4.3.5.2. The Gold 990 alloy in the precipitation-hardened condition.....	72
4.4. Conclusions.....	76
CHAPTER 5: The electrochemical behaviour of gold-based alloys in alkaline solution without ethylene glycol.....	77
5.1. Introduction.....	77
5.2. Experimental.....	77
5.3. Results and discussion.....	78

5.3.1. Gold.....	78
5.3.2. Platinum.....	79
5.3.3. The 60Au-40Pt alloy.....	81
5.3.3.1. The 60Au-40Pt alloy in the 1300°C heat treatment condition.....	81
5.3.3.2. The 60Au-40Pt alloy in the 1200°C (24 hours) heat treatment condition.....	82
5.3.3.3. The 60Au-40Pt alloy in the 1200°C (168 hours) heat treatment condition.....	83
5.3.3.4. The 60Au-40Pt alloy in the 800°C heat treatment condition.....	87
5.3.3.5 The 60Au-40Pt alloy in the 600°C heat treatment condition.....	88
5.3.4. The 50Au-50Pt alloy.....	89
5.3.4.1 The 50Au-50Pt alloy in the "ductile" condition.....	89
5.3.4.2 The 50Au-50Pt alloy in the solid solution condition.....	91
5.3.5. The Gold 990 alloy.....	94
5.3.5.1. The Gold 990 alloy in the solid solution condition.....	94
5.3.5.2. The Gold 990 alloy in the precipitation-hardened condition.....	94
5.4. Conclusions.....	96
CHAPTER 6: The electro-oxidation of ethylene glycol at gold-based alloys in an alkaline solution.....	98
6.1. Introduction.....	98
6.2. Experimental.....	98
6.3. Results and discussion.....	100
6.3.1. Gold.....	100
6.3.2. Platinum.....	102
6.3.3. The 60Au-40Pt alloy.....	106
6.3.3.1. The 60Au-40Pt alloy in the 1300°C heat treatment condition.....	106
6.3.3.2. The 60Au-40Pt alloy in the 1200°C (24 hours) heat treatment condition.....	108
6.3.3.3. The 60Au-40Pt alloy in the 1200°C (168 hours) heat treatment condition.....	111
6.3.3.4. The 60Au-40Pt alloy in the 800°C heat treatment condition.....	113
6.3.3.5 The 60Au-40Pt alloy in the 600°C heat treatment condition.....	116
6.3.4. The 50Au-50Pt alloy.....	118
6.3.4.1 The 50Au-50Pt alloy in the "ductile" condition.....	118

6.3.4.2 The 50Au-50Pt alloy in the solid solution condition.....	120
6.3.5. The Gold 990 alloy.....	122
6.3.5.1. The Gold 990 alloy in the solid solution condition.....	122
6.3.5.2. The Gold 990 alloy in the precipitation-hardened condition.....	124
6.3.6. Electrolysis of ethylene glycol at a fixed potential.....	128
6.3.6.1. Gold.....	129
6.3.6.2. Platinum.....	129
6.3.6.3. The 60Au-40Pt alloy in the 1300°C heat treatment condition.....	129
6.3.6.4. The 60Au-40Pt alloy in the 1200°C - 24 h heat treatment condition.....	130
6.3.6.5. The 50Au-50Pt alloy in the "ductile" heat treatment condition.....	130
6.3.6.6 The 50Au-50Pt alloy in the solid solution heat treatment condition.....	130
6.3.6.7. The Gold 990 alloy in the solid solution heat treatment condition.....	130
6.3.7. Electrolysis of ethylene glycol using potential pulsing.....	135
6.3.7.1. Gold.....	136
6.3.7.2. Platinum.....	140
6.3.7.3. The 60Au-40Pt alloy in the 1200°C - 24 h condition.....	143
6.3.7.4. The 50Au-50Pt alloy in the "ductile" condition.....	146
6.3.7.5 The 50Au-50Pt alloy in the solid solution condition.....	149
6.3.7.6. The Gold 990 alloy in the solid solution condition.....	152
6.4. Conclusions.....	158
CHAPTER 7: Conclusions and Recommendations.....	161
REFERENCES.....	164

Chapter 1

INTRODUCTION

The electro-oxidation of organic compounds at noble metal electrodes has been studied extensively for possible applications in electrochemical power sources (Parsons and VanderNoot, 1988) and electrochemical wastewater treatment (Comninellis, 1994). Gold is the noblest and most inert of all metals. It also possesses weak chemisorbing properties due to the absence of vacancies in its d-bands. Surprisingly, it still displays a wide range of electro-oxidation activity – especially in alkaline solutions (Burke and Nugent, 1998).

It is known that a bimetallic electrode is usually more active for the electro-oxidation of organics than the respective pure metals (Parsons and VanderNoot, 1988). The gold alloy containing 40% platinum has been identified (Stelmach et al., 1994) as being the most active for the oxidation of various organics in base. However, the effect of the microstructure of gold-platinum alloys on their electrochemical properties has largely been ignored in the past.

The Gold 990 alloy (Au-1wt% Ti) was developed originally for the jewellery industry (Gafner, 1989). The electrochemical properties of this alloy have not been investigated before. It is possible to heat treat Gold 990 to obtain two different heat treatment conditions: (a) with titanium in solid solution with the gold and (b) the precipitation-hardened condition, with small Au_4Ti precipitates.

This study has been subdivided into three main parts:

- In the first part, the heat treatments of the Au-Pt and the Au-Ti alloys are investigated. By employing different heat treatment temperatures and times, different microstructures are produced.
- In the second part, the electrochemical properties of the heat treated electrodes are studied in acid and alkaline solutions without an organic compound in the solution.
- In the third part, the electro-oxidation of ethylene glycol at Au-Pt and Gold 990 electrodes in different heat treatment conditions is investigated. Ethylene glycol was selected as a model organic compound due to the fact that its oxidation at noble metal electrodes has been studied extensively (Kadirgan et al., 1990; Hahn et al., 1987).

Chapter 2

THEORETICAL BACKGROUND

2. Electrochemical behaviour of pure gold in aqueous media

2.1. Gold in acidic media

A typical cyclic voltammogram recorded for a polycrystalline gold disc electrode in acid is shown in Figure 2.1 (Burke and Nugent, 1997). During the positive sweep, monolayer oxide (α -oxide) formation results in an increase in anodic current at 1.35 V versus the reversible hydrogen electrode (RHE). The charge associated with further monolayer oxidation for gold in acid tends to be distributed along a plateau with no major change until oxygen gas evolution commences at 2.0 V_{RHE} (not shown in Figure 2.1). During the negative sweep, the monolayer oxide reduction peak is observed at 1.1 V_{RHE} .

Birss and Xia (2001) formed α -oxide films at sputtered polycrystalline gold electrodes in 0.1 M H_2SO_4 solutions. The composition and properties of the film were established using potentiostatic, cyclic voltammetry, ellipsometric and in-situ mass measurement techniques. The α -oxide is proposed to be AuO at potentials below 1.5 V_{RHE} , and a mixture of AuO and Au_2O_3 above this, likely becoming primarily Au_2O_3 at still higher potentials. This is based on ellipsometric evidence and the measured mass to charge ratio of 8 g/mol electrons at all potentials.

2.2. Gold in alkaline media

Examples of cyclic voltammograms recorded for gold in base are shown in Figure 2.2 (Burke and Nugent, 1997). Monolayer oxide growth commences at 1.25 V_{RHE} . At more positive potentials, oxygen gas evolution occurs. Over the range of 1.6 to 2.0 V_{RHE} oxygen gas evolution is believed to be catalysed in a transient manner by some type of nascent hydrous gold oxide species formed at the monolayer oxide/aqueous solution interface (Burke and Nugent, 1997). Regular oxygen gas evolution on gold in base (as in acid) occurs only above 2.0 V_{RHE} .

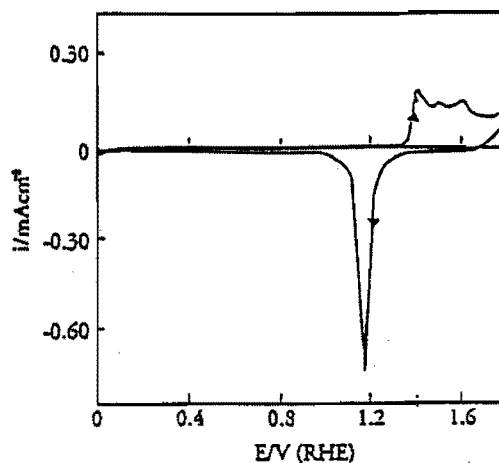


Figure 2.1. Typical cyclic voltammogram (0.0 to 1.80 V_{RHE} , 50mV/s, 25°C) recorded for a polycrystalline gold disc electrode in 1.0 mol/dm³ H_2SO_4 (Burke and Nugent, 1997).

An interesting feature of the negative sweep in Figure 2.2(b) is the appearance of a second cathodic peak at 0.85 V_{RHE} . The monolayer oxide reduction peak was observed in this case at 1.1 V_{RHE} and the subsequent peak is assumed to be due to the reduction of hydrous gold oxide species formed on the gold surface at the upper end of the cycle (Burke and Nugent, 1997).

2.3. Premonolayer oxidation of gold

Gold is frequently regarded as the ideal solid electrode system for fundamental investigations in electrochemistry. This is due to the fact that in the absence of redox active species in the aqueous phase, the system apparently exhibits only double layer (non-Faradaic) behaviour over the range of 0 to 1.3 V_{RHE} in acid and 0 to 1.2 V_{RHE} in base. However, there have been assertions that Faradaic behaviour due to the formation of oxy-species at the gold surface occurs within the double layer region. However, the extent of premonolayer oxidation (the coverage involved) is small. This makes it difficult to detect these species and the responses associated with them.

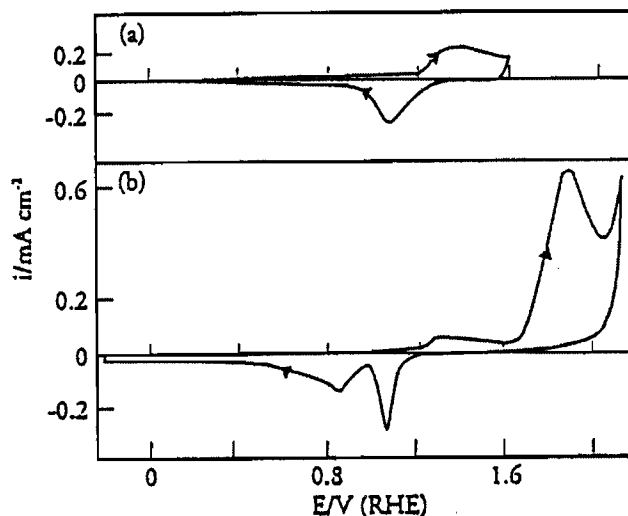


Figure 2.2. Typical cyclic voltammogram for a polycrystalline gold electrode in $1.0 \text{ mol/dm}^3 \text{ NaOH}$ at $25 \text{ }^\circ\text{C}$: (a) 0.0 to $1.60 \text{ V}_{\text{RHE}}$ at 50 mV/s ; (b) -0.2 to $2.1 \text{ V}_{\text{RHE}}$ at 10 mV/s (Burke and Nugent, 1997).

2.3.1. Premonolayer oxidation of gold in acid

Watanabe and Gerischer (1981) postulated on the basis of photoelectrochemical data that gold exhibited premonolayer oxidation extending over the potential range 0.85 to $1.35 \text{ V}_{\text{RHE}}$. They postulated that this incipient oxidation represented the formation of chemisorbed species (Au-OH and/or Au-O) with surface coverages up to 20%.

Hutton and Williams (1994), using Scanning Laser Microscopy, found that gold oxidised in the premonolayer region. They found that this incipient oxide was stable, only being removed by prolonged evolution of hydrogen gas.

Gordon and Johnson (1994) investigated gold electrodes in acid solution by means of an Electrochemical Quartz Crystal Microbalance (EQCM). They proposed that the species formed during premonolayer oxidation corresponded to adsorbed hydroxyl radicals, designated as AuOH . Figure 2.3(a) (Gordon and Johnson, 1994) shows a typical current-potential (I-E) curve obtained at a gold film electrode in 0.10 M HClO_4 . The very small anodic current observed during the positive potential scan in region A corresponds to charging of the electrical double layer. Region B during the positive scan corresponds to the premonolayer region and the slight increase in anodic current is concluded to result primarily from the formation of the submonolayer of hydrous oxide, designated as AuOH . The large wave in region C corresponds to the formation of the monolayer oxide. An electrochemical quartz crystal microbalance (EQCM) was

used to detect small surface mass changes during cyclic voltammetry. A decrease in frequency indicates an increase in mass. Figure 2.3(b) (Gordon and Johnson, 1994) shows the frequency-potential (f-E) curve recorded simultaneously with the I-E curve in Figure 2.3(a). During the positive scan there is no detectable change in frequency corresponding to double layer charging (region A). However, a rapid decrease in frequency (mass increase) by the amount Δf_B is observed in region B concomitantly with the formation of AuOH. Continuation of the positive scan through region C results in a further decrease in frequency by an amount Δf_C concomitantly with the formation of the monolayer oxide. Following scan reversal, the frequency remains constant until it increases very rapidly in the region corresponding to cathodic reduction of the monolayer oxide. Continuation of the negative scan back through the premonolayer region B results in further increase of frequency until the original value of f is attained in the double-layer region A.

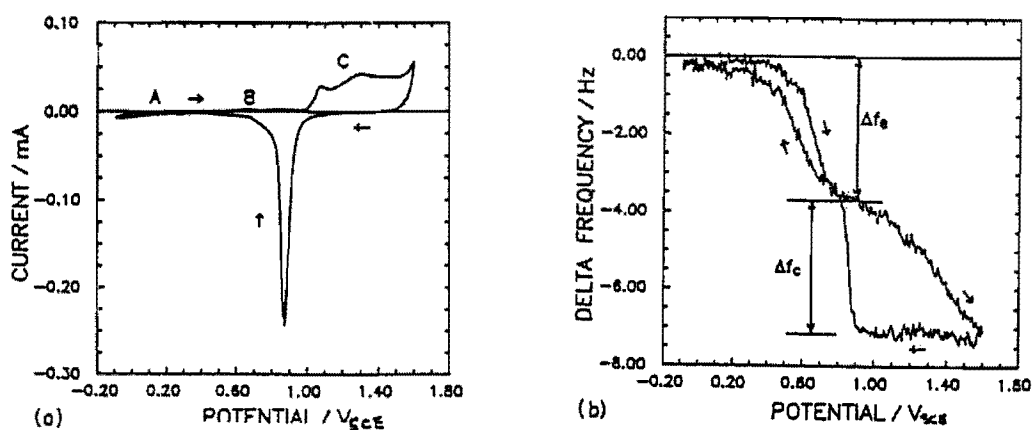


Figure 2.3. (a) Current-potential curve for Au EQCM film in 0.1 M HClO₄: scan rate 75 mV/s; no convective mixing. (b) Frequency-potential curve for Au EQCM film in 0.1 M HClO₄: scan rate 75 mV/s; no convective mixing. Obtained concomitant with I-E curve (Gordon and Johnson, 1994).

Gordon and Johnson (1994) proposed that the large values obtained for Δf_B and Δf_C in regions B and C respectively are the result of increased surface hydration as a consequence of the formation of AuOH (region B) and the monolayer oxide (region C). The magnitude of the increase was found to be independent of the nature of the acid. The mass increase in region B is consistent with an increase in surface hydration by about 32 H₂O molecules per AuOH site.

2.3.2. Premonolayer oxidation of gold in base

The electrochemical response due to premonolayer oxidation of gold in alkaline solutions tends to be of higher magnitude than in acid; the hydroxy species involved is more stable in solutions of high OH^- ion activity. Small peaks have been observed in the double layer region of cyclic voltammograms for gold in base (Burke and O'Leary, 1989).

Desilvestro and Weaver (1986) established, using Surface Enhanced Raman Spectroscopy (SERS), that the product of premonolayer oxidation was a hydroxy species, one that was of different character to the species involved in the regular monolayer oxidation reaction.

2.4. The electro-oxidation of chemical compounds at gold electrodes in aqueous media

Gold is the noblest and most inert of all metals. It is also a very weak chemisorber due to the absence of vacancies in its d-bands. It does, however, display a very wide range of electro-oxidation activity - especially in base (Vitt et al., 1990; Burke and Nugent, 1998).

Typical cyclic voltammograms for the electro-oxidation of formaldehyde, hydrazine, and ethylene glycol are shown in Figure 2.4 (Burke and Nugent, 1998). The following can be deduced from these cyclic voltammograms:

- i. The electro-oxidation of chemical compounds commences in the premonolayer region during the positive sweep. As soon as monolayer oxidation starts, oxidation of the compound is inhibited.
- ii. During the negative sweep, oxidation of the compound starts again as soon as the monolayer oxide has been reduced.
- iii. In general, chemical compounds are oxidised at gold before the formation of a surface oxide layer, while oxygen is evolved at a gold surface after the formation of the oxide layer.

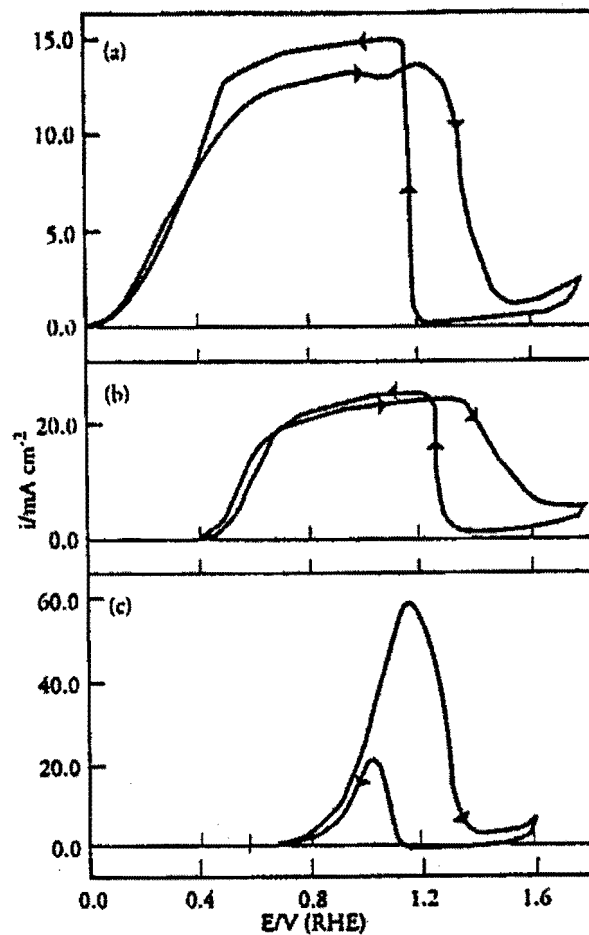


Figure 2.4. (a) Typical cyclic voltammogram (0 - 1.8 V, 5 mV/s) for a gold wire electrode in 1 mol/dm³ NaOH with HCHO, to a level of 0.1 mol/dm³, T = 25 °C; (b) Typical cyclic voltammogram (0 - 1.8 V, 50 mV/s) for a smooth gold electrode in N₂-stirred 1 mol/dm³ NaOH with N₂H₄, to a level of 0.1 mol/dm³, T = 25 °C; (c) Typical cyclic voltammogram (0 - 1.6 V, 50 mV/s) for a gold wire electrode in 1 mol/dm³ NaOH with 0.1 mol/dm³ ethylene glycol (CH₂OH)₂, T = 25 °C (Burke and Nugent, 1998).

2.4.1 Electro-oxidation by means of a submonolayer of adsorbed hydroxyl radicals

Electro-oxidation mechanisms have been proposed for oxidation at gold electrodes in acidic and alkaline solutions that involve adsorbed hydroxyl radicals (AuOH) (Vitt et al., 1990; Wen and Li, 1997). The adsorbed hydroxyl radicals are produced by means of the anodic discharge of H₂O in the premonolayer region (Vitt and Johnson, 1992).



The formation of the submonolayer of hydroxyl radicals is favoured in alkaline solutions, which explains the rather poor electro-oxidation properties of gold in acidic solutions. A mechanism has been proposed in which the adsorbed hydroxyl radicals participate in the oxygen-transfer step (Vitt et al., 1990). It has also been speculated that the AuOH species formed in the premonolayer region can assist in the adsorption of polar organic molecules. Oriented H₂O dipoles centred at catalytic AuOH sites may also influence the orientation of electro-active functional groups in reactants that must diffuse to these catalytic sites (Gordon and Johnson, 1994).

Vitt and co-workers (1990) proposed that adsorption is necessary for all compounds whose oxidation is accompanied by the transfer of oxygen via the electrode surface. A mechanism that involve three fundamental processes for the various adsorbed species has been devised for these anodic reactions:

- (1) oxygen transfer between the electrolyte and adsorbed hydroxyl radical (AuOH)
- (2) deprotonation and
- (3) electron transfer.

The mechanisms for various compounds seem to differ only in the order of these three reactions. For organic compounds (alcohols and aldehydes), deprotonation precedes electron transfer.

2.5. Alloys of gold

Noble metal alloys have been studied for the electro-oxidation of organic compounds, and some alloys display better activity than the pure metals. Most of the alloys that

have been studied are based on platinum (Parsons and VanderNoot, 1988; Stelmach et al., 1994).

2.5.1. Electrochemical behaviour of pure platinum

2.5.1.1. Mechanism of oxide formation

The early modelling of the initial stages of surface oxidation on platinum (Kozłowska et al., 1973) lead to the conclusion that two distinguishable and successive stages were involved:



followed by:



(potential range 1.1 to 1.4 V_{RHE}) also coupled with place-exchange, schematically represented by:



By using the electrochemical quartz-crystal nanobalance (EQCN) technique, Birss et al (1993) showed that the above two-step mechanism is inapplicable. The two-step mechanism would require a mass change of 17 g/mol electrons in step I and -1 g/mol electrons in step II. However, the anodic mass-response profile involves a continuous mass increase, contrary to the expectations according to mechanism I, II. It actually corresponds to the first stage (to 1.1 V_{RHE}) of oxide film development being formed as Pt/O, first to half-coverage by O-species up to 1.1 V_{RHE} . This is followed by completion of coverage by O-species up to 1.4 V_{RHE} coupled with place exchange between O and Pt (step III).

Thus, platinum surface oxide formation is believed to preferably involve discharge of water molecules directly forming 'PtO' species, process IV:



where the H_2O reagent is initially present at a platinum site in the inner region of the double-layer, i.e. residing at the metal surface. As the electrosorption of O species in process IV progresses, water molecules consumed in (IV) are replaced from the double-layer and appear on the surface of the developing oxide film, probably H-bonded to it.

The mechanism of platinum oxide formation is shown schematically in Figure 3.1 (Zolfaghari et al., 2002). The above mechanism has to include the anticipated participation of adsorbed H₂O molecules which, initially, are presumed to fully cover Pt sites (Fig. 2.5a). It is believed that the H₂O molecules are bridge-coordinated to two adjacent Pt atoms. The second step in the diagram (Fig. 2.5b) shows half coverage by O at 1.1 V_{RHE}. The third step in the diagram (Fig. 2.5c and 2.5d) illustrates how a nominally complete O monolayer on platinum eventually becomes developed through place-exchange between O and Pt over the two outer layers of the original platinum structure.

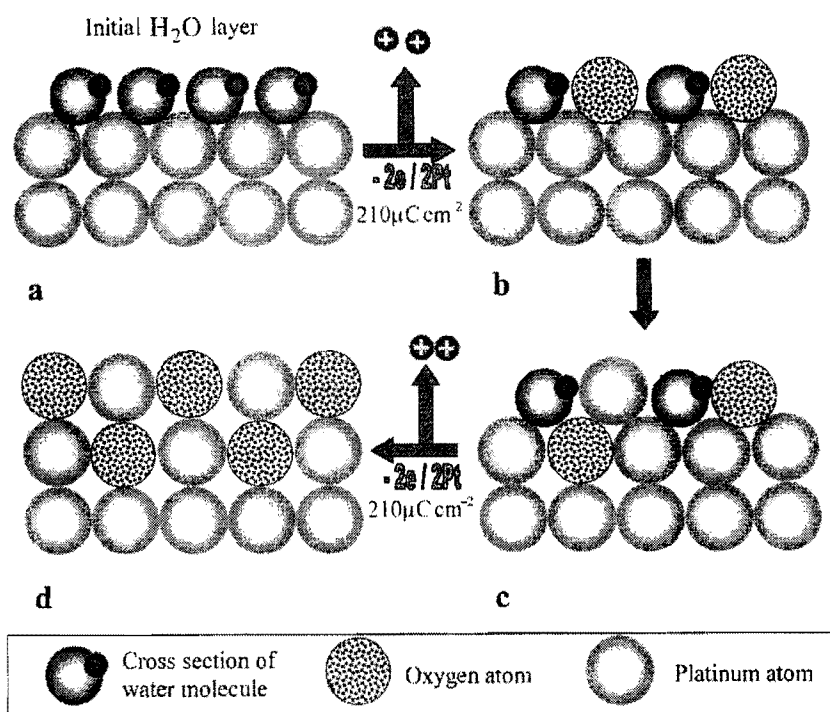


Figure 2.5. Cross-section of (a) initial water layer; (b) adsorbed O and H₂O; (c) adsorbed H₂O and place-exchanged O; (d) surface oxide (Zolfaghari et al., 2002).

A similar model of initial, two-electron oxidation of the platinum surface has also been proposed by Harrington and co-workers (1997) in their simulation of ac voltammetry behaviour over the region of Pt oxide-film formation. It was found that the shape of the ac voltammograms does not change much with frequency, suggesting a single time constant for oxide growth. No features were seen in the early stages of growth that can be assigned to the fast OH electrosorption, suggested previously to be the first step in oxide growth.

It was also suggested that although this mechanism is ruled out, some types of fast OH adsorption are still possible. Adsorption without charge transfer could be occurring. If OH electrosorption occurs in parallel with the slow oxide growth process, it might not be detectable by ac impedance. The admittances of the two processes would then be additive and a small admittance for OH electrosorption might contribute little to the total.

2.5.1.2. Electrochemical behaviour of platinum in alkaline solutions

Figure 2.6 (solid line) (Xia and Birss, 2000) shows a typical cyclic voltammogram of a Pt-coated quartz crystal in 0.1 M NaOH, as well as the associated frequency change (dashed line, inverse of mass change), measured during an oxidation/reduction scan between 0 and 1.6 V_{RHE} . In this range of potential the compact α -oxide film is formed (at ca. 0.6 V_{RHE}) and reduced, in peak C₁. The adsorption/desorption of a monolayer of hydrogen atoms is seen between 0.1 V and 0.4 V_{RHE} .

In Figure 2.6, a mass increase is seen, as expected, during Pt oxide formation, while oxide reduction is accompanied by an equivalent mass loss. From the integrated charge density during oxide reduction and the associated change in mass over the potential range of the cathodic peak, a ratio of 8.3g/mol e^- passed is obtained. A ratio of 8 g/mol electrons would be predicted for the formation of an anhydrous Pt oxide film, either PtO or PtO₂.

In the potential range of the hydrogen adsorption-desorption reaction it can be seen that as the potential is made more negative and hydrogen begins to adsorb, the electrode mass decreases, rather than increases, and vice versa during the positive scan. When hydrogen evolution commences in the negative scan, i.e. at 0.1 V_{RHE} , the frequency drops somewhat and then increases again in the positive scan. It is likely that the mass change between 0.15 and 0.4 V is due to the desorption of OH⁻ in the cathodic scan and its readsorption during the positive scan. The results of Figure 2.6 suggest that, during hydrogen atom adsorption on Pt (0.4-0.15 V_{RHE}), adsorbed hydroxide is concurrently being desorbed, then readsorbing again in the anodic sweep.

QCMB experiments involving α -oxide growth in 0.1 M NaOH with time at constant potentials were carried out by Xia and Birss (2000). Figure 2.7(a, b) (Xia and Birss, 2000) show both the oxide reduction charge density (per apparent area) and its g/mol e^-

ratio as a function of anodising time at two potentials: 1.3 and 1.6 V_{RHE} respectively. In both cases, the oxide reduction charge increases logarithmically with anodising time, reaching a near steady-state value after ca. 6 min (Fig. 2.7a) and 4 min (Fig. 2.8b).

Figure 2.7a shows that the mass to charge ratio for the oxide formed after very short times of anodising at 1.3 V_{RHE} is almost 9 g/mol electrons. While a ratio of 8 is expected for either PtO or PtO₂, this slightly higher value may indicate that the initial layer may have included some adsorbed OH⁻, or the formation of a small amount of PtOH or Pt(OH)₂ (expected ratio for both is 17g/mol e⁻). After 1 min of anodising at either 1.3 or 1.6 V, Figure 2.7(a,b) show similar ratios for the oxide film of 7.9 to 8.1 g/mol e⁻, the expected values for PtO or PtO₂. Unfortunately, the form of Pt oxide cannot be distinguished from the QCMB data.

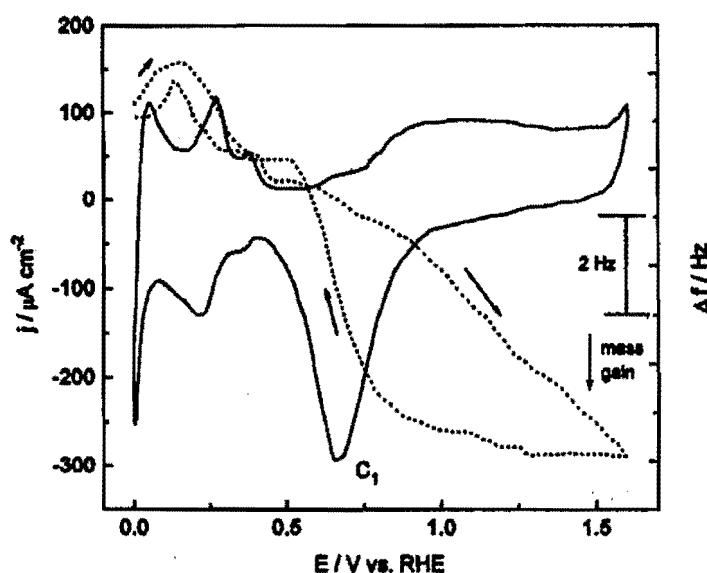


Figure 2.6. Cyclic voltammogram (solid line) and associated frequency change (dotted line) of a Pt-coated quartz crystal in 0.1 M NaOH between 0 and 1.6 V_{RHE} at 50mV/s (Xia and Birss, 2000).

Figure 2.8 (Xia and Birss, 2000) shows a plot of both the oxide reduction charge and the g/mol e⁻ ratios, monitored after 5 min at each of the anodising potentials between 1.2 and 1.9 V_{RHE} . The plot of the reduction charges appears to have two apparently linear segments, one for potentials less than 1.6 V, and one for potentials above this.

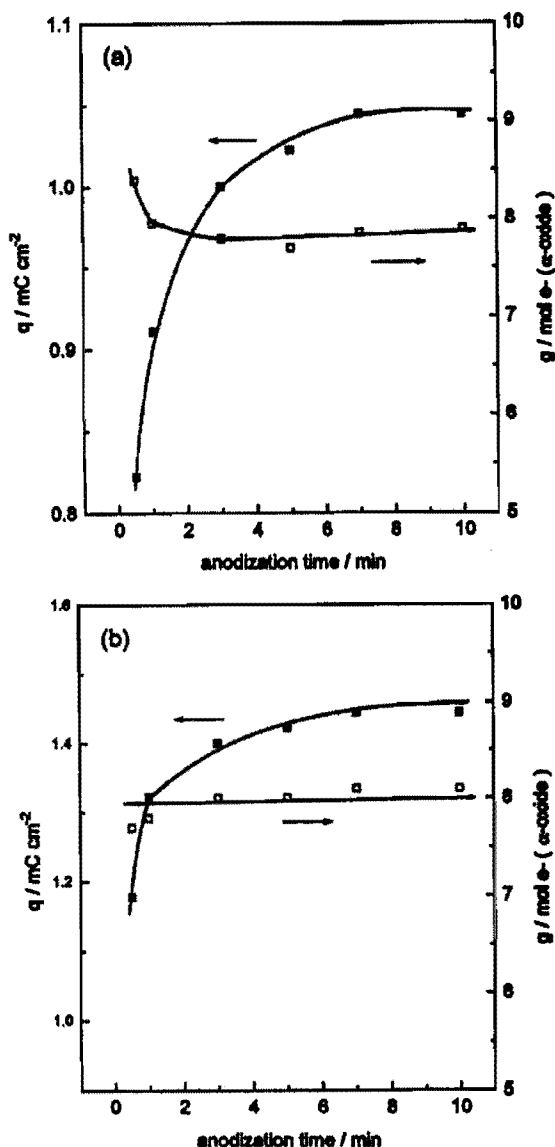


Figure 2.7: α -oxide reduction charge density (solid symbols) at 10 mV/s and its g/mol e^- ratio (open symbols) as a function of anodisation time of Pt-coated quartz crystal at (a) 1.3 V_{RHE} and (b) 1.6 V_{RHE} in 0.1 M NaOH (Xia and Birss, 2000).

Ellipsometric data (Xia and Birss, 2000) also indicates that the platinum oxide films, formed using potentials below 1.6 V_{RHE} , have different optical properties from those formed at potentials above 1.6 V_{RHE} . However, for all upper potential limits, except 1.2 V_{RHE} , the g/mol e^- ratio remains 8. These results has been interpreted as indicating that the oxide formed over the range 1.3 to 1.6 V_{RHE} is PtO, then changing to PtO₂ when the applied potential becomes higher than 1.6 V_{RHE} .

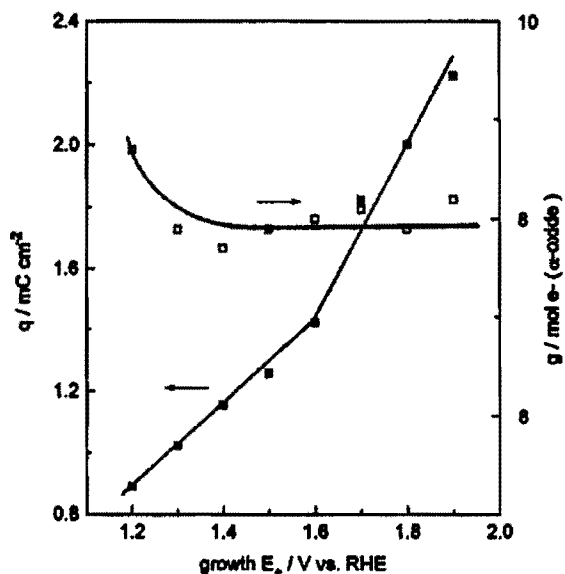


Figure 2.8. α -oxide reduction charge density (solid symbols) at 10 mV/s and its g/mol e^- ratio (open symbols) as a function of applied potential, after 5 minutes of anodisation of Pt-coated quartz crystal in 0.1 M NaOH (Xia and Birss, 2000).

2.5.1.3. Electrochemical behaviour of platinum in acid solutions

Figure 2.9 (solid curve) (Birss et al., 1993) shows a typical cyclic voltammogram of a Pt-coated quartz crystal in 0.1 M H_2SO_4 , as well as the associated mass changes (broken curve) measured during the experiment. A mass increase is seen, as expected, during Pt-oxide formation, while oxide reduction is marked by mass loss. From the integrated charge density during α -oxide reduction and the associated change in frequency over the potential range of the cathodic peak, a ratio of ca. 8 g/mol of electrons passed is obtained. This is similar to what was found for the oxide formed in alkaline solutions and suggests again that the α -oxide is anhydrous in nature (either PtO or PtO₂). However, ellipsometric data indicates that the platinum oxide film formed potentiostatically and by multicycling in 0.1 M H_2SO_4 has different optical properties than either of the two α -oxide films formed in base.

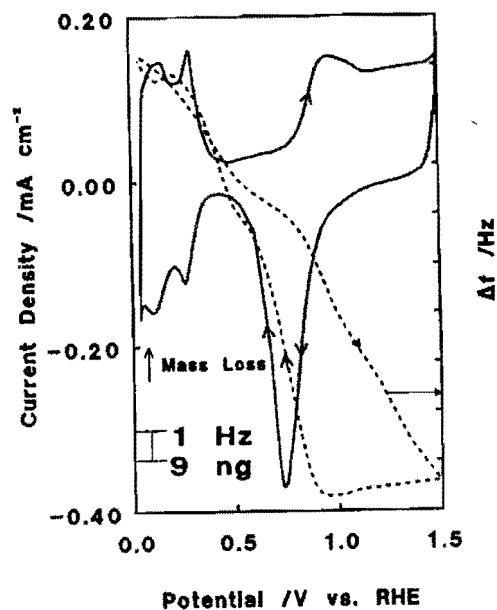


Figure 2.9. Cyclic voltammogram (solid line) and associated frequency change (dotted line) of a Pt coated quartz crystal in 0.1 M H₂SO₄; scanning rate 50 mV/s (Birss et al., 1993)

2.6. Gold-platinum alloys

The gold-platinum system has a miscibility gap (Figure 2.10) in the solid solution field (ASM Handbook, Volume 3: Alloy Phase Diagrams, 1992). The Pt-rich phase is frequently denoted as the α_1 phase and the Au-rich phase as α_2 .

There was interest in gold-platinum alloys during the 1950's and 1960's when they were used as spinning jets in the viscose rayon process (Darling, 1962).

2.6.1. Cold rolling of Au-Pt alloys

The whole range of alloys can be cold worked after quenching from temperatures not higher than 1000°C. The most ductile material is achieved by annealing at 1000°C, after which the temperature can be slowly dropped before water-quenching from 850°C (Darling, 1962).

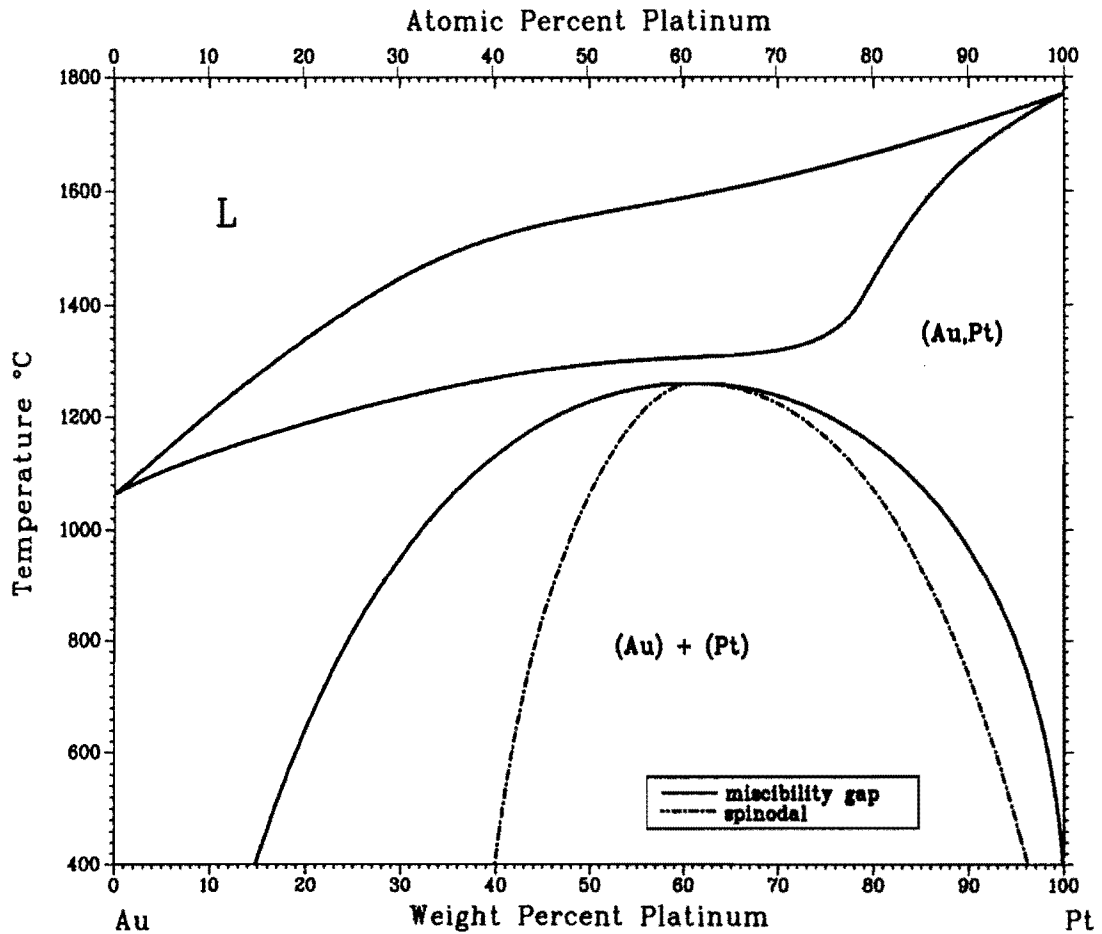


Figure 2.10. The Au-Pt phase diagram (ASM Handbook, Volume 3: Alloy Phase Diagrams, 1992)

2.6.2. Precipitation in Au-Pt alloys

The rate of precipitation depends upon the curvature of the free energy composition curves. The spinodal (Figure 2.10), being the locus of the inflexion points of the isothermal free energy composition curves, forms a lower limit of metastable equilibrium. Between the spinodal and the two-phase field exists a thermodynamic potential barrier that must be overcome before nucleation can occur, with the result that precipitation is retarded in this area (Darling, 1962).

2.6.3. Electrochemical behaviour of Au-Pt alloys

2.6.3.1. Homogeneous alloys

Woods (1971) studied the surface composition of Pt-Au alloys quenched from the region of continuous solid solution. Even though x-ray diffraction indicated that the alloys were homogeneous, the alloy electrodes gave current-potential curves (1 M H_2SO_4) that were equivalent to the sum of a pure platinum and a pure gold surface (Figure 2.11 (Woods, 1971)). It was suggested that this result can be explained if either:

1. Platinum and gold atoms in a homogeneous alloy have hydrogen and oxygen electroadsorption properties equal to that of platinum and gold atoms in the pure metals or
2. The surface of platinum/gold alloys always consists of the equilibrium phases even though the bulk is homogeneous.

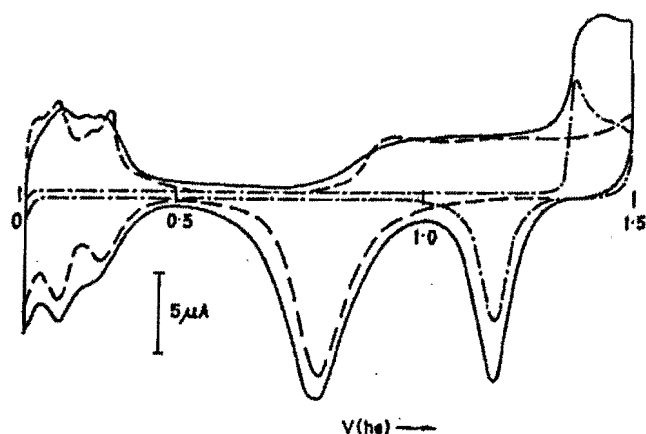


Figure 2.11. Current-potential curves showing hydrogen and oxygen adsorption in 1 M H_2SO_4 for a linear potential sweep of 40 mV/s. (----) Pt; (-.-.-) Au and (—) homogeneous 65%Pt-35%Au alloy (Woods, 1971).

2.6.3.2. Heterogeneous alloys

Breiter (1965) studied the anodic formation and cathodic reduction of oxygen layers on Au-Pt alloys in acid solutions. Platinum-gold alloys with gold contents ranging from 5 to 70 at% were studied. The alloys had to be annealed at 875°C before wires of 0.3 mm

diameter could be drawn. Heterogeneous (two-phased) Au-Pt alloys were produced with this heat treatment (Fig. 2.10). Current-potential curves were measured in 1 N H₂SO₄ at a sweep rate of 30 mV/s. The current-potential curves of the 20, 40 and 60at% Au alloys are shown in Figure 2.12 (Breiter, 1965). The most notable feature of Figure 2.12 is the fact that the alloys have two reduction waves. The first wave between 1.4 and 1.0 V_{SHE} is attributed to the reduction of the oxygen layer on “gold” and the second one between 1.0 V and 0.6 V_{SHE} to that of the layer on “platinum”. “Gold” is designated as being either gold atoms or the gold-rich phase of the heterogeneous alloys, while “platinum” is designated as being either platinum atoms or the platinum-rich phase of the alloys. The first reduction wave increased in height with increasing gold content while the second decreased (Fig. 2.12). The peaks of the two reduction waves appeared at slightly less anodic potentials on the alloys than on the respective pure metals. This indicates that the reduction of the oxygen layer on the two phases occurs with slightly larger hindrance than on the pure metals.

2.6.4. Electro-oxidation of chemical compounds at Au-Pt alloy electrodes

In alkaline media, the electro-oxidation activity of Au-Pt alloy electrodes is enhanced when compared with the respective metals (Stelmach et al., 1994; Beden et al., 1982). There are a few possible explanations for this synergistic effect of gold-platinum alloys.

2.6.5. Possible explanations for synergism on Au-Pt alloys

2.6.5.1. The bifunctional theory

The idea is that surface gold atoms adsorb oxygen-containing species, while surface platinum atoms adsorb the organic compound. The two different species interact leading to a final product. The two sites together give the complete reaction unit (Parsons and VanderNoot, 1988).

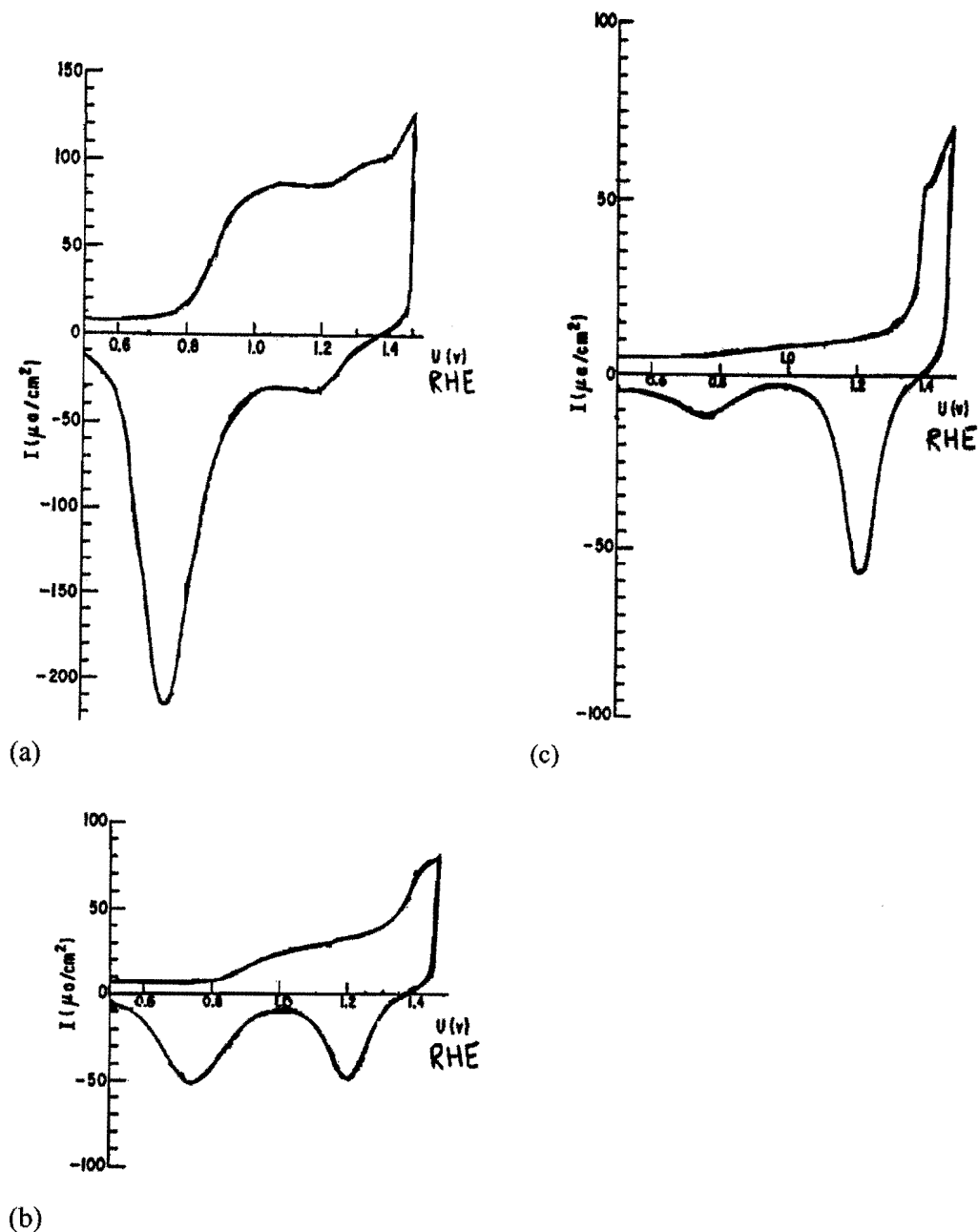


Figure 2.12. Current-potential curves for heterogeneous Au-Pt alloys containing (a) 20%, (b) 40% and (c) 60% Au in 1 N H_2SO_4 . Sweep rate 30 mV/s (Breiter, 1965).

2.6.5.2. Changes in adsorption features

Stelmach and co-workers (1994) found an increased rate of electro-oxidation of formaldehyde at alloy electrodes in comparison with the respective pure metals. They proposed that the energy of adsorption for the various forms of the substrate molecule is decreased sufficiently in order to facilitate further oxidative desorption of

intermediates and to suppress the adsorption of strongly bound intermediates. The adsorptivity of the surface remains high enough to support electro-oxidation.

2.6.5.3. The Third-Body effect

The formation of poisonous species adsorbed on more than one surface site is suppressed. For the electro-oxidation of formic acid, it was found that a platinum atom that is surrounded by gold atoms has the highest activity. A single platinum atom cannot be “poisoned” by the strongly bound intermediate since it needs adsorption sites that are only available on larger platinum clusters (Rach and Heitbaum, 1987).

2.6.5.4. The creation of Lewis acid surface sites on alloy electrodes

It is thought that the introduction of an alloying element that has a d-orbital occupancy less than that of the matrix will result in surface states at the alloy that function as Lewis acid sites. Furthermore, it is speculated that these surface sites enable adsorption of reactant species that are Lewis bases because of the existence of non-bonded electron pairs in these compounds e.g. the O-atoms in hydroxyl moieties of alcohols and carbohydrates, and N-atoms in amino acids (Mho and Johnson, 2001). This speculation is supported by successful modelling of the variations in the half-wave potential of the anodic voltammetric wave for dimethyl sulfoxide at β -PbO₂ film electrodes as a function of the variation in the level of doping by Bi (Popovic et al., 1998). The electrocatalytic benefit of reactant adsorption is explained on the basis of increase in residence time for the reactant species within the applied electric field at the electrode/solution interface.

Mho and Johnson (2001) studied the electrocatalytic response of carbohydrates at Cu-Mn alloy electrodes. The occupancy of the outermost d-orbital is lower for Mn (3d⁵) than that of Cu (3d¹⁰). The alloy composition of Cu:Mn = 95:5 was chosen to correspond to a homogeneous solid solution. The voltammetric responses observed for carbohydrates in 0.10 M NaOH were significantly larger at the preanodised CuMn electrodes as compared to preanodised pure Cu electrodes. It is speculated that the observed electrocatalytic effect comes as a beneficial consequence of the preadsorption of the carbohydrates at Mn sites (Lewis acid) in the preanodised CuMn surface.

Lewis acid surface sites will also be formed at gold-platinum alloys. The electron configuration of gold is $[\text{Xe}]4f^{14}5d^{10}6s^1$ and the electron configuration for platinum is $[\text{Xe}]4f^{14}5d^96s^1$.

2.7. The 60Au-40Pt alloy electrode

The Au-Pt alloy containing 60wt% Au has been identified previously (Stelmach et al., 1994) as the most active for the oxidation of aliphatic alcohols (Beltowska-Brzezinska, 1979), ethylene glycol (Eggert (Stelmach, 1994)) and formaldehyde (Beltowska-Brzezinska and Heitbaum, 1985) in alkaline media.

However, from the Au-Pt phase diagram (Fig. 2.10), it can be seen that different heat treatment temperatures can be used to produce different amounts of the α_1 and α_2 phases. The compositions of the two phases can also be changed by employing different heat treatment temperatures.

For the 60Au-40Pt alloy, annealing at 1100-1260°C will produce a homogeneous solid solution. Heat treatments at temperatures lower than 1100°C will produce a heterogeneous two-phased microstructure (Fig. 2.10). The different weight fractions of α_1 and α_2 , and their composition as a function of heat treatment temperature are shown in Table 2.1 for the 60Au-40Pt alloy. The lever rule was applied in order to calculate the various weight fractions.

Table 2.1: Equilibrium weight fractions and composition of phases in a 60wt% Au-40wt% Pt alloy as functions of temperature.

Temp. (°C)	Weight fraction of α_1	Composition of α_1		Weight fraction α_2	Composition of α_2	
		Wt%	Wt%		Wt%	Wt%
		Au	Pt		Au	Pt
1000	0.13	12	88	0.87	68	32
800	0.21	5	95	0.79	75	25
600	0.26	2	98	0.74	81	19
400	0.30	0	100	0.70	85	15

It will be interesting to study the electrochemical behaviour of the 60Au-40Pt alloy in different heat treatment conditions. The electro-oxidation of an organic compound, such as ethylene glycol, can be used to determine the effect of microstructure on the electrochemical properties of the alloy.

2.8. The electro-oxidation of ethylene glycol at noble metal electrodes

Ethylene glycol, $(\text{CH}_2\text{OH})_2$, is a non-toxic diol-alcohol. It has the advantage of involving a large number of electrons per molecule in its oxidation (the oxidation reaction needs 8 electrons per molecule when the final product is oxalate (Hauffe and Heitbaum, 1978)). The electro-oxidation of ethylene glycol at noble metal electrodes has been studied extensively, due to the interest of using it as a fuel for alcohol fuel cells (Christensen and Hamnett, 1989; Kadirgan et al., 1990; Beden et al., 1982, Hahn et al., 1987).

2.8.1. The electro-oxidation of ethylene glycol at gold electrodes in acid

The cyclic voltammogram for the electro-oxidation of ethylene glycol at a gold electrode in acid is shown in Figure 2.13 (Beden et al., 1987). It can clearly be seen from Figure 2.13 that nearly no oxidation of ethylene glycol occurs at gold in acid.

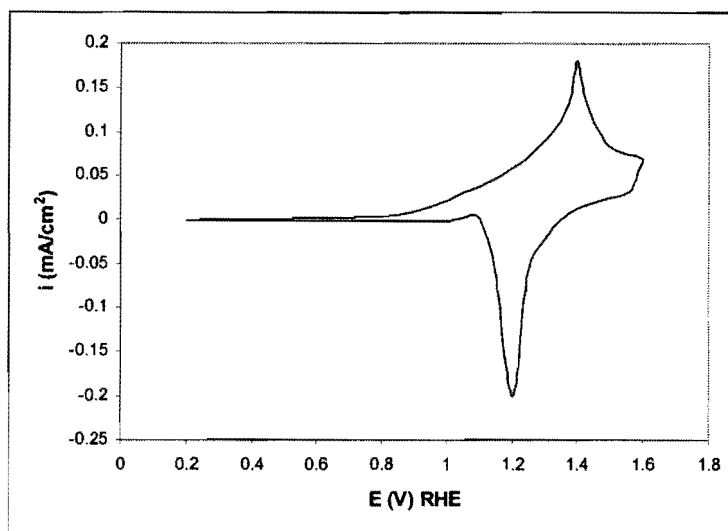


Figure 2.13. Oxidation of ethylene glycol at a gold electrode in acid medium. Conditions: 0.1 M HClO_4 , 0.1 M ethylene glycol, 25°C, 50 mV/s (After Beden et al., 1987).

2.8.2. The electro-oxidation of ethylene glycol at gold electrodes in base

A cyclic voltammogram for the electro-oxidation of ethylene glycol at a gold electrode in base is shown in Figure 2.14, together with the voltammogram of gold in the supporting electrolyte alone (Kadirgan et al., 1990). Ethylene glycol oxidation starts at $0.8 V_{\text{RHE}}$ during the positive sweep, giving a peak of 12 mA/cm^2 at approximately $1.2 V_{\text{RHE}}$ (peak A). The electro-oxidation of ethylene glycol is inhibited by the formation of the surface oxide on the gold electrode. During the negative sweep, oxidation of ethylene glycol commences only after the surface gold oxide has been reduced, reaching a current maximum of about 4 mA/cm^2 at $1 V_{\text{RHE}}$ (peak B). The positive and negative potential scans are almost superimposed in the potential range from 0.8 to $1 V_{\text{RHE}}$. Hauffe and Heitbaum (1978) found that the peak currents (peaks A and B) are somewhat smaller when the solution is stirred with argon gas. This can be explained by an accelerated transportation of intermediates into the solution.

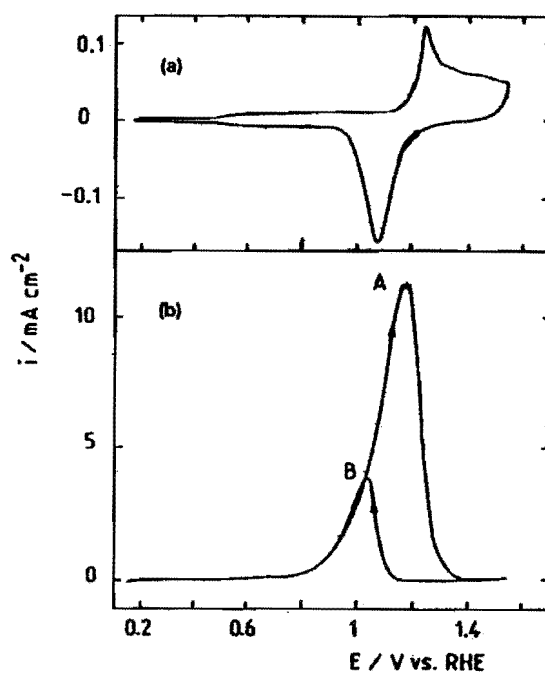


Figure 2.14. Cyclic voltammograms of a gold bead electrode (0.1 M NaOH , 25°C , 50 mV/s). (a) Without ethylene glycol; (b) with 0.1 M ethylene glycol (Kadirgan et al., 1990).

It is not possible to sustain long electrolysis of ethylene glycol at a fixed potential, because of poisoning phenomena that occurs at the electrode surface (Kadirgan et al., 1990). A cleaning procedure has to be used for sustainable electrolysis. The simplest technique is to use potential programs with potential plateaux separated repeatedly by a single cleaning potential sweep. The electrode surface and the poisons are oxidised at the upper potential limit. The surface oxides are reduced at the lower potential limit, before returning to the potential plateaux. The major product of electrolysis at 1.13 V_{RHE} is glycolate. Small quantities of oxalate, carbonate and formate are also formed (Kadirgan et al., 1990).

Kadirgan and co-workers (1990) used electromodulated infrared reflectance spectroscopy (EMIRS) to check for the presence of adsorbed CO-type poisons. These CO poisons would be formed by the rupture of the C-C bond during chemisorption at negative potentials. It was found the CO band is not present initially and that it grows during spectral accumulation performed to improve signal to noise ratio. However, the CO band is far from being the main infrared band observed. This implies that ethylene glycol does not dissociate immediately on gold at low potentials and that the CO poisoning species are formed only progressively. Glycolaldehyde and glyoxalate were found to be the main adsorbed species.

2.8.3. The electro-oxidation of ethylene glycol at platinum electrodes in acid

A cyclic voltammogram for the electro-oxidation of 0.1 M ethylene glycol in 0.1 M $HClO_4$ is shown in Figure 2.15 (Hahn et al., 1987). Several peaks and shoulders, labelled A to D are found.

Inhibition of hydrogen adsorption in the hydrogen region occurs due to adsorption of ethylene glycol. Electrochemically Modulated Infrared Reflectance Spectroscopy (EMIRS) was used by Hahn et al (1987) to study the adsorption of ethylene glycol. It was found that the adsorption is dissociative, leading to the formation of a poisoning linearly bonded CO species. Oxidation of the CO starts at 0.6 V_{RHE} , at the same potential where the overall oxidation process of ethylene glycol begins (Fig. 2.15).

By using in situ FTIR spectroscopy, Christensen and Hamnett (1989) identified the main products of ethylene glycol oxidation in acid as glycolic acid and CO_2 .

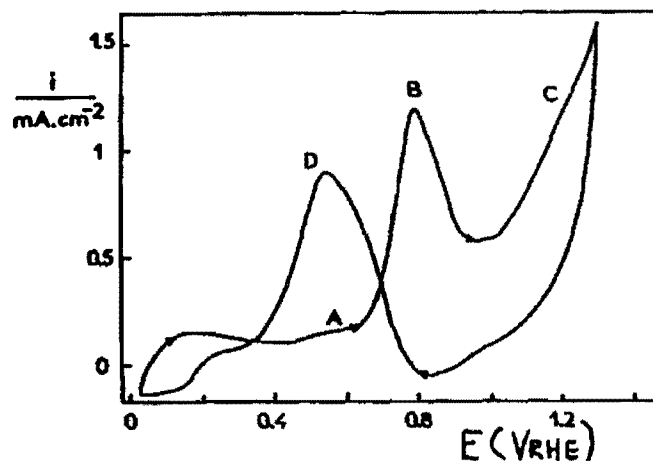


Figure 2.15. Cyclic voltammogram for the oxidation of 0.1 M ethylene glycol in 0.1 M HClO_4 , on platinum. Conditions: 100 mV/s, 25°C (Hahn et al., 1987).

2.8.4. The electro-oxidation of ethylene glycol at platinum electrodes in base

Cyclic voltammograms of a platinum electrode in 1 M NaOH in the absence and in the presence of 0.1 M ethylene glycol are shown in Figure 2.16 (Kadirgan et al., 1983). Ethylene glycol oxidation begins at 0.35 V_{RHE} during the positive sweep, giving a steep rise A at 0.65 V_{RHE} , then a peak B of 6.6 mA/cm^2 at 0.73 V_{RHE} and a small peak C at 1.05 V_{RHE} . The decrease of current after peak B is related to the formation of surface oxides on the platinum electrode. Ethylene glycol oxidation takes place during the negative sweep after the reduction of the surface oxides, reaching a maximum rate of 2 mA/cm^2 at 0.63 V_{RHE} (peak D). The current densities obtained in alkaline solution are much higher than in acid solution (Figure 2.15). The oxidation process also appears to be less irreversible in alkaline than in acid medium, in which the main oxidation peaks of ethylene glycol are separated by more than 250 mV during the positive and negative sweeps (Fig. 2.15).

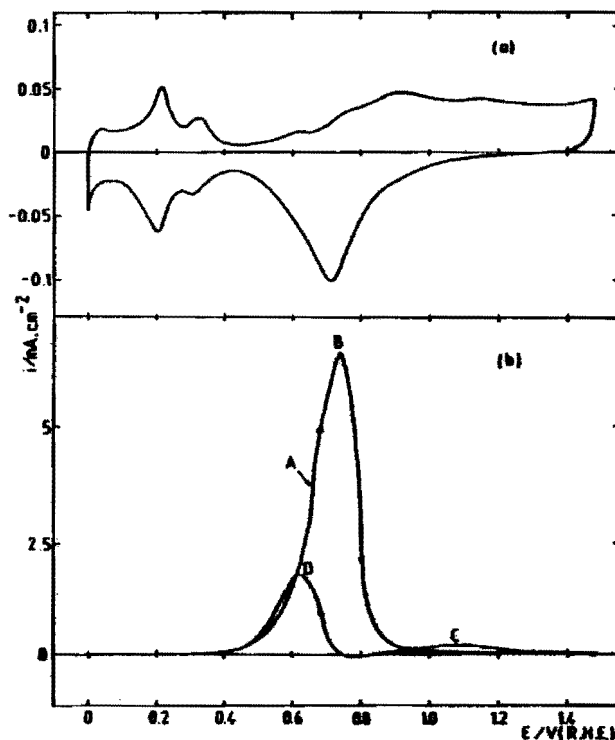


Figure 2.16. Cyclic voltammograms of a Pt bead electrode (1 M NaOH, 25°C, 50 mV/s): (a) without ethylene glycol; (b) with 0.1 M ethylene glycol (Kadirgan et al., 1983).

Electrochemically Modulated Infrared Reflectance Spectroscopy (EMIRS) was used by Hahn et al (1987) to study the adsorption of ethylene glycol at platinum in alkaline solutions. The adsorption was found to be dissociative. However, almost equal amounts of bridge-bonded and linearly bonded CO species were found in alkaline solutions. This is in contrast to acidic solutions, where only linearly bonded CO species were found (Hahn et al., 1987). An important shift towards lower wavenumbers of the linearly-bonded CO band centre was observed when the pH was increased. This might be due to interactions with the solvent or with adsorbed OH species, and a decrease of the CO coverage. The adsorption of molecular ethylene glycol may also play a role. The drastic change in the CO coverage as a function of pH is most probably related to a change in the electrocatalytic activity of platinum towards the oxidation of ethylene glycol when changing from acid to alkaline solutions.

The main products of ethylene glycol oxidation in base at platinum are glycolate, oxalate and CO_3^{2-} , determined by in situ FTIR (Christensen and Hamnett, 1989).

2.8.5. The electro-oxidation of ethylene glycol at Au-Pt electrodes in base

The cyclic voltammograms for ethylene glycol oxidation in base at Au, Pt and a 50Au-50Pt alloy electrode are shown in Figure 2.17 (Beden et al., 1982). The Au-Pt alloy electrode was prepared by electrolytic codeposition of the two metals on a platinum bead. The alloy electrode was then annealed by warming it to red heat in a hydrogen flame. For the alloy electrode it can be seen that during the positive sweep, electro-oxidation of ethylene glycol occurs in two main peaks. The first peak is in the same potential range as pure platinum and the second peak corresponds to oxidation on pure gold. However, the current densities obtained with the alloy electrode are much higher than those on the pure metals. At the Pt-region, the electro-oxidation activity is enhanced eight times and at the Au-region two times.

The 60Au-40Pt alloy electrode has been found to be the most active for ethylene glycol oxidation (Eggert (Stelmach, 1994)). However, the effect of the heat treatment condition of this alloy (Table 3.1) on the electro-oxidation of ethylene glycol needs to be considered.

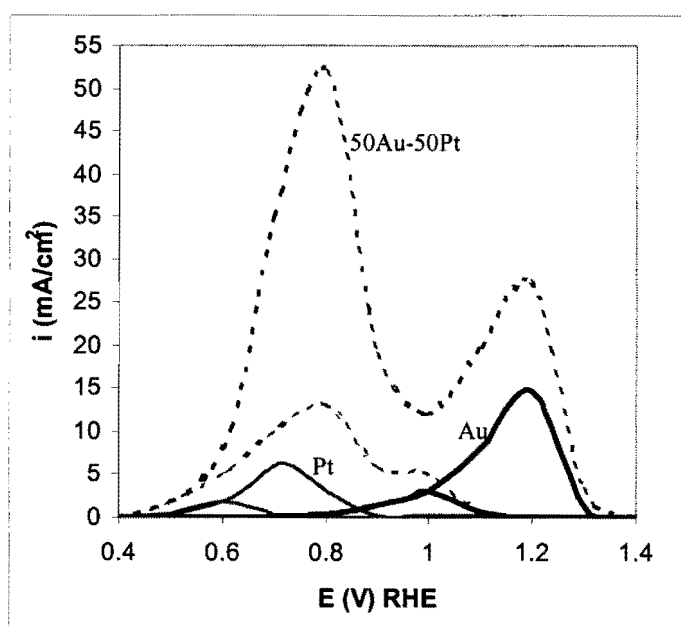


Figure 2.17. Cyclic voltammograms for ethylene glycol electro-oxidation in 1 M NaOH (0.1 M ethylene glycol, 25 °C, 50 mV/s) on a platinum bead electrode, a gold bead electrode and a 50Au-50Pt alloy electrode (After Beden et al., 1982).

2.9. The Au-1wt% Ti alloy (Gold 990)

The Au-1wt% Ti alloy was originally developed to produce an alloy with at least 990 fineness, with colour close to that of pure gold and with durability as good as that of standard jewellery alloys (Gafner, 1989).

The addition of 1 wt% (4 at%) of titanium to gold substantially hardens the precious metal and enhances its wear resistance. The enhanced hardening is due to the formation of fine Au_4Ti precipitates under the appropriate thermo-mechanical treatments (The Au-Ti phase diagram (ASM Handbook, Volume 3: Alloy Phase Diagrams, 1992) is shown in Figure. 2.18). The addition of titanium to gold satisfies two important criteria for achieving optimum precipitation hardening:

- 1) It has a high solubility in gold at elevated temperature, which maximises its dissolution into gold.
- 2) The gold-titanium system has a shallow solvus curve towards pure gold, which enables a significant proportion of titanium to be retained in supersaturated solid solution on quenching. The Au_4Ti compound, which constitutes the strengthening precipitate, is substantially harder than the gold matrix and so gives rise to a substantial reinforcement.

2.9.1. Preparation of Gold 990

The alloy is prepared (Gafner, 1989) by melting together the constituents in a vacuum induction furnace, and casting the alloy into a suitable ingot. It is then precipitation hardened in two stages by first carrying out a solution heat-treatment, involving a heating stage at 800°C in air, or a vacuum or inert atmosphere, followed by quenching the ingot in water. Tests have shown that no significant loss of titanium occurs when solutionising is in air, because a protective surface layer forms. This brown layer can subsequently be removed mechanically or by dipping the alloy in a 10% $K_2S_2O_7$ solution in water. Precipitation hardening is accomplished by heating the alloy at a lower temperature, typically at 400-500°C, with or without an intermediate cold working stage.

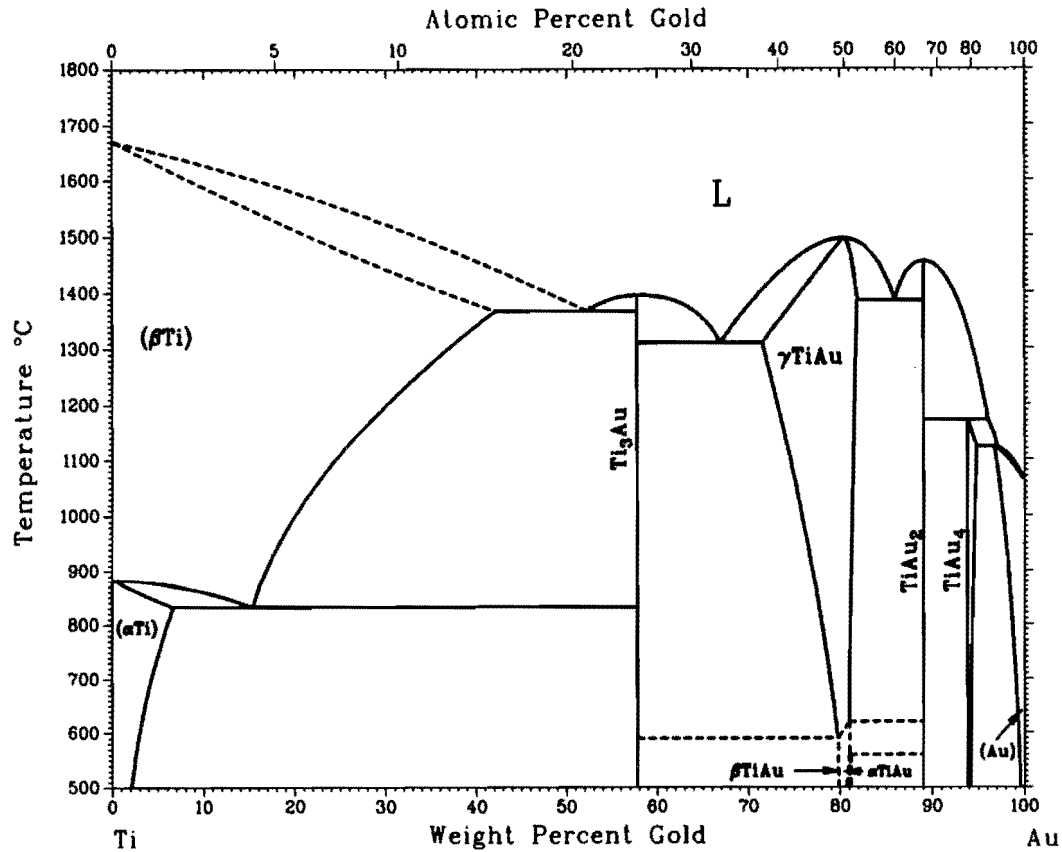


Figure 2.18. The Au-Ti phase diagram (ASM Handbook, Volume 3: Alloy Phase Diagrams, 1992).

It would be of interest to investigate the electrochemical properties of the alloy in two different heat treatment conditions (Fig. 2.18):

- 1) With titanium in solid solution.
- 2) In the precipitation-hardened condition (with Au₄Ti precipitates).

2.9.2. The electrochemical behaviour of pure titanium

Potentiodynamic polarisation curves for titanium in 0.5 M H₂SO₄ were measured at 303, 313 and 323 K by Shibata and Zhu (1995) and are shown in Figure 2.19.

An active-passive transition is found at around -0.49 V_{Ag/AgCl}. The critical current for passivation and the passive current increase with temperature. It is interesting that a second peak appears around 2.1 V_{Ag/AgCl}, which decreases with increase in temperature. The origin of this peak is still uncertain. According to Armstrong (1977) it could be due to a phase transformation of the originally formed oxide. The steady passive current was again reached beyond this second peak. A rapid current increase then

follows due to oxygen evolution. The oxygen evolution potential shifted in the negative direction with increase in temperature.

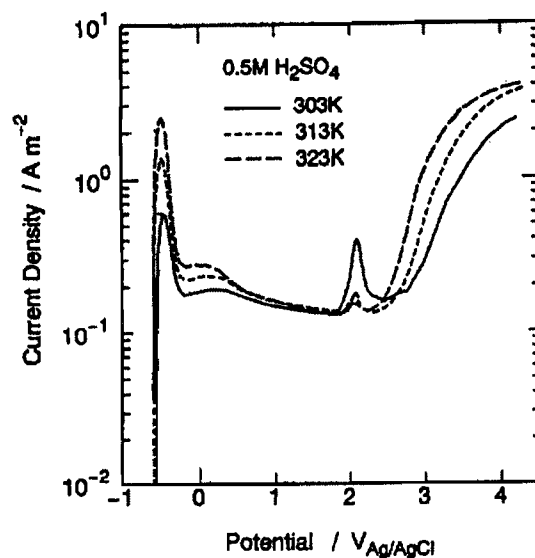


Figure 2.19. Anodic polarisation curves of Ti in 0.5 M H_2SO_4 solution at 303, 313 and 323 K (Shibata and Zhu, 1995).

The frequency and current responses as a function of the potential for titanium in 5 M H_2SO_4 are shown in Figure 2.20 (Herranen and Carlsson, 2001). As expected, the anodic current corresponding to dissolution of titanium is first accompanied by an increase in frequency (this corresponds to a decrease in mass). After reaching the passivation potential at -470 mV_{SCE} , with the corresponding critical current density (i_c), the current decreases as a result of oxide formation. However, the mass continues to decrease in the active-passive region. This indicates that the passive layer is not intact until a passive potential of about -150 mV_{SCE} is reached. An increase in mass is observed in the passive region. A second current density peak at 1.72 V_{SCE} was only found in 0.1 M H_2SO_4 - proposed to be due to a phase transformation of the oxide (Armstrong, 1977).

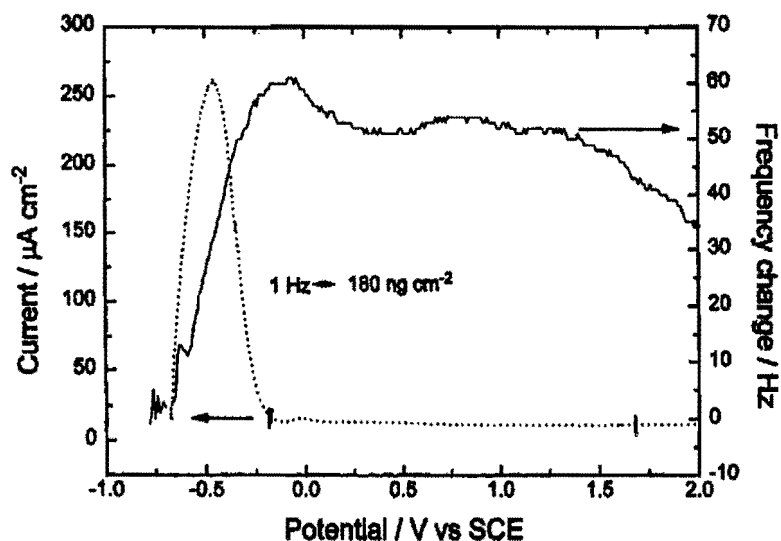


Figure 2.20. Current and frequency changes as functions of the potential of Ti in 5 M H_2SO_4 (Herranen and Carlsson, 2001).

A number of studies of the structure and composition of passive films on titanium have been reported. Armstrong (1977) studied the electrochemical behaviour of titanium films in 1 M HClO_4 and 0.5 M H_2SO_4 and characterised the surface oxide by XPS and AES. This indicated a mixture of metal oxides (TiO_2 , Ti_2O_3 and TiO). Electrodes prepared at a larger anodic charge (potentials up to 2 V_{SCE}) showed more TiO_2 character.

Pure titanium is expected to be in the passive condition at the potentials applied for cyclic voltammetry of gold electrodes (0 – 1.8 V_{RHE} in acid and 0 – 1.6 V_{RHE} in base, Figures 2.1 and 2.2). This fact is also supported by the Pourbaix diagram for titanium shown in Figure 2.21 (Pourbaix, 1974).

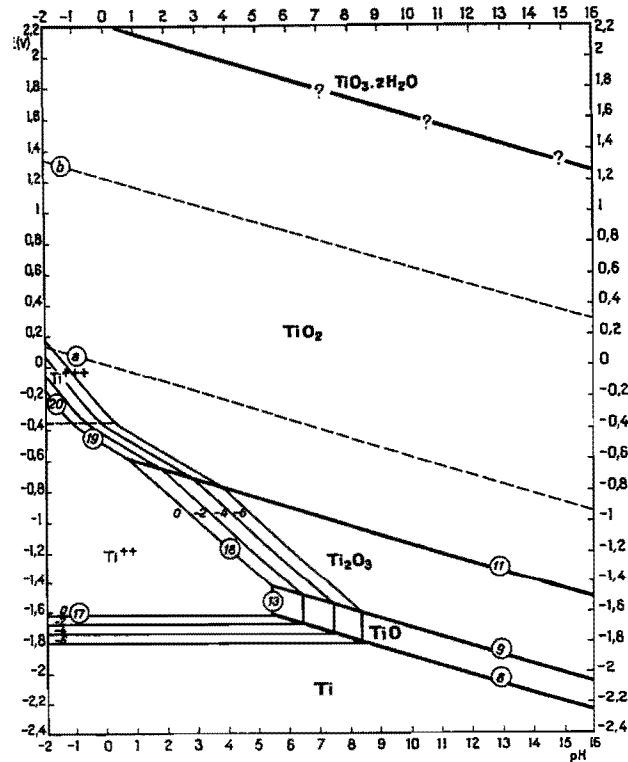


Figure 2.21: Potential – pH equilibrium diagram for the system titanium – water, at 25°C (Pourbaix, 1974).

2.10. Conclusions

- Even though gold is a weak chemisorber, it displays a wide range of electro-oxidation activity, especially in alkaline solutions.
- It is believed that organic compounds are oxidised at gold anodes in the presence of a submonolayer of adsorbed hydroxyl radicals (AuOH) before monolayer oxide formation.
- A bimetallic electrode is usually more active for the electro-oxidation of organics than the respective pure metals.
- The 60Au-40Pt alloy electrode has been identified in the literature as being the most active for the electro-oxidation of various organics in base. However, the effect of the microstructure of the alloy on its electrochemical properties has largely been ignored in the past.
- The electro-oxidation of ethylene glycol at noble metal electrodes has been studied extensively. This organic compound can therefore be used as a model compound to study the effect of heat treatment condition on the electrochemical properties of the gold alloys.

- The Gold 990 alloy was developed originally for the jewellery industry. The electrochemical properties of this alloy have not been studied before.

Chapter 3

THE HEAT TREATMENT OF Au-Pt ALLOYS AND THE GOLD 990 ALLOY

3.1. Introduction

The gold alloy containing 40% platinum has been identified (Stelmach et al., 1994) as being the most active for the oxidation of various organic compounds in alkaline solutions. However, the effect of the microstructure of gold-platinum alloys on their electrochemical properties has largely been ignored in the past. The purpose of this chapter is to discuss the microstructures of the 60Au-40Pt alloy obtained after different heat treatments. The spinodal decomposition reaction in the 50Au-50Pt alloy is also discussed.

The Gold 990 alloy (Au-1wt%Ti) is a precipitation-hardenable alloy. The different heat treatments of the Gold 990 alloy will also be reviewed in this chapter.

3.2. The 60Au-40Pt alloy

Gold and platinum (both 99.99%) were melted together (in the required ratio) in an arc-furnace with a water-cooled copper hearth under a protective argon atmosphere. The sample (approximately 10 g) was turned around after each melt and re-melted three times to ensure homogeneity.

3.2.1. The 60Au-40Pt alloy heat treated at 1300°C

The 1300°C heat treatment of the 60Au-40Pt alloy is shown schematically in Figure 3.1. Partial melting of the sample will occur at 1300°C. The liquid phase will be gold-rich with a composition of approximately 85Au-15Pt. The solid phase will be platinum-rich. The composition of this phase is difficult to estimate, due to the fact that the solidus line is almost horizontal at these temperatures. A small deviation from 1300°C will result in

large deviations in the composition of this phase. For the same reason, the lever rule cannot be used to accurately predict the amount of each phase that will be formed. However, the Pt-rich phase obtained by this heat treatment will have a higher gold content than the Pt-rich phases formed in the miscibility gap (Figure 3.1).

The sample was kept at 1300°C for 1 hour before quenching in water. After quenching, the sample was cold-rolled to a thickness of approximately 2 mm. A disk with a diameter of 6 mm was subsequently punched. The sample was mounted in a resin by using a black phenolic thermosetting powder. It was polished using diamond paste (6, 5 and finally 1 μm). The microstructure was studied by means of optical microscopy and scanning electron microscopy (SEM).

The microstructure of the 60Au-40Pt alloy after the 1300°C heat treatment is shown in Figure 3.2. Etching was not required to produce the microstructure shown in Figure 3.2. It can be seen that the Pt-rich areas formed by this heat treatment are relatively large, with typical diameters of 30 –50 μm (Figure 3.2).

Back-scattered electron imaging cannot be used to study the Au-rich and Pt-rich areas, because the atomic weights of gold and platinum are similar (196.97 and 195.08 g/mol respectively). However, the Au-rich and Pt-rich phases can be distinguished by elemental mapping using energy dispersive X-ray analysis in a scanning electron microscope.

An elemental map (using energy-dispersive X-ray analysis based on the L lines of the two metals) of the 60Au-40Pt alloy heat treated at 1300°C is shown in Figure 3.3. The elemental map confirms that optical microscopy without etching of the sample can be employed to study the microstructures of Au-Pt alloys (Compare Figures 3.2 and 3.3).

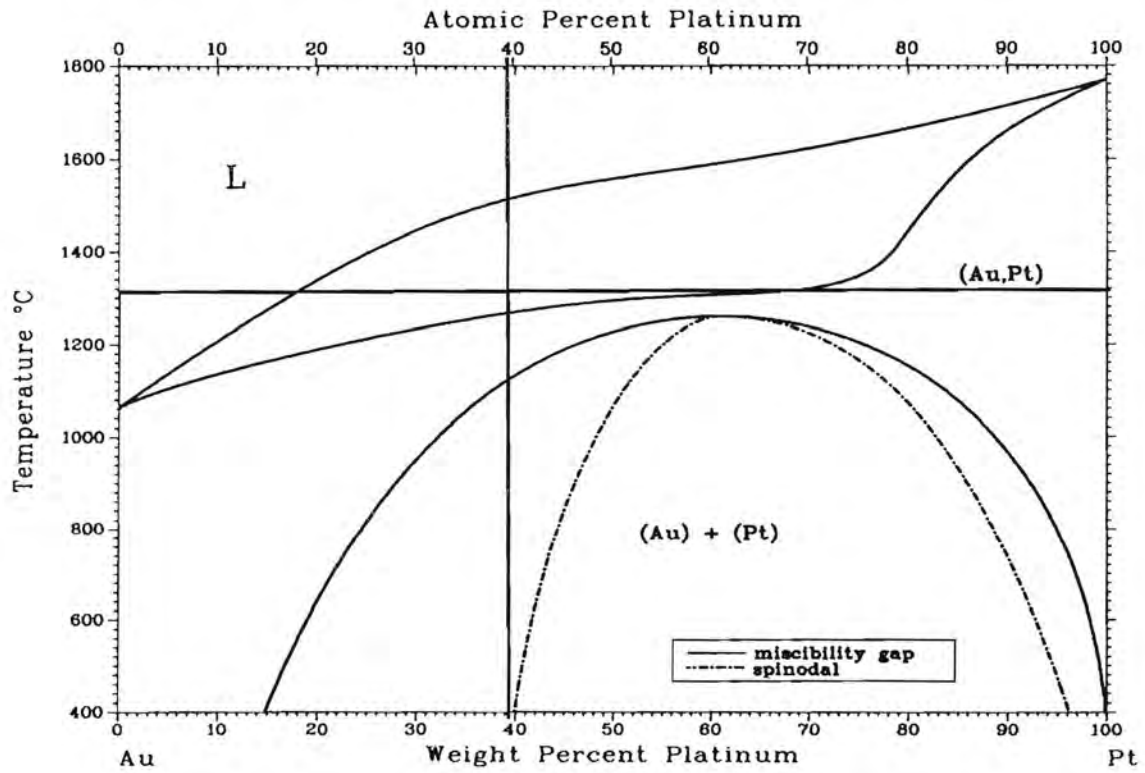


Figure 3.1. The 1300°C heat treatment of the 60Au-40Pt alloy (*ASM Handbook, Volume 3: Alloy Phase Diagrams, 1992*)

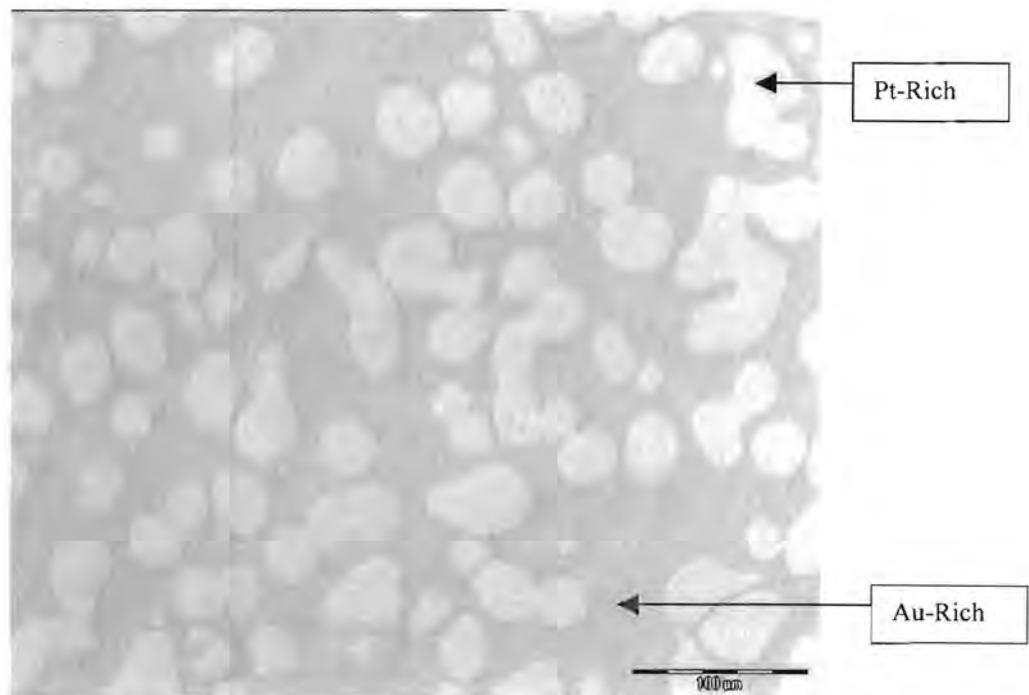


Figure 3.2. Optical photomicrograph of the 60Au-40Pt alloy after heat treatment at 1300°C for 1 hour (No etching).

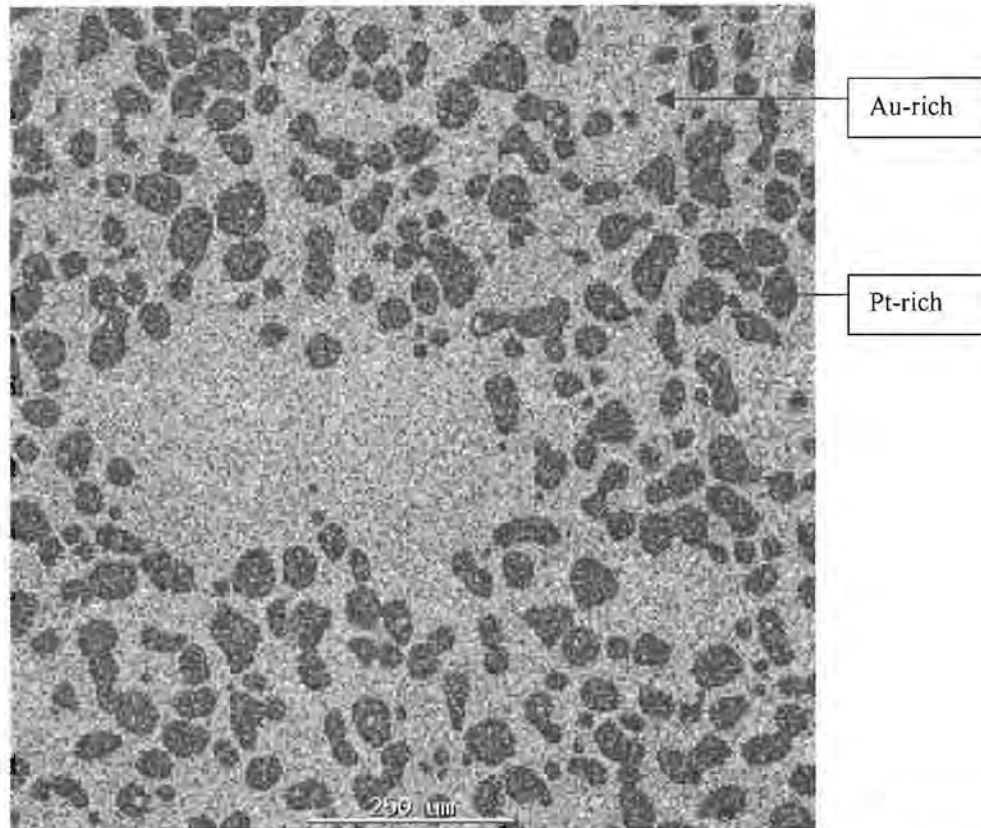


Figure 3.3: Elemental map (based on L lines of energy-dispersive X-ray analysis) of the 60Au-40Pt alloy heat treated at 1300°C.

3.2.2. The 60Au-40Pt alloy heat treated at 1200°C

Samples of the 60Au-40Pt alloy in the 1300°C heat treatment condition were heat treated at 1200°C, followed by water quenching. The 1200°C heat treatment of the 60Au-40Pt alloy is shown schematically in Figure 3.4. This heat treatment is designed to produce a homogeneous solid solution of platinum in gold. Due to the fact that the Pt-rich areas are relatively large in the 1300°C condition (Fig. 3.2), the influence of time at 1200°C was investigated by heat treating two samples for different times. The first sample was treated at 1200°C for 24 hours and the second sample for 168 hours (1 week).

The samples were polished using diamond paste (6, 5 and finally 1 μm). The microstructures were studied by means of optical microscopy and scanning electron microscopy (SEM). X-ray diffraction (XRD) was used to confirm whether a solid solution was produced after the solutionising heat treatment.

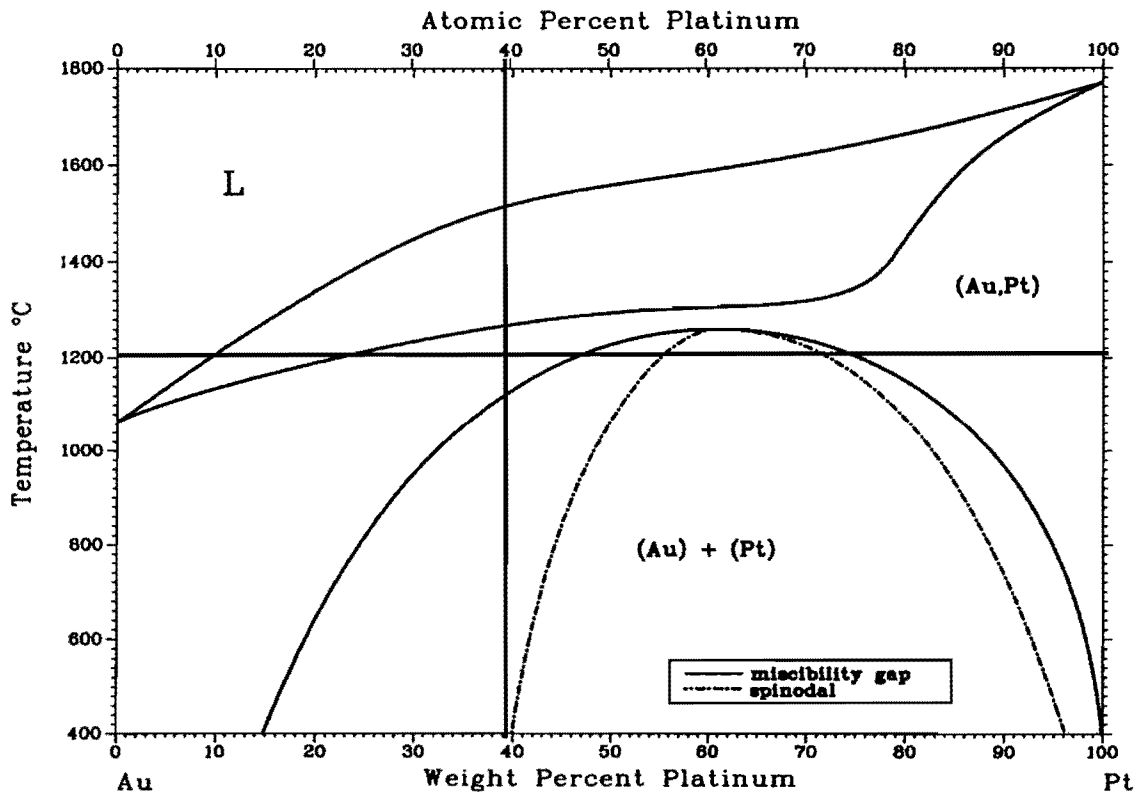


Figure 3.4. The 1200°C heat treatment of the 60Au-40Pt alloy (ASM Handbook, Volume 3: Alloy Phase Diagrams, 1992)

3.2.2.1. The 60Au-40Pt alloy heat treated at 1200°C for 24 hours

The X-ray diffraction patterns for the 1300°C and the 1200°C heat treated samples are shown in Figure 3.5. The 1300°C treated sample has two peaks, corresponding to the Au-rich and Pt-rich phases. Two peaks are observed because of the difference in lattice parameters of the two phases. Both phases are face-centered cubic (fcc). The 1200°C treated sample only has one peak, showing that the solutionising heat treatment was successful. The “prestik” peaks in Figure 3.5 are due to the sample holder that was used during XRD.

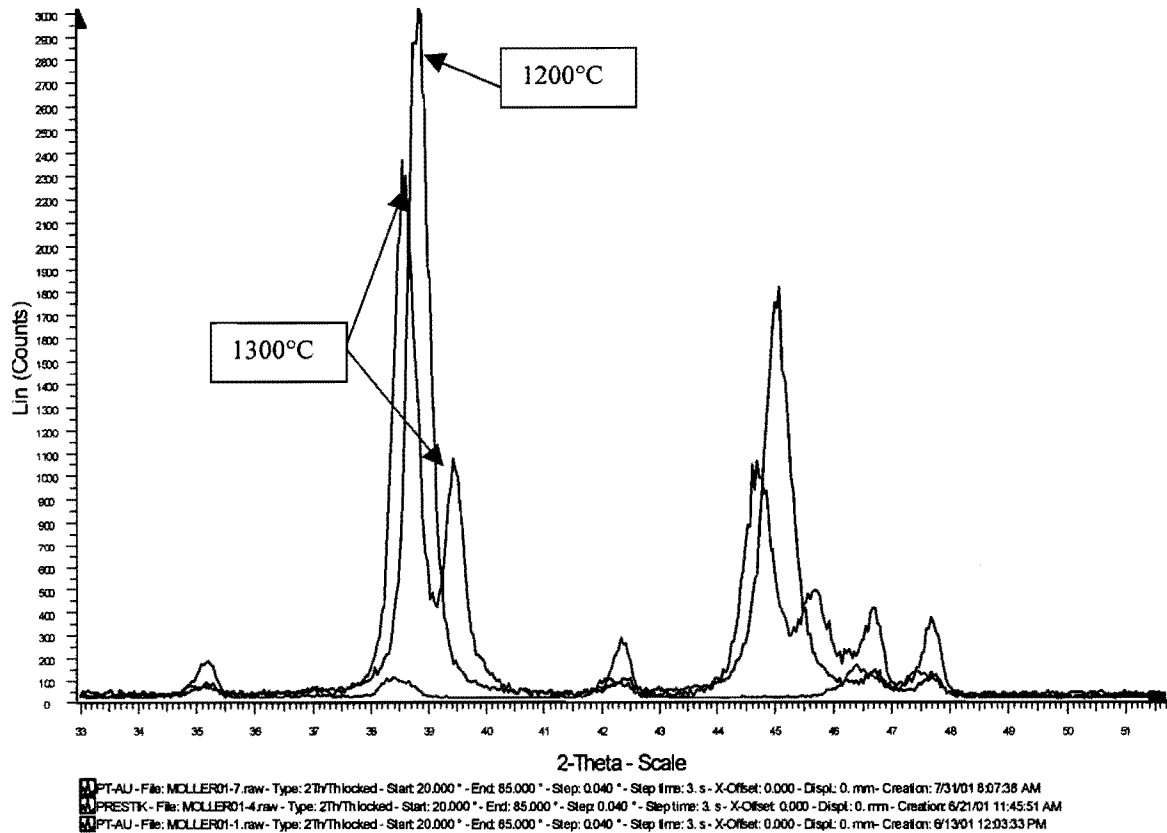


Figure 3.5. X-ray diffraction patterns of the samples heat treated at 1300°C and at 1200°C.

The microstructure of the 60Au-40Pt alloy after heat treatment at 1200°C for 24 hours is shown in Figure 3.6. The microstructure confirms that a single-phase solid solution was produced. However, it can be seen that porosity resulted during this heat treatment.

The porosity is not due to shrinkage during solidification, because at 1200°C no liquid is formed. It can, however, be explained by the Kirkendall effect.

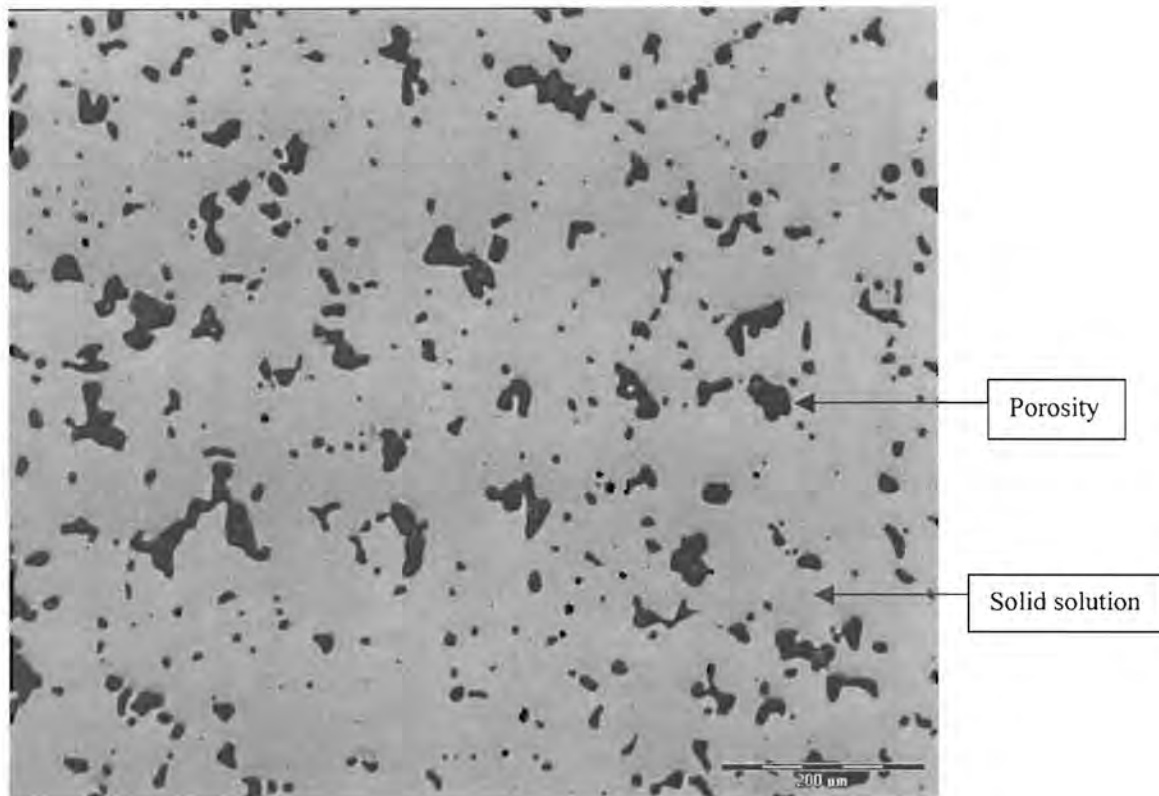


Figure 3.6. Optical photomicrograph of the 60Au-40Pt alloy after heat treatment at 1200°C for 24 hours (No etching).

3.2.2.2. Kirkendall porosity

The rate at which two types of atoms of a binary solution diffuse is not the same. The element with the lower melting point diffuses faster (Reed-Hill and Abbaschian, 1994: 367). The melting points of gold and platinum are 1064°C and 1769°C respectively (Fig. 3.1).

During the homogenising heat treatment (1200°C), the gold atoms diffused faster than the platinum atoms. Since every time an atom makes a jump a vacancy moves in the opposite direction, an unequal flow in the two types of atoms must result in an equivalent flow of vacancies in the reverse direction.

Figure 3.7 shows an optical micrograph of the sample in the 1300°C condition. During the 1200°C heat treatment, more gold atoms left the Au-rich areas than platinum atoms arrived to take their place - resulting in the observed porosity.

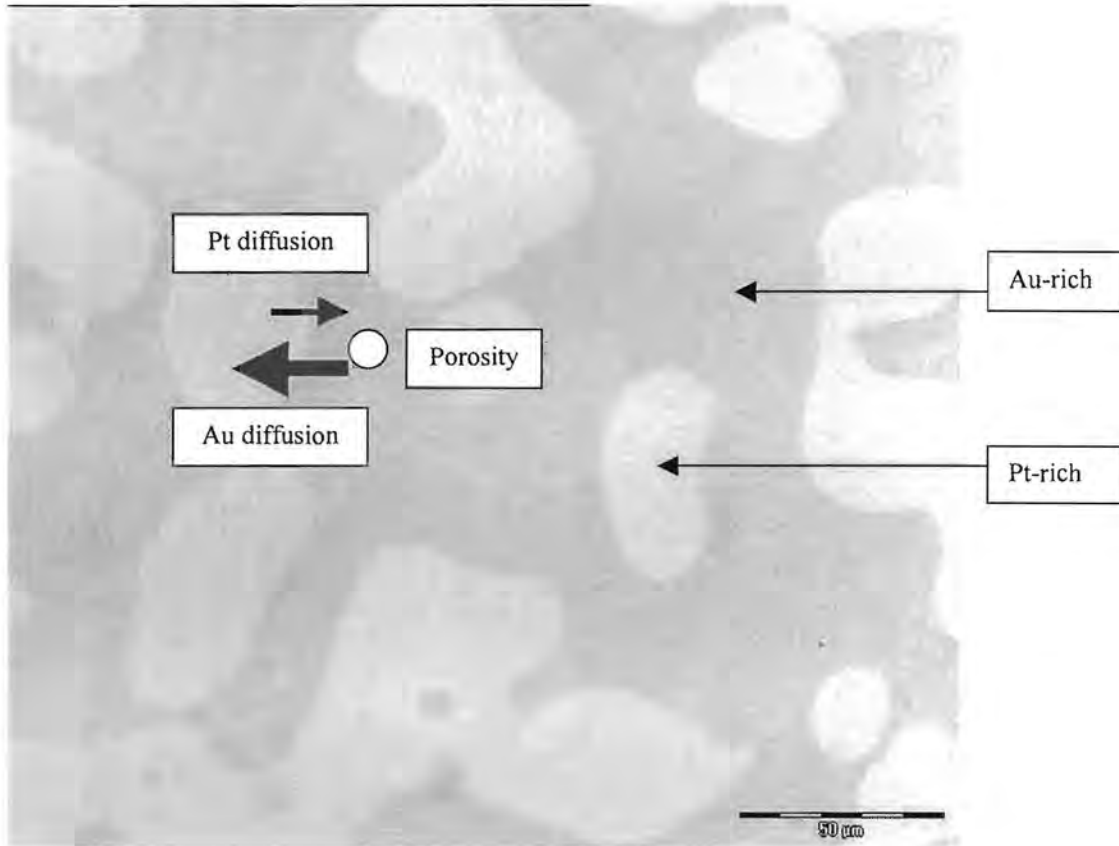


Figure 3.7. Pore formation in the 60Au-40Pt alloy due to the Kirkendall effect.

The Kirkendall effect in Au-Pt alloys has been reported by Bolk (1958). It is also known that failure of aged Cu-Au thin films frequently occurs due to Kirkendall porosity (Feinstein and Bindell, 1979).

3.2.2.3. The 60Au-40Pt alloy heat treated at 1200°C for 168 hours

The microstructure of the 60Au-40Pt alloy after heat treatment at 1200°C for 168 hours is shown in Figure 3.8.

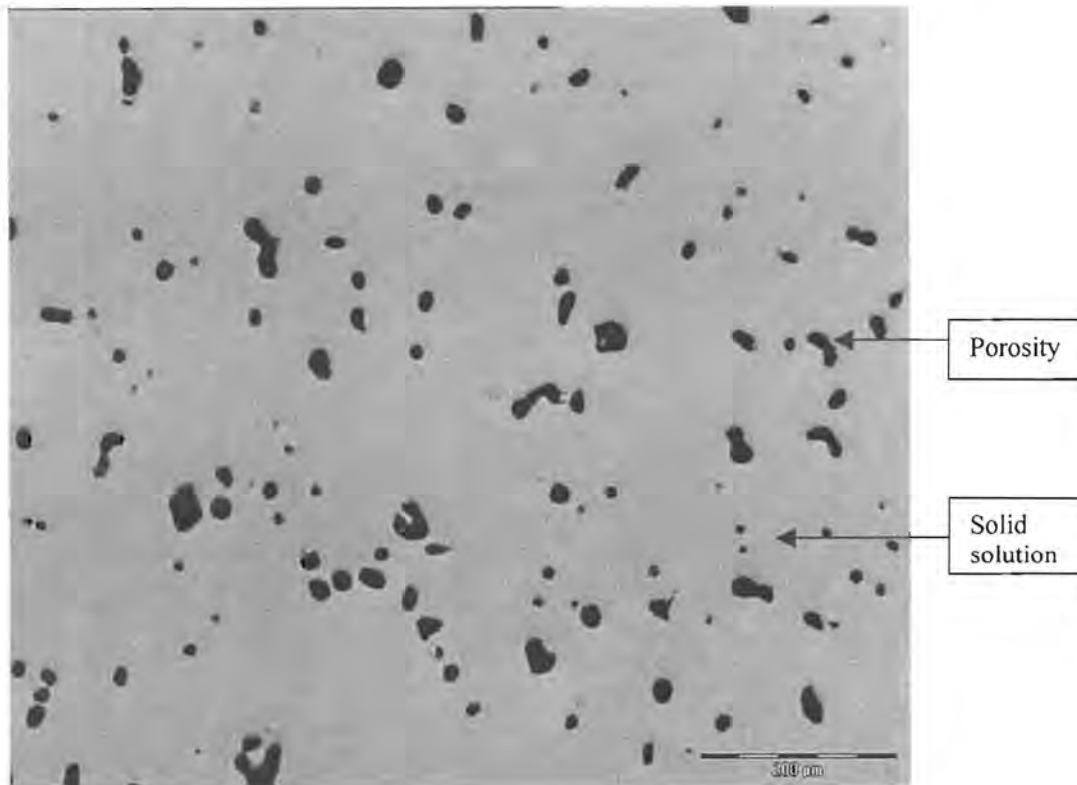


Figure 3.8. Optical photomicrograph of the 60Au-40Pt alloy after heat treatment at 1200°C for 168 hours.

There are fewer pores in the sample heat treated for 168 hours than the sample heat treated for 24 hours (Figures 3.6 en 3.8.). This is probably due to sintering of the pores during the longer heat treatment.

3.2.3. The 60Au-40Pt alloy heat treated directly at 1200°C

In order to produce a 60Au-40Pt sample with less Kirkendall porosity, it was decided to heat treat another sample at 1200°C without the intermediate 1300°C heat treatment step. The 1300°C heat treatment had resulted in large Pt-rich areas (Fig. 3.2) which, in turn, resulted in large pores during the subsequent solutionising heat treatment (Fig. 3.6). A new sample was therefore produced by button-arc melting, and heat treated at 1200°C for 24 hours. The sample was quenched in water after the heat treatment.

From Figure 3.9 it can be seen that diffusion during homogenisation at 1200°C to eliminate solidification segregation resulted in the formation of small pores. No large pores, such as in Figure 3.6, were formed.

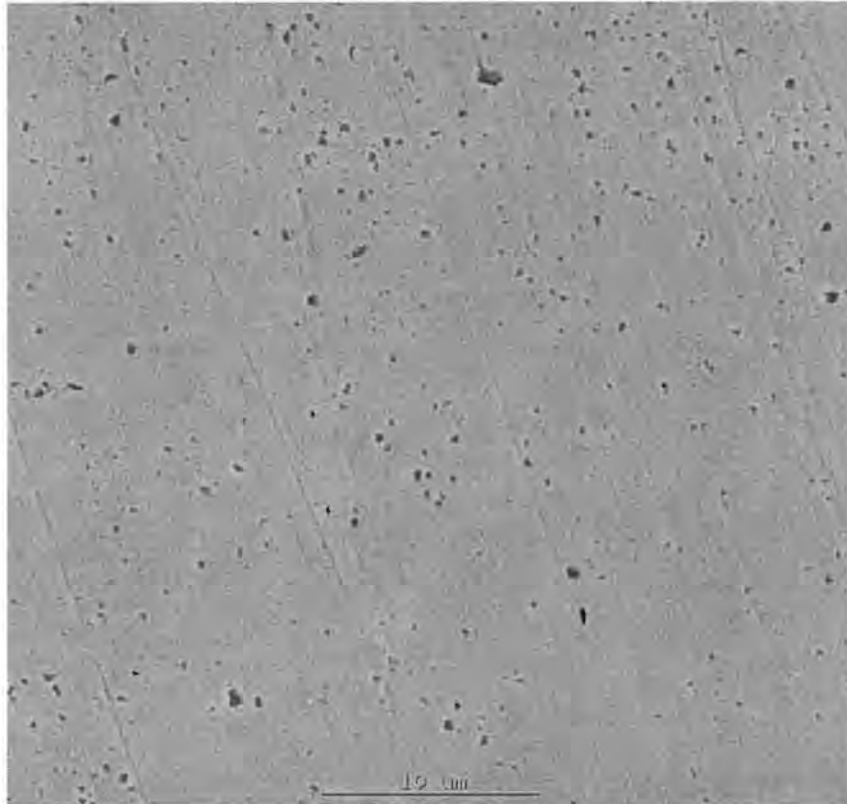


Figure 3.9. Scanning electron micrograph showing small pores in the 60Au-40Pt sample heat treated directly at 1200°C.

It is known that a heat treatment at 1200°C followed by quenching produces brittle material (Darling, 1962). This sample did indeed crack during rolling and discs could not be manufactured for electrochemical testing. A SEM investigation of the crack surface revealed that intergranular cracking occurred during rolling (Fig. 3.10). Intercrystalline cracking in Au-Pt alloys quenched from 1200°C has been attributed to partly suppressed grain boundary precipitation (Darling, 1962).

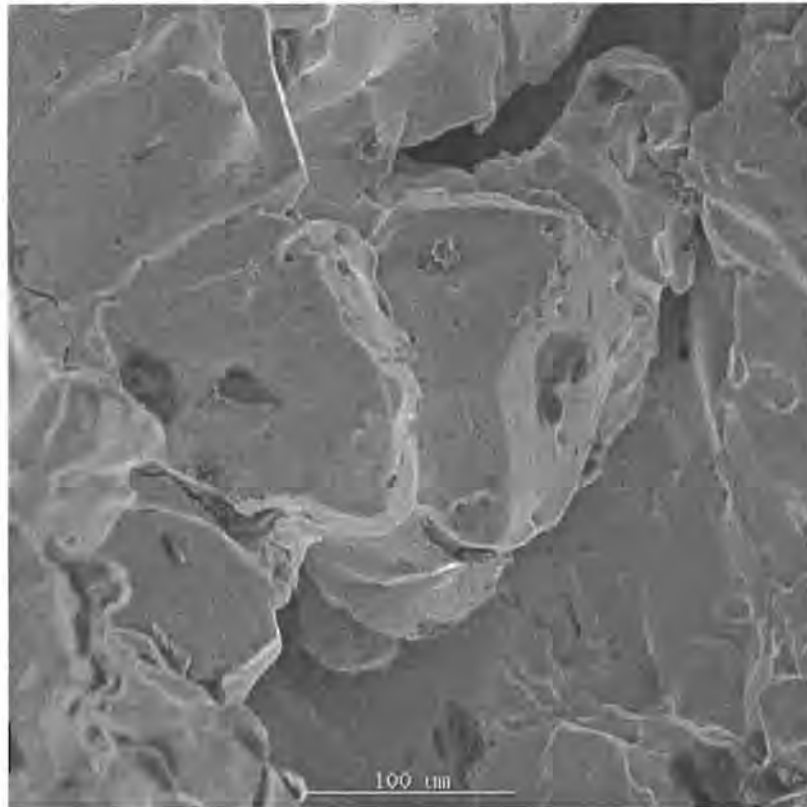


Figure 3.10. Scanning electron micrograph of a crack surface of the 60Au-40Pt sample heat treated directly at 1200°C

3.2.4. The 60Au-40Pt miscibility gap heat treatments

Porous samples in the solid solution condition (1200°C) were heat treated at 800 and 600°C. The predicted equilibrium weight fractions of α_1 (Pt-rich) and α_2 (Au-rich), and their composition as a function of heat treatment temperature, are shown in Table 3.1. The lever rule was applied to calculate the various weight fractions.

3.2.4.1. The 60Au-40Pt alloy heat treated at 800°C for 50 hours

A porous sample in the solid solution condition (1200°C-24h) was heat treated at 800°C for 50 hours, followed by water quenching. The 800°C heat treatment is shown schematically in Figure 3.11.

Table 3.1. Equilibrium weight fractions and composition of phases in a 60wt% Au-40wt% Pt alloy as functions of temperature

Temp. (°C)	Weight fraction of α_1	Composition of α_1		Weight fraction α_2	Composition of α_2	
		Wt%	Wt%		Wt%	Wt%
		Au	Pt		Au	Pt
800	0.21	5	95	0.79	75	25
600	0.26	2	98	0.74	81	19

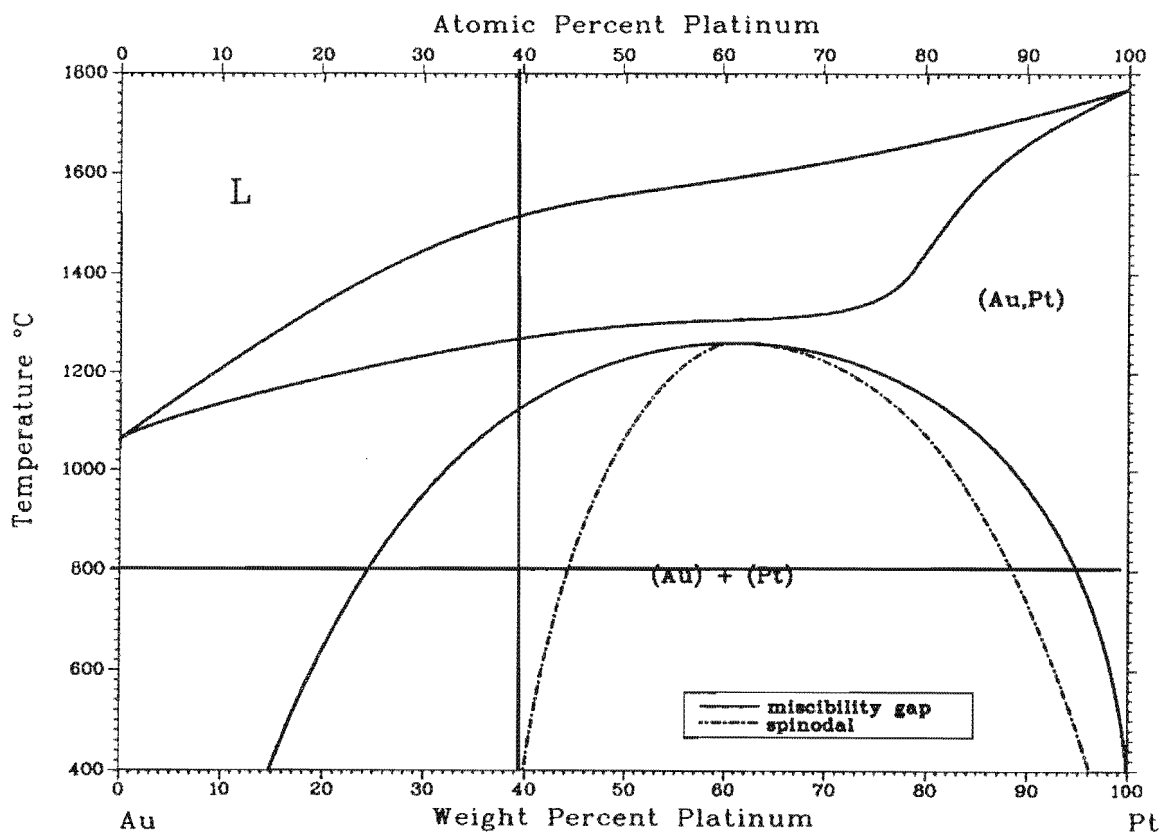


Figure 3.11. The 800°C heat treatment of the 60Au-40Pt alloy (ASM Handbook, Volume 3: Alloy Phase Diagrams, 1992)

The 60Au-40Pt alloy at 800°C lies outside the spinodal phase area (Figure 3.11). Conventional nucleation and growth of the Pt-rich areas is therefore expected.

An elemental map (using energy-dispersive X-ray analysis based on the L lines of the two metals) of the 60Au-40Pt alloy heat treated at 800°C for 50 hours is shown in Figure 3.12. The distribution of phases indicates that heterogeneous nucleation of the Pt-rich areas occurred, probably on grain boundaries. The Pt-rich areas are small, with diameters of only 1 to 3 μm .

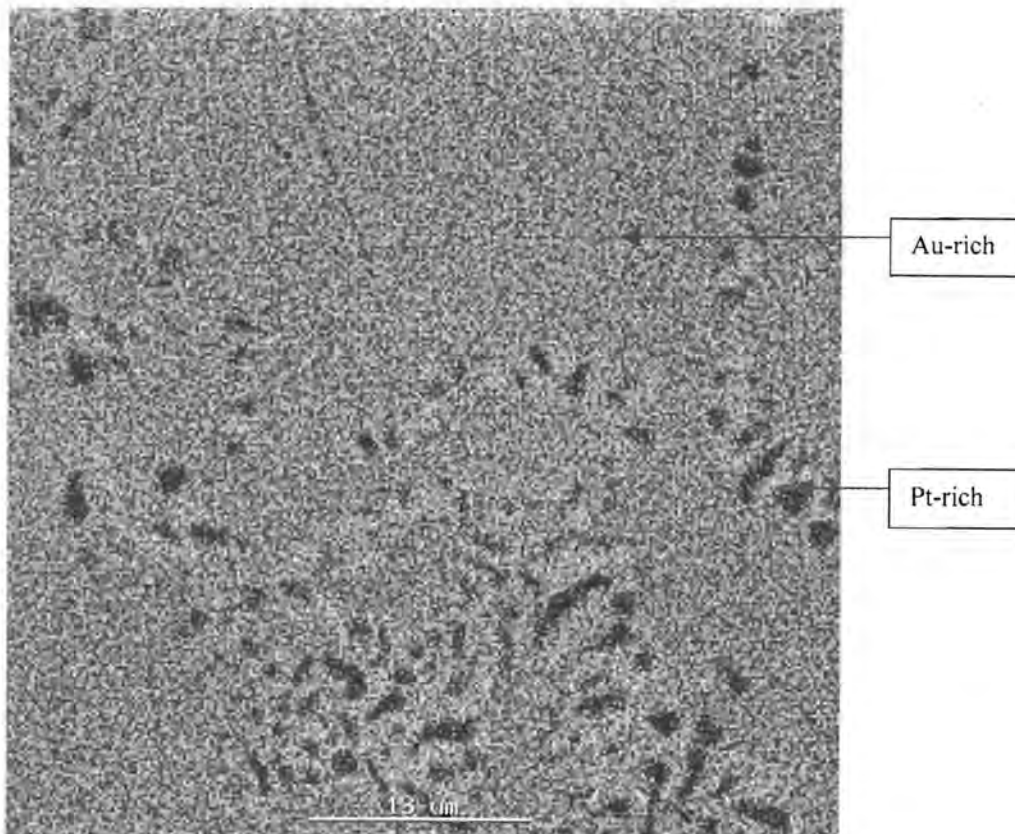


Figure 3.12. Elemental map (based on L lines of energy-dispersive X-ray analysis) of the 60Au-40Pt alloy heat treated at 800°C for 50 h.

The porosity also played an important role during the nucleation of the Pt-rich areas. In Figure 3.13, small Pt-rich areas are seen in close vicinity of a pore.

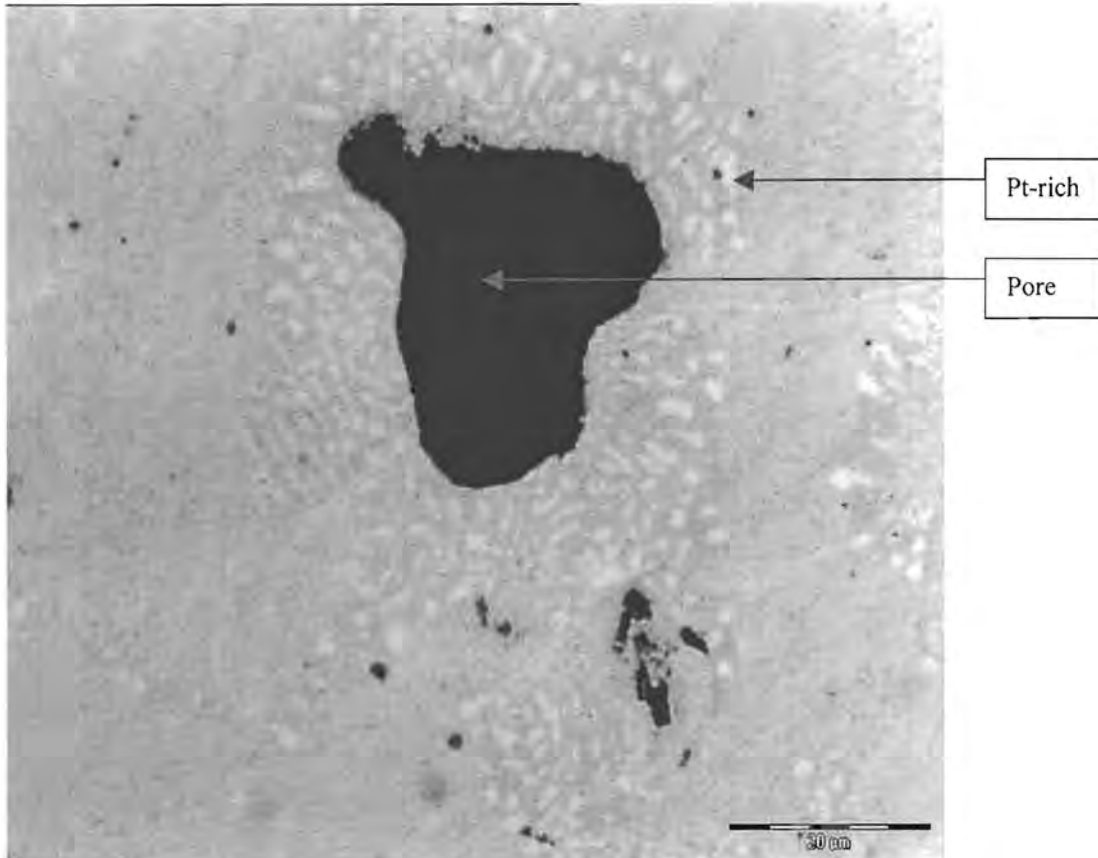


Figure 3.13. Optical photomicrograph of small Pt-rich areas near a pore after a heat treatment at 800°C for 50 h.

3.2.4.2. The 60Au-40Pt alloy heat treated at 600°C for 100 hours

A porous sample in the solid solution condition (1200°C-24h) was heat treated at 600°C for 100 hours, followed by water quenching. The 600°C heat treatment is shown schematically in Figure 3.14.

The 60Au-40Pt alloy at 600°C also lies outside the spinodal phase area (Figure 3.14). Conventional nucleation and growth of the Pt-rich areas is once again expected.

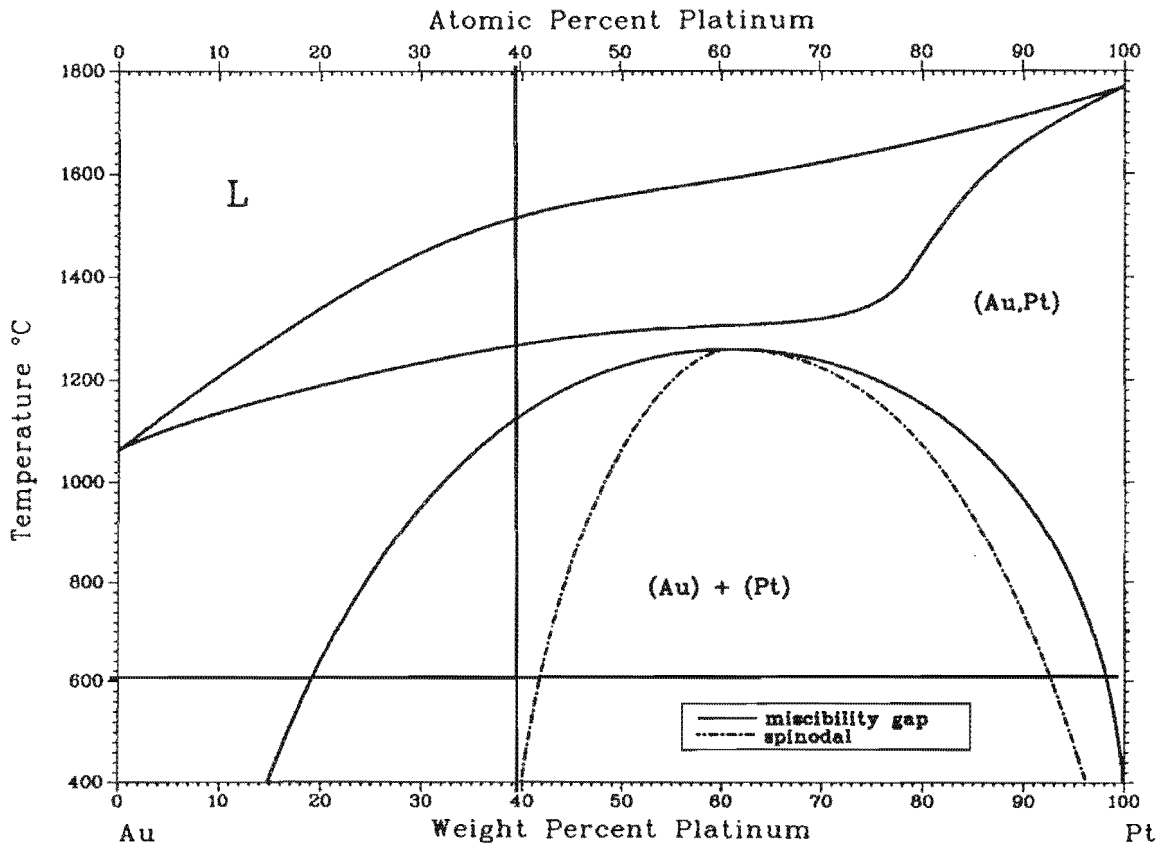


Figure 3.14. The 600°C heat treatment of the 60Au-40Pt alloy (*ASM Handbook, Volume 3: Alloy Phase Diagrams, 1992*)

An elemental map (using energy-dispersive X-ray analysis based on the L lines of the two metals) of the 60Au-40Pt alloy heat treated at 600°C for 100 hours is shown in Figure 3.15.

Heterogeneous nucleation of the Pt-rich areas is observed for the 60Au-40Pt alloy heat treated at 800°C (Fig. 3.12) and 600°C (Fig. 3.15). For compositions outside the spinodal decomposition area (Fig. 3.14), second-phase formation is by conventional nucleation and growth. In order to study spinodal decomposition in Au-Pt alloys, the 50Au-50Pt alloy was investigated.

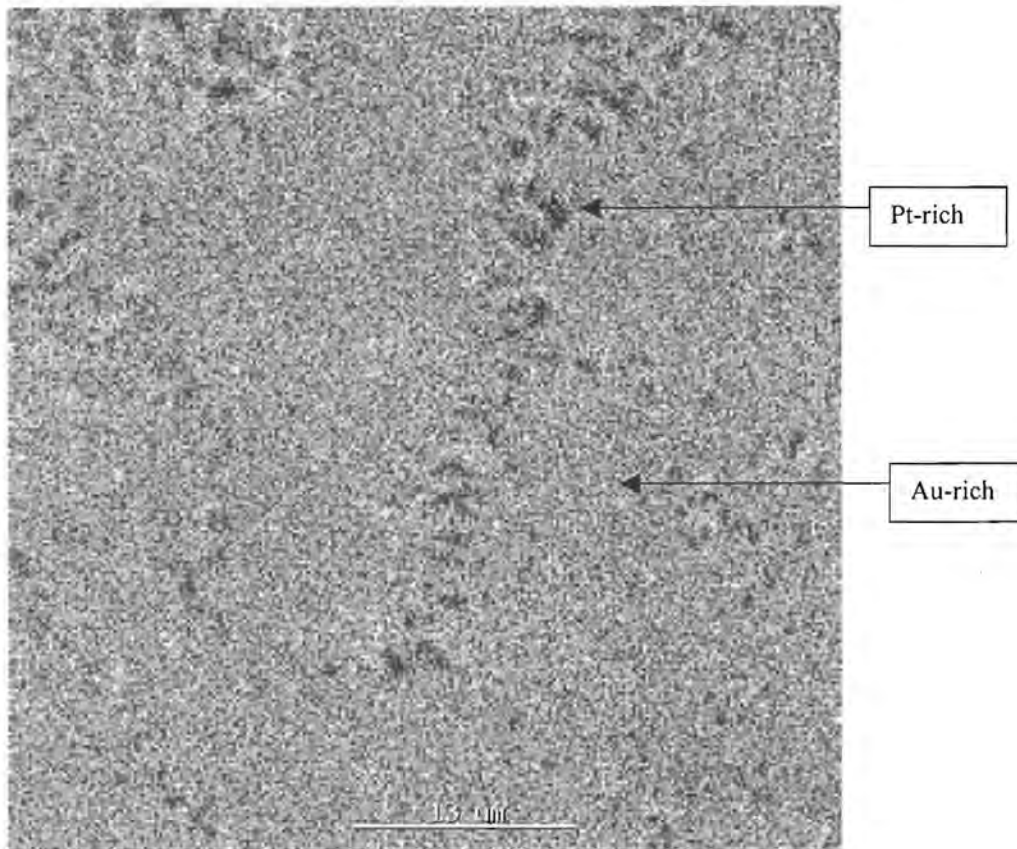


Figure 3.15. Elemental map (based on L lines of energy-dispersive X-ray analysis) of the 60Au-40Pt alloy heat treated at 600°C for 100 h.

3.3. The 50Au-50Pt alloy

Gold and platinum (both 99.99%) were melted together (in the required ratio) in an arc-furnace with a water-cooled copper hearth under a protective argon atmosphere. The sample was turned around after each melt and re-melted three times to ensure homogeneity.

3.3.1 The 50Au-50Pt alloy in the “ductile” condition

A 50Au-50Pt sample was given a heat treatment according to Darling (1962) to produce ductile material. The following procedure was used:

- The sample was placed in the furnace at 1000°C for 2 hours.

- The sample was left in the furnace, and the temperature was reduced to 800°C. The furnace took approximately 1.5 hours (between 85 and 100 minutes) to reach the desired temperature of 800°C.
- Once the temperature reached 800°C, the sample was left in the furnace for a further 2 hours.
- The sample was rapidly cooled by water quenching.

The sample was in the furnace for approximately 5.5 hours. It was then cold rolled. The whole process (heat treatment and cold rolling) was performed three times. The sample therefore spent 16.5 hours (5.5 x 3) in total in the furnace. The two temperature limits of the “ductile” heat treatment are shown in Figure 3.16.

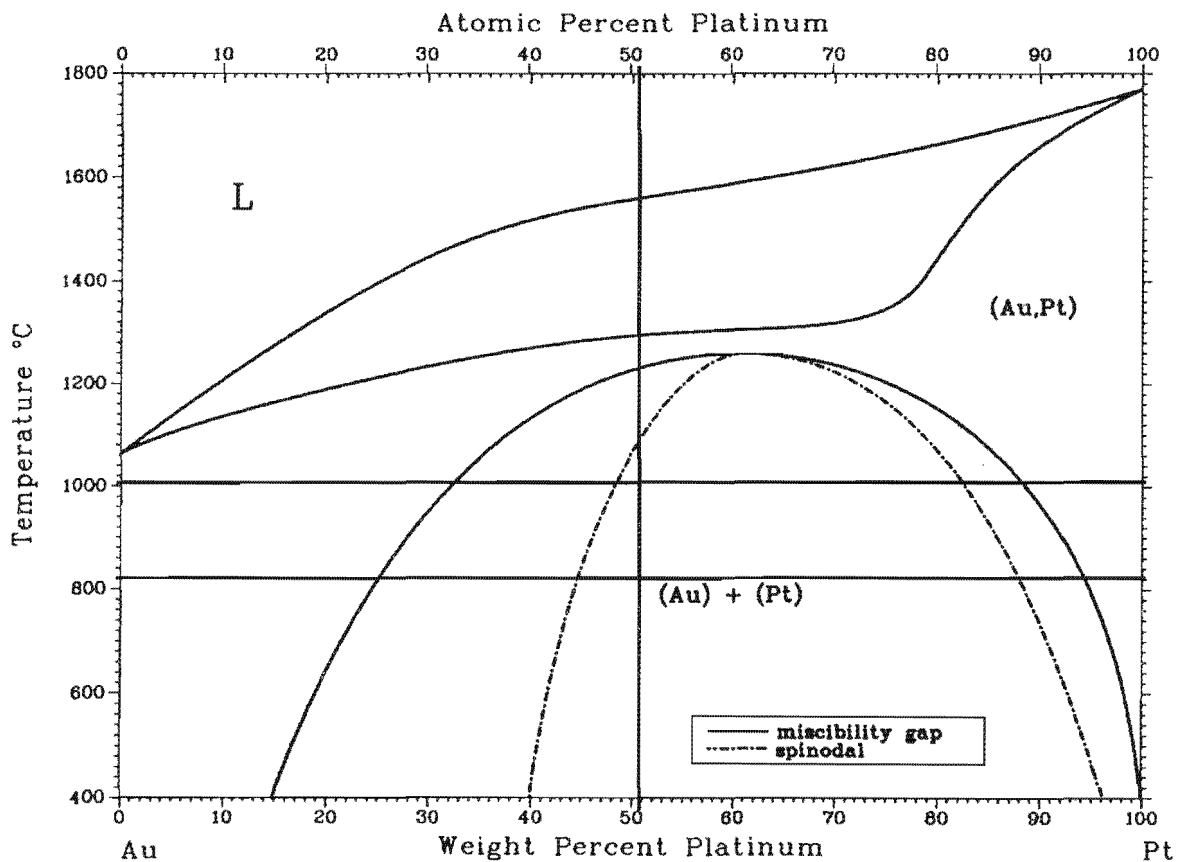


Figure 3.16. The “ductile” heat treatment of the 50Au-50Pt alloy (ASM Handbook, Volume 3: Alloy Phase Diagrams, 1992)

From Figure 3.16, it is seen that this alloy composition lies in the spinodal decomposition area in the temperature range of 800 to 1000°C.

A disc of 6 mm diameter was punched from the cold-rolled material and was mounted in resin by using a black phenolic thermosetting powder. The sample was polished with diamond paste (down to 1 μm) and the microstructures were studied by optical microscopy.

The microstructure of the 50Au-50Pt alloy in the ductile condition is shown in Figure 3.17.

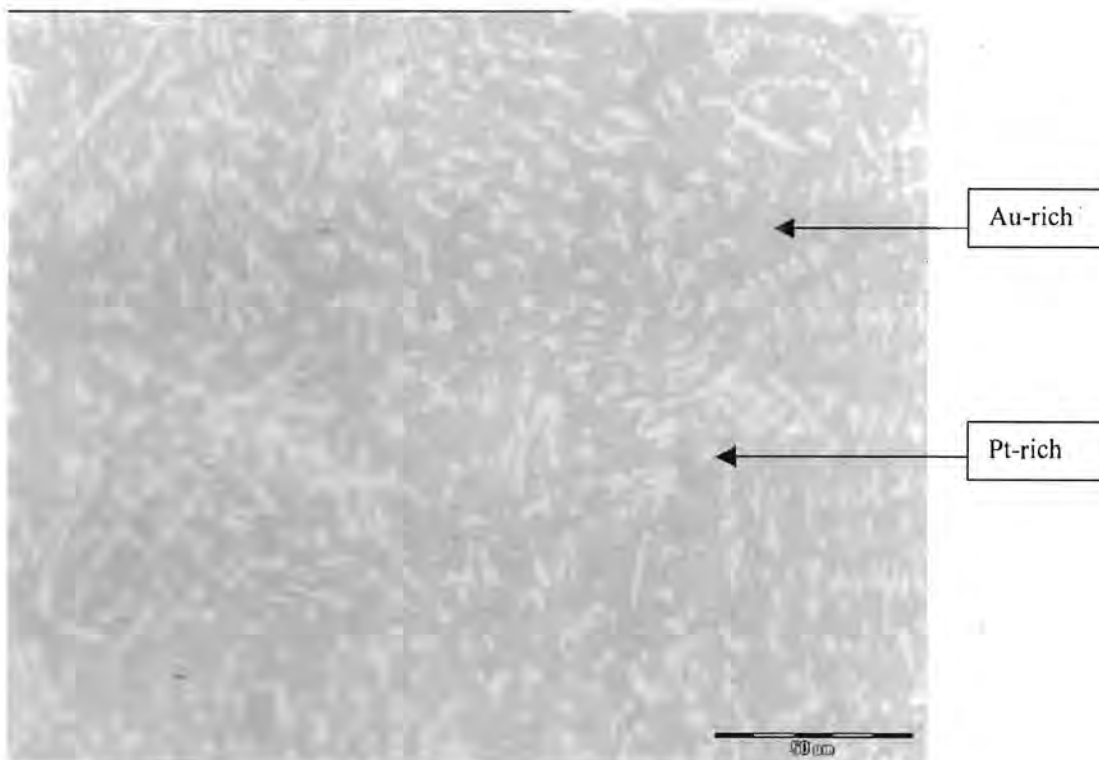


Figure 3.17. Optical photomicrograph of the 50Au-50Pt alloy after the “ductile” heat treatment.

Figure 3.17 shows that nucleation of the Pt-rich areas occurred simultaneously throughout the matrix producing a uniform microstructure. Uniform microstructures are obtained during spinodal decomposition, because there is no thermodynamic barrier to nucleation (Cahn, 1970). In this type of transformation, no definite distinguishable nuclei are formed initially, as the interface between the matrix and the precipitate is diffuse

through a sinusoidal variation in composition throughout the matrix. As time increases, the amplitudes of the composition variation will increase. This requires “uphill” diffusion – solute separation therefore occurs against the concentration gradient.

3.3.2. The 50Au-50Pt alloy in the solid solution condition

A sample in the “ductile” heat treatment condition was solutionised at 1250°C for 24 hours followed by water quenching. This heat treatment is shown in Figure 3.18.

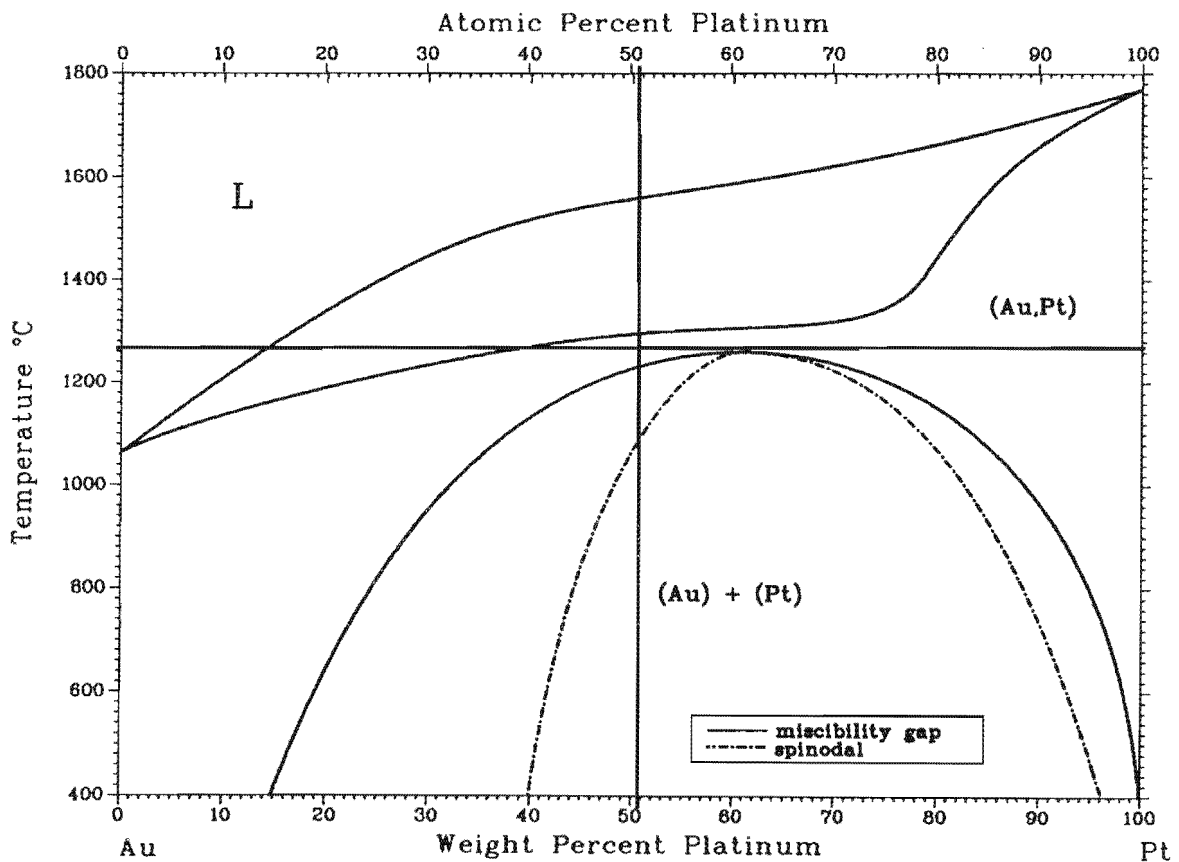


Figure 3.18. The solid solution heat treatment of the 50Au-50Pt alloy (ASM Handbook, Volume 3: Alloy Phase Diagrams, 1992)

The microstructure of the 50Au-50Pt alloy in the solutionised condition is shown in Figure 3.19. Only one phase (solid solution) can be observed and no significant porosity

was formed during solutionising in this case. The reason why spinodal alloys do not form Kirkendall porosity during solutionising is not clear. It may be that the Pt-rich areas were too small prior to solutionising to produce significant porosity (Compare the sizes of the Pt-rich areas in Figures 3.2 and 3.17 before solutionising).

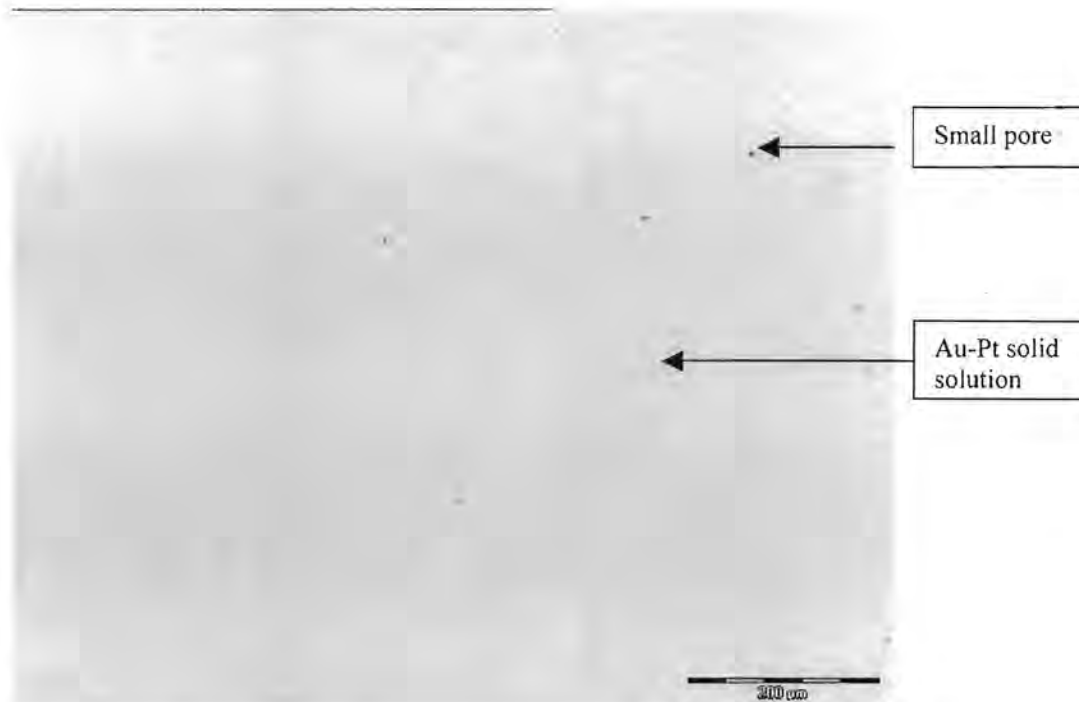


Figure 3.19. Optical photomicrograph of the 50Au-50Pt alloy in the solutionised condition.

3.4. The Gold 990 alloy

The metals were melted together (in the required ratio) in an arc-furnace with a water-cooled copper hearth under an argon protective atmosphere. The sample was turned around after each melt and re-melted three times to ensure homogeneity.

3.4.1. The Gold 990 alloy in the solid solution condition

Gold 990 samples were solutionised in air at 800°C for 1 hour (Figure 3.20). The samples were subsequently quenched in water and the brown tarnish layer removed mechanically.

The Vickers hardness (5kg load) of the material in this condition was found to be approximately 50 kg/mm².

3.4.2. The Gold 990 alloy in the precipitation-hardened condition

A solutionised Gold 990 sample was precipitation-hardened by a heat treatment in air at 500°C for 1 hour followed by quenching in water (Figure 3.20). The Vickers hardness value (5kg load) after the heat treatment was found to be 150 kg/mm². The increase in the hardness is due to the formation of nanosized Au₄Ti precipitates (Gafner, 1989).

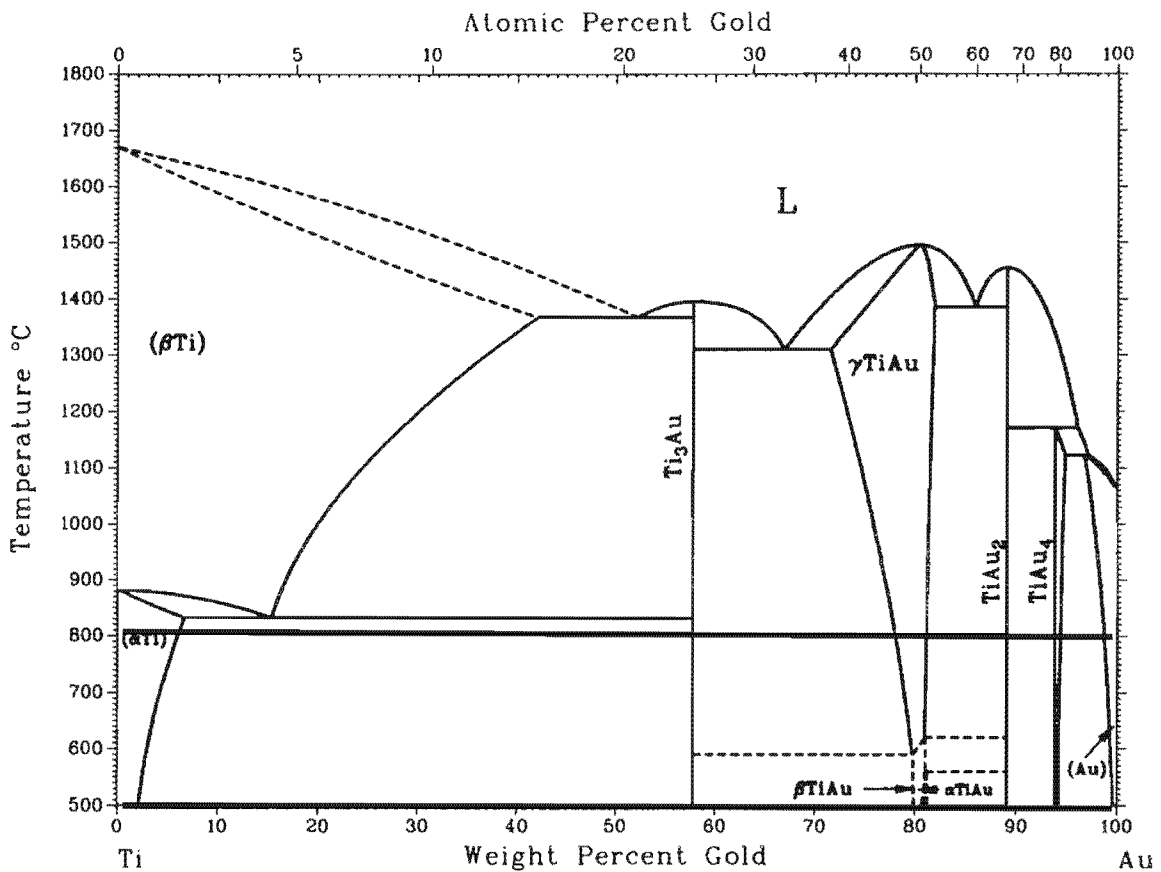


Figure 3.20. The Gold 990 alloy heat treatments (ASM Handbook, Volume 3: Alloy Phase Diagrams, 1992).

3.5. Conclusions

- The 60Au-40Pt alloy heat treated at 1300°C followed by water quenching has large Pt-rich areas in a Au-rich matrix.
- Solutionising of the 1300°C treated sample leads to the formation of Kirkendall porosity.
- The 60Au-40Pt alloy heat treated directly at 1200°C (without the intermediate 1300°C heat treatment) is brittle and cracked during cold rolling. A disc of this sample could therefore not be manufactured for electrochemical testing.
- Heterogeneous nucleation of Pt-rich areas occurs during the miscibility gap heat treatments of the 60Au-40Pt alloy.
- Spinodal decomposition occurs when a 50Au-50Pt alloy is heat treated in the miscibility gap. No significant Kirkendall porosity is found when this sample is solutionised.
- The Gold 990 alloy was heat treated to produce two different conditions: a solid solution and a precipitation-hardened condition.

This chapter indicated that different microstructures can be obtained in the Au-Pt alloys by varying the heat treatments of the samples. The Gold 990 alloy was heat treated to produce samples in the solid solution condition and the precipitation-hardened condition. The influence of the heat treatment condition of the samples on their electrochemical behaviour will be discussed in the following chapters.

Chapter 4

THE ELECTROCHEMICAL BEHAVIOUR OF GOLD-BASED ALLOYS IN ACID SOLUTION WITHOUT ETHYLENE GLYCOL

4.1. Introduction

The heat treatments of the gold-based alloys were discussed in the previous chapter. By employing different heat treatments, different microstructures could be produced in alloys with the same composition. The purpose of this chapter is to investigate the electrochemical behaviour of all the electrodes in acid solution without ethylene glycol. Cyclic voltammetry was used to study electrode surface oxidation, oxide reduction and the oxygen and hydrogen gas evolution reactions. In order to have a better understanding of the electrochemical behaviour of alloy electrodes, experiments were also conducted with gold and platinum electrodes.

4.2. Experimental

The experimental work was performed with polycrystalline gold (99.9%), platinum (99.9%), 60Au-40Pt, 50Au-50Pt and Gold 990 electrodes. The electrodes were disc-shaped with 6mm diameter. All the electrodes were mounted in a resin by using a black phenolic thermosetting powder. Electrical contact was achieved by drilling a hole through the rear of the mounting and tapping M6 thread. A Pine analytical rotator was used as electrode rotator. The apparent surface area of 0.28 cm² was used in all cases to calculate current densities. The higher real surface areas of the porous electrodes are expected to give higher apparent current densities than the non-porous electrodes. This will give an indication on how the porosity of these electrodes will influence their electrochemistry.

A water-jacketed perspex electrochemical cell was used for all the experiments. The cell had an inside diameter of 90 mm and a height of 100 mm. Approximately 400 ml electrolyte was used. The distance between the working electrode and the bottom of the cell was about 60 mm. The temperature was controlled at 25°C. The cover of the perspex

cell had six openings which allowed the insertion of two counter electrodes, the working electrode, the Luggin capillary, the tube for nitrogen purging and a thermometer.

The experiments were conducted in 0.5 M H₂SO₄ solution. The solution was prepared by using CP grade H₂SO₄ from Chemical Suppliers (Pty) Ltd and double distilled water. Prior to each experiment, the solution was purged with nitrogen for 30 minutes to remove dissolved oxygen. The electrodes were polished before the experiments with diamond paste (down to 1 μm) and ultrasonically cleaned in 0.5 M H₂SO₄.

A Solartron 1287 Electrochemical Interface was used for the cyclic voltammetry experiments. The electrode potential was cycled between the values for onset of O₂ and H₂ evolution until the I-E curves were reproducible. It was found that approximately 15 cycles are needed to obtain reproducible I-E curves. The fifteenth cycle is used in all cyclic voltammograms shown in this chapter. The scan rate employed was 50 mV/s. The electrochemical experiments in acid solution without ethylene glycol were conducted without rotating the electrodes or stirring the solution. Platinum wire was used as counter electrode. All potentials quoted in this study are with respect to the silver/silver chloride reference electrode (SSC). Electrochemical impedance spectroscopy was performed with a Solartron 1250 Frequency Response Analyser.

4.3. Results and discussion

4.3.1. Gold

Cyclic voltammograms for gold are shown in Figure 4.1. These voltammograms agree well with those found in the literature (Fig. 2.1). Monolayer oxide formation commences at 1.05 V_{SSC} during the positive sweep followed by oxygen gas evolution at higher potentials. The surface oxide is reduced at 0.9 V_{SSC} during the negative sweep. More oxide is formed during the positive sweep when a higher upper potential limit is used. This results in a larger oxide reduction peak during the subsequent negative sweep. The potential for the oxide reduction peak is then also shifted to slightly more negative potentials (Fig. 4.1).

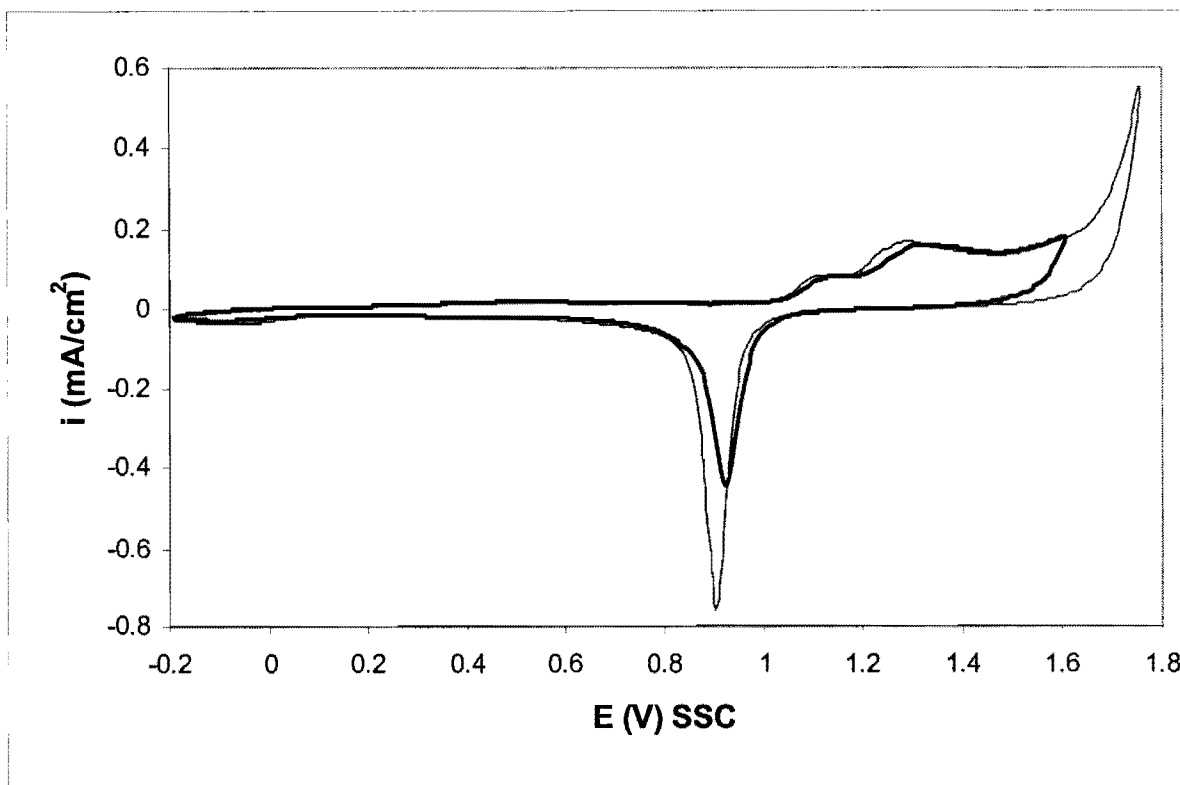


Figure 4.1. Cyclic voltammograms for gold in 0.5 M H_2SO_4 . Scan rate 50 mV/s, 25°C.

4.3.2. Platinum

A cyclic voltammogram for platinum is shown in Figure 4.2. This voltammogram agrees well with those found in the literature (Fig. 2.9). Hydrogen desorption/adsorption occurs in the region of -0.2 to $0.1 V_{SSC}$. Surface oxidation commences at approximately $0.55 V_{SSC}$. The surface oxide is reduced during the negative sweep at $0.5 V_{SSC}$.

Cyclic voltammograms for platinum with different upper potential limits (1.4 and $1.6 V_{SSC}$) are shown in Figure 4.3. The higher upper potential limit leads to a much larger oxide reduction peak because more oxide is formed with a high upper potential limit. The peak is also shifted significantly to more negative potentials. Possibly some PtO_2 is formed with the high upper potential limit and only PtO with the low upper potential limit (Xia and Birss, 2000).

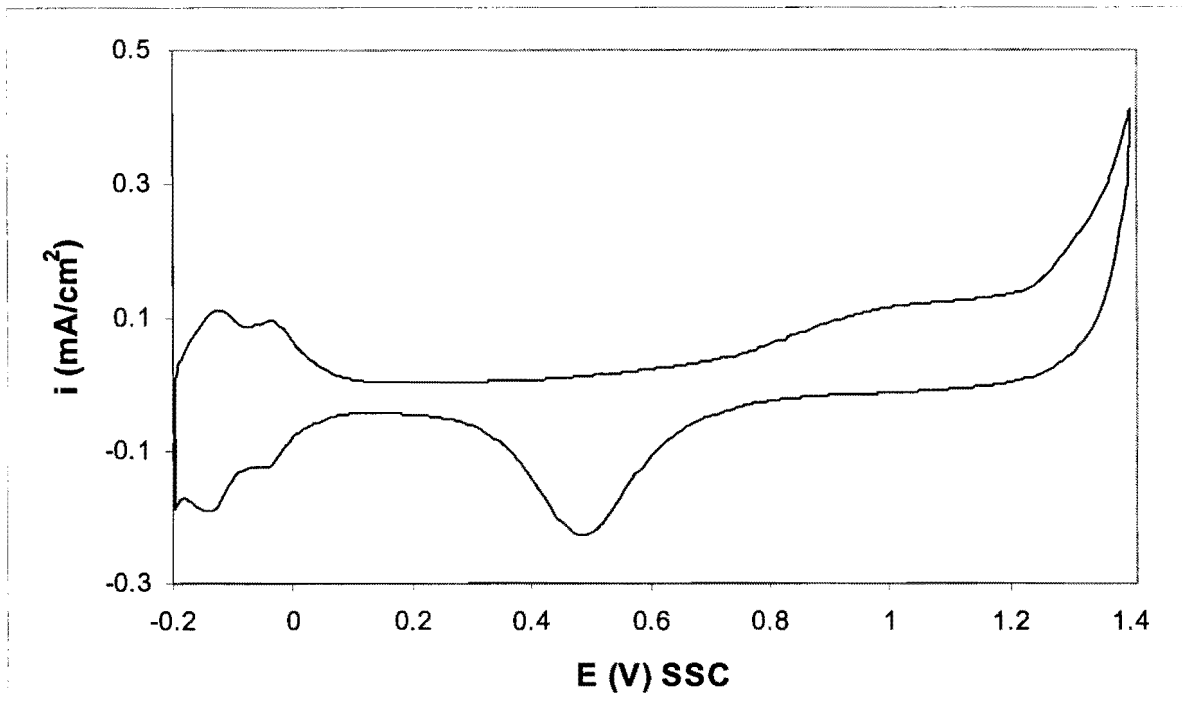


Figure 4.2. Cyclic voltammogram for platinum in 0.5 M H_2SO_4 . Scan rate 50 mV/s, 25°C.

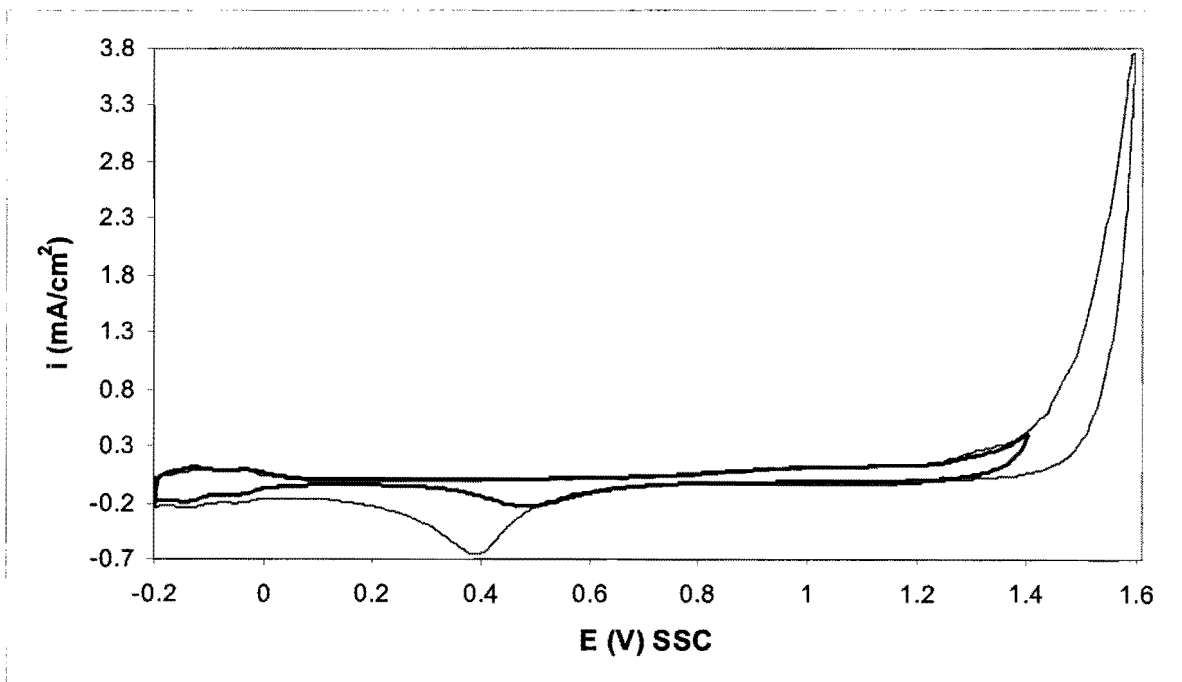


Figure 4.3. Cyclic voltammograms for platinum in 0.5 M H_2SO_4 . Scan rate 50 mV/s, 25°C.

Cyclic voltammograms for gold and platinum with the same upper potential limit ($E_{up} = 1.5$ V) are shown in Figure 4.4. It is seen that oxygen gas evolution occurs at lower potentials on platinum than on gold. The lack of a hydrogen adsorption/desorption region on gold is also evident. A larger oxide reduction peak is found for platinum than gold. This is due to the fact that surface oxide formation commences at lower potentials on platinum.

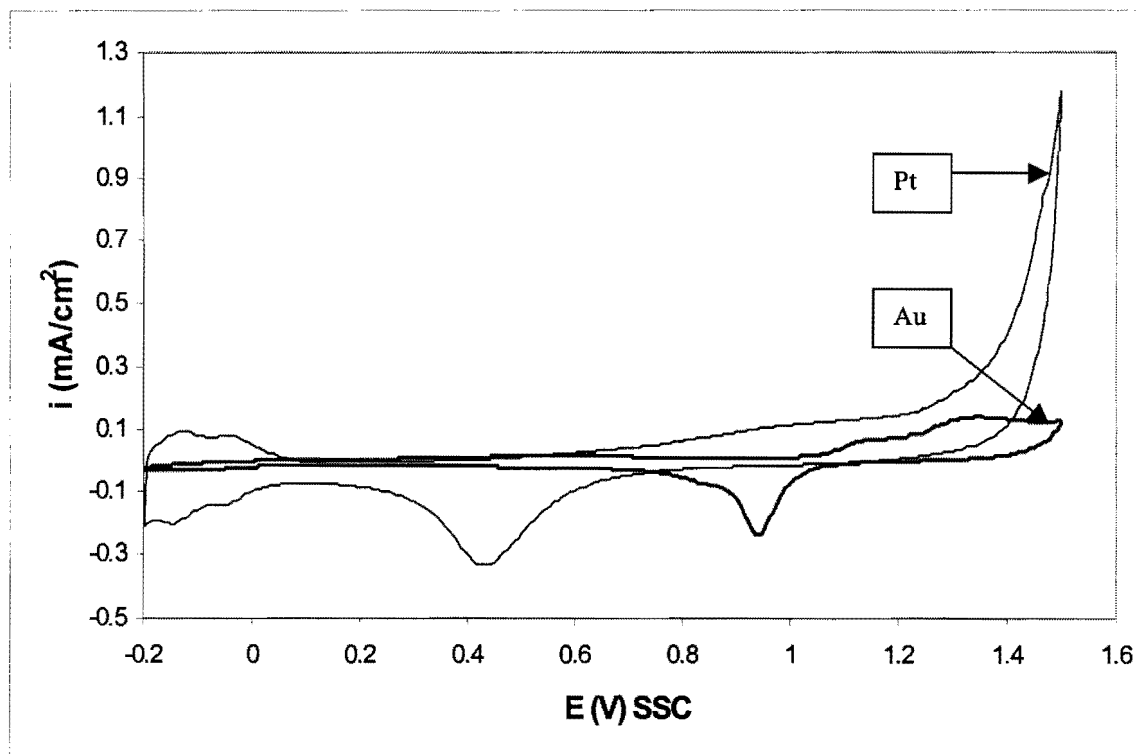


Figure 4.4. Cyclic voltammograms for platinum and gold in 0.5 M H_2SO_4 . Scan rate 50 mV/s, 25°C. $E_{up} = 1.5$ V.

4.3.3. The 60Au-40Pt alloy

4.3.3.1. The 60Au-40Pt alloy in the 1300°C heat treatment condition

The two-phased microstructure of this alloy is shown in Figure 3.2. Cyclic voltammograms for the 1300°C treated electrode are shown in Figure 4.5 and features corresponding to both pure gold and platinum can be seen. The alloy has a hydrogen adsorption/desorption region (-0.2 to 0.1 V_{SSC}). Two oxide reduction peaks are found. The one peak corresponds to that of platinum and the other to gold. An increase in the upper potential limit causes an increase in the oxide reduction peaks and the peaks are shifted in the negative direction. The effect is more pronounced with the platinum (or platinum-rich) oxide reduction peak than with the gold (or gold-rich) oxide reduction peak. The current density for oxygen gas evolution at 1.6 V_{SSC} is higher than on pure gold, but lower than on pure platinum.

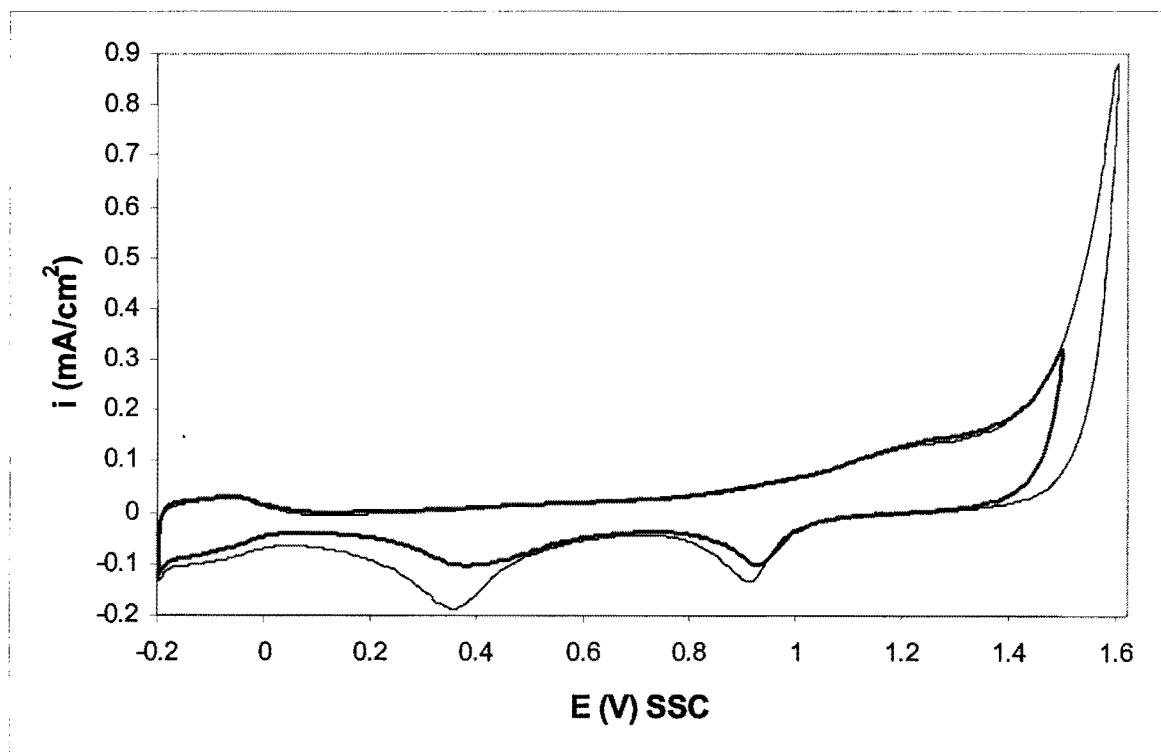


Figure 4.5. Cyclic voltammograms for the 1300°C heat treated sample (60Au-40Pt) in 0.5 M H₂SO₄. Scan rate 50 mV/s, 25°C.

4.3.3.2. The 60Au-40Pt alloy in the 1200°C (24 hours) heat treatment condition

The microstructure of this single-phased, but porous sample is shown in Figure 3.6. The sample was in the 1300°C treated condition prior to the heat treatment at 1200°C for 24 hours. Cyclic voltammograms for this electrode are shown in Figure 4.6. The apparent current densities obtained with this electrode are very high due to the porosity (the apparent surface area is used to calculate current density). Another interesting feature of the cyclic voltammograms is that two oxide reduction peaks are observed, even though the electrode is a solid solution of platinum in gold. The oxide reduction peaks occur at slightly more negative potentials than on the pure metals. Woods (1971) also found that gold-platinum solid solutions had two oxide reduction peaks. If one considers the mechanism of platinum oxide formation (Fig. 2.5), it is difficult to understand how platinum atoms surrounded by gold atoms can have an oxide reduction peak in the same potential region as pure platinum. The same applies to gold atoms that are surrounded by platinum atoms in a solid solution.

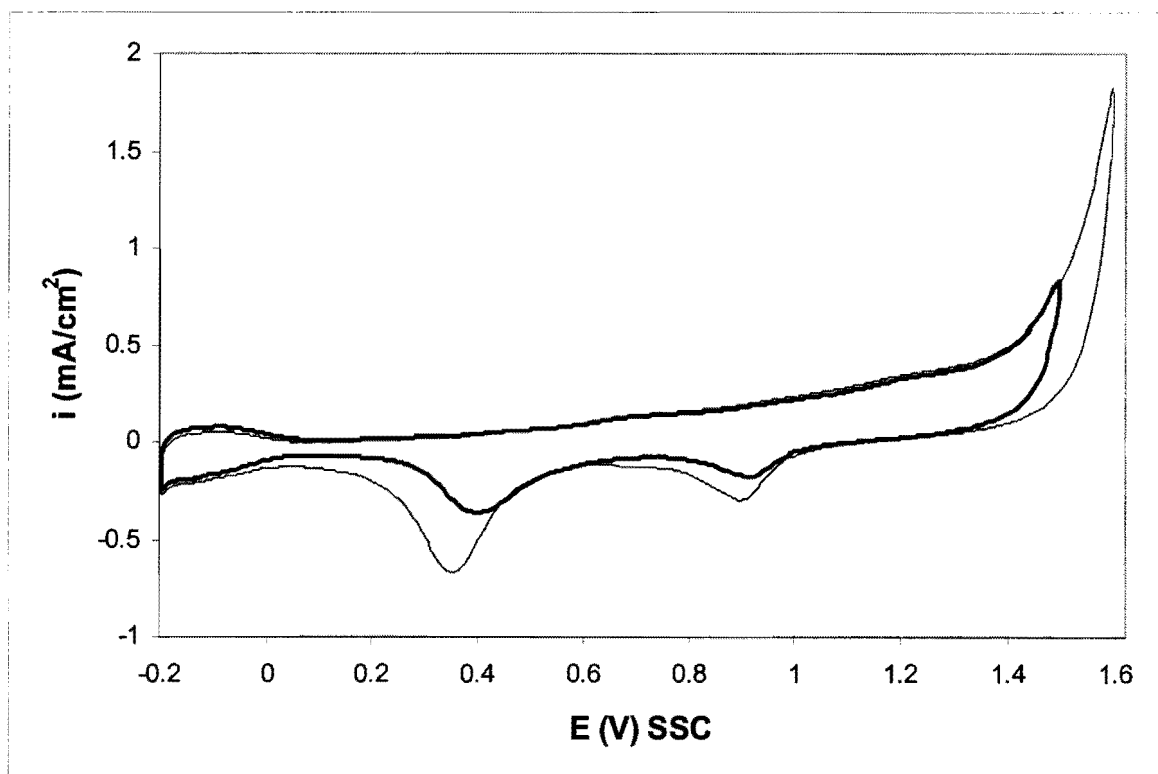


Figure 4.6. Cyclic voltammograms for the 1200°C- 24 hour heat treated sample (60Au-40Pt) in 0.5 M H_2SO_4 . Scan rate 50 mV/s, 25°C.

Cyclic voltammograms for the non-porous 1300°C treated sample and the porous 1200°C sample heat treated for 24 hours are shown in Figure 4.7. From the increased apparent current density, it is clear that the porosity increases the surface area significantly.

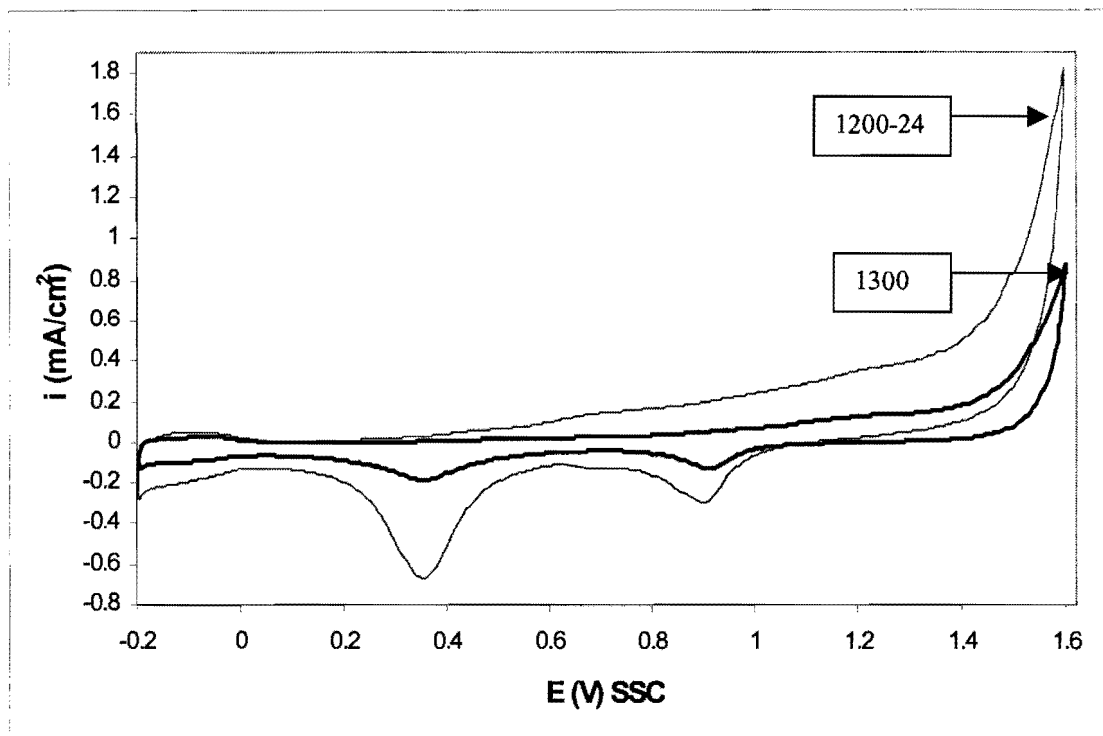


Figure 4.7. Cyclic voltammograms for the 1300°C heat treated sample and the 1200°C – 24 hour heat treated sample (60Au-40Pt) in 0.5 M H₂SO₄. Scan rate 50 mV/s, 25°C.

4.3.3.3. The 60Au-40Pt alloy in the 1200°C (168 hours) heat treatment condition

The microstructure of this sample is shown in Figure 3.8. The sample was in the 1300°C treated condition prior to the heat treatment at 1200°C for 168 hours. Cyclic voltammograms for this electrode are shown in Figure 4.8. Two oxide reduction peaks are also found for this solutionised sample.

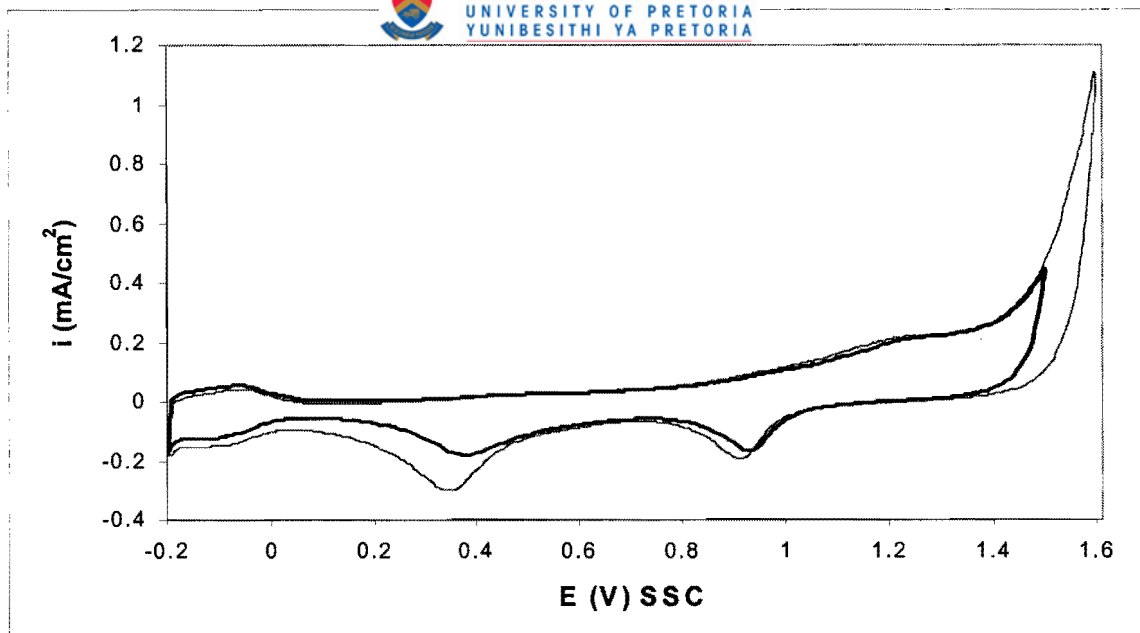


Figure 4.8. Cyclic voltammograms for the 1200°C – 168 hour heat treated sample (60Au-40Pt) in 0.5 M H₂SO₄. Scan rate 50 mV/s, 25°C.

The porosity of the sample heat treated for 168 hours appears to be less than for the sample heat treated for 24 hours (Figures 3.6 and 3.8). The same conclusion is reached when the cyclic voltammograms of the two samples are compared (Fig. 4.9), since the apparent current density is lower for the sample which received the longer heat treatment.

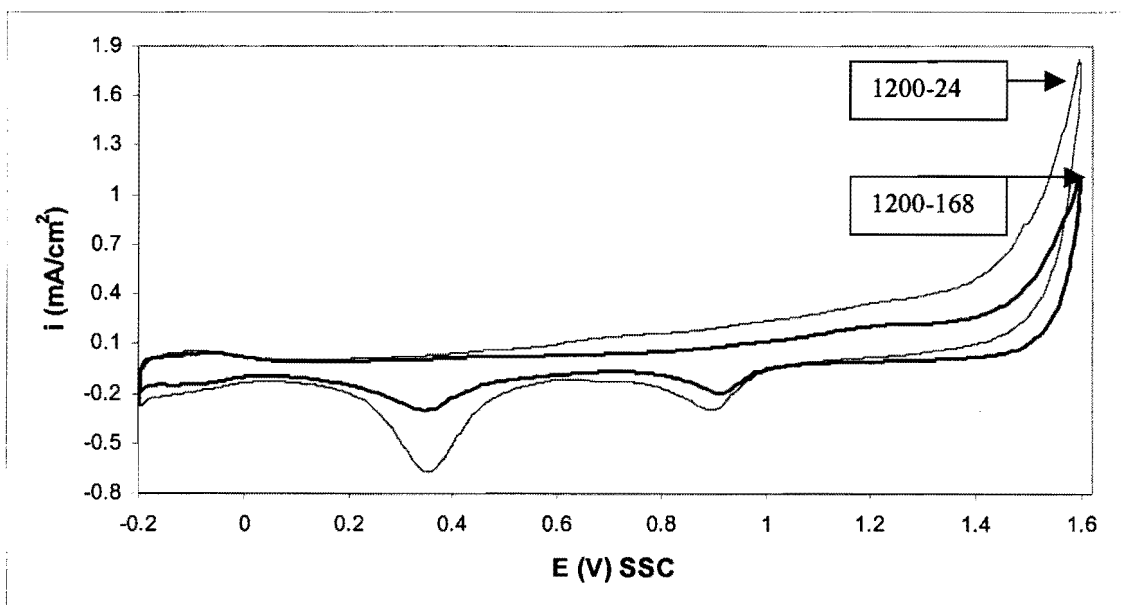


Figure 4.9. Cyclic voltammograms for the 1200°C heat treated samples (60Au-40Pt) in 0.5 M H₂SO₄. Scan rate 50 mV/s, 25°C.

Electrochemical Impedance Spectroscopy (EIS) can be used to compare surface areas of electrodes. An electrochemical double layer is formed at the interface between an electrode and an electrolyte at a given potential. In the absence of faradaic reactions, smooth and clean surfaces show ideal capacitive behaviour as described by (Song et al., 2000):

$$Z = 1/(j\omega C_d) \quad (1)$$

where the double layer capacitance C_d is independent of frequency (ω is the angular frequency). The ideal behaviour is represented as a vertical line in the Nyquist plot of impedance. However, the impedance of solid electrodes deviates from the purely capacitive behaviour. This causes a deviation of the vertical line in the Nyquist plot by a constant angle α , which falls in the range 0° - 45° . For ideally smooth electrodes α should be 0° , whereas for extremely rough or porous surfaces, α should be close to 45° (Song et al., 2000).

The non-ideality or frequency dispersion (the term “frequency dispersion” indicates that the apparent capacitance is a function of the frequency, which is not the case for an ideal capacitor) has been described by the constant phase element (CPE) (Rammelt and Reinhard, 1990). The impedance of the CPE can be written as:

$$Z = 1/[(T(j\omega))^n] \quad (2)$$

where n is the roughness parameter (ranges between 0.5 and 1). $T = C_d$ only if $n=1$. T is expressed in units of farads per square centimetre per second to the power n .

n can be related to α by:

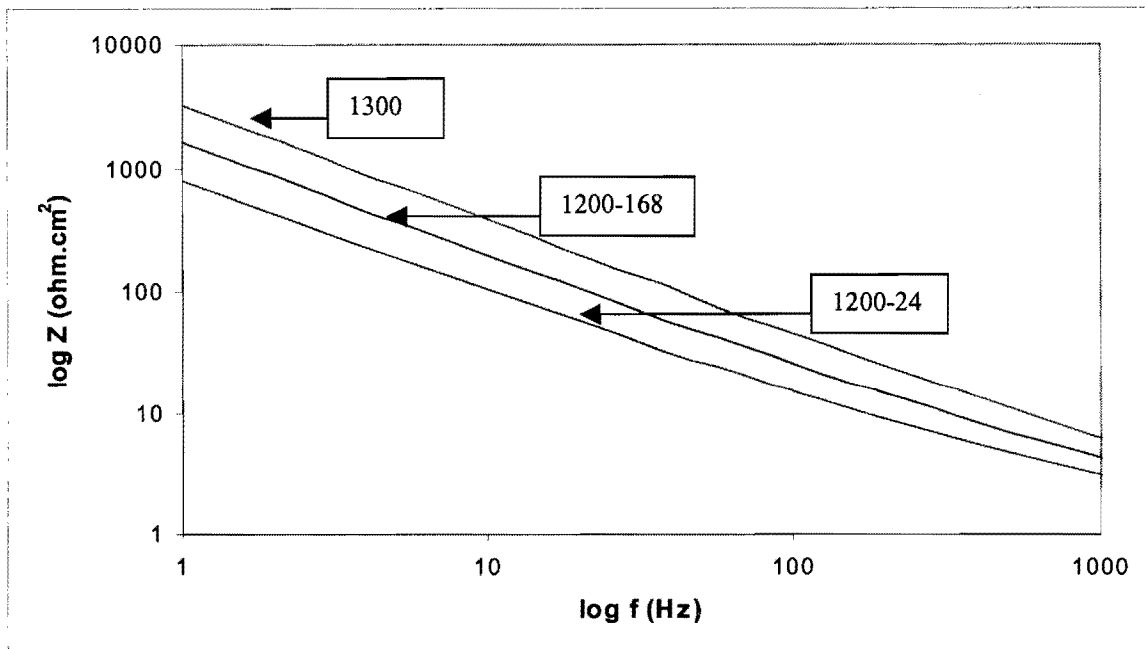
$$\alpha = (1-n)90^\circ \quad (3)$$

The CPE element can be caused by several effects (Song et al., 2000): diffusion in a diffusion-limited system, geometric factors, sluggish processes such as adsorption of anions, surface reconstruction and transformation in adlayer, and crystallographic heterogeneity.

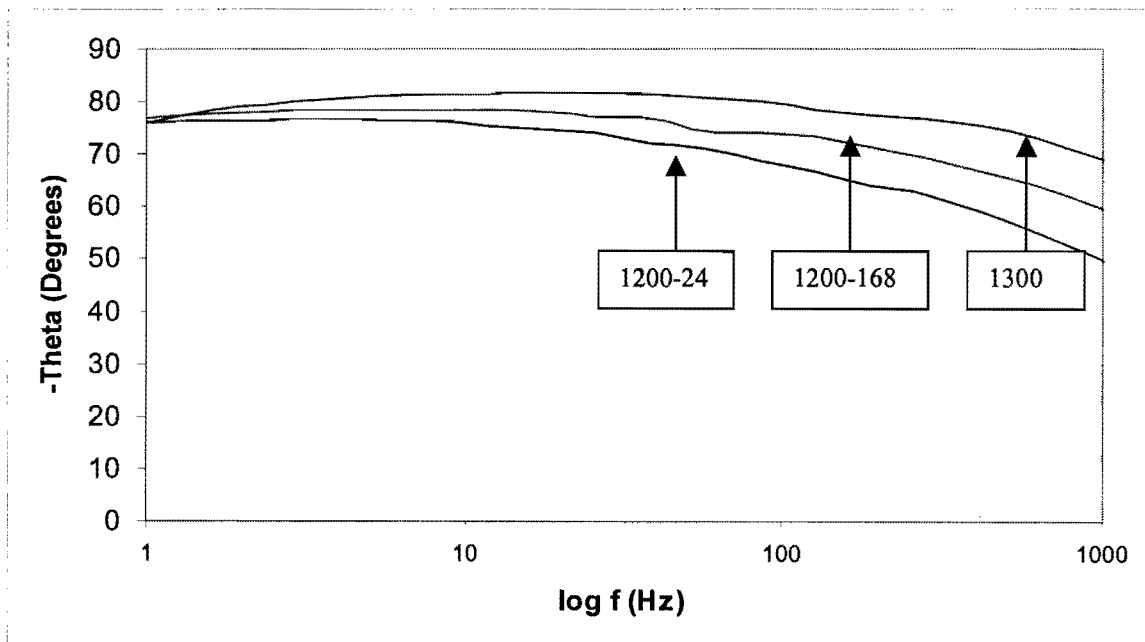
In cases of highly porous electrodes, geometric factors are the most important among the origins of frequency dispersion in the absence of faradaic reactions.

In Figure 4.10(a), the impedance as a function of frequency is shown for the 60Au-40Pt electrodes. Impedance spectroscopy was performed in 0.5 M H_2SO_4 at a potential of 0.1 V_{SSC} . This potential was chosen because the current at the electrode will then be a

minimum and reactions occurring at the electrode surface will be avoided. The phase angle (θ) as a function of the frequency is shown in Figure 4.10(b).



(a)



(b)

Figure 4.10. (a) Impedance spectroscopy at $0.1 V_{SSC}$ for the 60Au-40Pt samples in $0.5 M H_2SO_4$; (b) the phase angle over the same frequency range.

The phase angles were fairly constant over the frequency range, dropping to lower values at higher frequencies (Fig. 4.10b). Purely capacitive behaviour is represented by a θ of -90° . A low Z value corresponds to a high surface area in the frequency range where the capacitance dominates the impedance. The phase angles in Figure 4.10(b) show that the capacitance dominated the impedance over most of this frequency range. Figure 4.10 confirms that the sample heat treated at 1200°C for 24 hours has a higher surface area than the sample heat treated for 168 hours. Both porous samples have higher surface areas than the non-porous 1300°C heat treated sample, as expected.

4.3.3.4. The 60Au-40Pt alloy in the 800°C heat treatment condition

The microstructure of this sample is shown in Figure 3.12. The sample was in the 1200°C -24h (porous, single-phased) heat treated condition prior to the heat treatment at 800°C for 50 hours. Cyclic voltammograms for this electrode are shown in Figure 4.11. The current densities of this sample are slightly higher than the solutionised sample heat treated at 1200°C for 24 hours. This suggests that the heat treatment at 800°C resulted in additional porosity or the linking up of the porosity already present before the heat treatment.

4.3.3.5. The 60Au-40Pt alloy in the 600°C heat treatment condition

The microstructure of this sample is shown in Figure 3.15. The sample was in the 1200°C -24h (porous, single-phased) heat treated condition prior to the heat treatment at 600°C for 100 hours. Cyclic voltammograms for this electrode are shown in Figure 4.12. The most notable feature of Figure 4.12 is the very high apparent current densities due to oxygen gas evolution. The equilibrium composition of the platinum-rich areas in this sample is 98Pt-2Au (Table 3.1). The fact that these areas are nearly pure platinum may explain the low oxygen gas evolution potential.

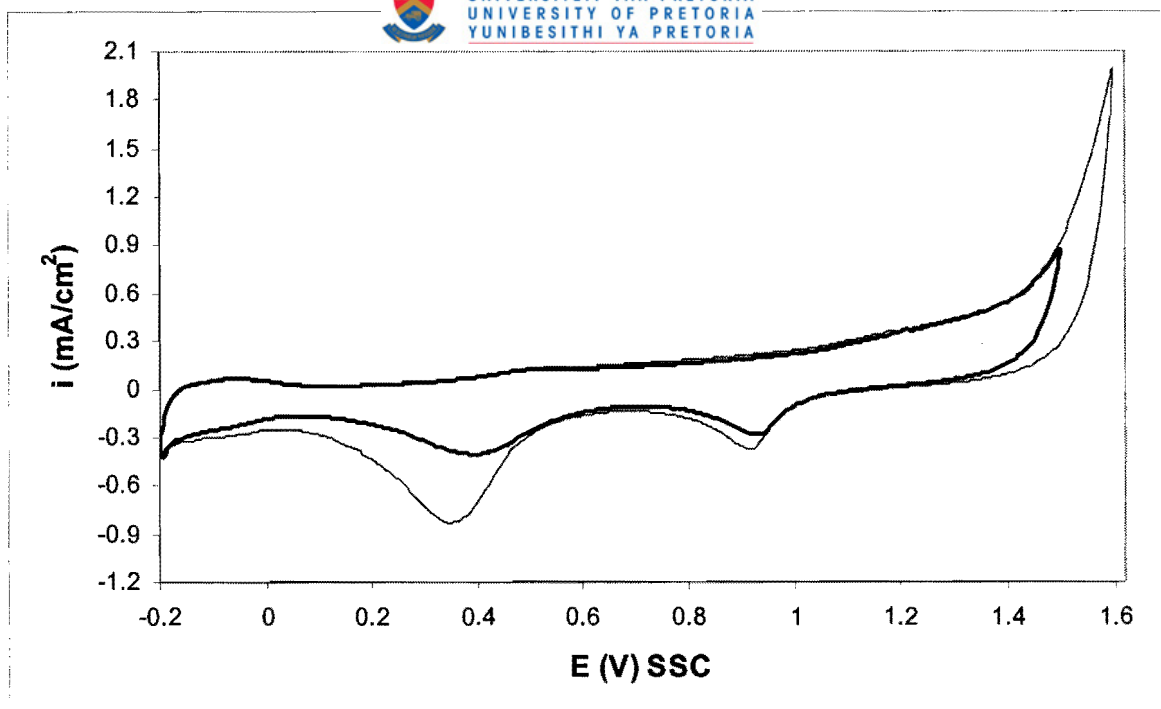


Figure 4.11. Cyclic voltammograms for the 800°C heat treated sample (60Au-40Pt) in 0.5 M H₂SO₄. Scan rate 50 mV/s, 25°C.

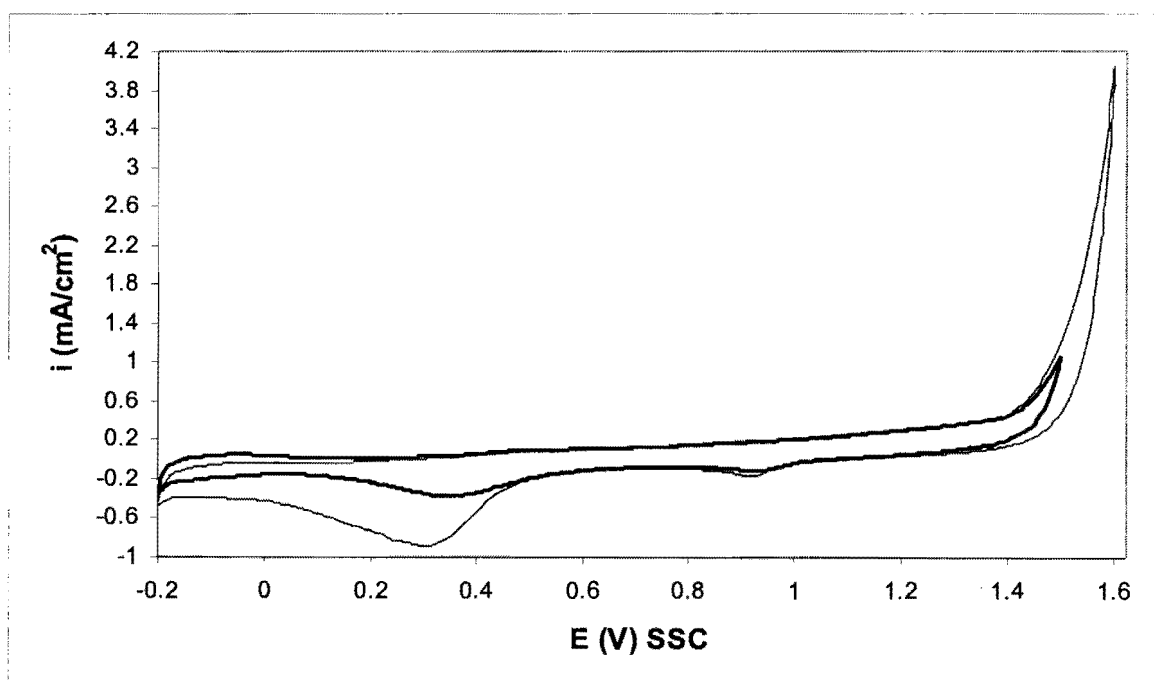


Figure 4.12. Cyclic voltammograms for the 600°C heat treated sample (60Au-40Pt) in 0.5 M H₂SO₄. Scan rate 50 mV/s, 25°C.

The equilibrium gold content of the platinum-rich phase in the 800°C heat treated sample is higher than that of the 600°C heat treated sample (Table 3.1). This causes the oxygen gas evolution reaction on the 800°C treated sample to be inhibited more than on the 600°C heat treated sample (Fig. 4.13).

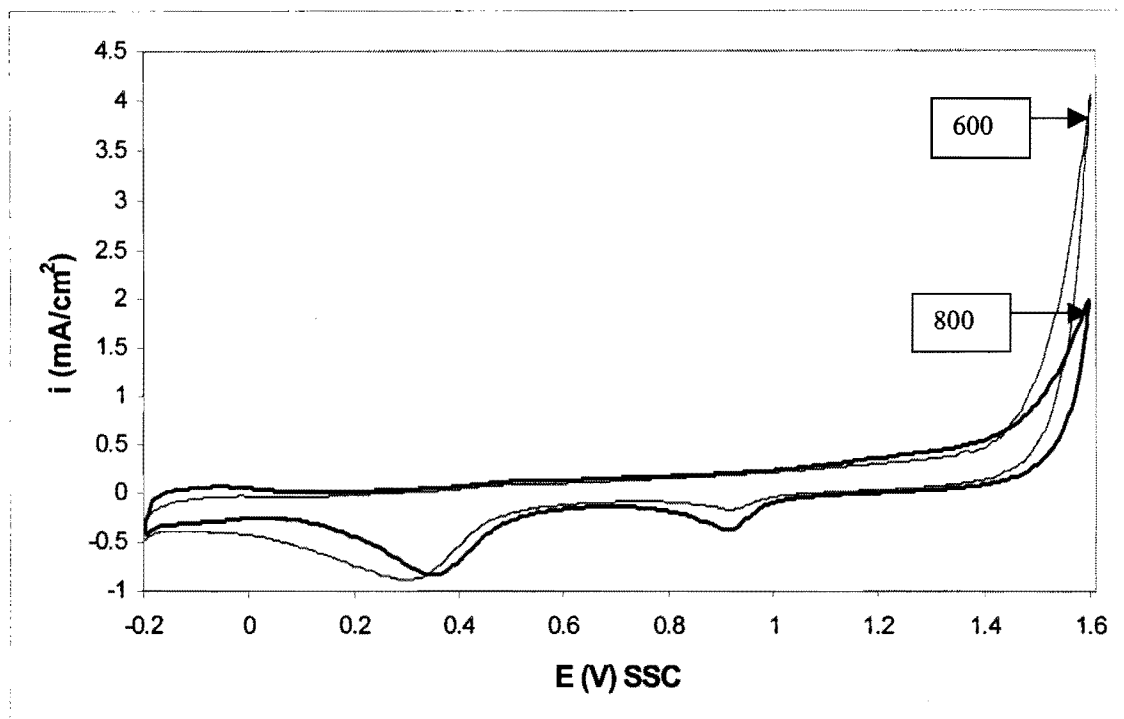


Figure 4.13. Cyclic voltammograms for the miscibility gap heat treated samples (60Au-40Pt) in 0.5 M H_2SO_4 . Scan rate 50 mV/s, 25°C.

4.3.4. The 50Au-50Pt alloy

4.3.4.1. The 50Au-50Pt alloy in the “ductile” condition

The microstructure (two-phased, fine microstructure) of this sample is shown in Figure 3.17. Cyclic voltammograms for this electrode are shown in Figure 4.14. The current densities obtained on the ductile 50Au-50Pt sample are similar to the 60Au-40Pt electrode in the 1300°C (two-phased, coarse microstructure) heat treatment condition (Fig. 4.5).

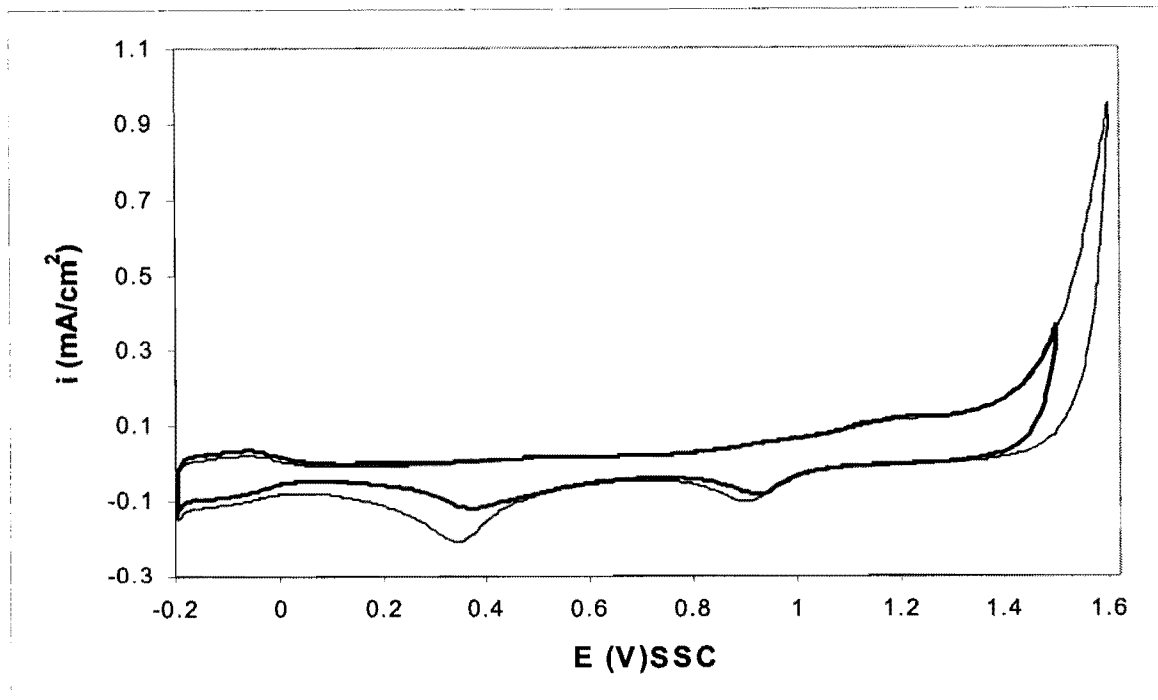


Figure 4.14. Cyclic voltammograms for the “ductile” heat treated sample (50Au-50Pt) in 0.5 M H_2SO_4 . Scan rate 50 mV/s, 25°C.

4.3.4.2. The 50Au-50Pt alloy in the solid solution condition

The microstructure of this sample (single-phased, non-porous) is shown in Figure 3.19. Cyclic voltammograms for this electrode are shown in Figure 4.15. As was the case with the solutionised 60Au-40Pt electrodes, this sample also has two oxide reduction peaks.

Kirkendall porosity was not found in the sample after the solid solution heat treatment, and it can be seen that the two 50Au-50Pt samples have similar current densities (Fig. 4.16). The oxygen gas evolution reaction is inhibited on the solid solution sample compared to the ductile (two-phased) sample. If one considers the two temperature limits that were used for the “ductile” heat treatment (Fig. 3.16), it is seen that the Pt-rich areas of this sample have an equilibrium gold content of 5 to 10 %. The platinum atoms in the Pt-rich phase of this sample are therefore surrounded by fewer gold atoms than the platinum atoms in the solid solution sample. This results in oxygen evolution at a lower overpotential at the “ductile” sample.

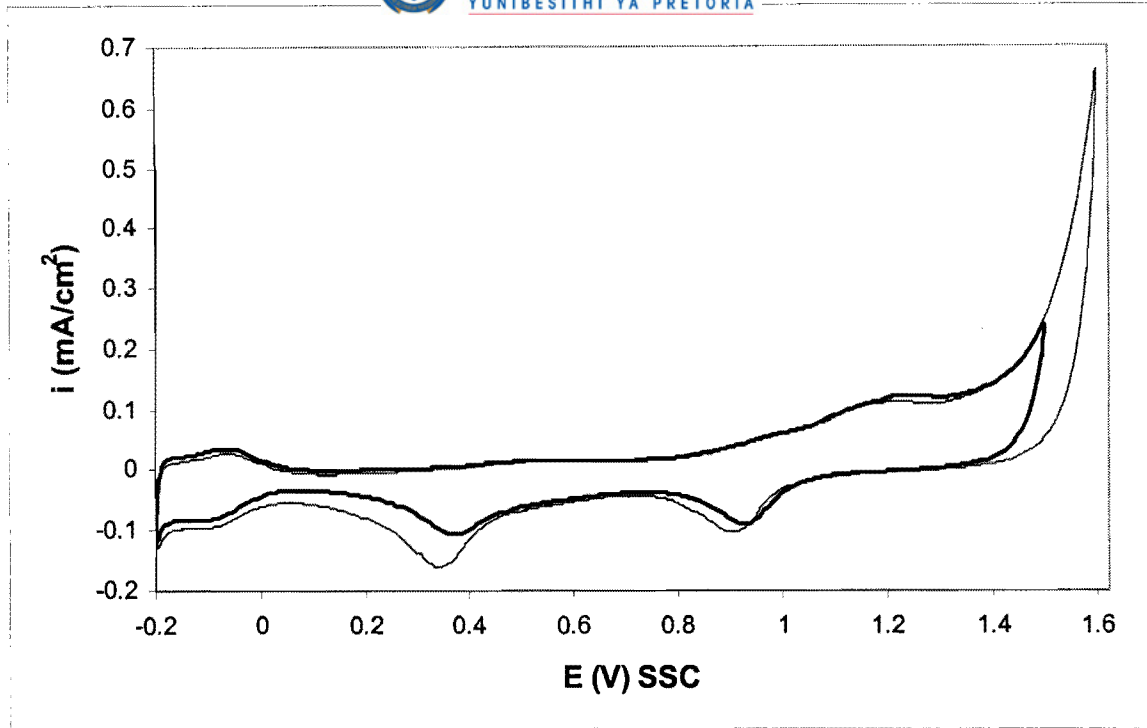


Figure 4.15. Cyclic voltammograms for the solutionised sample (50Au-50Pt) in 0.5 M H_2SO_4 . Scan rate 50 mV/s, 25°C.

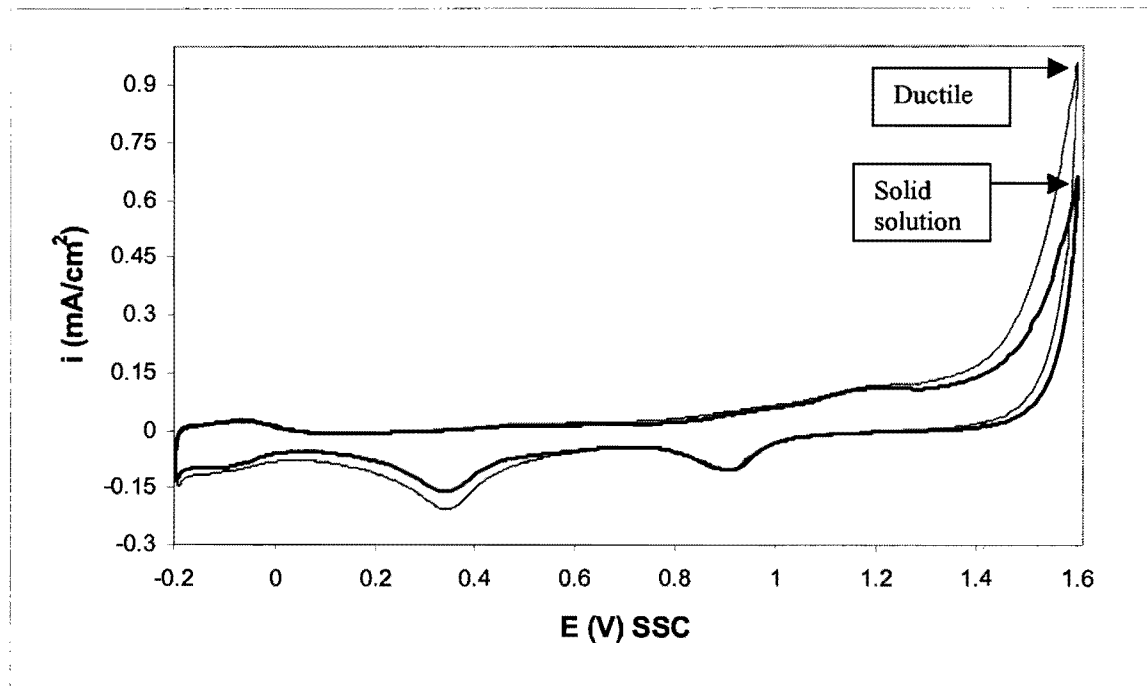


Figure 4.16. Cyclic voltammograms for the 50Au-50Pt samples in 0.5 M H_2SO_4 . Scan rate 50 mV/s, 25°C.

Impedance spectroscopy was performed in 0.5 M H₂SO₄ at a potential of 0.1 V_{SSC}. In Figure 4.17(a), the impedance as a function of frequency is shown for the 50Au-50Pt electrodes. The phase angle (θ) as a function of the frequency is shown in Figure 4.17(b). The 60Au-40Pt sample in the 1300°C heat treatment condition is included for comparison. Figure 4.17 shows that the surface areas of the 50Au-50Pt electrodes are similar. This confirms that Kirkendall porosity was not formed during the solid solution heat treatment. The impedance of the 60Au-40Pt sample in the 1300°C heat treatment condition is also similar to the 50Au-50Pt alloy electrodes. This implies that the impedance of Au-Pt alloys in 0.5 M H₂SO₄ at a potential of 0.1 V_{SSC} is not influenced much by composition, but rather by the surface area.

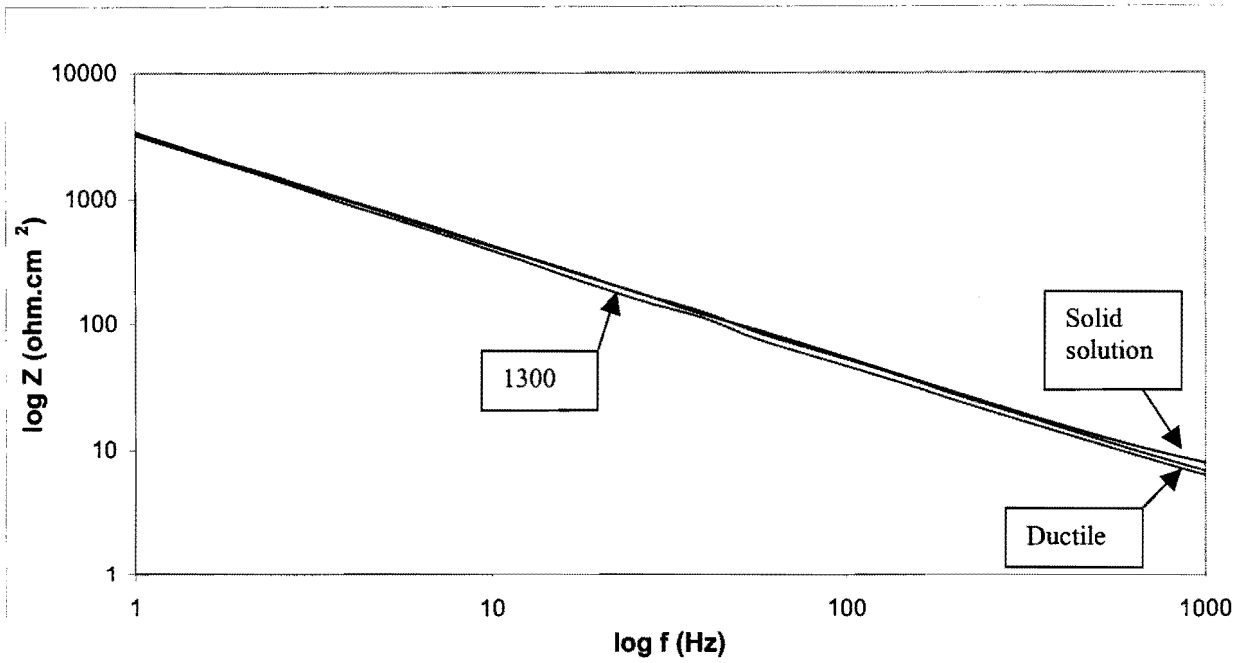
4.3.5. The Gold 990 alloy

4.3.5.1. The Gold 990 alloy in the solid solution condition

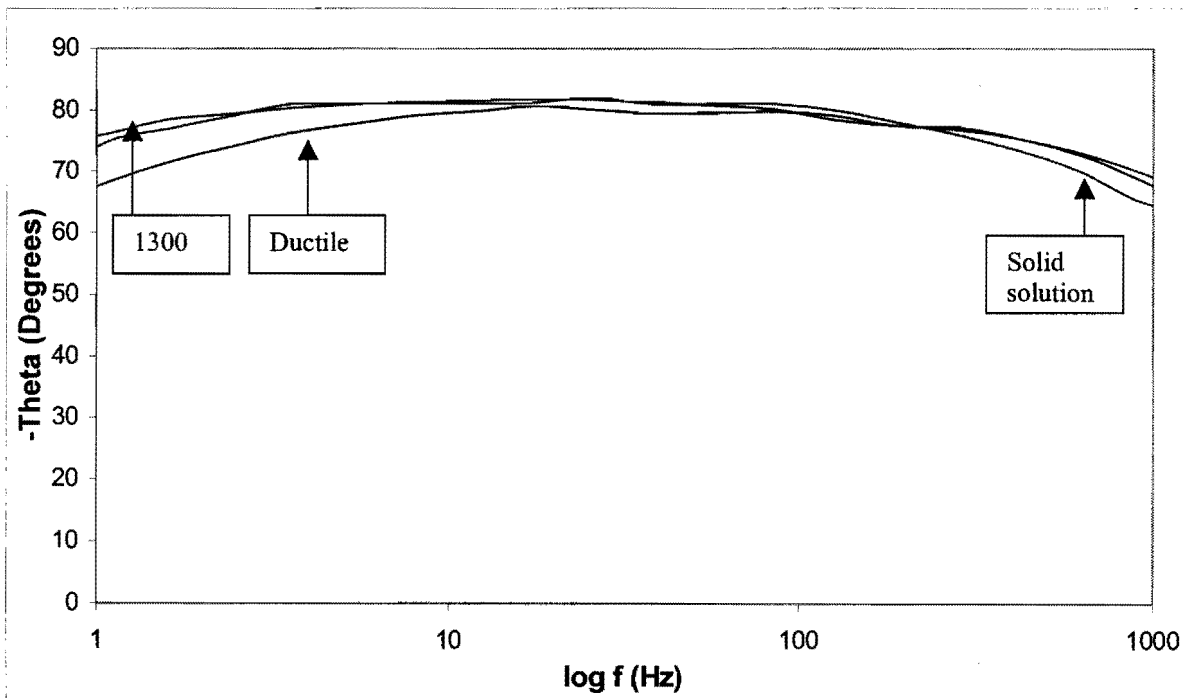
This sample has 1 wt% (4 at%) titanium in solid solution with the gold. The Vickers hardness of the sample in this condition is HV₅ = 50 kg/mm². Cyclic voltammograms for this sample are shown in Figure 4.18. The behaviour of Gold 990 in the solid solution condition is similar to pure gold (Fig. 4.1).

4.3.5.2. The Gold 990 alloy in the precipitation-hardened condition

This sample is hardened by the presence of small Au₄Ti precipitates. The Vickers hardness of the sample in this condition is HV₅ = 150 kg/mm². Cyclic voltammograms for this sample are shown in Figure 4.19. The behaviour of Gold 990 in the precipitation-hardened condition is also similar to pure gold (Fig. 4.1).



(a)



(b)

Figure 4.17. (a) Impedance spectroscopy at $0.1 V_{SSC}$ for the 50Au-50Pt samples in $0.5 M H_2SO_4$; (b) the phase angle over the same frequency range. The $1300^\circ C$ heat treated sample (60Au-40Pt) is included for comparison.

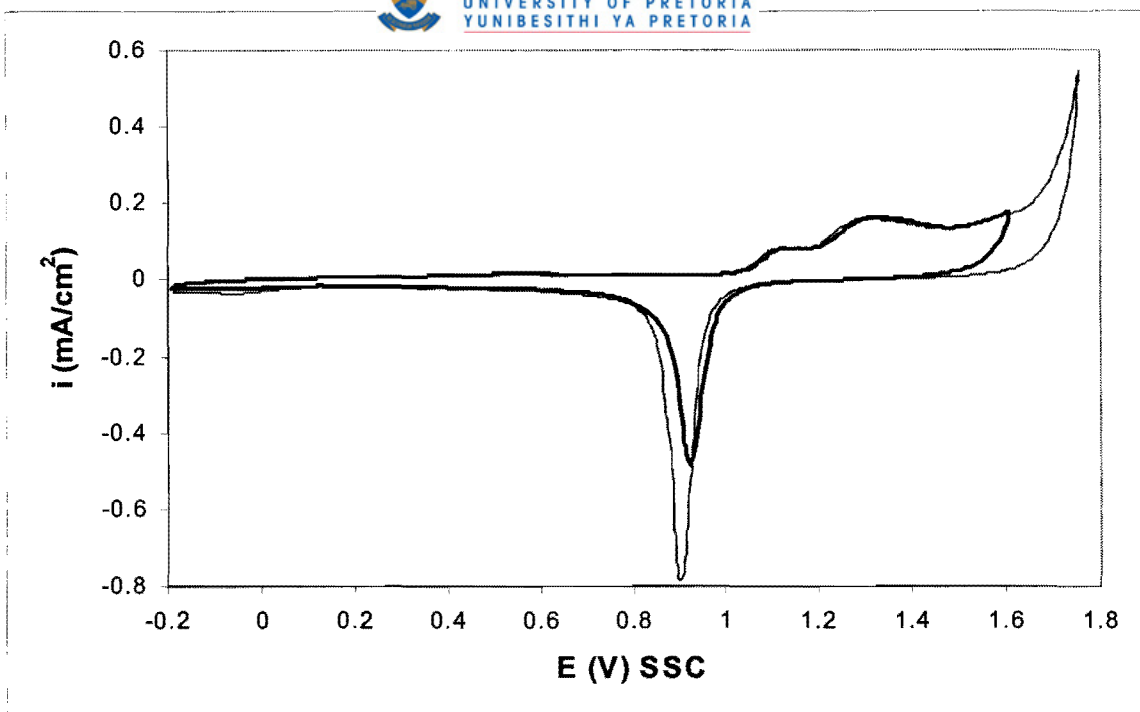


Figure 4.18. Cyclic voltammograms for the Gold 990 sample in the solid solution condition in 0.5 M H₂SO₄. Scan rate 50 mV/s, 25°C.

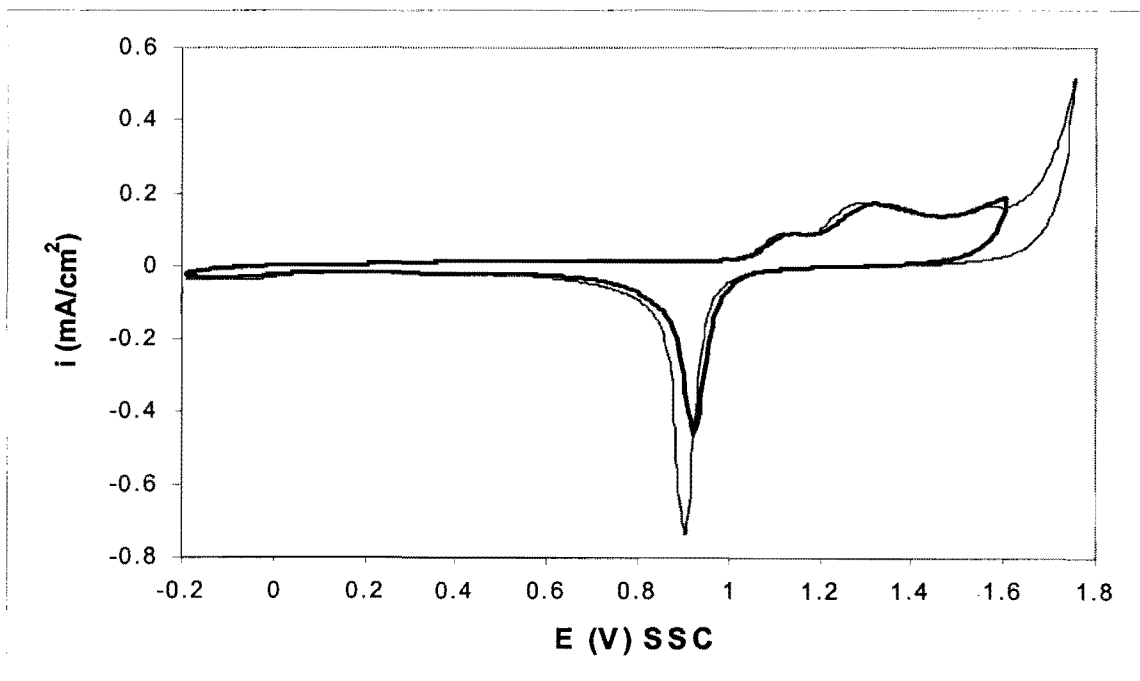


Figure 4.19. Cyclic voltammograms for the Gold 990 sample in the precipitation hardened condition in 0.5 M H₂SO₄. Scan rate 50 mV/s, 25°C.

The cyclic voltammograms for the two Gold 990 electrodes and pure gold are compared in Figure 4.20. The cyclic voltammograms of the three electrodes are similar to such a degree that they are difficult to distinguish in Figure 4.20.

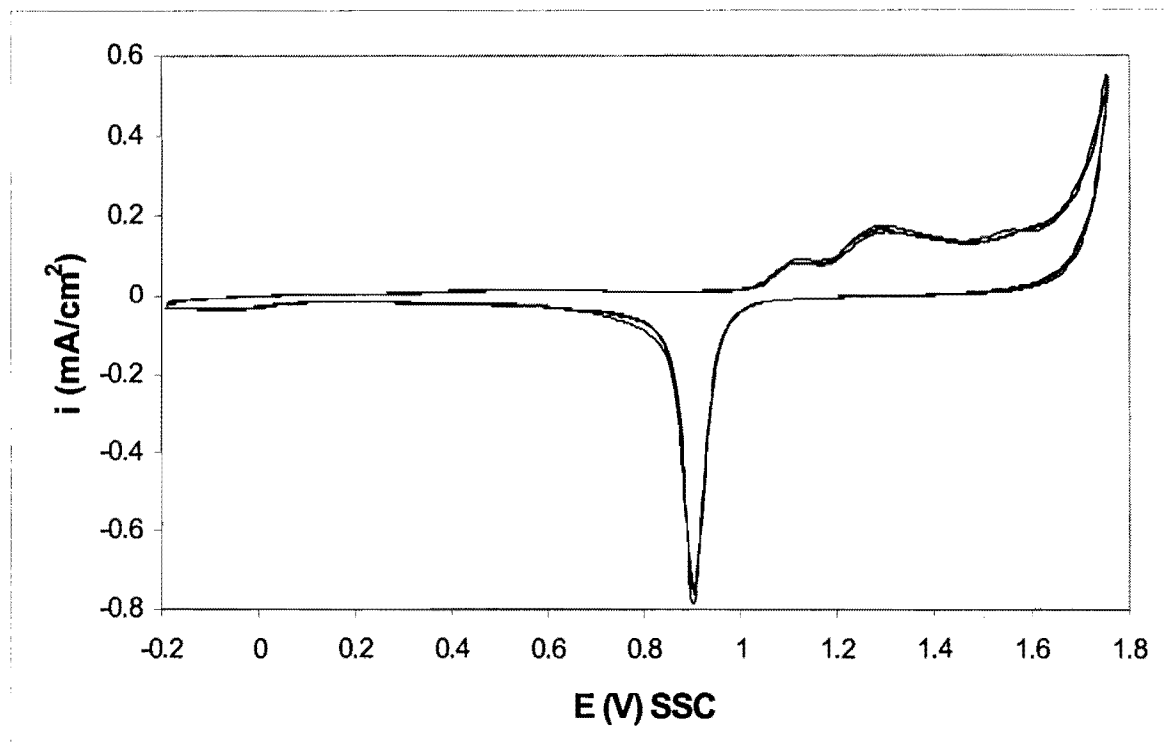


Figure 4.20. Cyclic voltammograms for gold and the Gold 990 samples in 0.5 M H_2SO_4 . Scan rate 50 mV/s, 25°C.

The similarities may be due to the following possible reasons:

- The titanium content of 4 at% may be too low to have a significant influence on the electrochemical behaviour of gold.
- The titanium may be in the passive condition (Fig 2.21).
- The titanium may have dissolved selectively from the Gold 990 alloy resulting in a pure gold surface.

4.4. Conclusions

The electrochemical behaviour of the investigated gold-based alloys in 0.5 M H₂SO₄ can be summarised by the following conclusions:

- The cyclic voltammograms of the Au-Pt alloys have features corresponding to both pure gold and platinum.
- The Au-Pt alloys in the solid solution condition have two oxide reduction peaks. The one peak corresponds to oxide reduction of platinum and the other to oxide reduction of gold.
- The high surface areas of the porous electrodes result in higher currents. The current densities of these electrodes are therefore higher when the apparent surface area is considered.
- The 60Au-40Pt alloy electrode in the 600°C heat treatment condition has a lower oxygen evolution overpotential than the other Au-Pt alloys. This can be explained by the fact that the platinum-rich areas in this sample only contain 2 % gold.
- The surface areas of the 50Au-50Pt alloy electrode in the “ductile” condition and in the solid solution condition are similar. Kirkendall porosity is absent in the 50Au-50Pt solutionised alloy.
- The cyclic voltammograms of pure gold and the Gold 990 electrodes are similar.

The electrochemical behaviour of the electrodes in alkaline solution is discussed in the next chapter.

Chapter 5

THE ELECTROCHEMICAL BEHAVIOUR OF GOLD-BASED ALLOYS IN ALKALINE SOLUTION WITHOUT ETHYLENE GLYCOL

5.1. Introduction

The electrochemical properties of the Au-Pt and Gold 990 electrodes in acid solution without ethylene glycol were discussed in the previous chapter. Cyclic voltammetry was used to study electrode surface oxidation, oxide reduction and the oxygen and hydrogen gas evolution reactions. The purpose of this chapter is to present results of similar electrochemical experiments in alkaline solution without ethylene glycol. In order to have a better understanding of the electrochemical behaviour of the alloy electrodes, experiments were also conducted with gold and platinum electrodes.

5.2. Experimental

The experimental work was performed with polycrystalline gold (99.99%), platinum (99.99%), 60Au-40Pt, 50Au-50Pt and Gold 990 electrodes. The electrodes were disc-shaped with 6mm diameter. All the electrodes were mounted in a resin by employing a black phenolic thermosetting powder. Electrical contact was achieved by drilling a hole through the rear of the mounting and tapping M6 thread. A Pine analytical rotator was used as electrode rotator. The apparent surface area of 0.28 cm² was used in all cases to calculate current densities. The higher real surface areas of the porous electrodes are expected to give higher apparent current densities than the non-porous electrodes.

A water-jacketed perspex electrochemical cell was used for all the experiments. A water-jacketed perspex electrochemical cell was used for all the experiments. The cell had an inside diameter of 90 mm and a height of 100 mm. Approximately 400 ml electrolyte was used. The distance between the working electrode and the bottom of the cell was about 60 mm. The temperature was controlled at 25°C. The cover of the perspex cell had six

openings which allowed the insertion of two counter electrodes, the working electrode, the Luggin capillary, the tube for nitrogen purging and a thermometer.

The experiments were conducted in 0.5 M NaOH solution. The solution was prepared by using double distilled water and CP grade NaOH pellets from Associated Chemical Enterprises (Pty) Ltd. Prior to each experiment, the solution was purged with nitrogen for 30 minutes to remove dissolved oxygen. The electrodes were polished before the experiments with diamond paste (down to 1 μm) and ultrasonically cleaned in 0.5 M NaOH. A Solartron 1287 Electrochemical Interface was used for the cyclic voltammetry experiments. The electrode potential was cycled between the values for onset of O_2 and H_2 evolution until the I-E curves were reproducible. It was found that approximately 15 cycles are needed to obtain reproducible I-E curves. The fifteenth cycle is used in all cyclic voltammograms shown in this chapter. The scan rate employed was 50 mV/s. The electrochemical experiments in alkaline solution without ethylene glycol were conducted without rotating the electrodes or stirring the solution. Platinum wire was used as counter electrode. All potentials quoted in this study are with respect to the silver/silver chloride reference electrode (SSC). Electrochemical impedance spectroscopy was performed with a Solartron 1250 Frequency Response Analyser.

5.3. Results and discussion

5.3.1. Gold

Cyclic voltammograms for gold are shown in Figure 5.1. These voltammograms agree well with those found in the literature (Fig. 2.2). Monolayer oxide formation commences at 0.1 V_{SSC} during the positive sweep followed by oxygen gas evolution at higher potentials. The surface oxide is reduced at 0.06 V_{SSC} during the negative sweep. It is seen that the reactions occur at lower potentials in base than in acid (Fig. 4.1). A small cathodic peak at $-0.18 V_{\text{SSC}}$ is also observed during the negative sweep. This peak is thought to be due to the reduction of hydrous gold oxide species formed on the gold surface at the upper end of the cycle (Burke and Nugent, 1997).

More oxide is formed during the positive sweep when a higher upper potential limit is used. This results in a larger oxide reduction peak during the subsequent negative sweep.

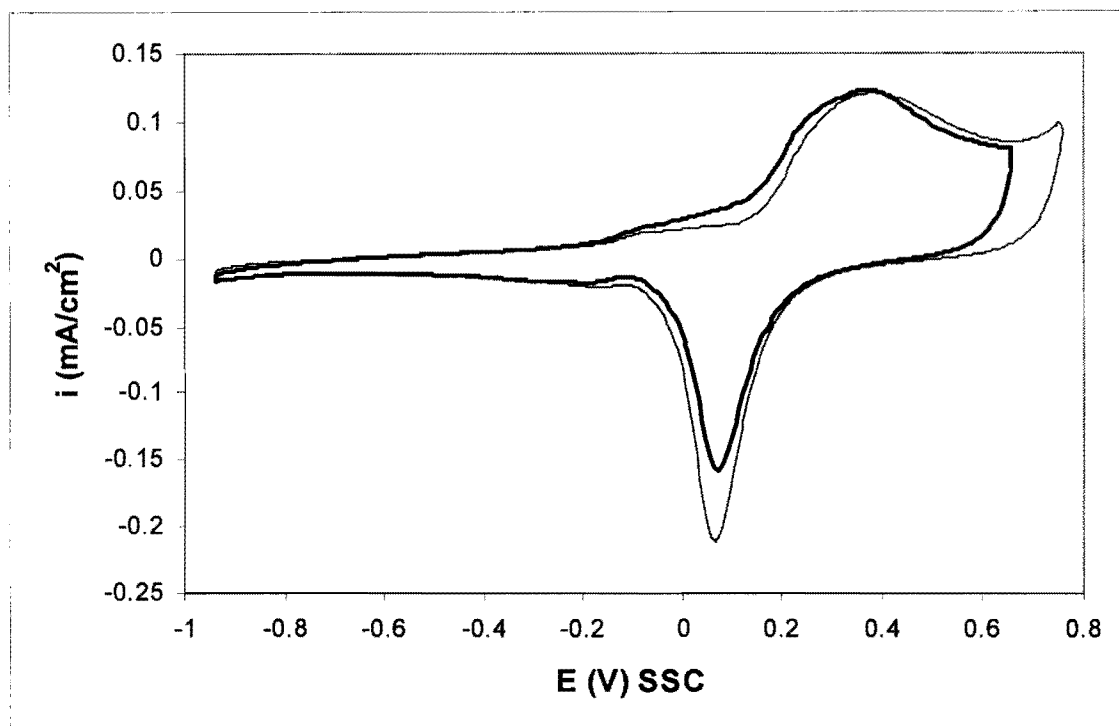


Figure 5.1. Cyclic voltammograms for gold in 0.5 M NaOH. Scan rate 50 mV/s, 25°C.

5.3.2. Platinum

A cyclic voltammogram for platinum is shown in Figure 5.2. This voltammogram agrees well with those found in the literature (Fig. 2.6). Hydrogen desorption/adsorption occurs in the region of -0.9 to -0.55 V_{SSC}. Surface oxidation commences at approximately -0.4 V_{SSC}. The surface oxide is reduced during the negative sweep at -0.3 V_{SSC}. Hydrogen gas evolution occurs at potentials negative of -0.9 V_{SSC}.

Cyclic voltammograms for platinum with different upper potential limits (0.65 and 0.75 V_{SSC}) are shown in Figure 5.3. The higher upper potential limit leads to a larger oxide reduction peak because more oxide is formed. The peak is not shifted to more negative potentials as was found for platinum in acid solution (Fig. 4.3). A higher upper potential limit than those used here is probably needed to form PtO₂ rather than PtO.

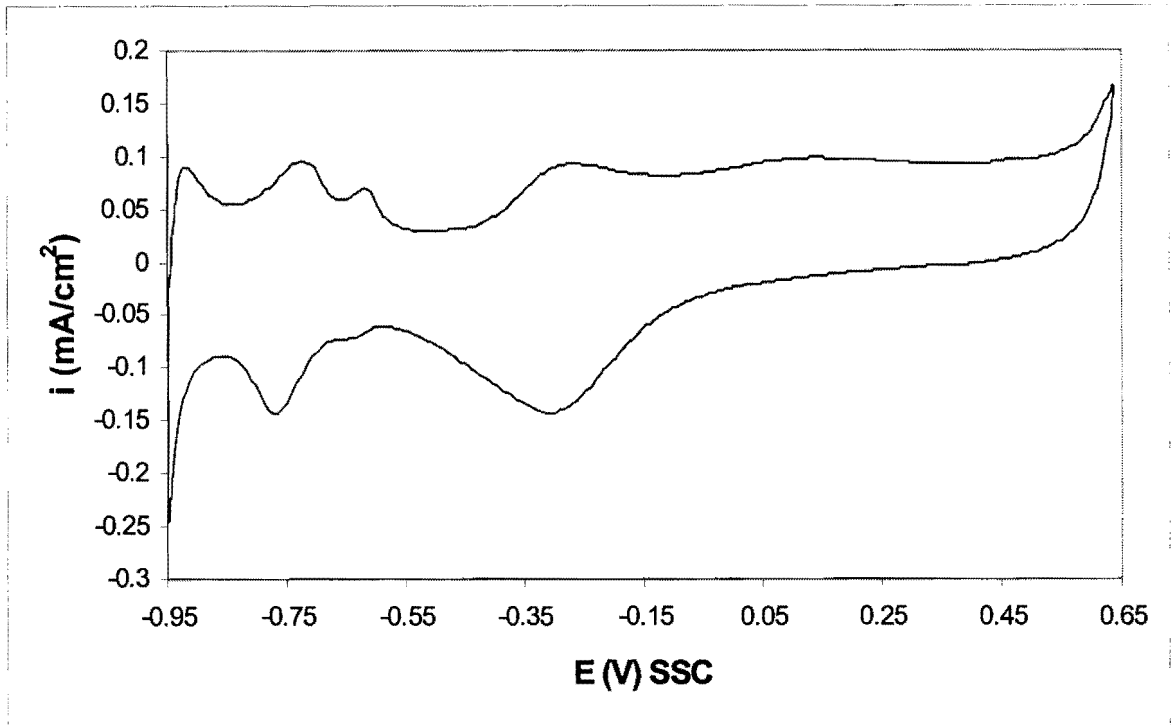


Figure 5.2. Cyclic voltammogram for platinum in 0.5 M NaOH. Scan rate 50 mV/s, 25°C.

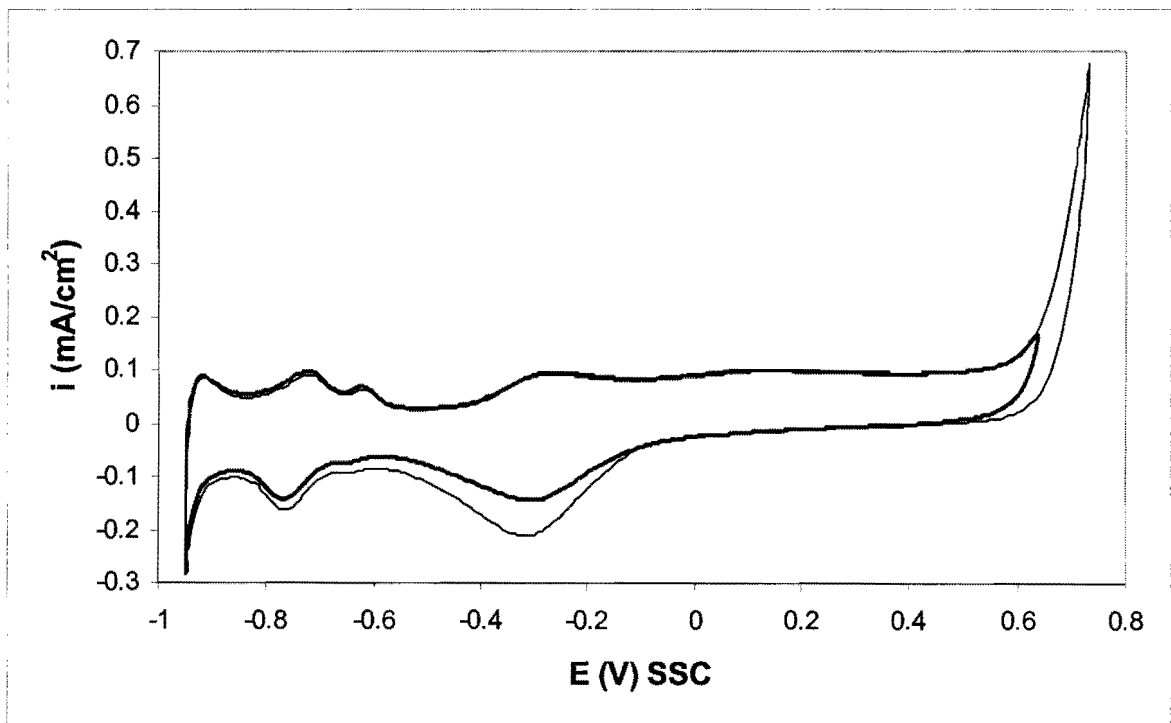


Figure 5.3. Cyclic voltammograms for platinum in 0.5 M NaOH. Scan rate 50 mV/s, 25°C.

Cyclic voltammograms for gold and platinum with the same upper potential limit ($E_{up} = 0.75$ V) is shown in Figure 5.4. It is seen that oxygen gas evolution occurs at lower potentials on platinum than on gold. The lack of a hydrogen adsorption/desorption region on gold is also evident. The same observations were made for gold and platinum in acid solution (Fig. 4.4).

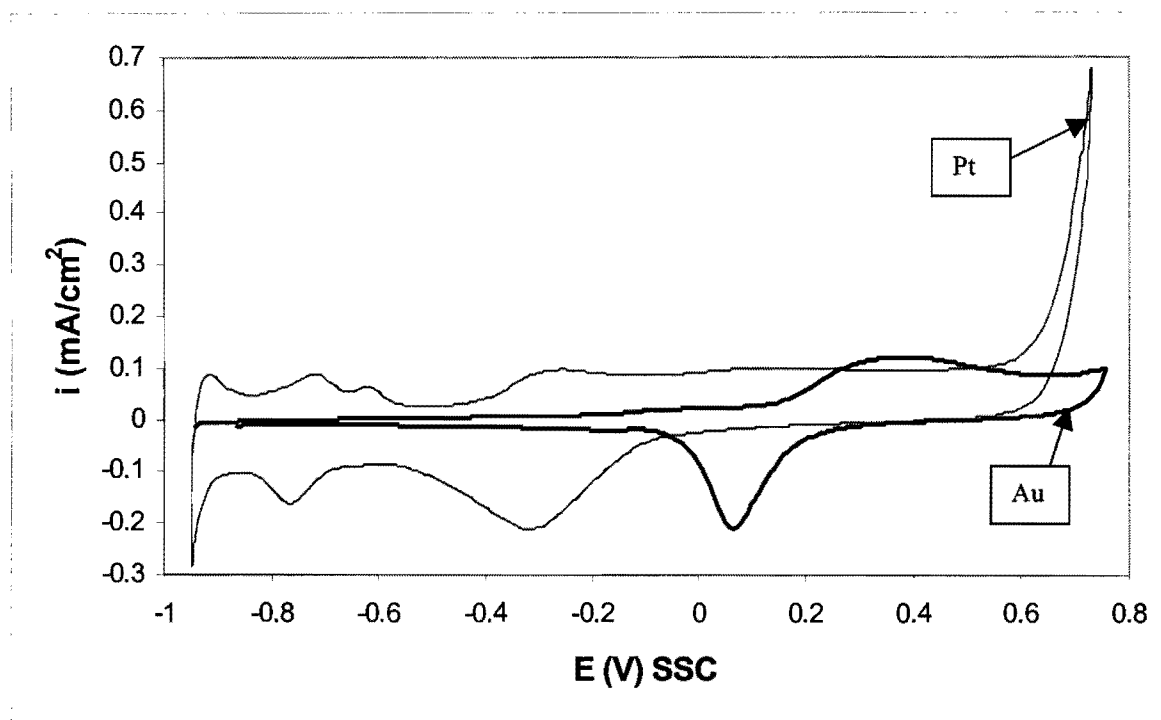


Figure 5.4. Cyclic voltammograms for platinum and gold in 0.5 M NaOH. Scan rate 50 mV/s, 25°C. $E_{up} = 0.75$ V.

5.3.3. The 60Au-40Pt alloy

5.3.3.1. The 60Au-40Pt alloy in the 1300°C heat treatment condition

The two-phased microstructure of this alloy is shown in Figure 3.2. Cyclic voltammograms for the 1300°C treated electrode are shown in Figure 5.5 and features corresponding to both pure gold and platinum can be seen. The alloy has a hydrogen adsorption/desorption region (-0.9 to -0.55 V_{SSC}). Surface oxide forms at platinum or

(platinum-rich areas) at $-0.4 V_{SSC}$ during the positive sweep. Surface oxide formation at gold (or gold-rich areas) commences at $0.1 V_{SSC}$. Two oxide reduction peaks are found in the same potential regions for oxide reduction on pure platinum and pure gold. An increase in the upper potential limit causes an increase in the oxide reduction peak, once again due to more oxide formation with the higher upper potential limit. The current density for oxygen gas evolution at $0.75 V$ is higher than on pure gold, but lower than on pure platinum. Hydrogen gas evolution occurs at potentials negative of $-0.9 V_{SSC}$.

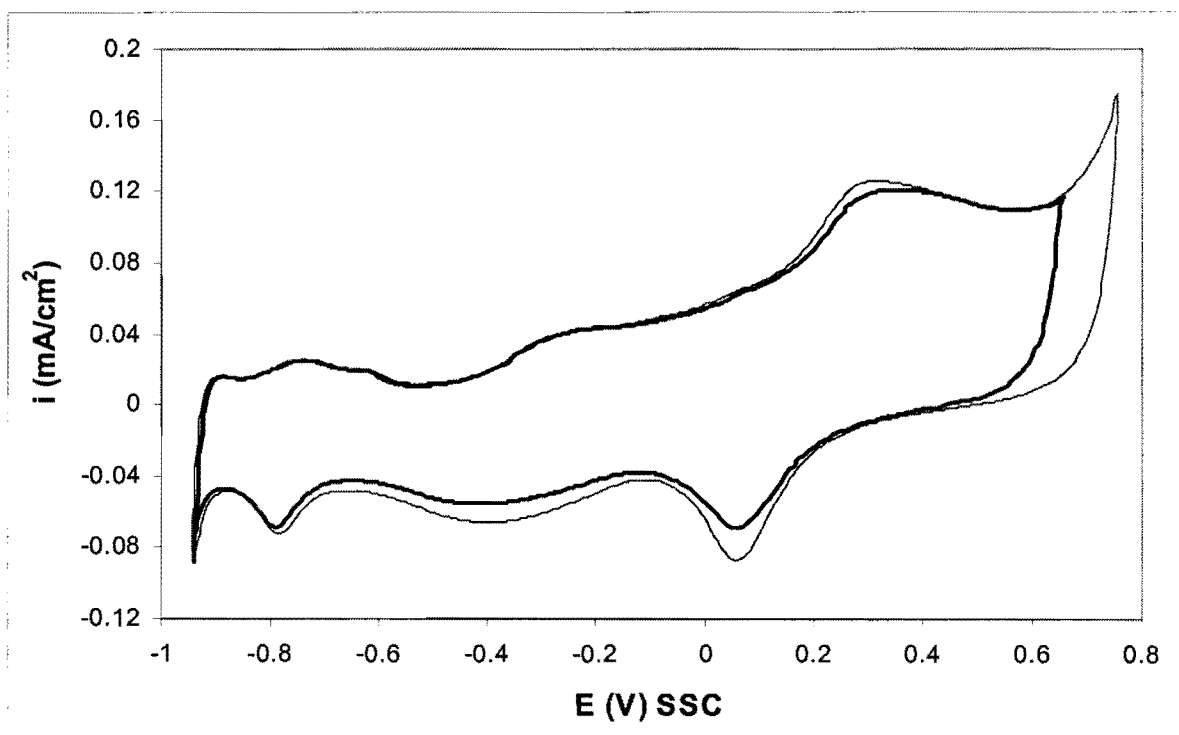


Figure 5.5. Cyclic voltammograms for the 1300°C heat treated sample (60Au-40Pt) in 0.5 M NaOH. Scan rate 50 mV/s, 25°C.

5.3.3.2. The 60Au-40Pt alloy in the 1200°C (24 hours) heat treatment condition

The microstructure of this sample (single-phased, porous) is shown in Figure 3.6. The sample was in the 1300°C treated condition prior to the heat treatment at 1200°C for 24 hours. Cyclic voltammograms for this electrode are shown in Figure 5.6. The apparent current densities obtained with this electrode are very high due to the porosity (the

apparent surface area is used to calculate current density). As was the case in acid solution (Fig. 4.6), two oxide reduction peaks are observed, even though the electrode is a solid solution of platinum in gold.

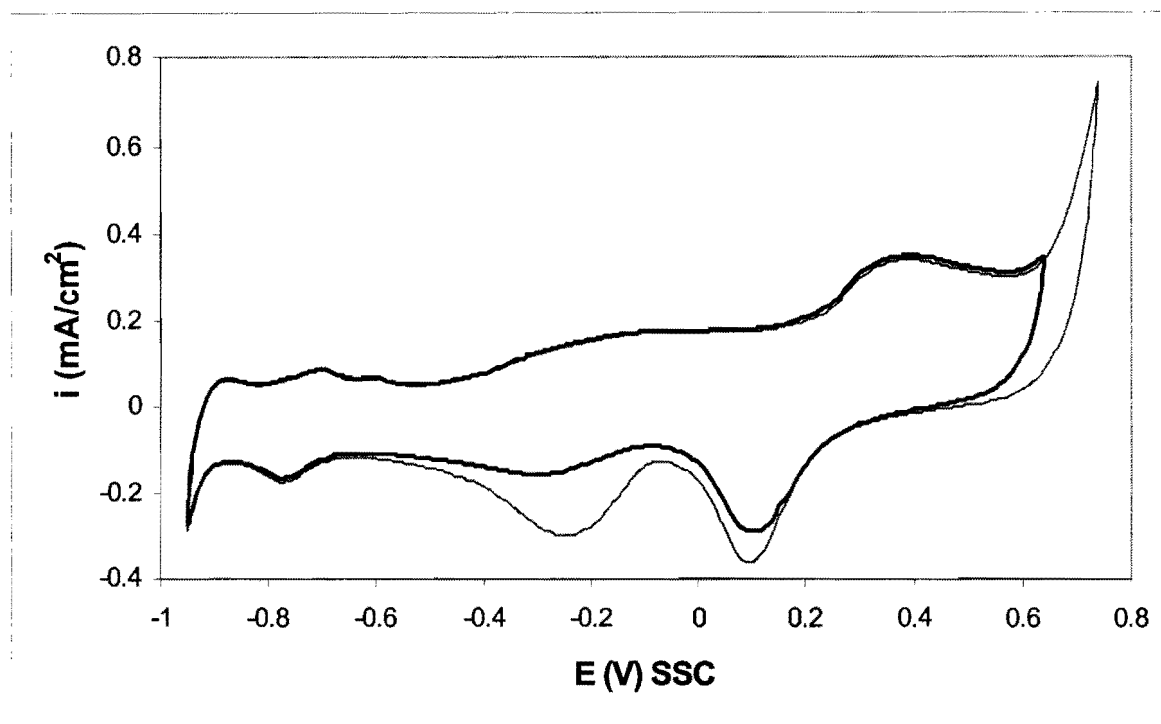


Figure 5.6. Cyclic voltammograms for the 1200°C - 24 hour heat treated sample (60Au-40Pt) in 0.5 M NaOH. Scan rate 50 mV/s, 25°C.

Cyclic voltammograms for the non-porous 1300°C treated sample and the porous 1200°C sample heat treated for 24 hours are shown together in Figure 5.7. From the increased apparent current density it is clear that the porosity increases the surface area significantly. The same effect was observed in acid (Fig. 4.7).

5.3.3.3. The 60Au-40Pt alloy in the 1200°C (168 hours) heat treatment condition

The microstructure of this sample (single-phased, porous) is shown in Figure 3.8. The sample was in the 1300°C treated condition prior to the heat treatment at 1200°C for 168

hours. Cyclic voltammograms for this electrode are shown in Figure 5.8. Two oxide reduction peaks are also found for this solutionised sample.

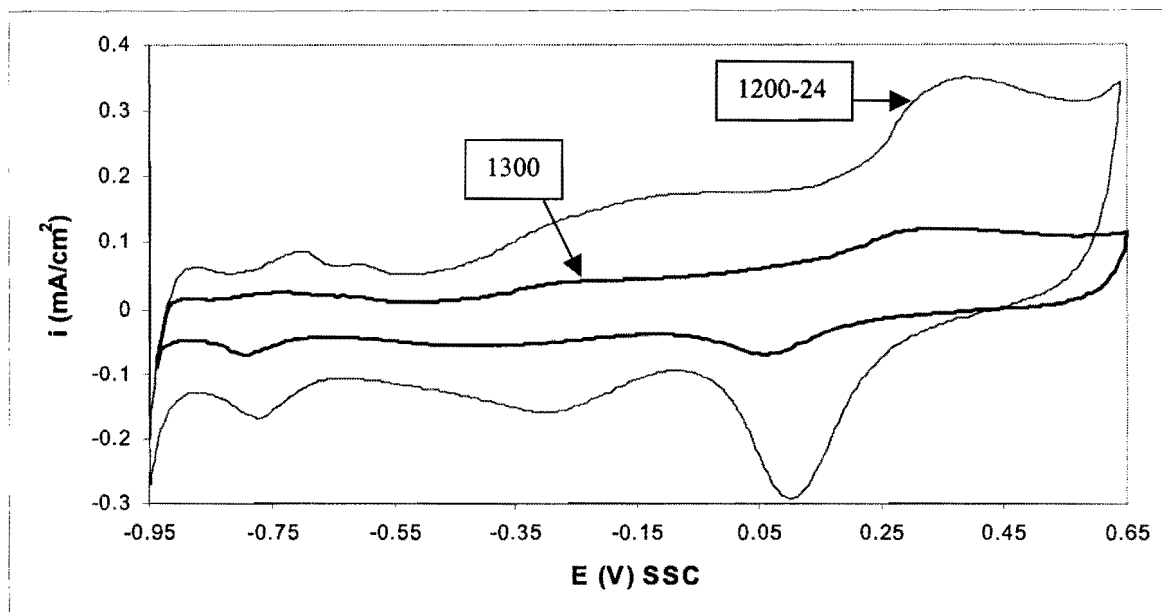


Figure 5.7. Cyclic voltammograms for the 1300°C heat treated sample and the 1200°C – 24 hour heat treated sample (60Au-40Pt) in 0.5 M NaOH. Scan rate 50 mV/s, 25°C.

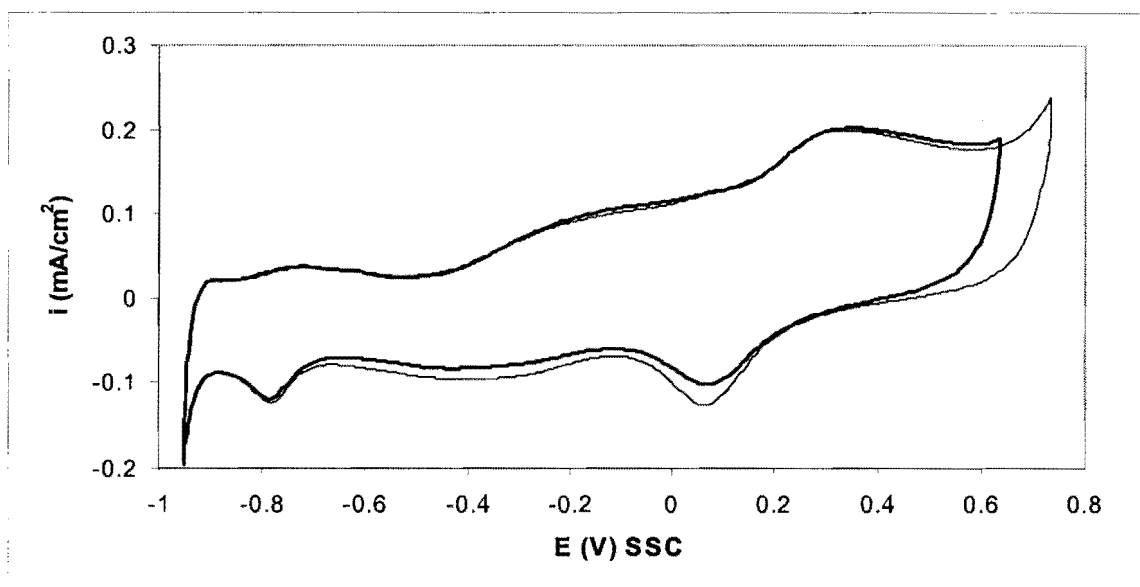


Figure 5.8. Cyclic voltammograms for the 1200°C – 168 hour heat treated sample (60Au-40Pt) in 0.5 M NaOH. Scan rate 50 mV/s, 25°C.

The apparent current densities obtained with the 1200°C – 24h sample are larger than with the 1200°C – 168h sample in acid (Fig. 4.9) and in base (Fig. 5.9). The porosity of the sample heat treated for 168 hours therefore appears to be less than for the sample heat treated for 24 hours (Figures 3.6 and 3.8).

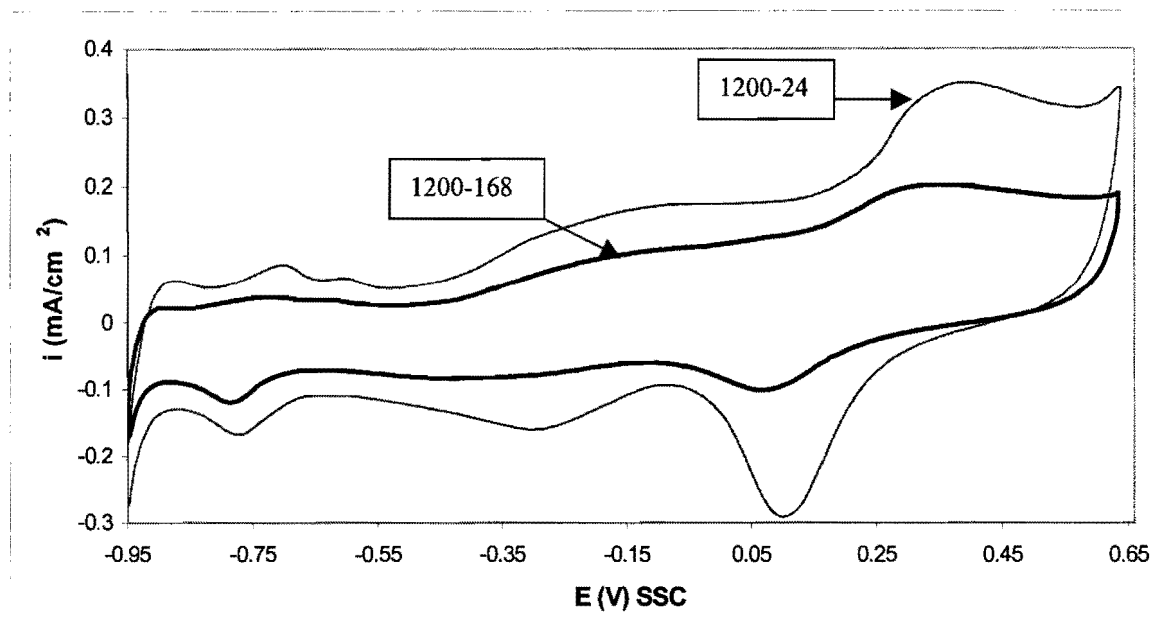


Figure 5.9. Cyclic voltammograms for the 1200°C heat treated samples (60Au-40Pt) in 0.5 M NaOH. Scan rate 50 mV/s, 25°C.

Electrochemical Impedance Spectroscopy (EIS) was used in 0.5 M H₂SO₄ to compare the surface areas of the electrodes (Fig. 4.10). The experiments were repeated in 0.5 M NaOH and the impedance as a function of frequency is shown for the 60Au-40Pt electrodes in Figure 5.10(a). Impedance spectroscopy was performed at a potential of $-0.5 V_{SSC}$. This potential was chosen because the current at the electrode will then be a minimum and reactions occurring at the electrode surface will be avoided.

The phase angle (θ) as a function of the frequency is shown in Figure 5.10(b). The phase angles were fairly constant over the frequency range, dropping to lower values at higher frequencies. Purely capacitive behaviour is represented by a θ of -90° .

A low Z value corresponds to a high surface area in the frequency range where the capacitance dominates the impedance. The phase angles in Figure 5.10(b) show that the

capacitance dominated the impedance over most of this frequency range. Figure 5.10(a) therefore indicates that the 1200°C-24h electrode has a higher surface area than the 1200°C-168h electrode. The porous electrodes have higher surface areas than the non-porous electrode.

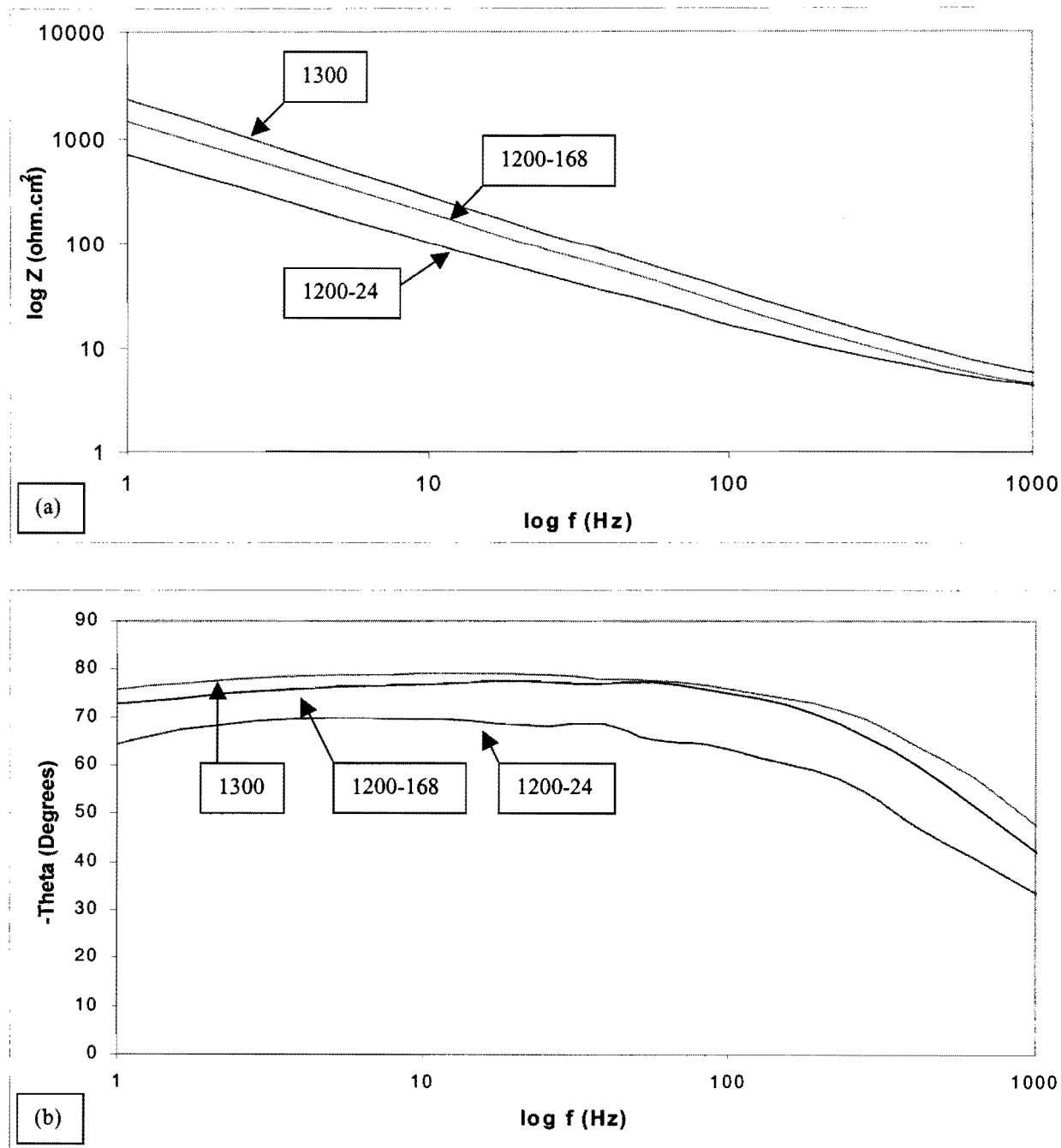


Figure 5.10.(a) Impedance spectroscopy at $-0.5 V_{SSC}$ for the 60Au-40Pt samples in 0.5 M NaOH (b) the phase angle over the same frequency range.

5.3.3.4. The 60Au-40Pt alloy in the 800°C heat treatment condition

The microstructure of this sample is shown in Figure 3.12. The sample was in the 1200°C (24 h) porous, but single-phase heat treated condition prior to the heat treatment at 800°C for 50 hours. Cyclic voltammograms for this electrode are shown in Figure 5.11. The oxygen gas evolution overpotential is low on this electrode (Fig. 5.9). The low equilibrium gold content of the platinum-rich areas (Table 3.1) is probably responsible for this observation. The platinum oxide reduction peak is very large when the upper potential limit is 0.75 V (Fig. 5.11). This may be related to oxygen gas evolution at the upper end of the cycle. It must also be remembered that platinum-rich areas nucleated at the pores during the heat treatment at 800°C (Fig. 3.13). The surface area of the pores is therefore probably platinum-rich.

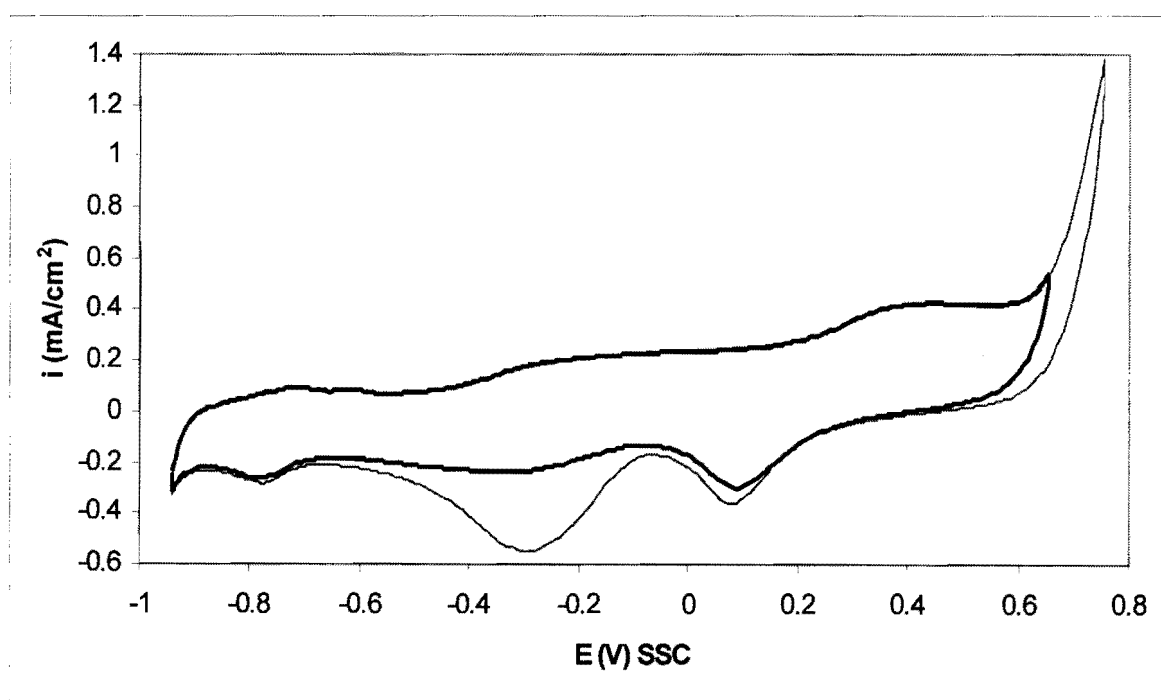


Figure 5.11. Cyclic voltammograms for the 800°C heat treated sample (60Au-40Pt) in 0.5 M NaOH. Scan rate 50 mV/s, 25°C.

5.3.3.5. The 60Au-40Pt alloy in the 600°C heat treatment condition

The microstructure of this sample is shown in Figure 3.15. The sample was in the 1200°C (24 h) heat treated condition prior to the heat treatment at 600°C for 100 hours. Cyclic voltammograms for this electrode are shown in Figure 5.12. High current densities due to oxygen gas evolution are also obtained. The equilibrium composition of the platinum-rich areas in this sample is 98Pt-2Au (Table 3.1). The fact that these areas are nearly pure platinum may explain the low oxygen gas evolution potential.

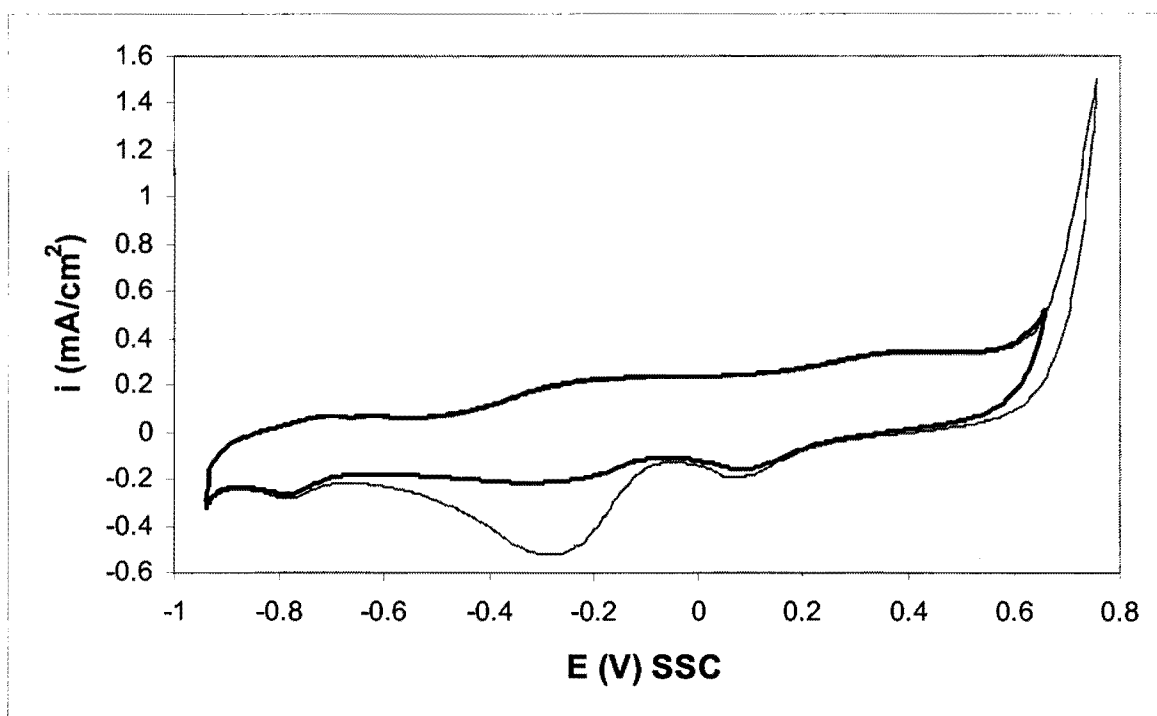


Figure 5.12. Cyclic voltammograms for the 600°C heat treated sample (60Au-40Pt) in 0.5 M NaOH. Scan rate 50 mV/s, 25°C.

In acid solution, it seems as if only a few percent of gold in platinum is needed to inhibit the oxygen gas evolution reaction. There is only 5 % Au in the platinum-rich areas in the 800°C heat treated sample, but the oxygen gas evolution reaction on this sample is inhibited more than on the 600°C heat treated sample in acid (Fig 4.13). The oxygen gas evolution reaction in alkaline solution is not inhibited on the 800°C heat treated sample

compared to the 600°C heat treated sample (Fig. 5.13). This implies that the presence of gold in the platinum-rich phase is not as effective in inhibiting the oxygen evolution reaction in base. The oxygen gas evolution reaction at gold in acid commences at approximately 1.65 V_{SSC} (Fig. 4.1) and in base at 0.75 V_{SSC} (Fig. 5.1). The corresponding values for oxygen evolution at platinum are 1.25 V_{SSC} in acid (Fig. 4.2) and 0.60 V_{SSC} in base (Fig. 5.2). These values compare well with those found in the literature. Burke and Nugent (1997) found that oxygen evolution starts at gold in acid at 1.7 V_{SSC} (1 M H_2SO_4 , 25°C) and in base at 0.7 V_{SSC} (1 M NaOH, 25°C). Heyd and Harrington (1992) found a potential of 1.28 V_{SSC} for the onset of oxygen evolution at platinum in acid (0.5 M H_2SO_4 , 25°C). For platinum in base (0.1 M NaOH, 25°C), a potential of 0.62 V_{SSC} was found by Xia and Birss (2000). The difference in potential at which oxygen starts to be evolved at gold and platinum is generally about 0.40 V in acid and 0.10 - 0.15 V in base. Burke and Nugent (1997) postulated that oxygen gas evolution at gold in base over the range 0.7 – 1.0 V_{SSC} is catalysed in a transient manner by some type of hydrous gold oxide species. They pointed out that regular oxygen gas evolution at gold in base occurs only above 1.0 V_{SSC} . The presence of gold in the platinum-rich areas will therefore be not so effective in inhibiting the oxygen evolution reaction in base as it is in acid. This is unfortunate, as oxygen gas evolution lowers the current efficiency during the electro-oxidation of organic compounds (Bock and MacDougall, 2000).

5.3.4. The 50Au-50Pt alloy

5.3.4.1. The 50Au-50Pt alloy in the “ductile” condition

The microstructure of this sample (two-phased, fine microstructure) is shown in Figure 3.17. Cyclic voltammograms for this electrode are shown in Figure 5.14. The current densities obtained on the ductile 50Au-50Pt sample are similar to the 60Au-40Pt electrode in the 1300°C (two-phased, non-porous) heat treatment condition (Fig. 5.5).

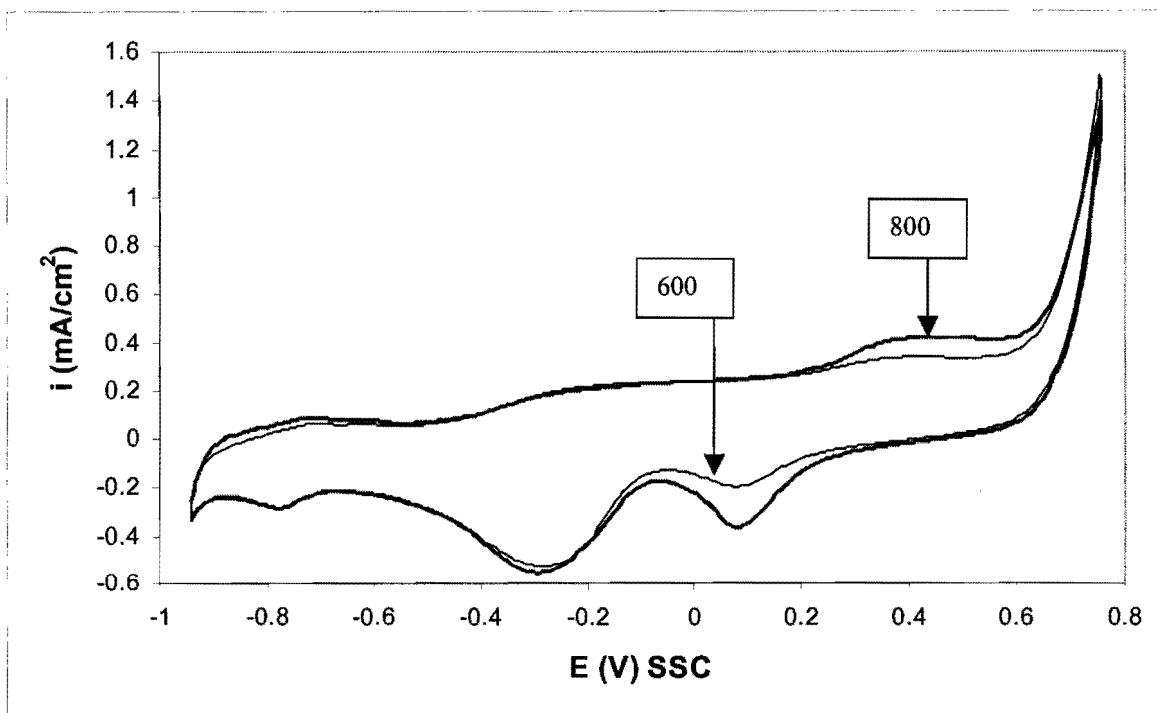


Figure 5.13. Cyclic voltammograms for the miscibility gap heat treated samples (60Au-40Pt) in 0.5 M NaOH. Scan rate 50 mV/s, 25°C.

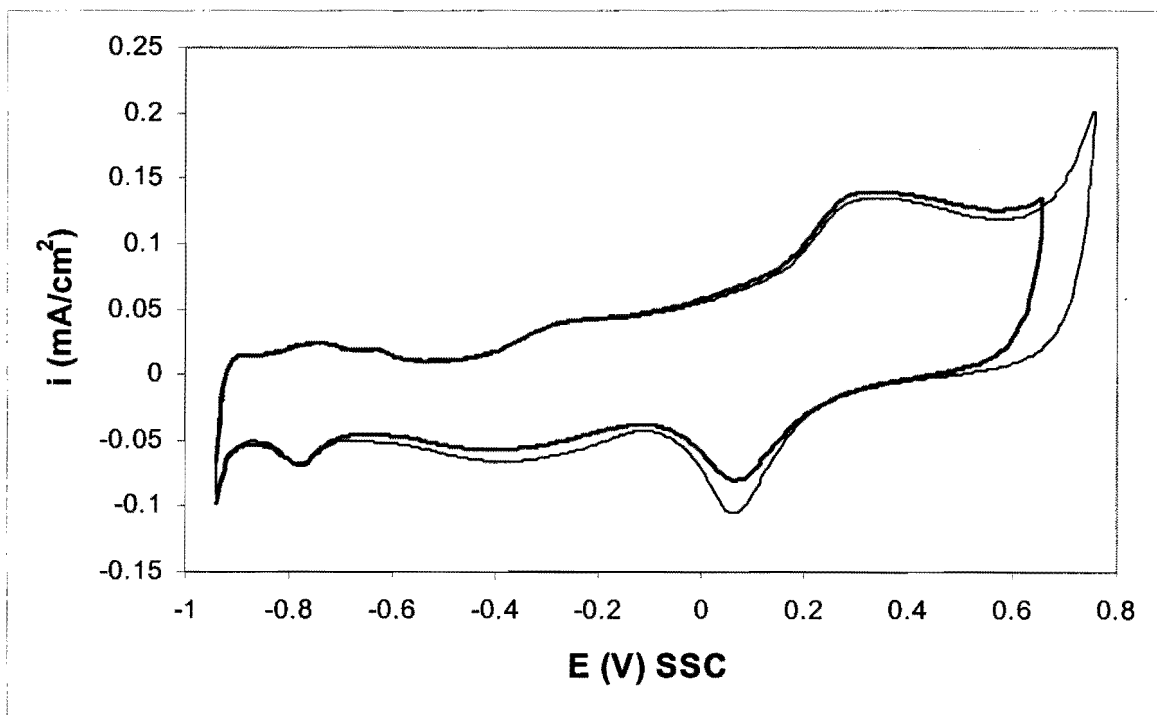


Figure 5.14. Cyclic voltammograms for the "ductile" heat treated sample (50Au-50Pt) in 0.5 M NaOH. Scan rate 50 mV/s, 25°C.

5.3.4.2. The 50Au-50Pt alloy in the solid solution condition

The microstructure of this sample is shown in Figure 3.19. Cyclic voltammograms for this electrode are shown in Figure 5.15. This electrode also has two oxide reduction peaks, despite being in the solid solution condition.

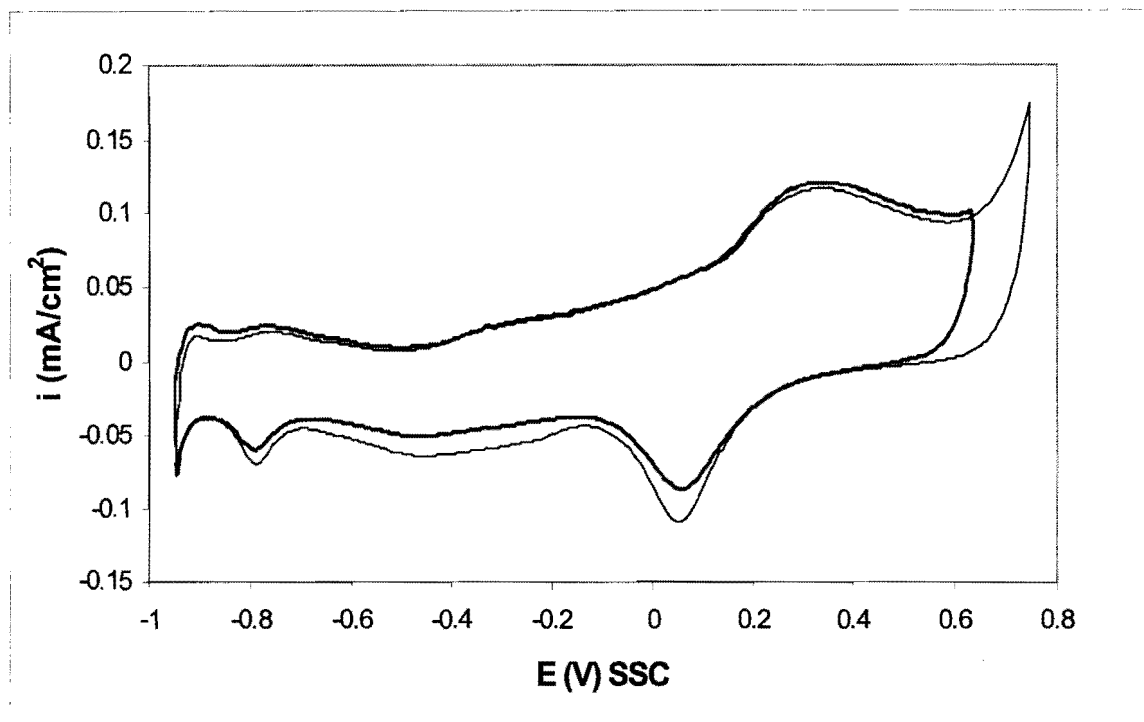


Figure 5.15. Cyclic voltammograms for the solutionised sample (50Au-50Pt) in 0.5 M NaOH. Scan rate 50 mV/s, 25°C.

The two 50Au-50Pt samples have similar current densities (Fig. 5.16). A similar result was obtained in acid (Fig. 4.16) and the reason once again is the absence of Kirkendall porosity in the sample after the solid solution heat treatment. The oxygen gas evolution reaction at the two electrodes is similar in base (Fig. 5.16). This was not the case in acid, where the oxygen evolution reaction was inhibited more at the solid solution electrode compared to the two-phased “ductile” sample (Fig. 4.16). This observation is in line with that in the previous section, namely that gold is less effective at inhibiting oxygen evolution in base than in acid.

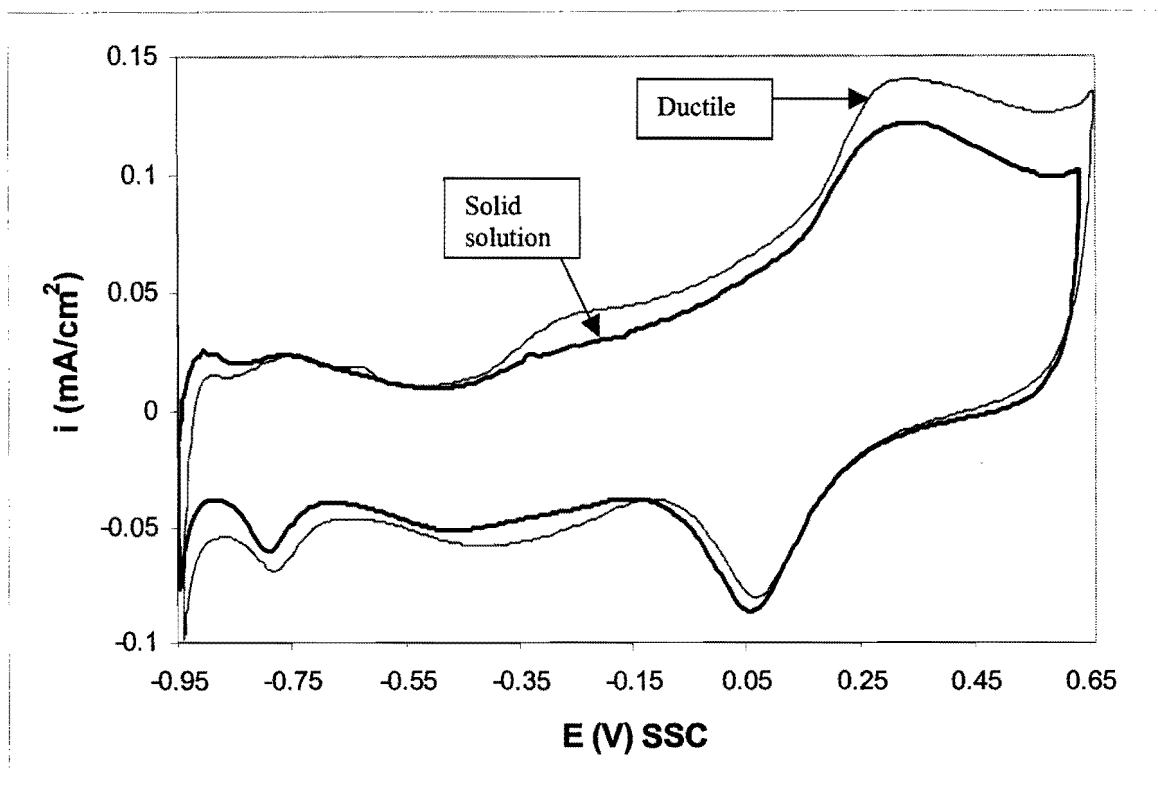


Figure 5.16. Cyclic voltammograms for the 50Au-50Pt samples in 0.5 M NaOH. Scan rate 50 mV/s, 25°C.

Impedance spectroscopy was performed in 0.5 M NaOH at a potential of $-0.5 V_{SSC}$. In Figure 5.17(a), the impedance as a function of frequency is shown for the 50Au-50Pt electrodes. The phase angle (θ) as a function of the frequency is shown in Figure 5.17(b). The phase angles were fairly constant over the frequency range, dropping to lower values at higher frequencies. The 60Au-40Pt sample in the 1300°C heat treatment condition is included for comparison. Figure 5.17 shows that the surface areas of the 50Au-50Pt electrodes in both heat treatment conditions are similar. The impedance of the 60Au-40Pt sample in the 1300°C heat treatment condition is also similar to the 50Au-50Pt alloy electrodes. This confirms the results of the impedance spectroscopy performed in acid (Fig. 4.17).

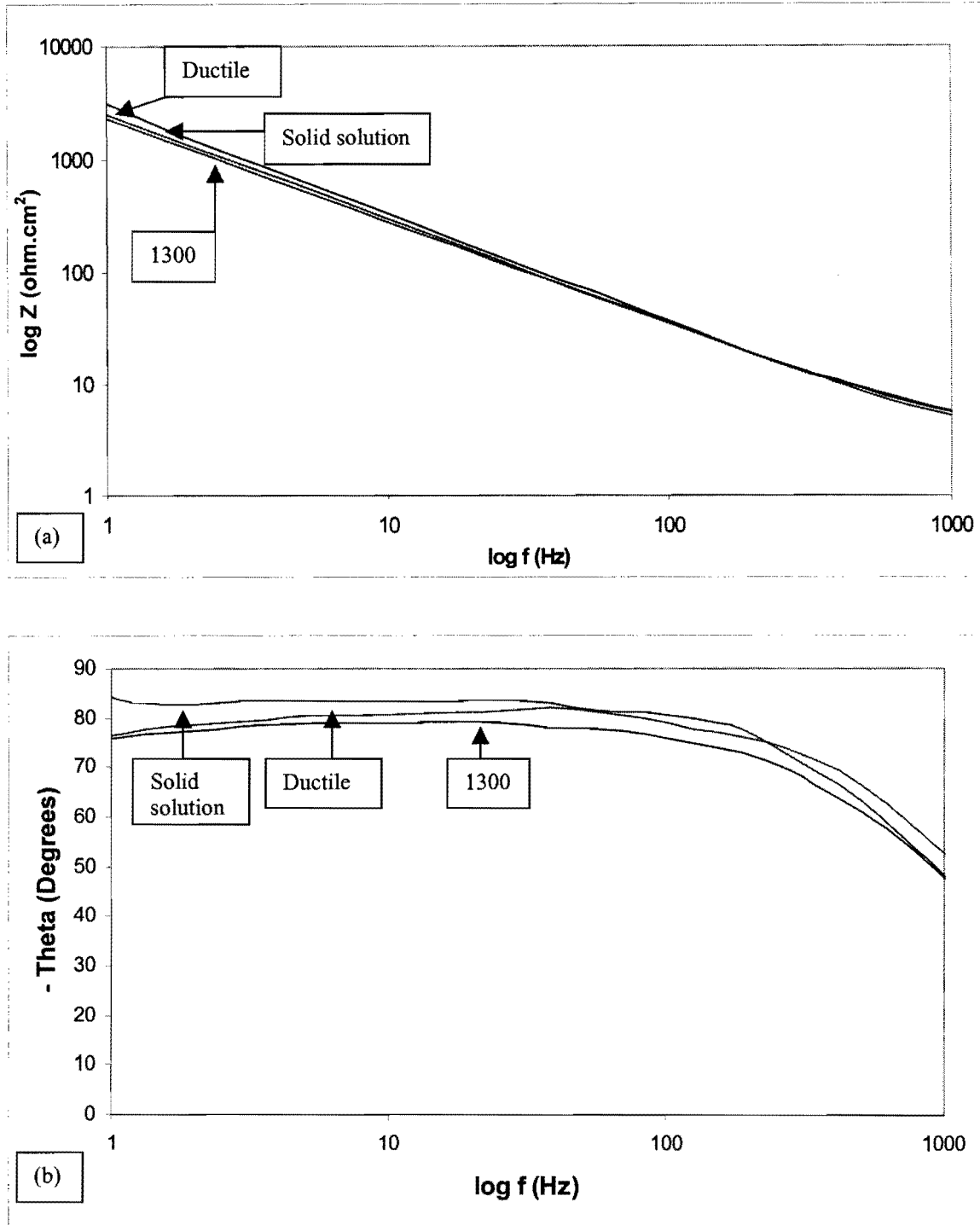


Figure 5.17. (a) Impedance spectroscopy of the 50Au-50Pt samples in 0.5 M NaOH at $-0.5 V_{SSC}$. (b) The phase angle over the same frequency range. The 1300°C heat treated sample (60Au-40Pt) is included for comparison.

5.3.5. The Gold 990 alloy

5.3.5.1. The Gold 990 alloy in the solid solution condition

This sample has 1 wt% (4 at%) titanium in solid solution with the gold. The Vickers hardness of the sample in this condition is $HV_5 = 50 \text{ kg/mm}^2$. Cyclic voltammograms for this sample are shown in Figure 5.18. The behaviour of Gold 990 in the solid solution condition is similar to pure gold (Fig. 5.1), as was the case in acid solutions (Fig. 4.18).

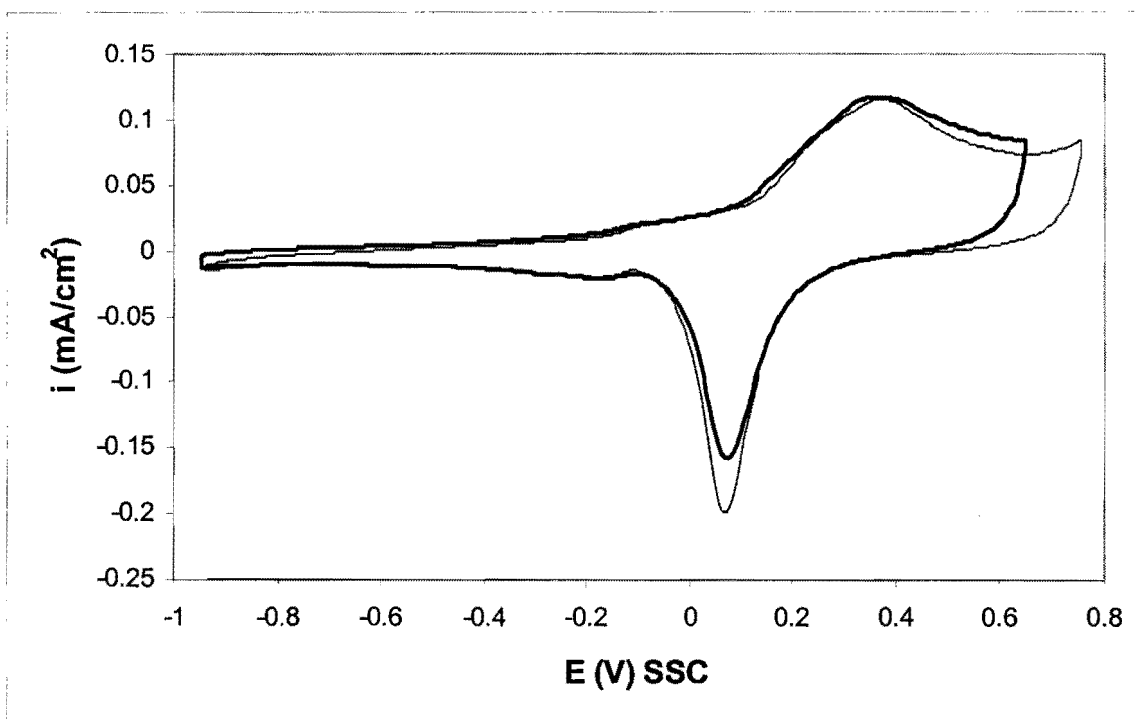


Figure 5.18. Cyclic voltammograms for the Gold 990 sample in the solid solution condition in 0.5 M NaOH. Scan rate 50 mV/s, 25°C.

5.3.5.2. The Gold 990 alloy in the precipitation-hardened condition

This sample is hardened by the presence of small Au_4Ti precipitates. The Vickers hardness of the sample in this condition is $HV_5 = 150 \text{ kg/mm}^2$. Cyclic voltammograms

for this sample are shown in Figure 5.19. The behaviour of Gold 990 in the precipitation-hardened condition is also similar to pure gold (Fig. 5.1).

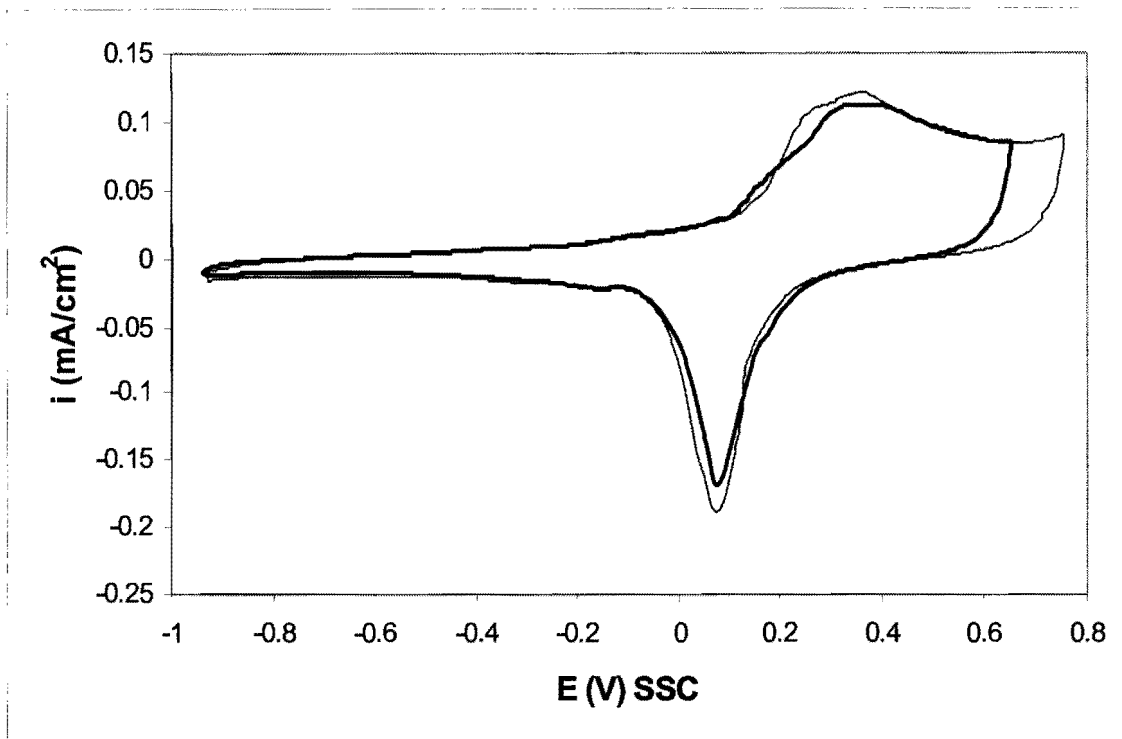


Figure 5.19. Cyclic voltammograms for the Gold 990 sample in the precipitation hardened condition in 0.5 M NaOH. Scan rate 50 mV/s, 25°C.

The cyclic voltammograms for the two Gold 990 electrodes and pure gold are compared in Figure 5.20. The cyclic voltammograms of the three electrodes are similar in alkaline solutions. This agrees with the result found in sulphuric acid (Fig. 4.20). The possible reasons for the similarities have already been discussed in Chapter 4 and are repeated below:

- The titanium content of 4 at% may be too low to have a significant influence on the electrochemical behaviour of gold.
- The titanium may be in the passive condition (Fig 2.21).
- The titanium may have dissolved selectively from the Gold 990 alloy resulting in a pure gold surface.

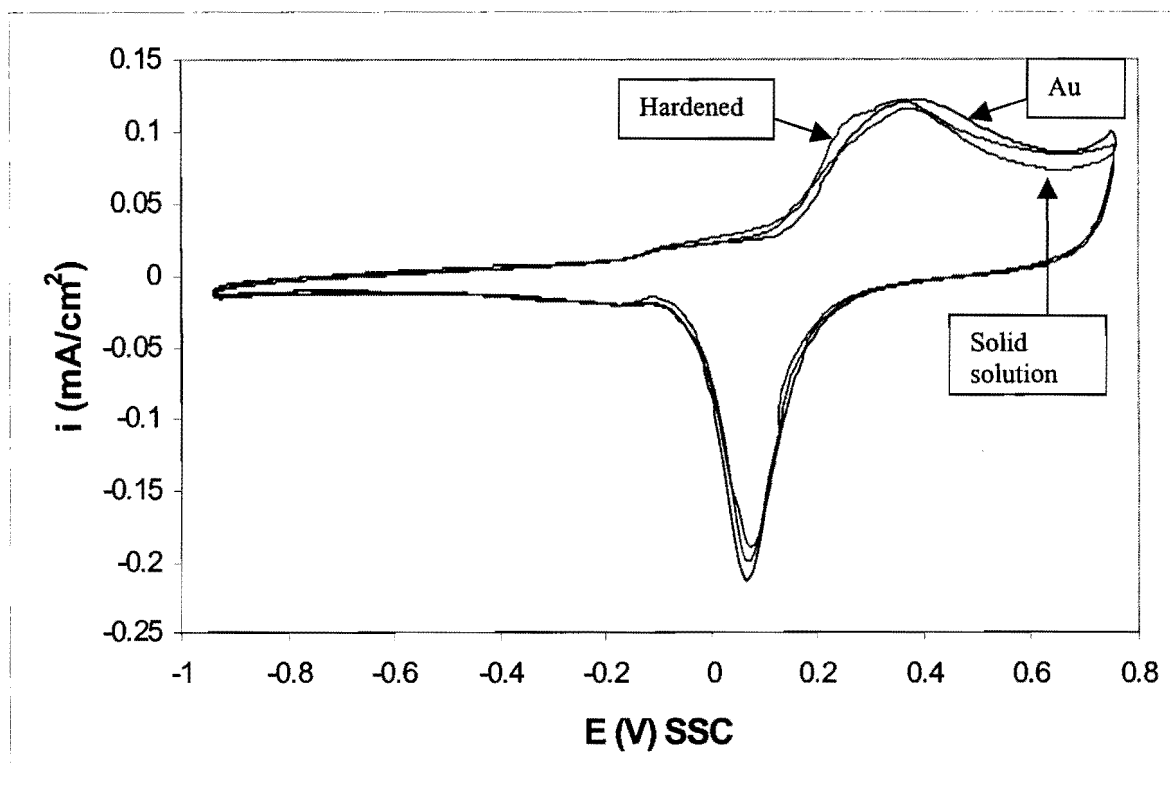


Figure 5.20. Cyclic voltammograms for gold and the Gold 990 samples in 0.5 M NaOH. Scan rate 50 mV/s, 25°C.

5.4. Conclusions

The electrochemical properties of the gold-based alloys in 0.5 M NaOH have been investigated. The most important results can be summarised as follows:

- All reactions occur at a lower potential in base than in acid.

Many of the results obtained in base are similar to what was observed in acid. These include:

- The cyclic voltammograms of the Au-Pt alloys have features corresponding to both pure gold and platinum.
- The Au-Pt alloys in the solid solution condition have two oxide reduction peaks. The one peak corresponds to oxide reduction of platinum and the other to oxide reduction of gold.

- The high surface areas of the porous electrodes result in higher currents. The current densities of these electrodes are therefore higher when the apparent surface area is considered.
- The surface areas of the 50Au-50Pt alloy electrode in the “ductile” condition and in the solid solution condition are similar. Kirkendall porosity is absent in the 50Au-50Pt solid solution alloy.
- The cyclic voltammograms of pure gold and the Gold 990 electrodes are similar.

The oxygen gas evolution reaction in alkaline solution is not inhibited on the 800°C heat treated sample compared to the 600°C heat treated sample (Fig. 5.13). This is in contrast to what was found in acid solution (Fig. 4.13).

The electrochemical properties of the gold-based alloys without organics in solution have been discussed in Chapters 4 and 5. The information gathered with these experiments will be useful to understand the electro-oxidation reactions of organic compounds at the electrodes. The objective of the next chapter is to investigate the electro-oxidation of ethylene glycol at the gold-based alloys.

Chapter 6

THE ELECTRO-OXIDATION OF ETHYLENE GLYCOL AT GOLD-BASED ALLOYS IN AN ALKALINE SOLUTION

6.1. Introduction

The heat treatments of the Au-Pt and Gold 990 samples were investigated in Chapter 3. This was followed by a discussion of the electrochemical properties of the Au-Pt and Gold 990 electrodes in acid (Chapter 4) and in alkaline solutions (Chapter 5) without ethylene glycol.

The purpose of this chapter is to study the electro-oxidation of ethylene glycol at the gold-based alloys in an alkaline solution. High current densities for ethylene glycol oxidation at gold (Kadirgan et al., 1990) and at platinum (Kadirgan et al., 1983) were found in solutions of high pH. By contrast, the electro-oxidation of ethylene glycol at gold (Beden et al., 1987) and at platinum (Hahn et al., 1987) in acid solutions occurs to a lesser extent. It has also been shown by Beden and co-workers (1982) that a synergistic effect is found when gold-platinum alloys are used for the electro-oxidation of ethylene glycol in alkaline solutions. If one considers the possible mechanisms for the synergistic effect observed for Au-Pt alloys (Section 2.6.5), it is expected that the distribution of the gold and platinum atoms at the surface of the electrode will influence the electro-oxidation properties of the alloy. The effect of the microstructure of the alloys on the electro-oxidation of ethylene glycol in alkaline solution was therefore studied and will be discussed in this chapter.

6.2. Experimental

The experimental work was performed with polycrystalline gold (99.99%), platinum (99.99%), 60Au-40Pt, 50Au-50Pt and Gold 990 electrodes. The electrodes were disc-shaped with 6mm diameter. All the electrodes were mounted in a resin by employing a black phenolic thermosetting powder. Electrical contact was achieved by drilling a hole through the rear of the mounting and tapping M6 thread. A Pine analytical rotator was

used as electrode rotator. The apparent surface area of 0.28 cm^2 was used in all cases to calculate current densities. The electrodes were polished before the experiments with diamond paste (down to $1 \text{ }\mu\text{m}$) and ultrasonically cleaned in 0.5 M NaOH .

A water-jacketed perspex electrochemical cell was used for all the experiments. The cell had an inside diameter of 90 mm and a height of 100 mm . Approximately 400 ml electrolyte was used. The distance between the working electrode and the bottom of the cell was about 60 mm . The temperature was controlled at 25°C . The cover of the perspex cell had six openings which allowed the insertion of two counter electrodes, the working electrode, the Luggin capillary, the tube for nitrogen purging and a thermometer.

“Proanalysis” ethylene glycol from Merck was used to prepare solutions containing 0.1 M ethylene glycol in 0.5 M NaOH . CP grade NaOH pellets from Associated Chemical Enterprises (Pty) Ltd were used, together with double distilled water.

A Solartron 1287 Electrochemical Interface was used for the cyclic voltammetry experiments. Platinum wire was used as counter electrode. All potentials quoted in this study are with respect to the silver/silver chloride reference electrode (SSC). The scan rate employed was 50 mV/s . Rotation of the electrodes produced an unacceptable high level of noise in the cyclic voltammograms and it was decided to rather stir the solution with a Heidolph MR 3001 K magnetic stirrer. A rotation speed of 500 revolutions per minute was used. The length of the magnet that was used is 40 mm and its diameter 8 mm (The water-jacketed perspex electrochemical cell has an inside diameter of 90 mm).

The cyclic voltammetry experiments of all the electrodes were performed by using the following procedure:

- The 0.5 M NaOH solution (without ethylene glycol) was purged with nitrogen for 30 minutes to remove dissolved oxygen.
- The electrode potential was cycled for fifteen cycles between the values for onset of O_2 and H_2 evolution until the I-E curves were reproducible. The cyclic voltammogram (15^{th} cycle) of the electrode was then compared to the cyclic voltammogram found in chapter 5. This was done to make certain that the solution did not contain impurities and that the behaviour of the electrode was similar to what was found in chapter 5.
- The ethylene glycol was added to the solution.

- The electrode was anodically activated at 1.2 V_{SSC} for 10 seconds (the solution was stirred during activation). Poisoning species and the electrode surface are oxidised at this potential. Oxygen gas evolution is also expected to occur at 1.2 V_{SSC}.
- The electrode potential was then cycled for 10 cycles between the values for onset of O₂ and H₂ evolution (the solution was stirred in one set of experiments and not stirred in the other set of experiments).
- The electrode was anodically reactivated at 1.2 V_{SSC} for 10 seconds (the solution was stirred during reactivation).
- The electrode potential was cycled once between the values for onset of O₂ and H₂ evolution to see if reactivation was successful (the solution was stirred in one set of experiments and not stirred in the other set of experiments).

6.3. Results and discussion

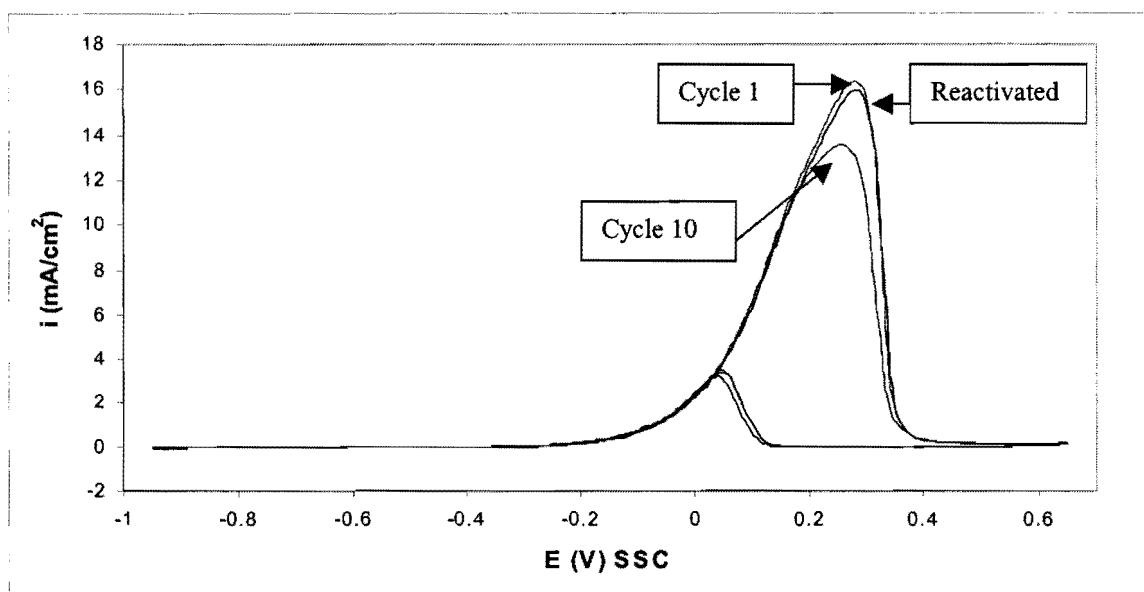
6.3.1. Gold

Cyclic voltammograms for gold in 0.5 M NaOH without ethylene glycol are shown in Figure 5.1. The cyclic voltammograms (1st and 10th cycles) with 0.1 M ethylene glycol in the solution are shown in Figure 6.1. The solution was not stirred in Figure 6.1(a) and stirred in Figure 6.1(b). The first cycles after anodic reactivation of the gold electrode are also shown in Figures 6.1(a) and (b).

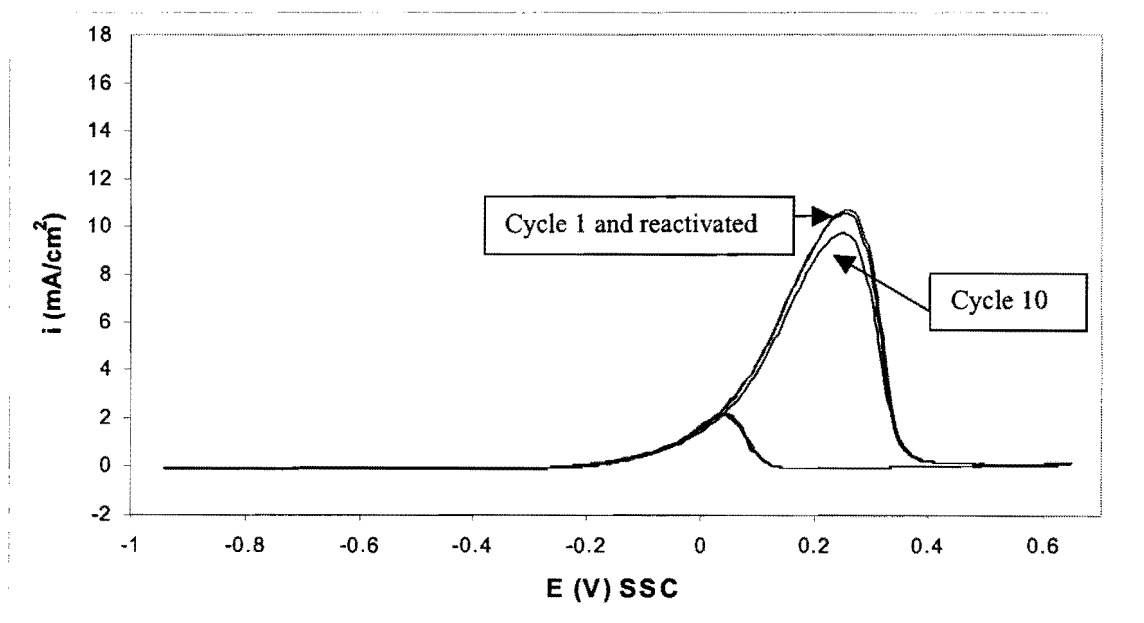
The voltammograms in Figure 6.1 compare well with those found in the literature (Fig. 2.14). It is seen from Figure 6.1 that ethylene glycol electro-oxidation commences during the positive sweep at a potential of $-0.3 V_{SSC}$. This is in the potential region before the surface oxide forms on gold (Figure 5.1). It has been suggested (Vitt et al., 1990) that organic compounds are oxidised in the presence of AuOH formed in the premonolayer region (also see section 2.4.1).

During the first positive scan, a peak of 16 mA/cm² at 0.27 V_{SSC} (Fig. 6.1(a)) is found when the solution is not stirred and a peak of 10.5 mA/cm² at 0.25 V_{SSC} (Fig. 6.1(b)) is

found when the solution is stirred. Hauffe and Heitbaum (1978) also found that the peak currents were smaller when the solution was stirred with argon gas. They postulated that



(a)



(b)

Figure 6.1. Cyclic voltammograms for the electro-oxidation of 0.1 M ethylene glycol in 0.5 M NaOH at a gold electrode (50mV/s, 25°C). (a) Solution not stirred; (b) Solution stirred.

stirring caused an accelerated transportation of partially oxidised intermediates into the solution. These intermediates cannot be oxidised at the electrode surface, resulting in lower current densities.

The electro-oxidation of ethylene glycol is inhibited by the surface oxide on the gold electrode from 0.25 to 0.65 V_{SSC} during the positive sweep (Fig 6.1). During the negative sweep, oxidation of ethylene glycol commences only after the surface gold oxide has been reduced (Figure 5.1), reaching a current density maximum of 3.5 mA/cm^2 (not stirred) and 2.2 mA/cm^2 (stirred) at 0.03 V_{SSC} .

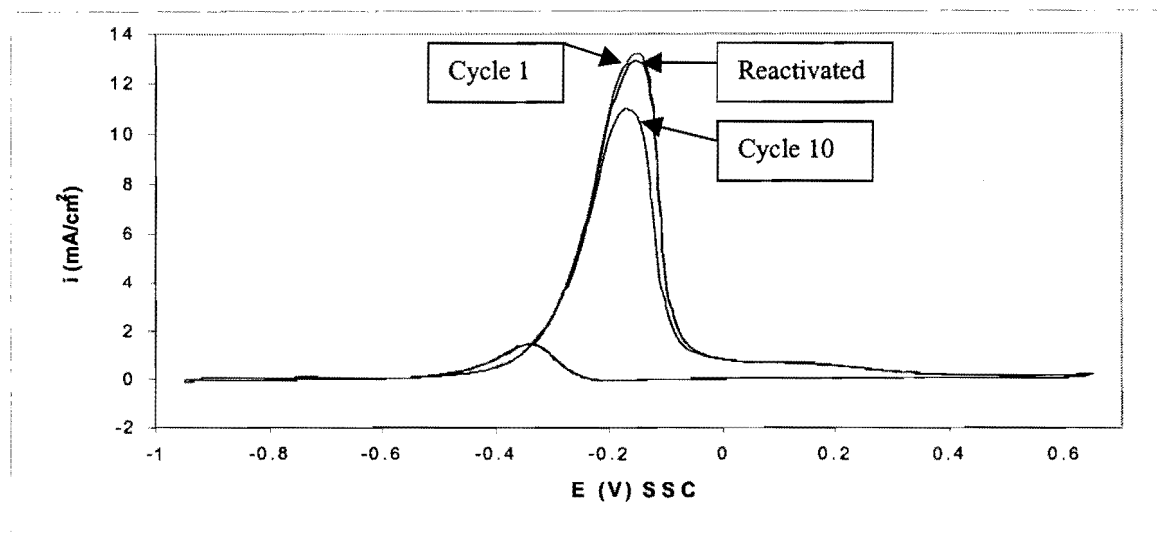
The peak current densities of the 10th cycles are lower than for the 1st cycles (Fig. 6.1(a), (b)). This occurs due to electrode poisoning. CO poisons are expected to form by the rupture of the C-C bond during chemisorption at negative potentials. Kadirgan and co-workers (1990) used electromodulated infrared reflectance spectroscopy (EMIRS) to study poison formation at gold electrodes during ethylene glycol electro-oxidation. They found that the CO band was not present initially and that it grew during spectral accumulation performed to improve signal to noise ratio. However, the CO band was far from being the main infrared band observed. It was therefore suggested that ethylene glycol does not dissociate immediately on gold at low potentials and that the CO poisoning species are formed only progressively. Glycolaldehyde and glyoxalate were found to be the main adsorbed species.

During the anodic reactivation procedure at 1.2 V_{SSC} , the poisons (and the electrode surface) are oxidised. The cyclic voltammograms (Fig. 6.1 (a), (b)) show that the original peak current densities (before poisoning) can be obtained after reactivation of the electrode.

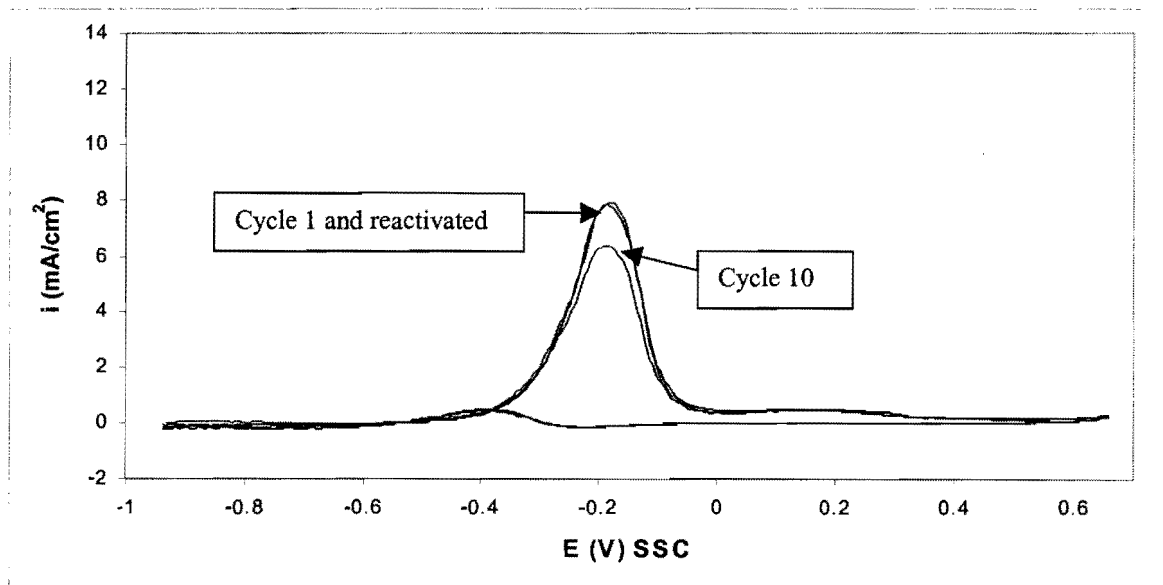
6.3.2. Platinum

Cyclic voltammograms for platinum in 0.5 M NaOH without ethylene glycol are shown in Figures 5.2 and 5.3.

The cyclic voltammograms (1st and 10th cycles) with 0.1 M ethylene glycol in the solution are shown in Figure 6.2. The solution was not stirred in Figure 6.2(a) and it was stirred in Figure 6.2(b). The first cycles after anodic reactivation of the platinum electrode are also shown in Figures 6.2(a) and (b).



(a)



(b)

Figure 6.2. Cyclic voltammograms for the electro-oxidation of 0.1 M ethylene glycol in 0.5 M NaOH at a platinum electrode (50mV/s, 25°C). (a) Solution not stirred; (b) Solution stirred.

The voltammograms in Figure 6.2 compare well with those found in the literature (Fig. 2.16). It is seen from Figure 6.2 that ethylene glycol electro-oxidation commences during the positive sweep at a potential of $-0.6 V_{SSC}$. This is, as with gold, in the potential region before the surface oxide is formed (Fig. 5.2). The electro-oxidation of ethylene glycol is apparently inhibited by the surface oxide on the platinum electrode. Xia and Birss (2000) postulated that hydroxide is adsorbed in the anodic sweep while hydrogen is desorbed over the potential region from -0.9 to $-0.55 V_{SSC}$ (Fig. 2.6). It is generally accepted that the electro-oxidation of ethylene glycol at platinum occurs in the presence of OH_{ads} species. (Enea and Ango, 1989).

During the first positive scan, a peak of 13.5 mA/cm^2 at $-0.15 V_{SSC}$ (Fig. 6.2(a)) is found when the solution is not stirred and a peak of 8 mA/cm^2 at $-0.18 V_{SSC}$ (Fig. 6.2(b)) is found when the solution is stirred.

During the negative sweep, oxidation of ethylene glycol commences only after the surface platinum oxide has been reduced (Figure 5.2), reaching a current density maximum of 1.5 mA/cm^2 (not stirred) and 0.4 mA/cm^2 (stirred) at $-0.35 V_{SSC}$.

The peak current densities of the 10th cycles are lower than for the 1st cycles (Fig. 6.2(a), (b)). As was the case for gold, this is apparently due to electrode poisoning. Hahn and co-workers (1987) studied the adsorption of ethylene glycol at platinum in alkaline solutions. In contrast to gold, the adsorption at platinum was found to be dissociative. Almost equal amounts of bridge-bonded and linearly bonded CO species were found. The linearly-bonded CO is thought to be responsible for the poisoning of the electrode.

The cyclic voltammograms (Fig. 6.2 (a), (b)) show that the original peak current densities at platinum (before poisoning) can also be obtained after reactivation of the electrode.

Cyclic voltammograms for ethylene glycol oxidation at gold and platinum (1st cycles, stirred) are compared in Figure 6.3. It is seen that higher current densities are found with gold compared to platinum. However, the oxidation peaks for ethylene glycol oxidation are located at more negative potentials for platinum than for gold.

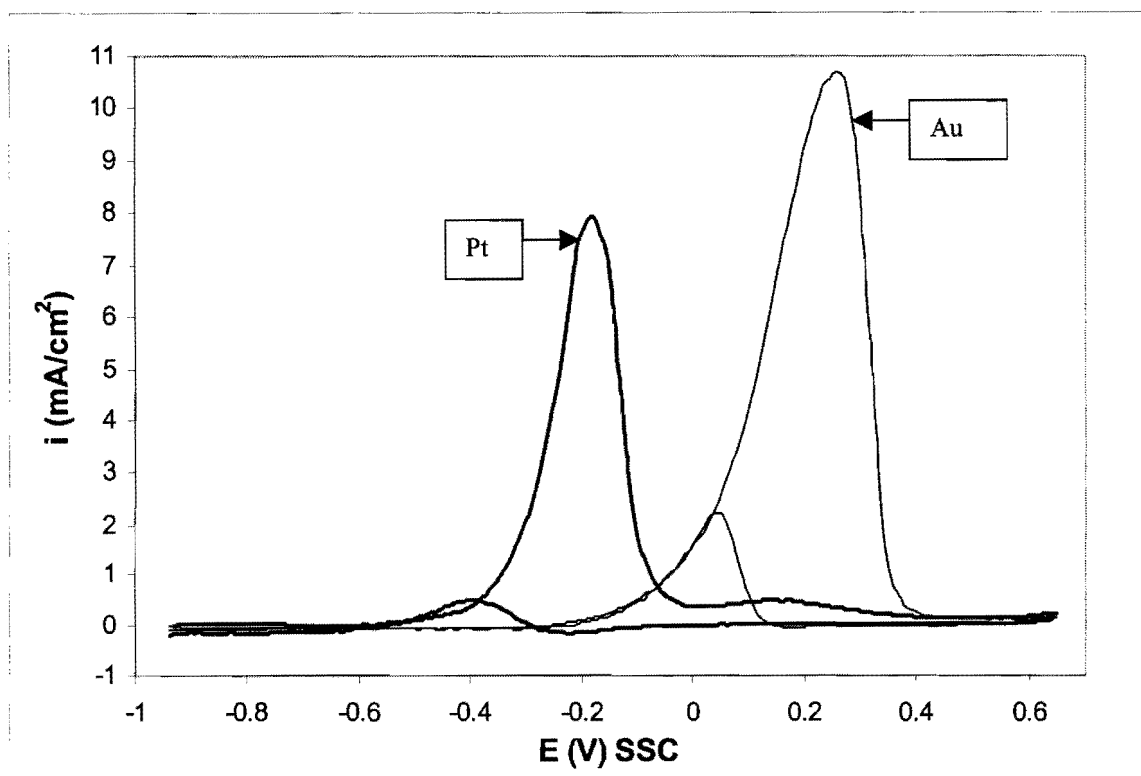


Figure 6.3. Cyclic voltammograms for the electro-oxidation of 0.1 M ethylene glycol in 0.5 M NaOH at gold and platinum electrodes (50mV/s, 25°C); 1st cycles, solution stirred.

Enea and Ango (1989) suggested that the adsorption of ethylene glycol at gold and platinum occur by different mechanisms. Gold is a weak chemisorber due to the absence of vacancies in its d-bands ($5d^{10}$ electron configuration). Platinum is a stronger chemisorber ($5d^9$ electron configuration) than gold. Dissociative adsorption of ethylene glycol on the surface of platinum is therefore significant and occurs even if at open circuit. This is presumably due to the interactions of the CH_2 groups with the metallic platinum sites. By contrast, such a dissociative adsorption does not take place at a gold surface: the applied potential must have positive values to allow adsorption of the OH groups at the surface and their subsequent dissociation (Enea and Ango, 1989). This may explain why the CO poisoning species are formed only progressively at gold, but are already present from the beginning at platinum (Kadirgan et al., 1990; Hahn et al., 1987).

6.3.3. The 60Au-40Pt alloy

6.3.3.1. The 60Au-40Pt alloy in the 1300°C heat treatment condition

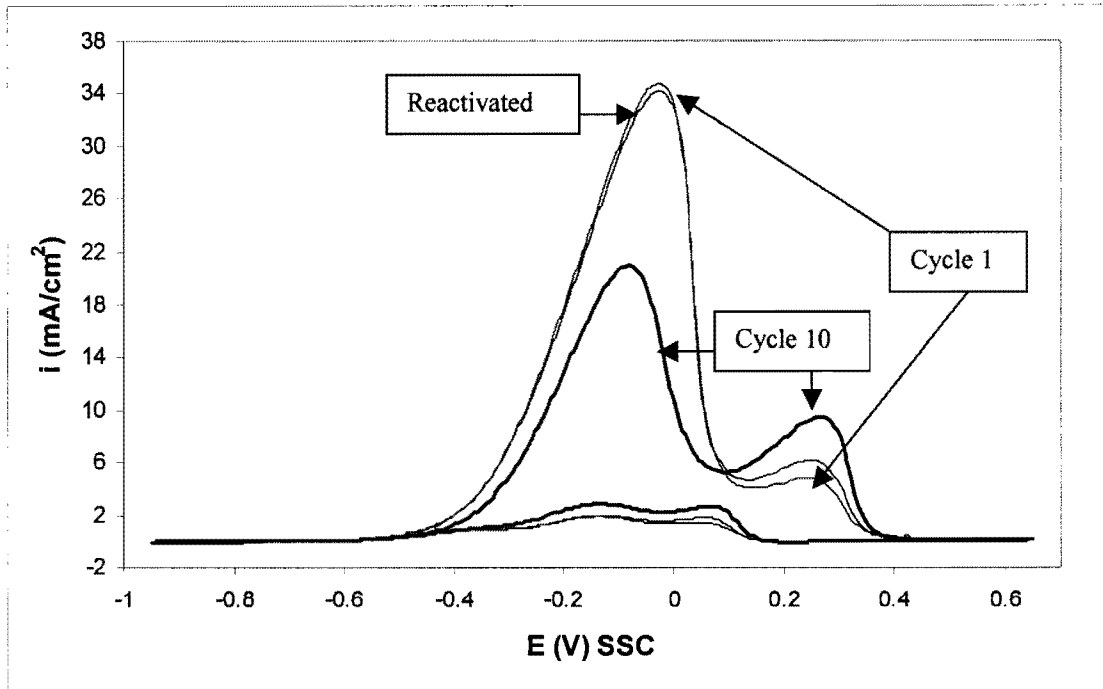
The two-phased microstructure of this alloy can be seen in Figure 3.2. Cyclic voltammograms for the 1300°C treated electrode in 0.5 M NaOH without ethylene glycol are shown in Figure 5.5.

The cyclic voltammograms (1st and 10th cycles) with 0.1 M ethylene glycol in the solution are shown in Figure 6.4. The solution was not stirred in Figure 6.4(a) and stirred in Figure 6.4(b). The first cycles after anodic reactivation of this electrode are also shown in Figures 6.4(a) and (b). The electro-oxidation of ethylene glycol at the alloy electrode occurs in two regions: the first region is in the same potential range as pure platinum and the second in the same potential range as pure gold.

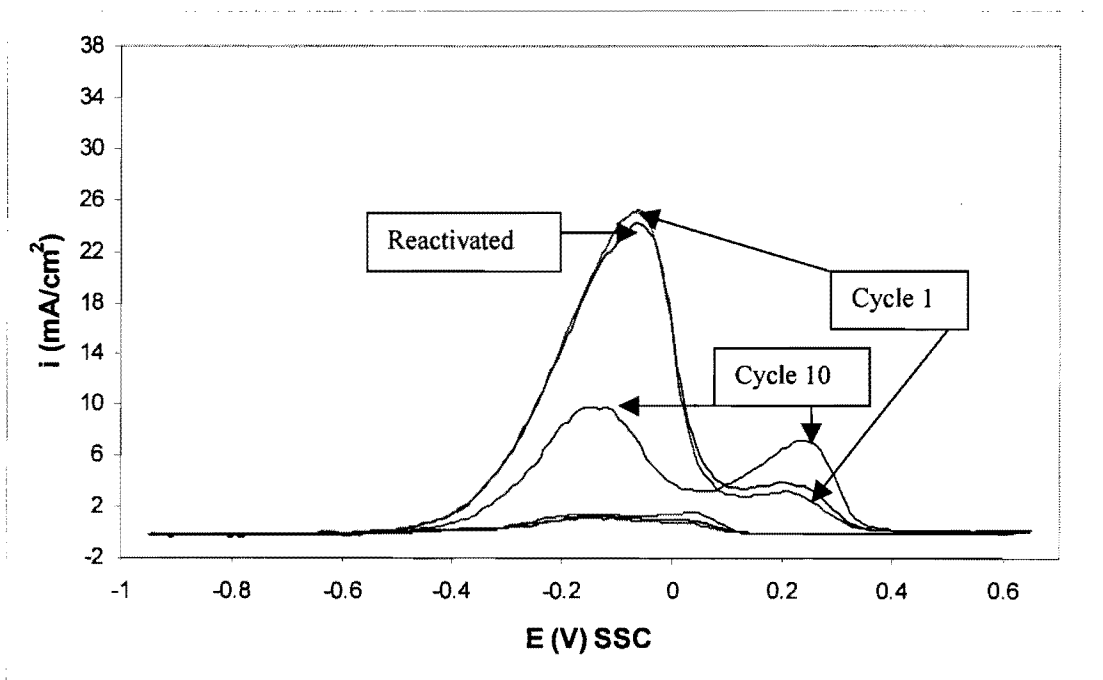
The peak current densities during the positive scan for this 60Au-40Pt electrode, pure gold and pure platinum are compared in Table 6.1.

Table 6.1. Peak current densities (in mA/cm²) during the positive scans for Au, Pt and the 1300°C electrode

Scan no.	Stirred?	Pt	1300°C (Pt region)	Au	1300°C (Au region)
1	No	13.5	34	16	4.5
1	Yes	8	25	10.5	3
10	No	11	21	13.5	9
10	Yes	6.5	10	9.5	7



(a)



(b)

Figure 6.4. Cyclic voltammograms for the electro-oxidation of 0.1 M ethylene glycol in 0.5 M NaOH at the 1300°C (60Au-40Pt) electrode (50mV/s, 25°C). (a) Solution not stirred; (b) Solution stirred.

From Table 6.1, it is seen that the activity of the platinum region of the alloy is enhanced compared to pure platinum. The current densities of the platinum region of the alloy decrease from scan 1 to scan 10. Surprisingly, the current densities of the gold region increase as the number of scans increases. The activity of the gold region is decreased compared to pure gold. These results differ from those of Beden and co-workers (1982), who found that the activities of both the platinum and the gold regions for a 50Au-50Pt electrode were enhanced compared with the pure metals (Fig 2.17). As with pure gold and pure platinum, the current densities of the alloy electrode are lower when the solution is stirred (Table 6.1).

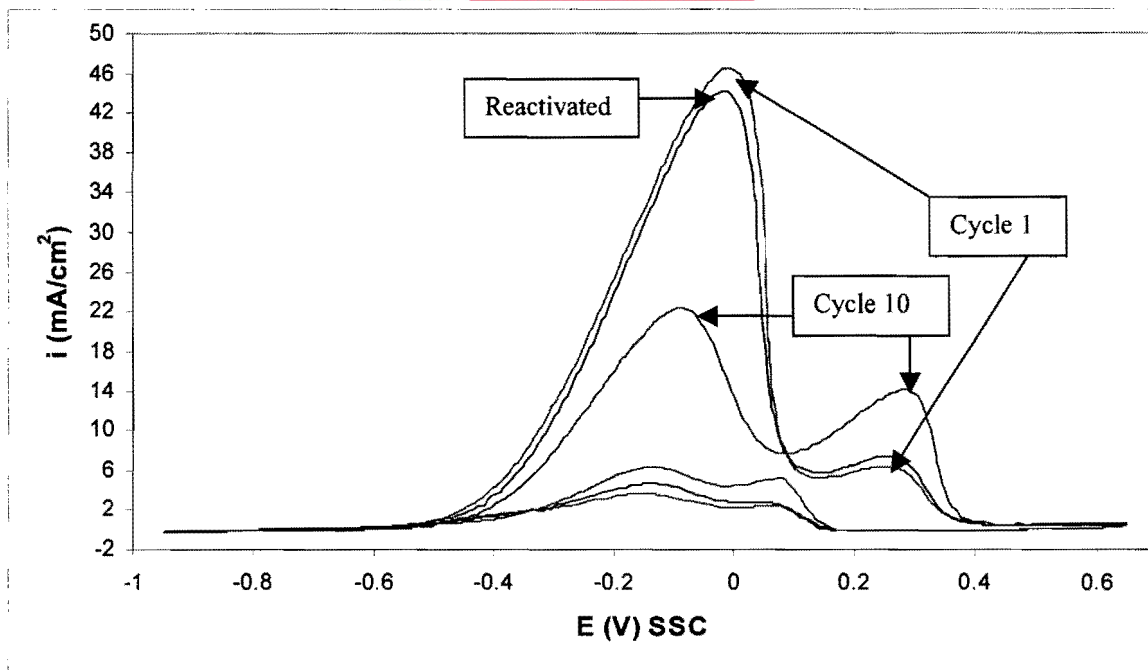
The anodic treatment at $1.2V_{SSC}$ after the 10th cycle reactivates the platinum region of the alloy electrode, but deactivates the gold region again (Fig. 6.4). It therefore seems as if the activities of the two regions are linked – the activity of the one is high when the activity of the other is low and vice versa.

6.3.3.2. The 60Au-40Pt alloy in the 1200°C (24 hours) heat treatment condition

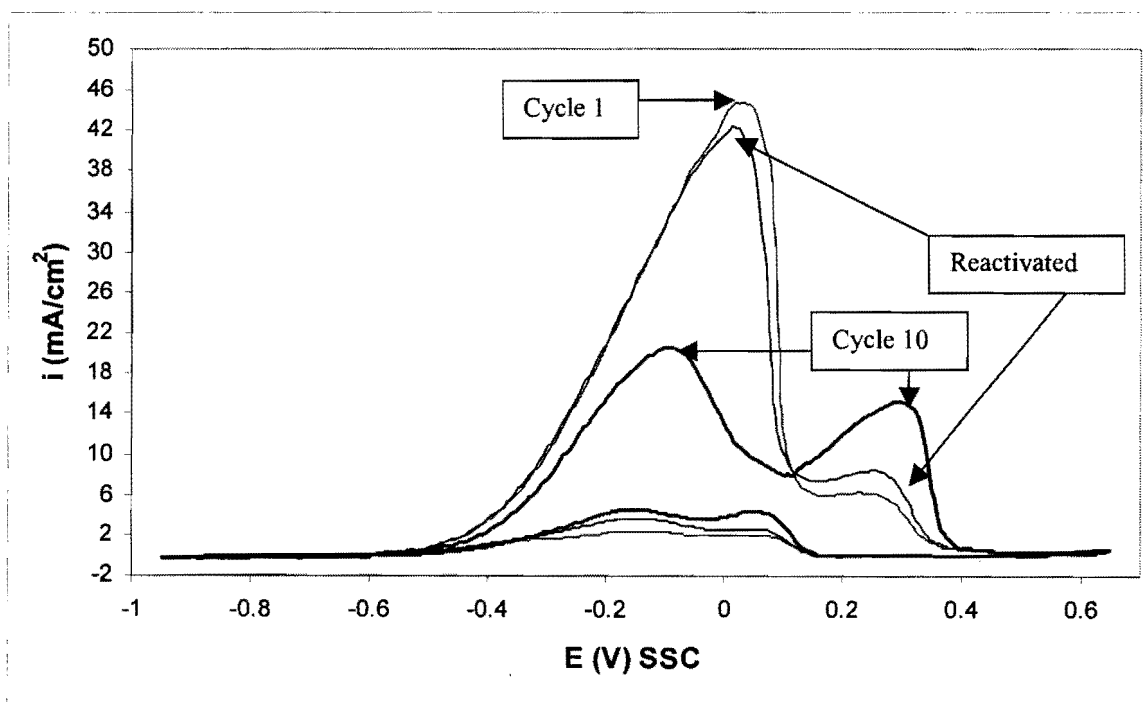
The microstructure of this alloy (single-phased, porous) can be seen in Figure 3.6. The sample was in the 1300°C heat treated condition prior to the heat treatment at 1200°C for 24 hours. Cyclic voltammograms for the 1200°C-24 h treated electrode in 0.5 M NaOH without ethylene glycol are shown in Figure 5.6.

The cyclic voltammograms (1st and 10th cycles) with 0.1 M ethylene glycol in the solution are shown in Figure 6.5. The solution was not stirred in Figure 6.5(a) and stirred in Figure 6.5(b). The first cycles after anodic reactivation of this electrode are also shown in Figures 6.5(a) and (b). The electro-oxidation of ethylene glycol at this solid solution electrode also occurs in two regions: the first region is in the same potential range as pure platinum and the second in the same potential range as pure gold.

The peak current densities during the positive scan for this 60Au-40Pt electrode, pure gold and pure platinum are compared in Table 6.2.



(a)



(b)

Figure 6.5. Cyclic voltammograms for the electro-oxidation of 0.1 M ethylene glycol in 0.5 M NaOH at the 1200°C-24h (60Au-40Pt) electrode (50mV/s, 25°C). (a) Solution not stirred; (b) Solution stirred.

Table 6.2. Peak current densities (in mA/cm²) during the positive scans for Au, Pt and the 1200°C-24 h electrode

Scan no.	Stirred?	Pt	1200°C-24h (Pt region)	Au	1200°C-24h (Au region)
1	No	13.5	46	16	6
1	Yes	8	45	10.5	6
10	No	11	22	13.5	14
10	Yes	6.5	21	9.5	15

Comparing Tables 6.1 and 6.2, it is seen that the porous solid solution electrode produces higher apparent current densities than the non-porous, two-phased 1300°C electrode. The higher apparent current densities of the porous electrode may be due to one of the following reasons:

- The extra surface area of the porous electrode produces higher apparent current densities and the phase difference between the two electrodes is negligible.
- The solid solution of platinum in gold (single phase) is more effective for the electro-oxidation of ethylene glycol than the two-phased microstructure and the porosity does not play an important role.
- The combination of the extra surface area of the porous electrode and the solid solution leads to higher apparent current densities.
- The solid solution decreases the activity, but the extra surface area due to the porosity still leads to higher apparent current densities.

It is difficult to say at this point which of the above scenarios is the correct one. The 50Au-50Pt electrodes (single-phased and two-phased, but both non-porous) should give valuable information to indicate which scenario is correct (see paragraph 6.3.4.). The 60Au-40Pt electrode heat treated at 1200°C for 168 hours will also give valuable information (see paragraph 6.3.3.3.), because the porosity of this electrode appears to be less than that of the 1200°C-24h electrode (compare Figures 3.6 and 3.8).

From Table 6.2 it is evident that stirring does not have a great effect on the current densities obtained with this electrode - the solution inside the pores is probably not affected much by stirring.

The anodic treatment at $1.2V_{SSC}$ after the 10th cycle once again reactivates the platinum region of the alloy electrode, but deactivates the gold region (Fig. 6.5).

6.3.3.3. The 60Au-40Pt alloy in the 1200°C (168 hours) heat treatment condition

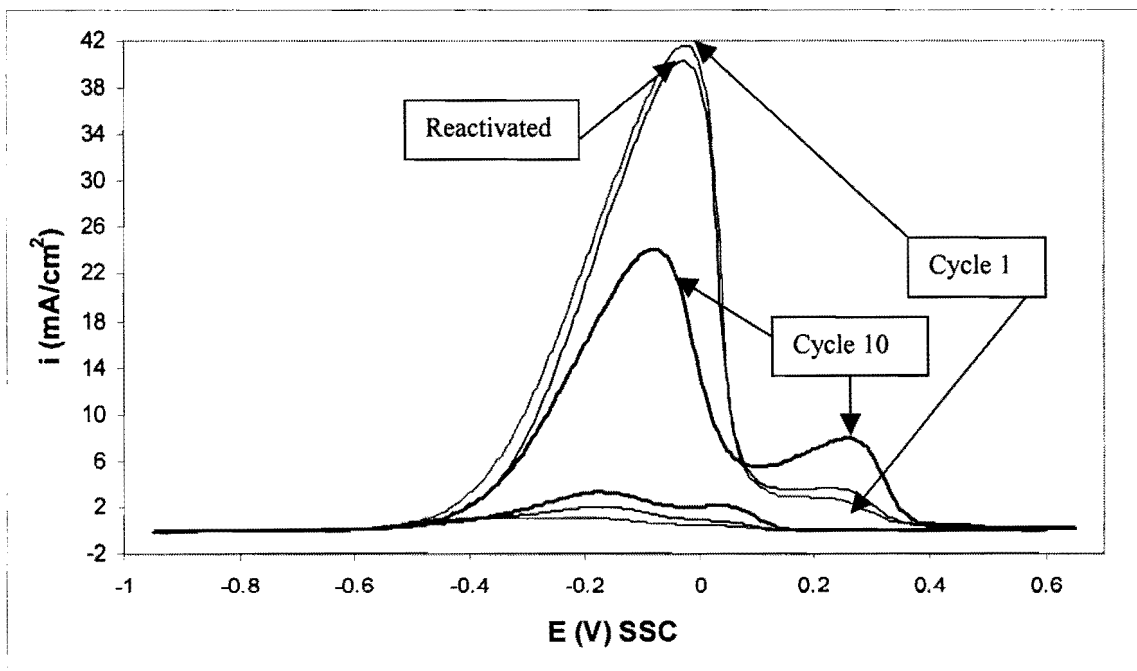
The microstructure of this alloy (single-phased; porous, but with less porosity than after the 24 hour treatment at 1200°C) can be seen in Figure 3.8. The sample was in the 1300°C heat treated condition prior to the heat treatment at 1200°C for 168 hours. Cyclic voltammograms for the 1200°C-168 h treated electrode in 0.5 M NaOH without ethylene glycol are shown in Figure 5.8.

The cyclic voltammograms (1st and 10th cycles) with 0.1 M ethylene glycol in the solution are shown in Figure 6.6. The solution was not stirred in Figure 6.6(a) and stirred in Figure 6.6(b). The first cycles after anodic reactivation of this electrode are also shown in Figures 6.6(a) and (b). Once again, the electro-oxidation of ethylene glycol at this solid solution electrode occurs in two regions: the first region is in the same potential range as pure platinum and the second in the same potential range as pure gold.

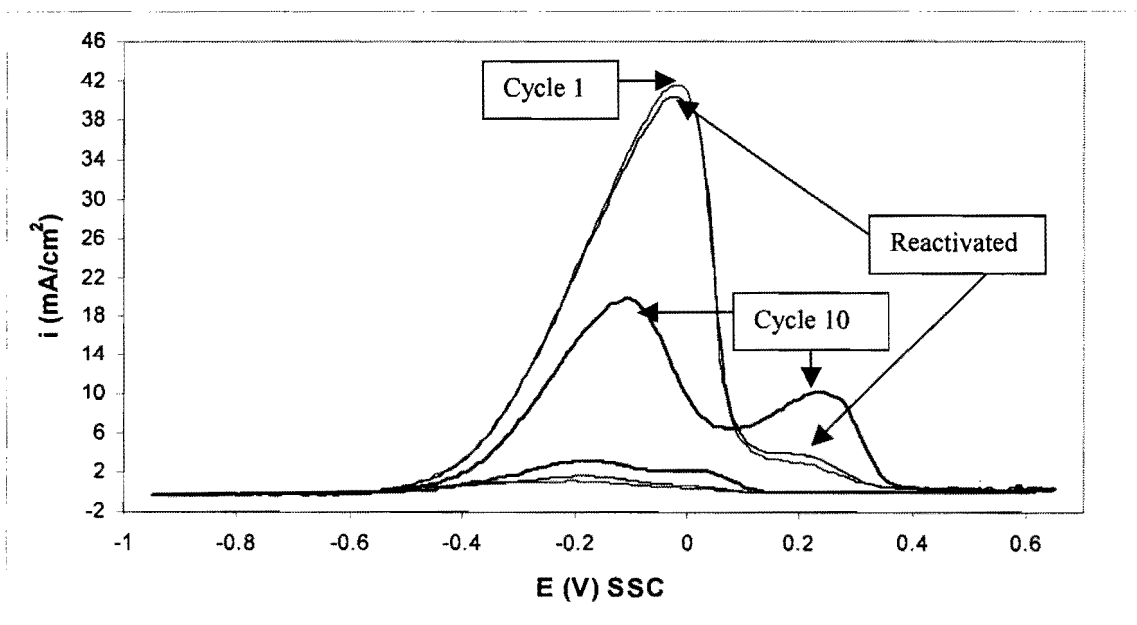
The peak current densities during the positive scan for this 60Au-40Pt electrode, pure gold and pure platinum are compared in Table 6.3.

Table 6.3. Peak current densities (in mA/cm²) during the positive scans for Au, Pt and the 1200°C-168 h electrode

Scan no.	Stirred?	Pt	1200°C-168h (Pt region)	Au	1200°C-168h (Au region)
1	No	13.5	42	16	3
1	Yes	8	41	10.5	3
10	No	11	24	13.5	8
10	Yes	6.5	20	9.5	10



(a)



(b)

Figure 6.6. Cyclic voltammograms for the electro-oxidation of 0.1 M ethylene glycol in 0.5 M NaOH at the 1200°C-168h (60Au-40Pt) electrode (50mV/s, 25°C). (a) Solution not stirred; (b) Solution stirred.

Comparing Tables 6.2 and 6.3, it is seen that the two porous solid solution electrodes produce rather similar apparent current densities (especially the Pt-regions). This is surprising if one considers the large difference in apparent current densities between the two electrodes without ethylene glycol in solution (Fig. 5.9). It therefore appears as if the extra surface area due to the porosity does not significantly increase the maximum apparent current densities for ethylene glycol electro-oxidation.

From Table 6.3 it is evident that stirring also does not have a great effect on the current densities obtained with this electrode.

The anodic treatment at $1.2V_{SSC}$ after the 10th cycle once again reactivates the platinum region of the alloy electrode, but deactivates the gold region (Fig. 6.6).

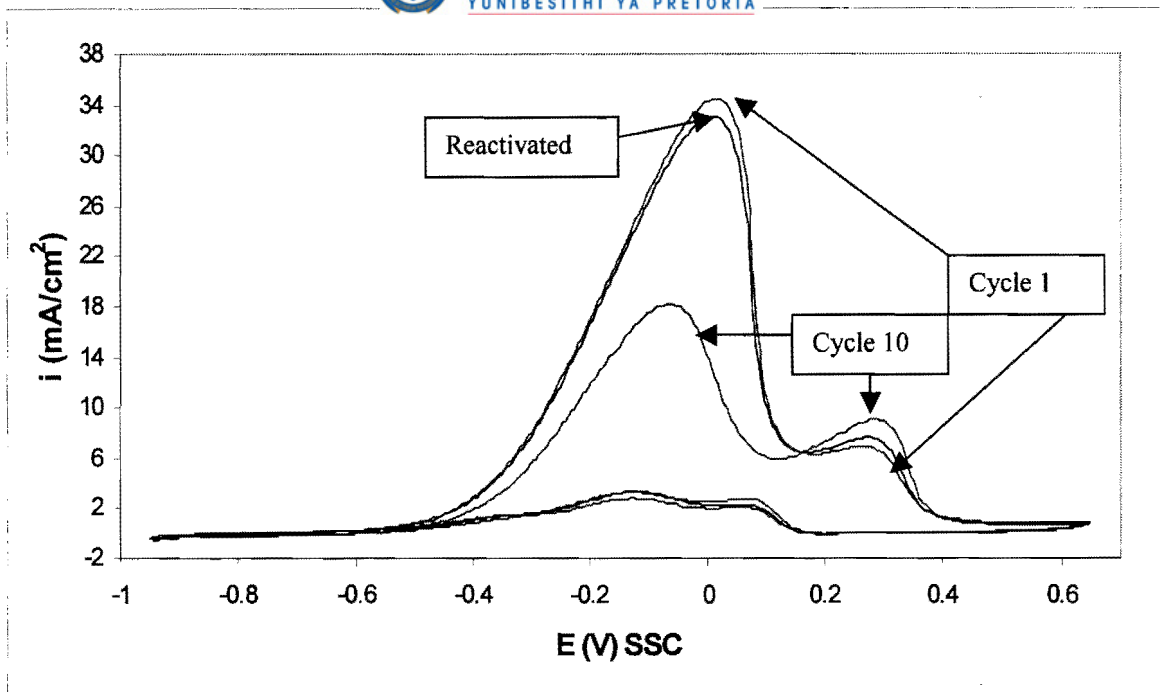
6.3.3.4. The 60Au-40Pt alloy in the 800°C heat treatment condition

The microstructure of this alloy (two-phased, porous) can be seen in Figure 3.12. The sample was in the 1200°C-24h (single-phased, porous) heat treatment condition prior to the heat treatment at 800°C for 50 hours. Cyclic voltammograms for the 800°C treated electrode in 0.5 M NaOH without ethylene glycol are shown in Figure 5.11.

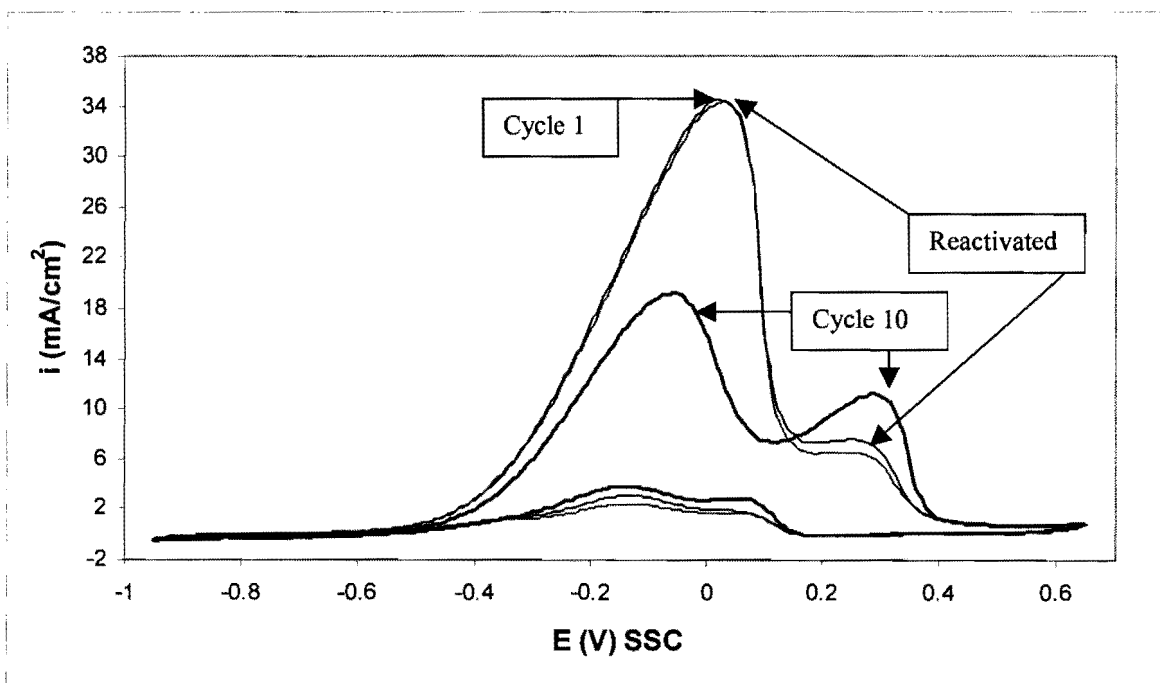
The cyclic voltammograms (1st and 10th cycles) with 0.1 M ethylene glycol in the solution are shown in Figure 6.7. The solution was not stirred in Figure 6.7(a) and stirred in Figure 6.7(b).

The first cycles after anodic reactivation of this electrode are also shown in Figures 6.7(a) and (b).

The peak current densities during the positive scan for this 60Au-40Pt electrode, pure gold and pure platinum are compared in Table 6.4.



(a)



(b)

Figure 6.7. Cyclic voltammograms for the electro-oxidation of 0.1 M ethylene glycol in 0.5 M NaOH at the 800°C (60Au-40Pt) electrode (50mV/s, 25°C). (a) Solution not stirred; (b) Solution stirred.

Table 6.4. Peak current densities (in mA/cm²) during the positive scans for Au, Pt and the 800°C electrode

Scan no.	Stirred?	Pt	800°C (Pt region)	Au	800°C (Au region)
1	No	13.5	34	16	7
1	Yes	8	34	10.5	6
10	No	11	18	13.5	9
10	Yes	6.5	19	9.5	11

Comparing Tables 6.2 and 6.4, it is seen that the solid solution electrode produces higher apparent current densities than the two-phased 800°C heat treated electrode (especially the Pt-regions, 1st scans). It therefore seems as if a solid solution is more effective for the electro-oxidation than a two-phased microstructure. This can perhaps be explained by the “third-body effect” (see section 2.6.5.3.). The formation of poisonous species adsorbed on more than one surface site is suppressed. A platinum atom cannot be “poisoned” by a strongly bound intermediate when it is surrounded by gold atoms. Adsorption sites that are only available on larger platinum clusters are needed (Rach and Heitbaum, 1987). Fewer platinum atoms are surrounded by gold atoms in the two-phased electrode (the equilibrium gold content of the platinum-rich areas of the 800°C treated alloy is shown in Table 3.1) than with the solid solution electrode. The two-phased electrode is therefore more likely to be poisoned and the current densities are lower.

From Table 6.4 it is evident again that stirring does not have a great effect on the current densities obtained with this porous electrode.

The anodic treatment at 1.2 V_{SSC} after the 10th cycle once again reactivates the platinum region of the alloy electrode, but deactivates the gold region (Fig. 6.7).

6.3.3.5. The 60Au-40Pt alloy in the 600°C heat treatment condition

The microstructure of this alloy (two-phased, porous) can be seen in Figure 3.15. The sample was in the 1200°C-24h (single-phased, porous) heat treatment condition prior to the heat treatment at 600°C for 100 hours. Cyclic voltammograms for the 600°C treated electrode in 0.5 M NaOH without ethylene glycol are shown in Figure 5.12.

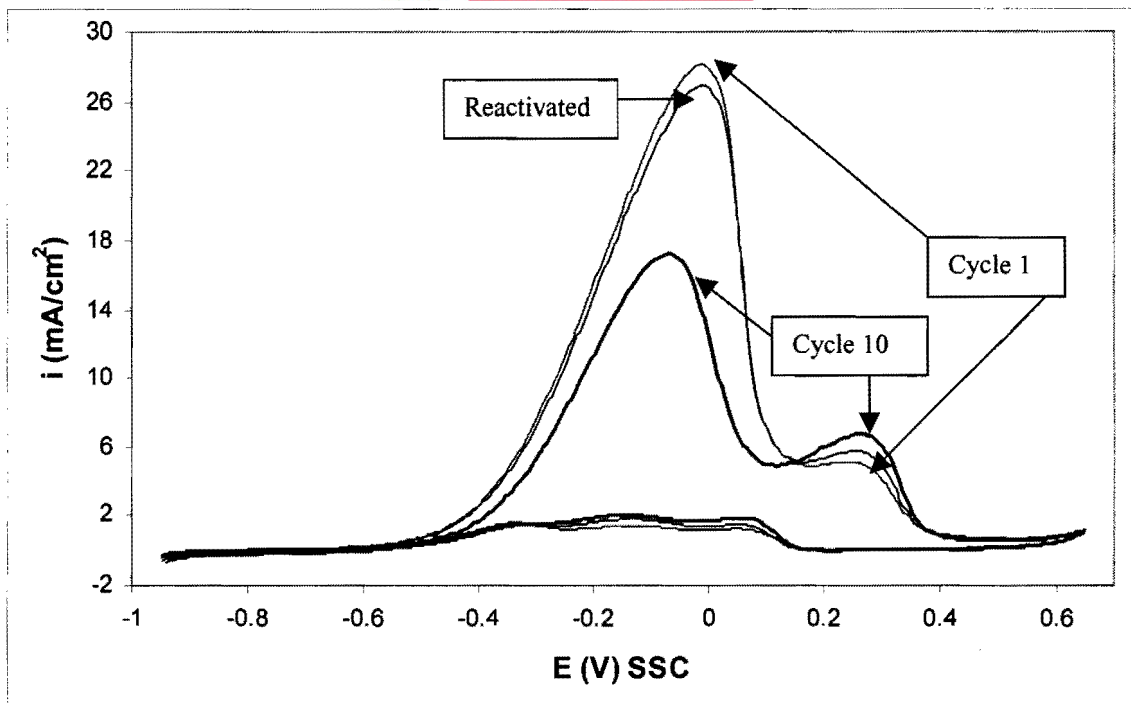
The cyclic voltammograms (1st and 10th cycles) with 0.1 M ethylene glycol in the solution are shown in Figure 6.8. The solution was not stirred in Figure 6.8(a) and stirred in Figure 6.8(b). The first cycles after anodic reactivation of this electrode are also shown in Figures 6.8(a) and (b).

The peak current densities during the positive scan for this 60Au-40Pt electrode, pure gold and pure platinum are compared in Table 6.5.

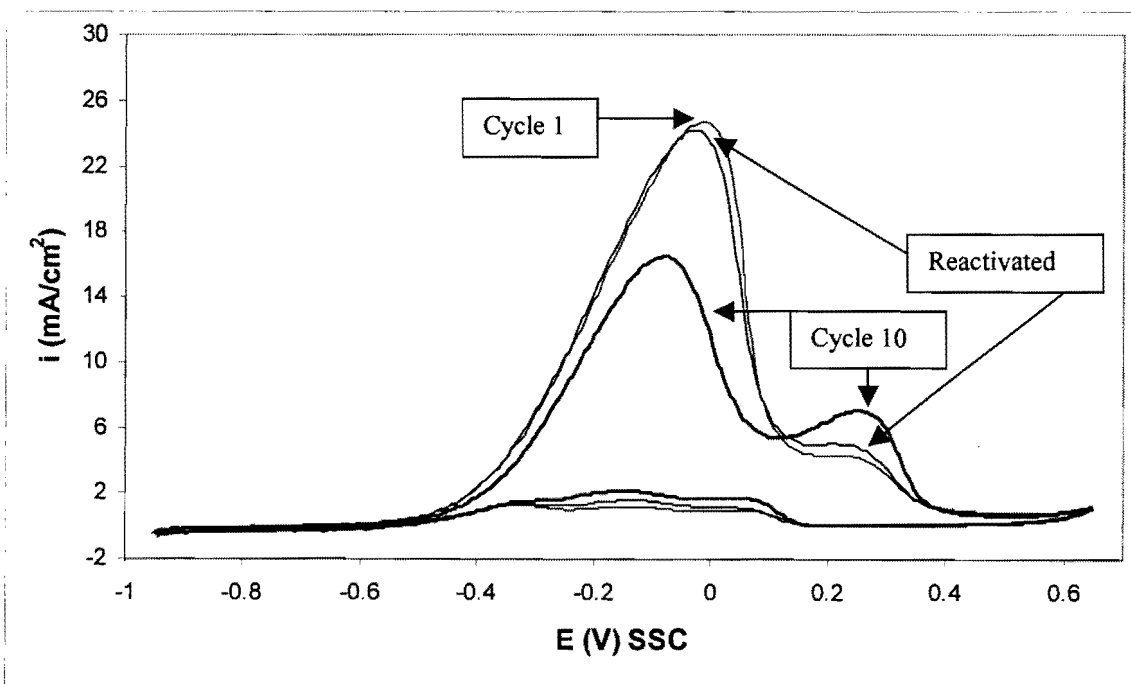
Table 6.5. Peak current densities (in mA/cm²) during the positive scans for Au, Pt and the 600°C electrode

Scan no.	Stirred?	Pt	600°C (Pt region)	Au	600°C (Au region)
1	No	13.5	28	16	5
1	Yes	8	25	10.5	4
10	No	11	17	13.5	7
10	Yes	6.5	16	9.5	7

Comparing Tables 6.4 and 6.5, it is seen that the 800°C electrode produces slightly higher apparent current densities than the 600°C heat treated electrode. The higher equilibrium gold content of the platinum-rich areas of the 800°C treated sample compared to the 600°C treated sample (Table 3.1) is probably responsible for this result.



(a)



(b)

Figure 6.8. Cyclic voltammograms for the electro-oxidation of 0.1 M ethylene glycol in 0.5 M NaOH at the 600°C (60Au-40Pt) electrode (50mV/s, 25°C). (a) Solution not stirred; (b) Solution stirred.

From Table 6.5 it is evident again that stirring does not have a great effect on the current densities obtained with porous electrodes.

As before, the anodic treatment at 1.2 V_{SSC} after the 10th cycle reactivates the platinum region of the alloy electrode, but deactivates the gold region (Fig. 6.7).

6.3.4. The 50Au-50Pt alloy

6.3.4.1. The 50Au-50Pt alloy in the “ductile” heat treatment condition

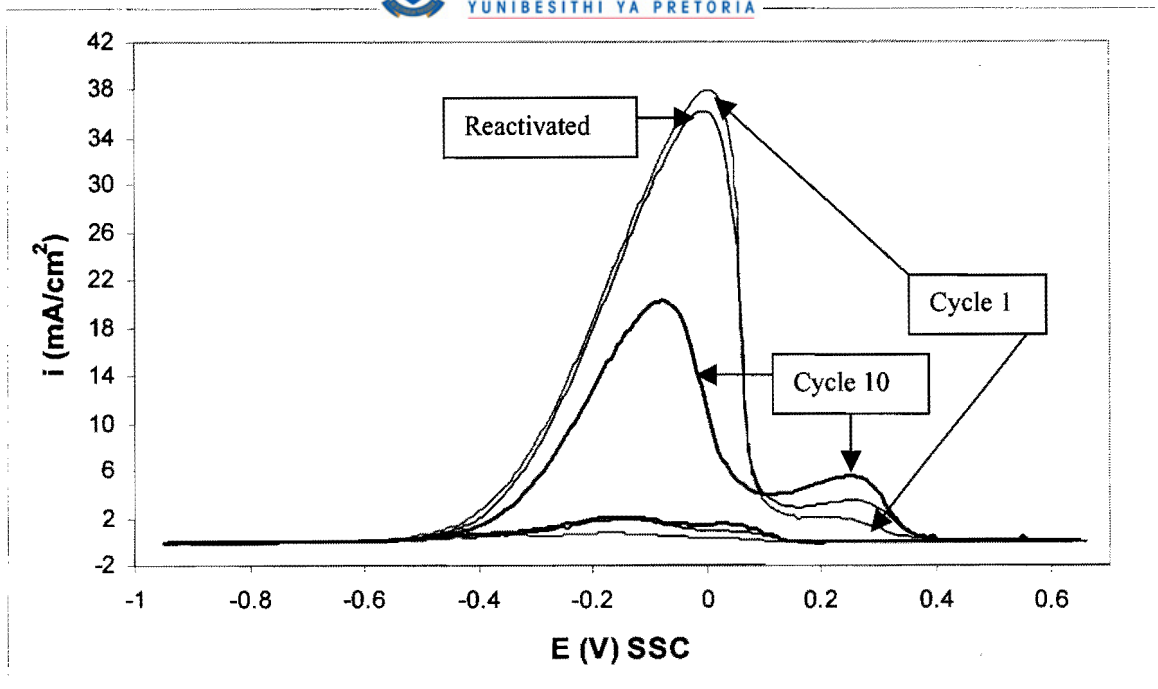
The microstructure of this sample (two-phased, fine microstructure, not porous) can be seen in Figure 3.17. Cyclic voltammograms for the “ductile” electrode in 0.5 M NaOH without ethylene glycol are shown in Figure 5.14.

The cyclic voltammograms for the “ductile” electrode in 0.5 M NaOH with 0.1 M ethylene glycol are shown in Figure 6.9. The first cycles voltammograms (1st and 10th cycles) with 0.1 M ethylene glycol in the solution are shown in after anodic reactivation of this electrode are also shown in Figures 6.9(a) and (b).

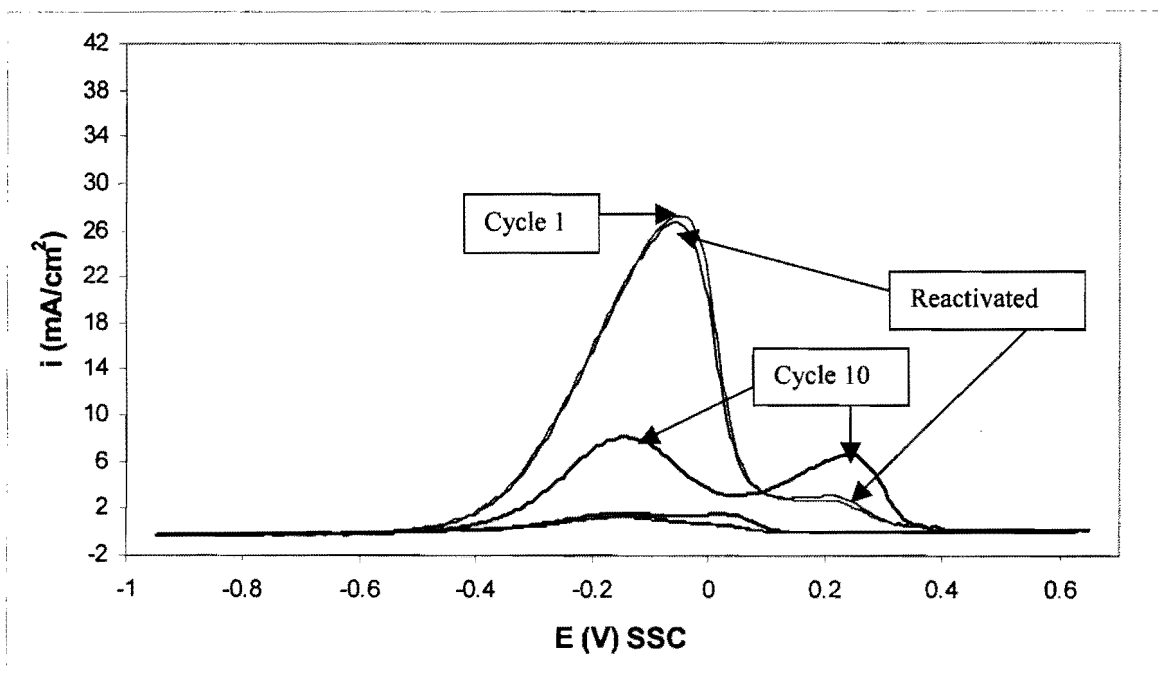
The peak current densities during the positive scan for this 50Au-50Pt electrode, pure gold and pure platinum are compared in Table 6.6.

Table 6.6. Peak current densities (in mA/cm²) during the positive scans for Au, Pt and the “ductile” 50Au-50Pt electrode

Scan no.	Stirred?	Pt	Ductile (Pt region)	Au	Ductile (Au region)
1	No	13.5	38	16	3
1	Yes	8	27	10.5	3
10	No	11	20	13.5	6
10	Yes	6.5	8	9.5	6



(a)



(b)

Figure 6.9. Cyclic voltammograms for the electro-oxidation of 0.1 M ethylene glycol in 0.5 M NaOH at the “ductile” (50Au-50Pt) electrode (50mV/s, 25°C). (a) Solution not stirred; (b) Solution stirred.

Comparing Tables 6.1 and 6.6, it is seen that the two-phased, non-porous 60Au-40Pt electrode and the two-phased, non-porous 50Au-50Pt electrode produce similar apparent current densities, despite differences in the compositions of the phases for the two electrodes (Figures 3.1 and 3.16). Solution stirring in both cases reduces the current densities significantly. This confirms that the non-porous electrodes are negatively affected by stirring.

The anodic treatment at 1.2 V_{SSC} after the 10th cycle once again reactivates the platinum region of the alloy electrode, but deactivates the gold region (Fig. 6.9).

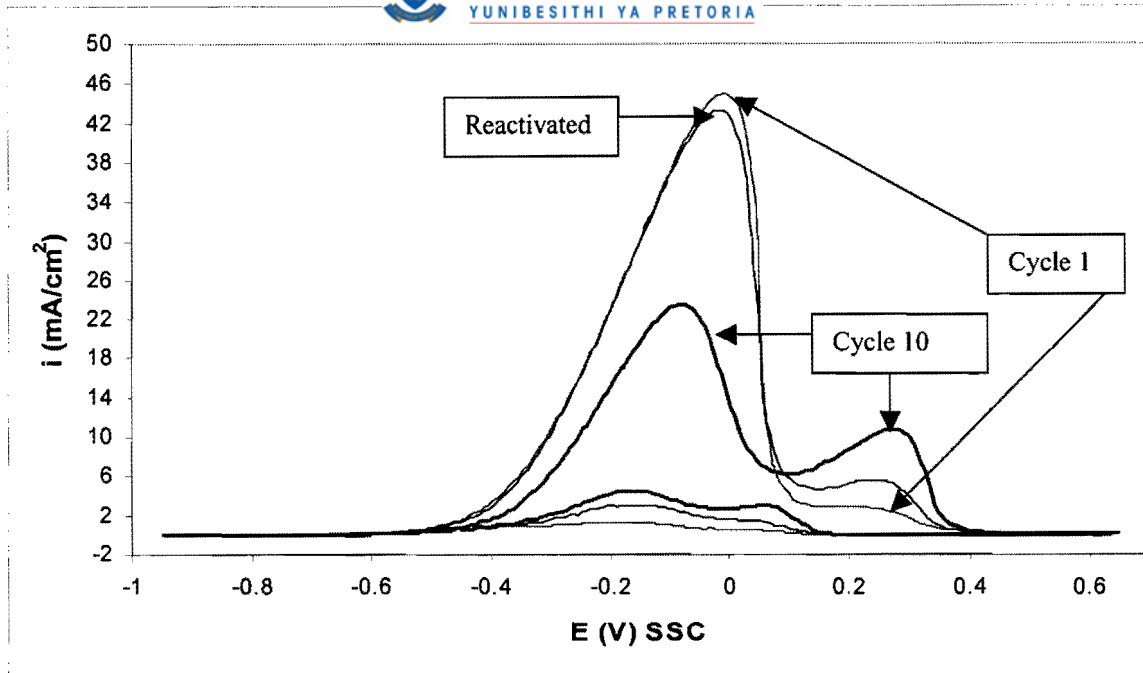
6.3.4.2. The 50Au-50Pt alloy in the solid solution heat treatment condition

The microstructure of this sample (single-phased, not porous) can be seen in Figure 3.19. The sample was in the “ductile” heat treatment condition prior to solutionising at 1250°C for 24 hours. Cyclic voltammograms for the solid solution electrode in 0.5 M NaOH without ethylene glycol are shown in Figure 5.15.

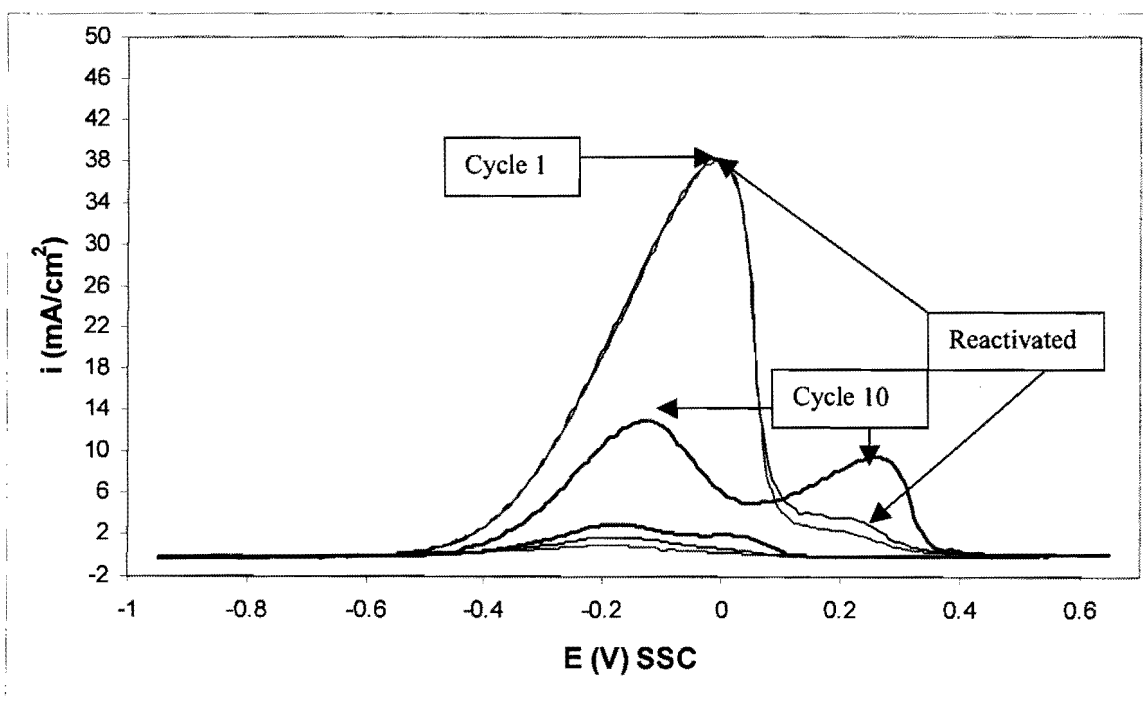
The cyclic voltammograms (1st and 10th cycles) with 0.1 M ethylene glycol in the solution are shown in Figure 6.10. The solution was not stirred in Figure 6.10(a) and stirred in Figure 6.10(b). The first cycles after anodic reactivation of this electrode are also shown in Figures 6.10(a) and (b). The peak current densities during the positive scan for this 50Au-50Pt electrode, pure gold and pure platinum are compared in Table 6.7.

Table 6.7. Peak current densities (in mA/cm²) during the positive scans for Au, Pt and the solid solution 50Au-50Pt electrode

Scan no.	Stirred?	Pt	Solid solution (Pt region)	Au	Solid solution (Au region)
1	No	13.5	45	16	3
1	Yes	8	38	10.5	2
10	No	11	24	13.5	11
10	Yes	6.5	13	9.5	9



(a)



(b)

Figure 6.10. Cyclic voltammograms for the electro-oxidation of 0.1 M ethylene glycol in 0.5 M NaOH at the solid solution (50Au-50Pt) electrode (50mV/s, 25°C). (a) Solution not stirred; (b) Solution stirred.

Comparing Tables 6.6 and 6.7, it is seen that the solid solution 50Au-50Pt electrode produces higher apparent current densities than the “ductile” (two-phased) 50Au-50Pt electrode. These two electrodes are both not porous. The difference in current densities can therefore only be due to the difference in phase compositions.

If one compares the 60Au-40Pt solid solution electrode (porous, Table 6.2) with the 50Au-50Pt solid solution electrode (not porous, Table 6.7), it is seen that the apparent current densities of the two electrodes are similar when the solution is not stirred. Solution stirring with the non-porous electrode reduces the current densities. The advantage of the porosity is therefore not to increase the maximum peak current densities, but rather to maintain a higher current density when the solution is stirred. The solution inside the pores is probably not affected much by stirring. The intermediates that are formed inside the pores during the electro-oxidation of ethylene glycol are therefore not transported away from the electrode as with the non-porous electrodes when the solution is stirred. The intermediates are oxidised further inside the pores, resulting in higher current densities.

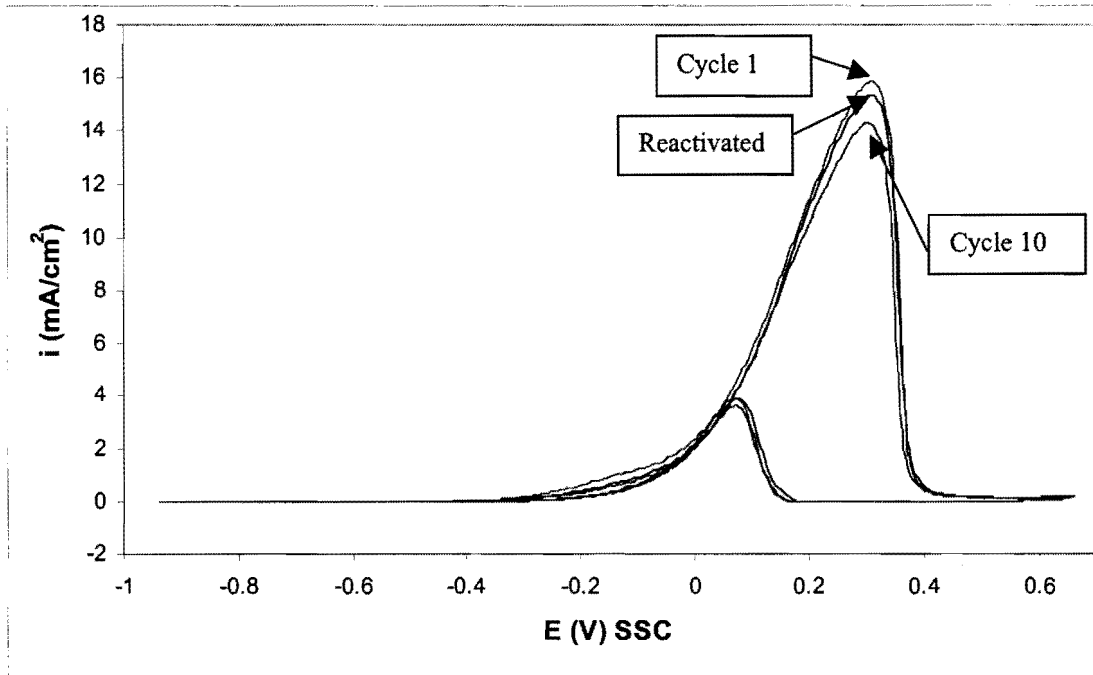
The anodic treatment at 1.2 V_{SSC} after the 10th cycle once again reactivates the platinum region of the alloy electrode, but deactivates the gold region (Fig. 6.10).

6.3.5. The Gold 990 alloy

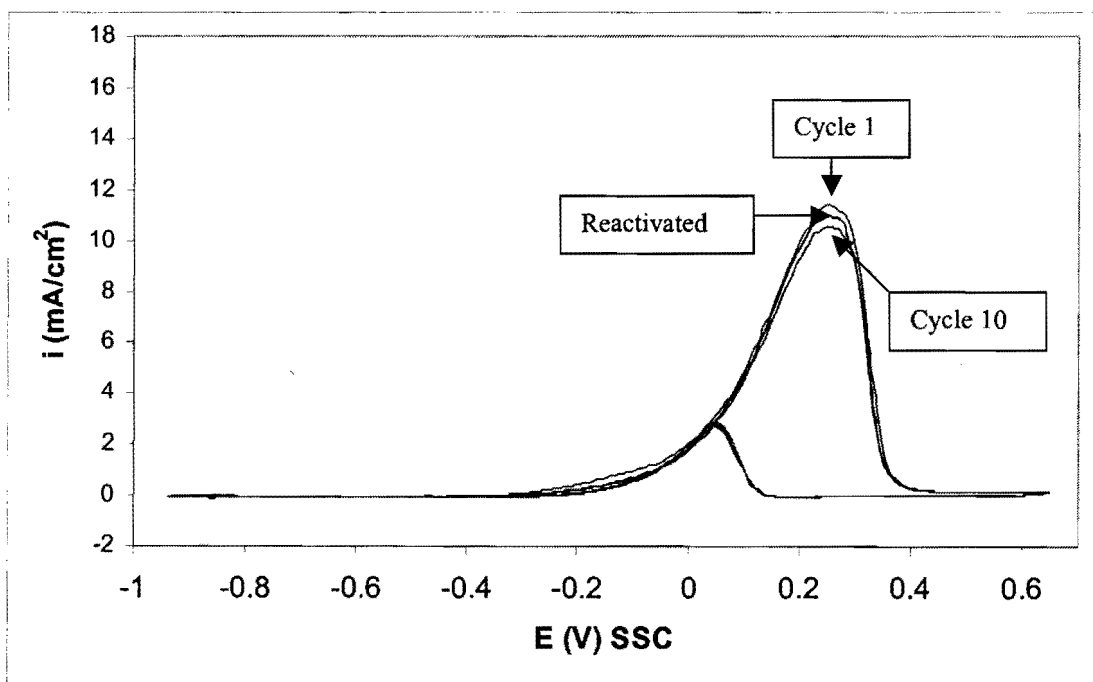
6.3.5.1. The Gold 990 alloy in the solid solution condition

This sample has 1 wt% (4 at%) titanium in solid solution with the gold. The Vickers hardness of the sample in this condition is HV₅ = 50 kg/mm². Cyclic voltammograms for this sample in 0.5 M NaOH without ethylene glycol are shown in Figure 5.18.

The cyclic voltammograms (1st and 10th cycles) with 0.1 M ethylene glycol in the solution are shown in Figure 6.11. The solution was not stirred in Figure 6.11(a) and stirred in Figure 6.11(b). The first cycles after anodic reactivation of this electrode are also shown in Figures 6.11(a) and (b).



(a)



(b)

Figure 6.11. Cyclic voltammograms for the electro-oxidation of 0.1 M ethylene glycol in 0.5 M NaOH at the solid solution Gold 990 electrode (50mV/s, 25°C). (a) Solution not stirred; (b) Solution stirred.

The peak current densities during the positive scan for this Gold 990 electrode and pure gold are compared in Table 6.8.

Table 6.8. Peak current densities (in mA/cm²) during the positive scans for Au and the solid solution Gold 990 electrode

Scan no.	Stirred?	Au	Solid solution (Gold 990)
1	No	16	16
1	Yes	10.5	11
10	No	13.5	14
10	Yes	9.5	10.5

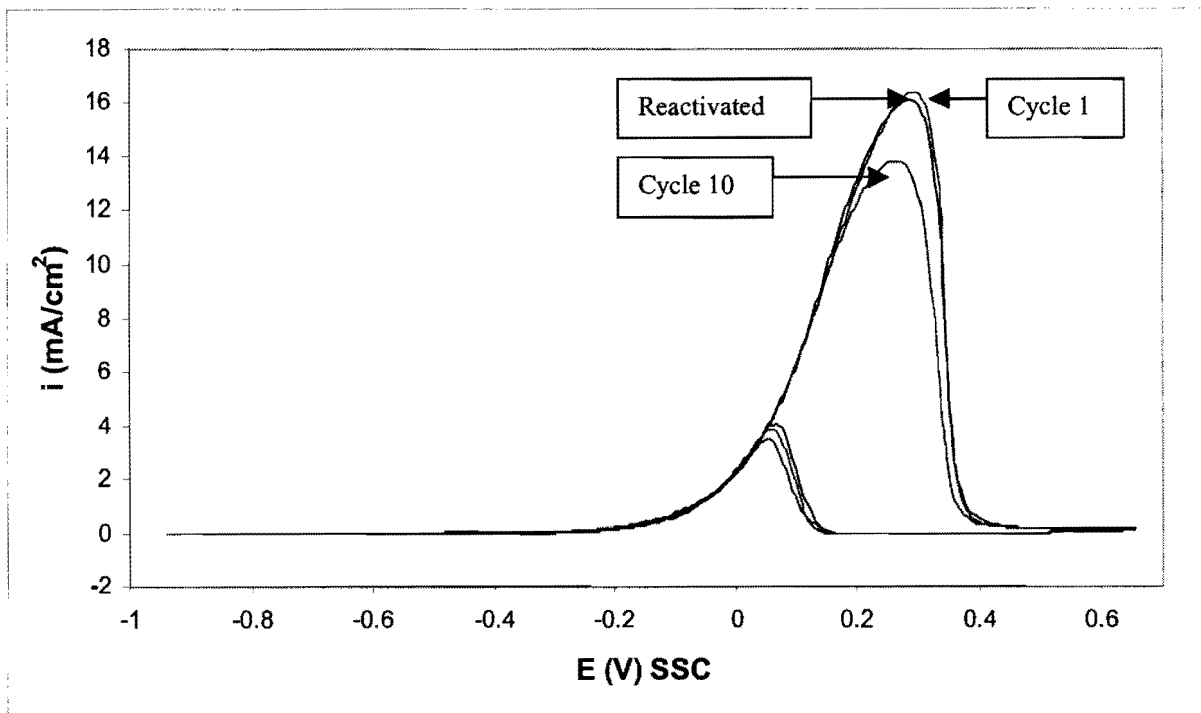
The behaviour of Gold 990 in the solid solution condition is similar to pure gold (Table 6.8).

The anodic treatment at 1.2 V_{SSC} after the 10th cycle reactivates the electrode (Fig. 6.11).

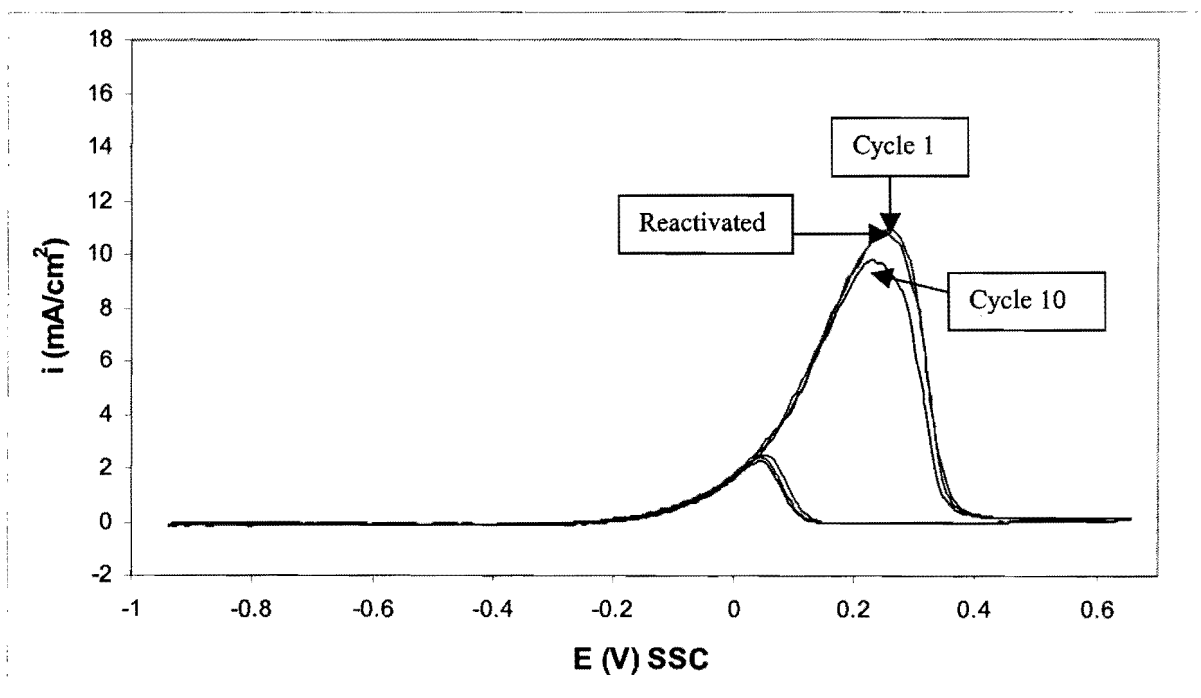
6.3.5.2. The Gold 990 alloy in the precipitation-hardened condition

This sample is hardened by the presence of small Au₄Ti precipitates. The Vickers hardness of the sample in this condition is HV₅ = 150 kg/mm². Cyclic voltammograms for this sample in 0.5 M NaOH without ethylene glycol are shown in Figure 5.19.

The cyclic voltammograms (1st and 10th cycles) with 0.1 M ethylene glycol in the solution are shown in Figure 6.12. The solution was not stirred in Figure 6.12(a) and stirred in Figure 6.12(b). The first cycles after anodic reactivation of this electrode are also shown in Figures 6.12(a) and (b).



(a)



(b)

Figure 6.12. Cyclic voltammograms for the electro-oxidation of 0.1 M ethylene glycol in 0.5 M NaOH at the precipitation-hardened Gold 990 electrode (50mV/s, 25°C). (a) Solution not stirred; (b) Solution stirred.

The peak current densities during the positive scan for this Gold 990 electrode and pure gold are compared in Table 6.9.

Table 6.9. Peak current densities (in mA/cm²) during the positive scans for Au and the precipitation-hardened Gold 990 electrode

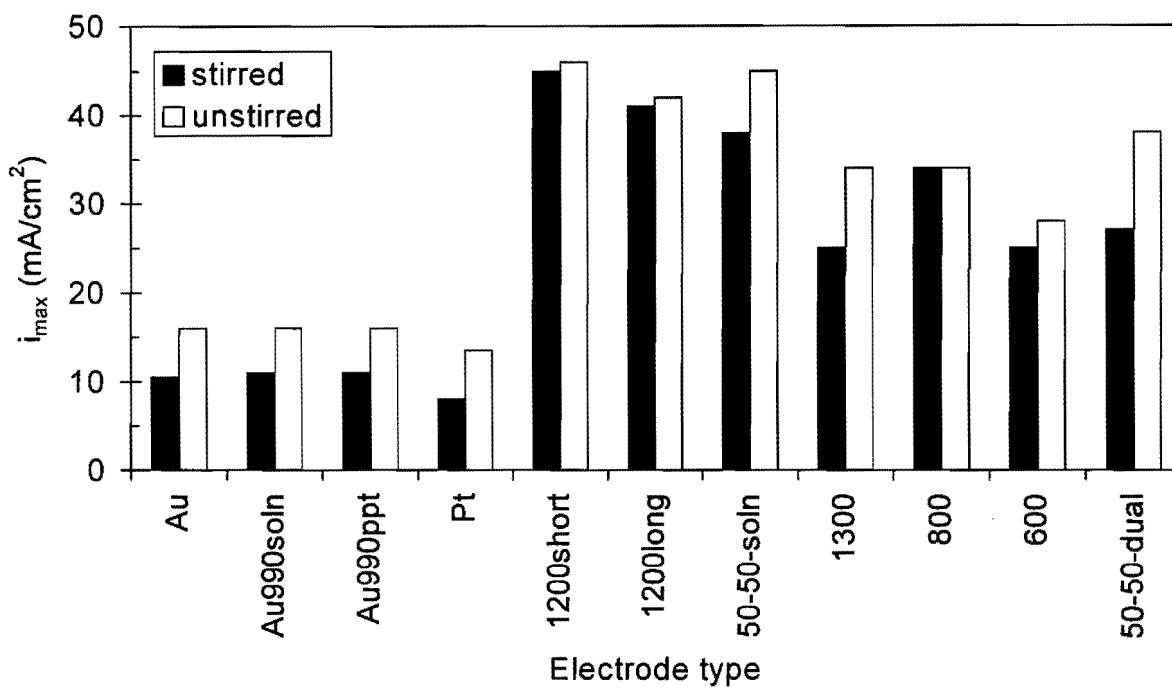
Scan no.	Stirred?	Au	Hardened (Gold 990)
1	No	16	16
1	Yes	10.5	11
10	No	13.5	14
10	Yes	9.5	10.5

The behaviour of Gold 990 in the precipitation-hardened condition is also similar to pure gold (Table 6.9). The possible reasons for the similarities between pure gold and Gold 990 have been discussed before (5.3.5.2.).

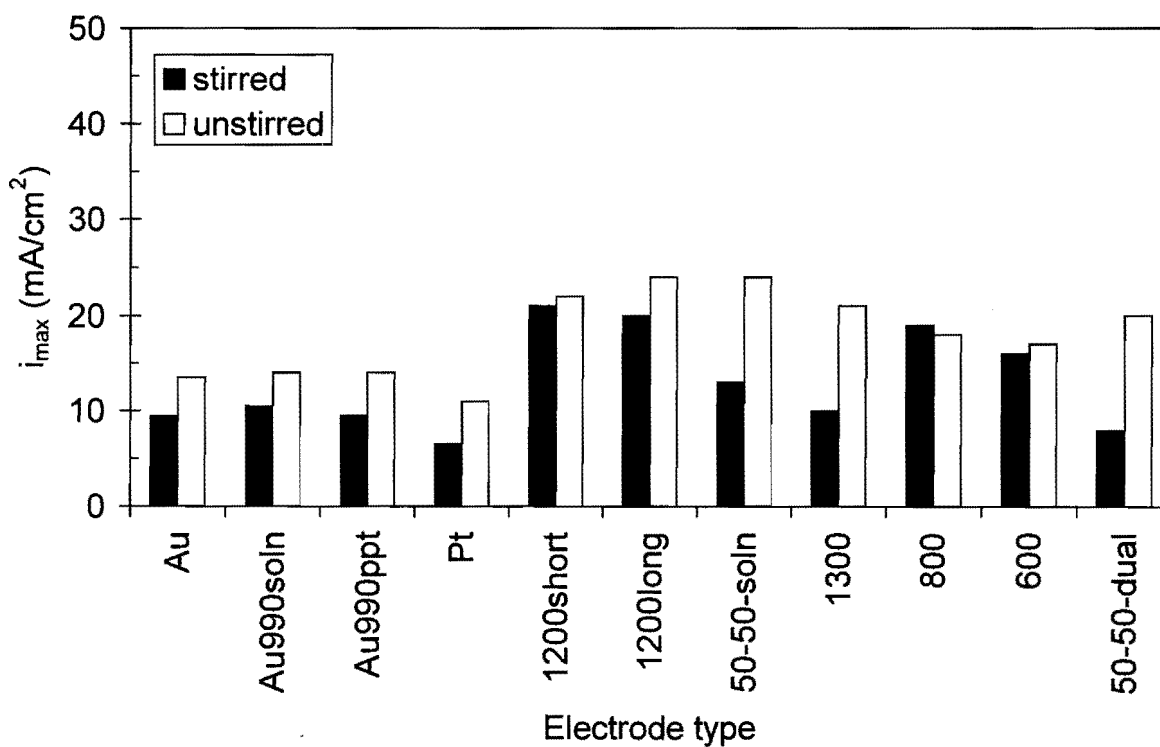
To summarise this section, the maximum peak current densities obtained at the electrodes during the first scan (Fig. 6.13(a)) and the tenth scan (Fig. 6.13(b)) are shown together for better comparison. Table 6.10 describes the electrodes in Figure 6.13.

Table 6.10. Description of the electrodes in Figure 6.13.

Code	Composition	Phase composition	Heat treatment
Au	Pure gold	-	-
Au990soln	Au - 1wt% Ti	Single	Solution treated
Au990ppt	Au - 1wt% Ti	Dual (contains Au ₄ Ti)	Precipitation hardened
Pt	Pure platinum	-	-
1200short	60Au-40Pt	Single-phase, porous	1200°C, 24 h
1200long	60Au-40Pt	Single-phase, porous	1200°C, 168 h
50-50-soln	50Au-50Pt	Single-phase, non-porous	1250°C
1300	60Au-40Pt	Dual phase, non-porous	1300°C
800	60Au-40Pt	Dual-phase, porous	800°C
600	60Au-40Pt	Dual-phase, porous	600°C
50-50-dual	50Au-50Pt	Dual-phase, non-porous	"Ductile"-treatment



(a)



(b)

Figure 6.13. The maximum peak current densities obtained at the different electrodes. (a) the first scan, (b) the tenth scan.

6.3.6. Electrolysis of ethylene glycol at a fixed potential

It is known that it is not possible to sustain long electrolysis of ethylene glycol at a fixed potential because of poisoning phenomena that occur at the electrode surface (Kadirgan et al., 1990).

Poisoning of selected electrodes during the electrolysis of ethylene glycol at a fixed potential was studied. The following procedure was used:

- The 0.5 M NaOH solution (without ethylene glycol) was purged with nitrogen for 30 minutes to remove dissolved oxygen.
- The electrode potential was cycled for fifteen cycles between the values for onset of O₂ and H₂ evolution until the I-E curves were reproducible.
- The ethylene glycol was added to the solution.
- The electrode was anodically activated at 1.2 V_{SSC} for 10 seconds (the solution was stirred during activation).
- The surface oxides formed during anodic activation were removed at -0.6 V_{SSC} for 10 seconds (the solution was stirred during the cathodic reduction of the surface oxides)
- The electrolysis of ethylene glycol was performed at a fixed potential (Table 6.11). The potential was selected from the cyclic voltammograms with ethylene glycol in solution. The solution was stirred in one set of experiments and not stirred in the other set of experiments. The results of all the different electrodes are presented on the same time and current density scales for better comparison.

Table 6.11. The potential of ethylene glycol electrolysis at the various electrodes

Electrode	Potential (V _{SSC})
Au	0.23
Pt	-0.20
60Au-40Pt electrodes	-0.05
50Au-50Pt electrodes	-0.05
Gold990 electrodes	0.23

6.3.6.1. Gold

The electrolysis of ethylene glycol at gold was performed at 0.23 V_{SSC} (Table 6.11) and the results are shown in Figure 6.14. The apparent current density at the start of electrolysis is 21 mA/cm^2 , but drops quickly due to electrode poisoning. The maximum apparent current density obtained with the cyclic voltammogram (Fig. 6.1) is 16 mA/cm^2 . This indicates that the electrode is partially poisoned during the positive scan (from -0.2 V to 0.27 V_{SSC}) and the maximum apparent current density during cyclic voltammetry is therefore lower than at the start of potentiostatic electrolysis.

Stirring of the solution results in an even faster decay of current density, perhaps because the transportation of intermediates into the solution is accelerated. These intermediates cannot be oxidised at the surface of the electrode, resulting in lower current densities.

6.3.6.2. Platinum

The electrolysis of ethylene glycol at platinum was performed at -0.20 V_{SSC} (Table 6.11) and the results are shown in Figure 6.15. The apparent current density at the start of electrolysis is 14 mA/cm^2 (slightly higher than the peak value obtained with cyclic voltammetry in Fig. 6.2), but also drops quickly due to electrode poisoning. As with gold, stirring of the solution results in an even faster decay of current density.

6.3.6.3. The 60Au-40Pt alloy in the 1300°C heat treatment condition

The electrolysis of ethylene glycol at this non-porous, two-phased electrode was performed at -0.05 V_{SSC} (Table 6.11) and the results are shown in Figure 6.16. The apparent current density at the start of electrolysis is 40 mA/cm^2 , but the alloy electrode unfortunately also poisons rapidly. As was the case with the pure metals, stirring of the solution also results in a faster decay of current density.

6.3.6.4. The 60Au-40Pt alloy in the 1200°C-24h heat treatment condition

The electrolysis of ethylene glycol at this porous, single-phased electrode was performed at $-0.05 V_{SSC}$ (Table 6.11) and the results are shown in Figure 6.17. The apparent current density at the start of electrolysis at this electrode is a high 60 mA/cm^2 . From Table 6.2 it is seen that stirring did not influence the current density much with the porous electrode. The results from Figure 6.17 show that stirring does produce lower current densities, but the effect is much smaller than with non-porous electrodes (Fig. 6.16).

6.3.6.5. The 50Au-50Pt alloy in the “ductile” heat treatment condition

The electrolysis of ethylene glycol at this non-porous, two-phased electrode was performed at $-0.05 V_{SSC}$ (Table 6.11) and the results are shown in Figure 6.18. The apparent current density at the start of electrolysis at this electrode is 40 mA/cm^2 . The electrolysis results from this sample are similar to that of the 1300°C heat treated 60Au-40Pt sample (Fig. 6.16, also compare Tables 6.1 and 6.6)

6.3.6.6. The 50Au-50Pt alloy in the solid solution heat treatment condition

The electrolysis of ethylene glycol at this non-porous, single-phased electrode was performed at $-0.05 V_{SSC}$ (Table 6.11) and the results are shown in Figure 6.19. The apparent current density at the start of electrolysis at this electrode is a high 52 mA/cm^2 . Higher apparent current densities are obtained with this single-phased 50Au-50Pt electrode than with the two-phased 50Au-50Pt electrode (Fig. 6.18). This confirms the cyclic voltammetry results (Tables 6.6 and 6.7).

6.3.6.7. The Gold 990 alloy in the solid solution heat treatment condition

The electrolysis of ethylene glycol at this electrode was performed at $0.23 V_{SSC}$ (Table 6.11) and the results are shown in Figure 6.20. The apparent current density at the start of

electrolysis at this electrode is 20.5 mA/cm^2 . Once again, the results obtained with this Gold 990 electrode are similar to that of pure gold (Fig. 6.14, Table 6.8).

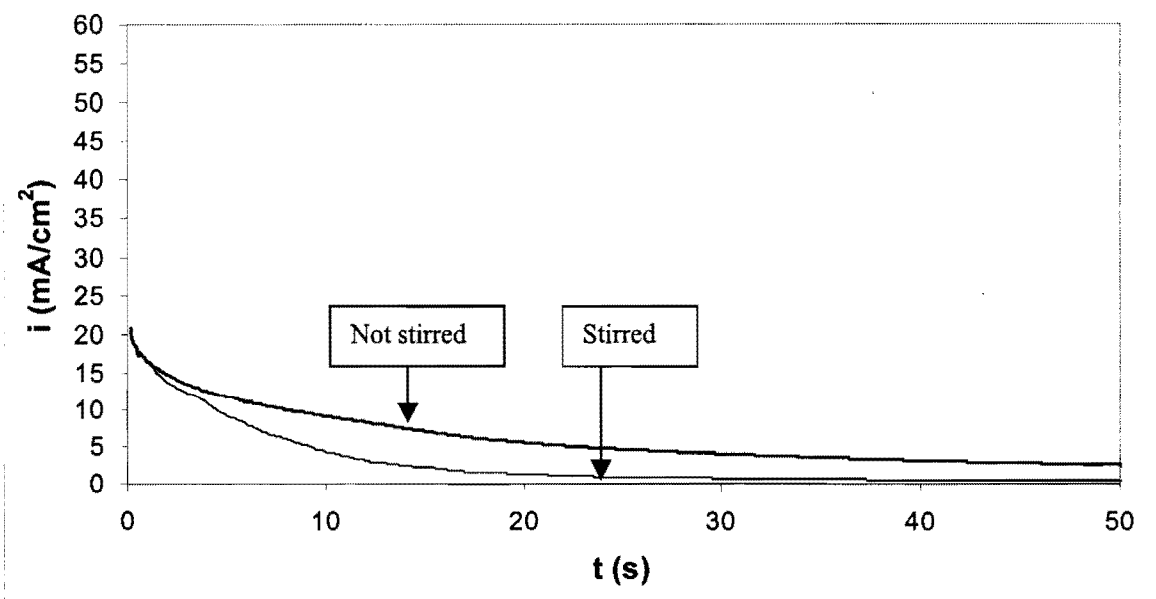


Figure 6.14. Electrolysis of ethylene glycol at gold at a fixed potential of $0.23 V_{ssc}$.

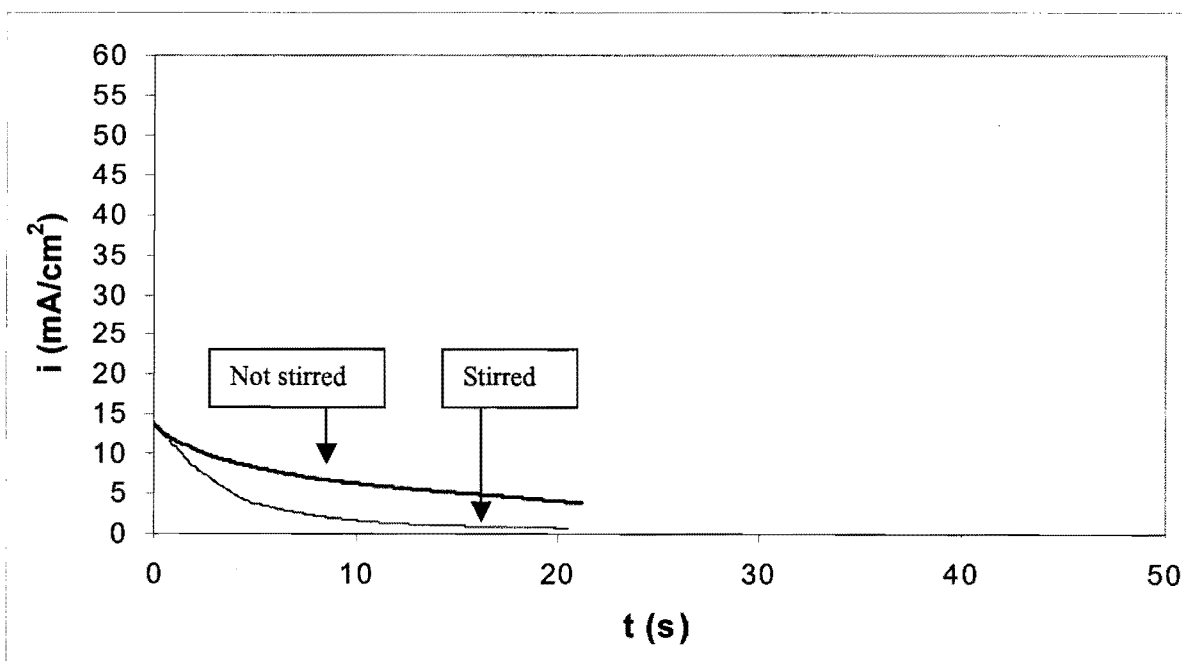


Figure 6.15. Electrolysis of ethylene glycol at platinum at a fixed potential of $-0.20 V_{ssc}$.

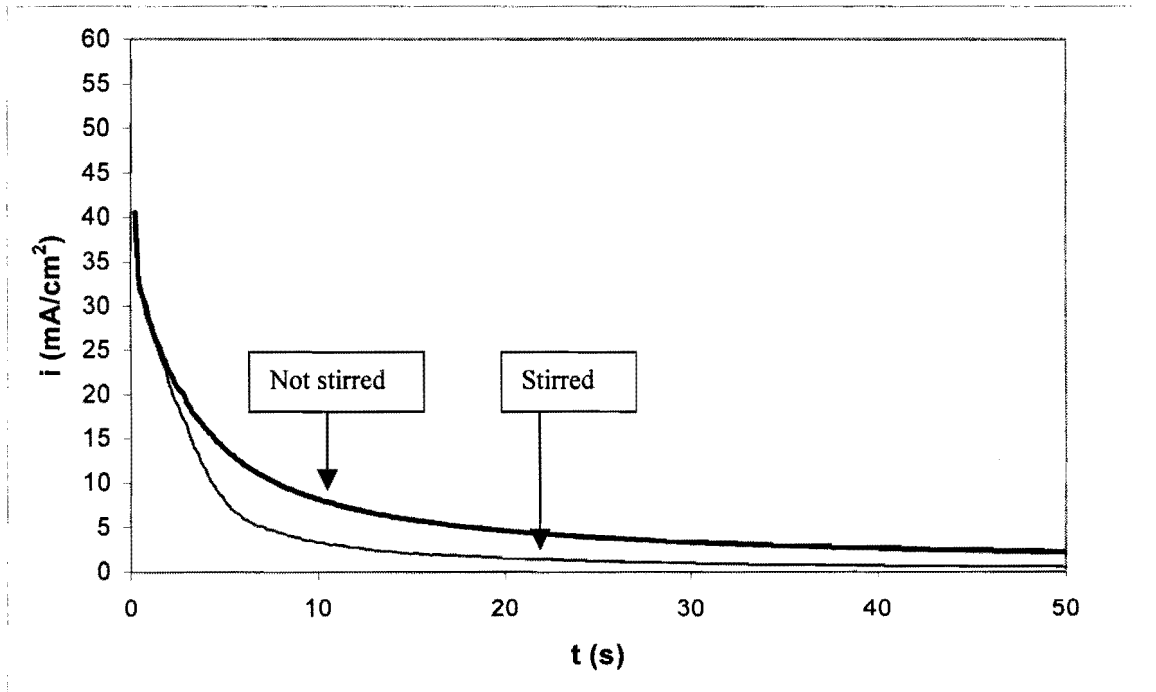


Figure 6.16. Electrolysis of ethylene glycol at the 1300°C (60Au-40Pt) electrode at a fixed potential of $-0.05 V_{SSC}$.

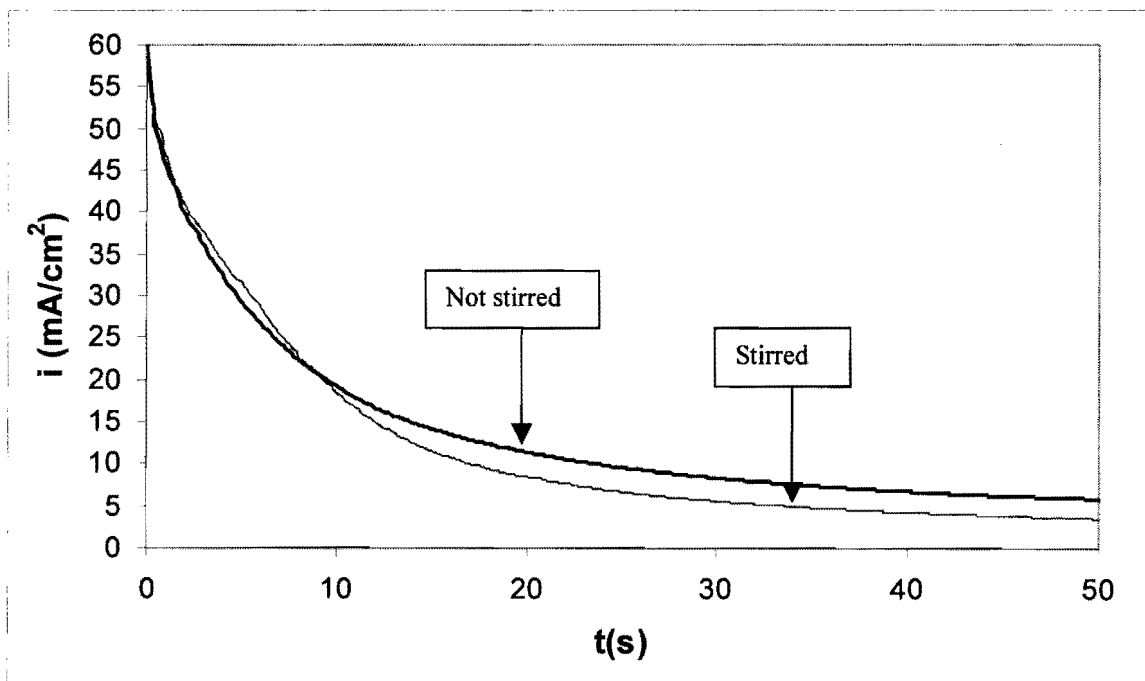


Figure 6.17. Electrolysis of ethylene glycol at the 1200°C-24h (60Au-40Pt) electrode at a fixed potential of $-0.05 V_{SSC}$.

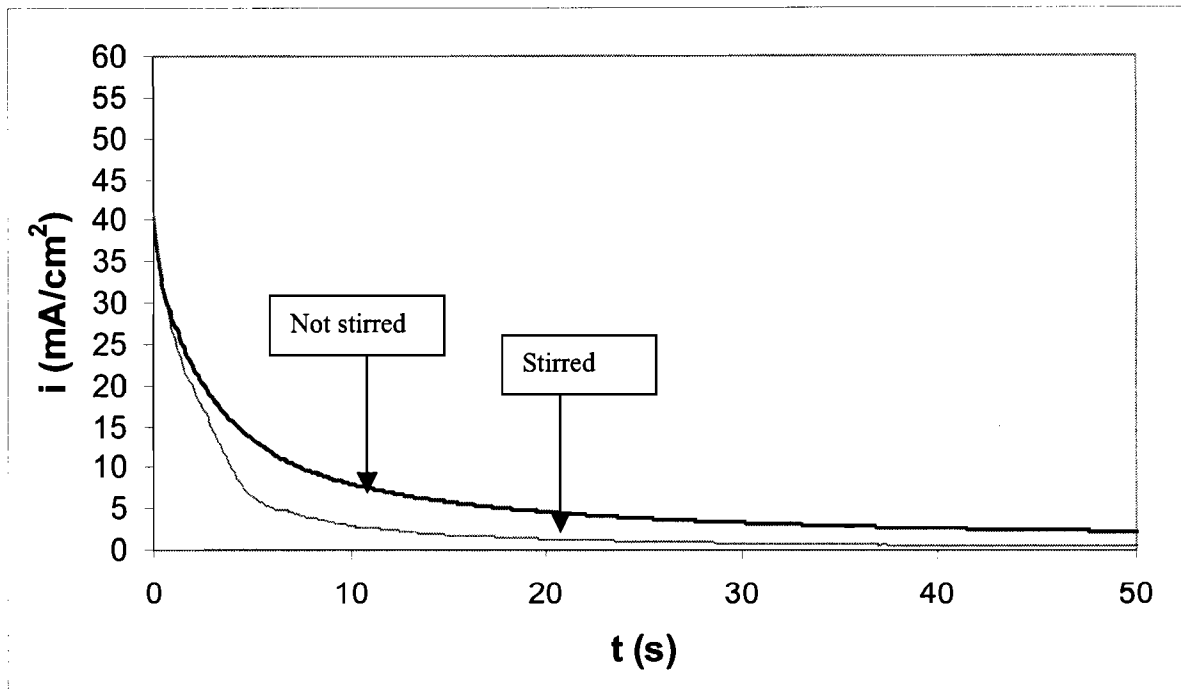


Figure 6.18. Electrolysis of ethylene glycol at the “ductile” (50Au-50Pt) electrode at a fixed potential of $-0.05 V_{SSC}$.

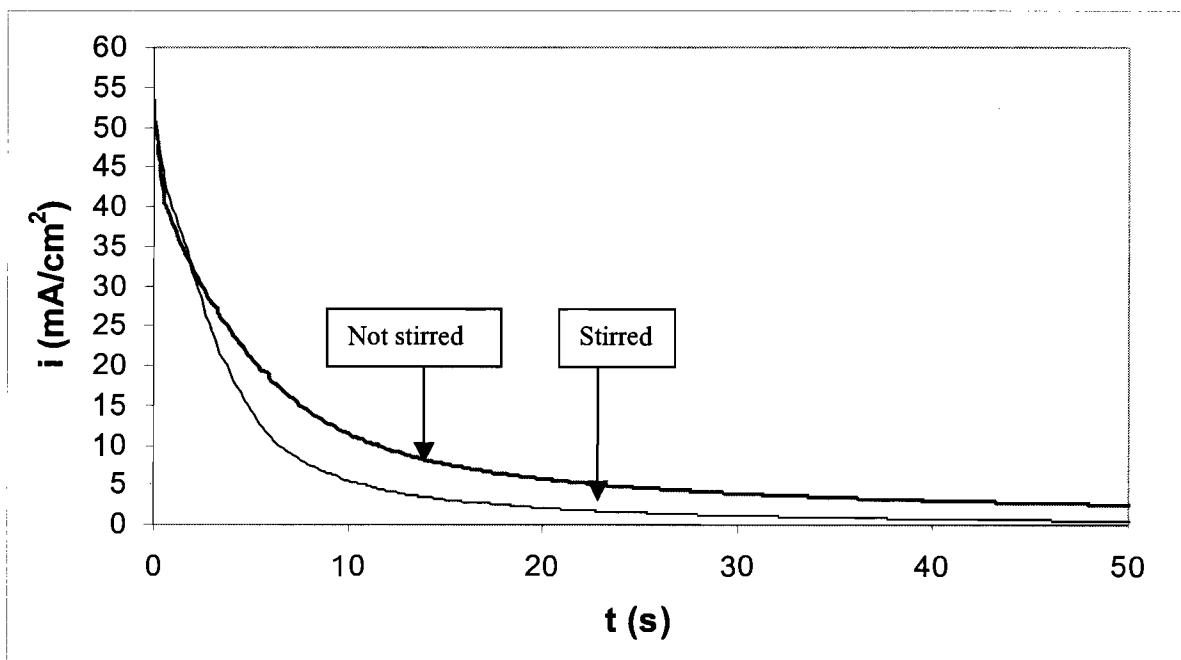


Figure 6.19. Electrolysis of ethylene glycol at the solid solution (50Au-50Pt) electrode at a fixed potential of $-0.05 V_{SSC}$.

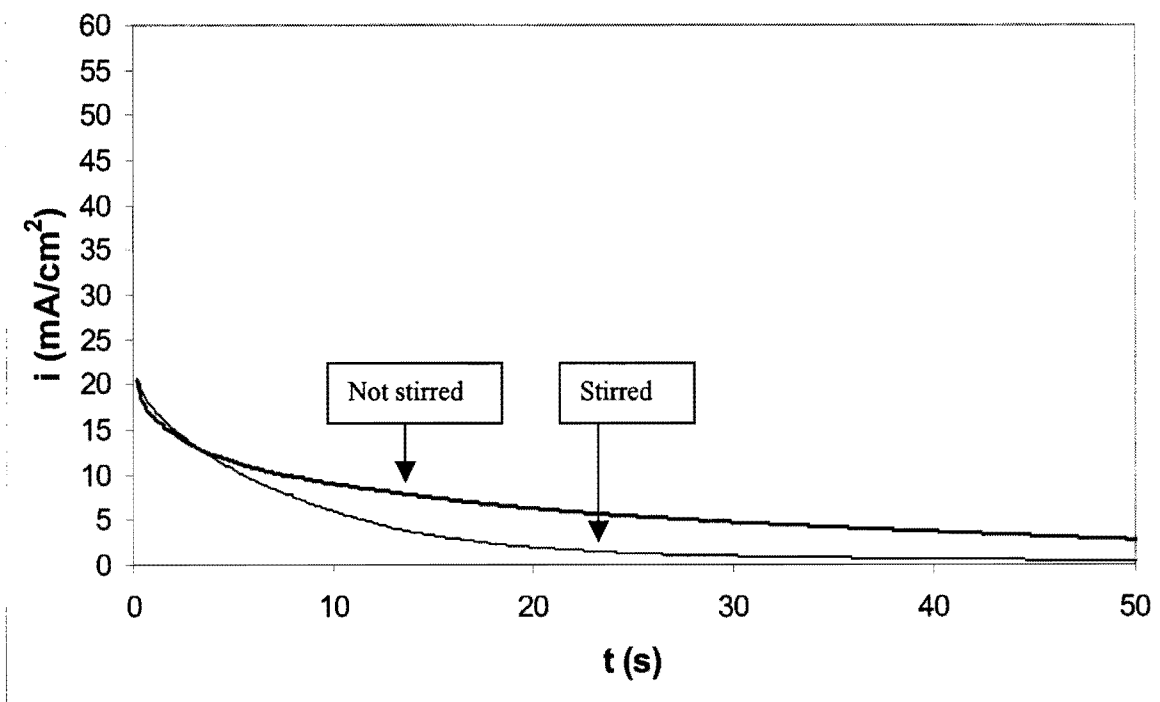


Figure 6.20. Electrolysis of ethylene glycol at the solid solution Gold 990 electrode at a fixed potential of $0.23 V_{SSC}$.

The following conclusions can be made based on Figures 6.14 to 6.20:

- All the electrodes are poisoned, resulting in a decrease in the apparent current densities with time.
- Stirring of the solution causes a decrease in the apparent current densities of all the electrodes, although the effect is smaller with the porous electrode.
- The current densities obtained at time $t = 0$ during potentiostatic electrolysis follow the same ranking as for the maximum peak current densities during cyclic voltammetry.
- The rate at which poisoning occurs at the electrodes differs. The time necessary for a 50% decrease in the initial current densities during electrolysis are shown in Table 6.12.

Table 6.12. The time (in seconds) necessary for a 50% decrease in the initial current densities during potentiostatic electrolysis

	Solution not stirred	Solution stirred
Au	7.5	4
Pt	7.5	3
1300°C (60Au-40Pt)	3	2
1200°C-24h (60Au-40Pt)	5	5
Ductile (50Au-50Pt)	2.5	2
Solid solution (50Au-50Pt)	3.5	3
Gold 990 (Solid solution)	7	5

The gold-platinum alloys poison at a faster rate than both pure gold and pure platinum (Table 6.12). The higher apparent current densities obtained at the alloy electrodes at the start of electrolysis probably lead to the formation of more poisoning species than at both pure gold and platinum.

6.3.7. Electrolysis of ethylene glycol using potential pulsing

The results of the electrolysis of ethylene glycol at a constant potential have shown that electrode poisoning occurs rapidly and that the current densities drop to low values in a matter of seconds. A cleaning procedure has to be used for sustainable electrolysis (Kadirgan et al., 1990).

Electrolysis of ethylene glycol at selected electrodes by employing the potential pulsing technique was studied. The following procedure was used:

- The 0.5 M NaOH solution (without ethylene glycol) was purged with nitrogen for 30 minutes to remove dissolved oxygen.
- The electrode potential was cycled for fifteen cycles between the values for onset of O₂ and H₂ evolution until the I-E curves were reproducible. The cyclic

voltammogram (15th cycle) of the electrode was then compared to the cyclic voltammogram found in chapter 5. This was done to make certain that the solution did not contain impurities and that the behaviour of the electrode was similar to what was found in chapter 5.

- The ethylene glycol was added to the solution.
- The potential was pulsed. The electrode was first cleaned anodically at 1.2 V_{SSC} for 1.5 seconds. The surface oxides formed during anodic activation were then removed at -0.6 V_{SSC} for 1.5 seconds. The cleaning cycle was chosen to be only 3 seconds to maximise the fraction of the total time spent at the electrolysis potential. It was expected to be long enough to remove the poisoning species. The electrolysis of ethylene glycol was performed for 10 seconds at the potentials shown in Table 6.11. The apparent current densities for ethylene glycol electro-oxidation decline to low levels after 10 seconds (Figures 6.14 to 6.20) and the electrode has to be cleaned again. The potential pulsing was performed for 100 cycles. The solution was stirred during the cleaning procedure and during electrolysis.

6.3.7.1. Gold

The electrolysis of ethylene glycol at gold was performed at 0.23 V_{SSC}. The first cycle (cleaning and electrolysis) is shown in Figure 6.21. In Figure 6.22(a), the current densities during cycles 1 – 10 are shown. Figure 6.22(b) shows the current densities for cycles 91 – 100. The current densities of the cleaning procedure have been omitted in Figure 6.22. From Figure 6.22(a) it is seen the initial current density after potential pulsing (cycle 1) was approximately 20 mA/cm², falling to 3.5 mA/cm² after 10 seconds. The time necessary for a 50% decrease of the initial current density is 3.5 seconds, which agrees well with Table 6.12 (remember that the solution was stirred during potential pulsing).

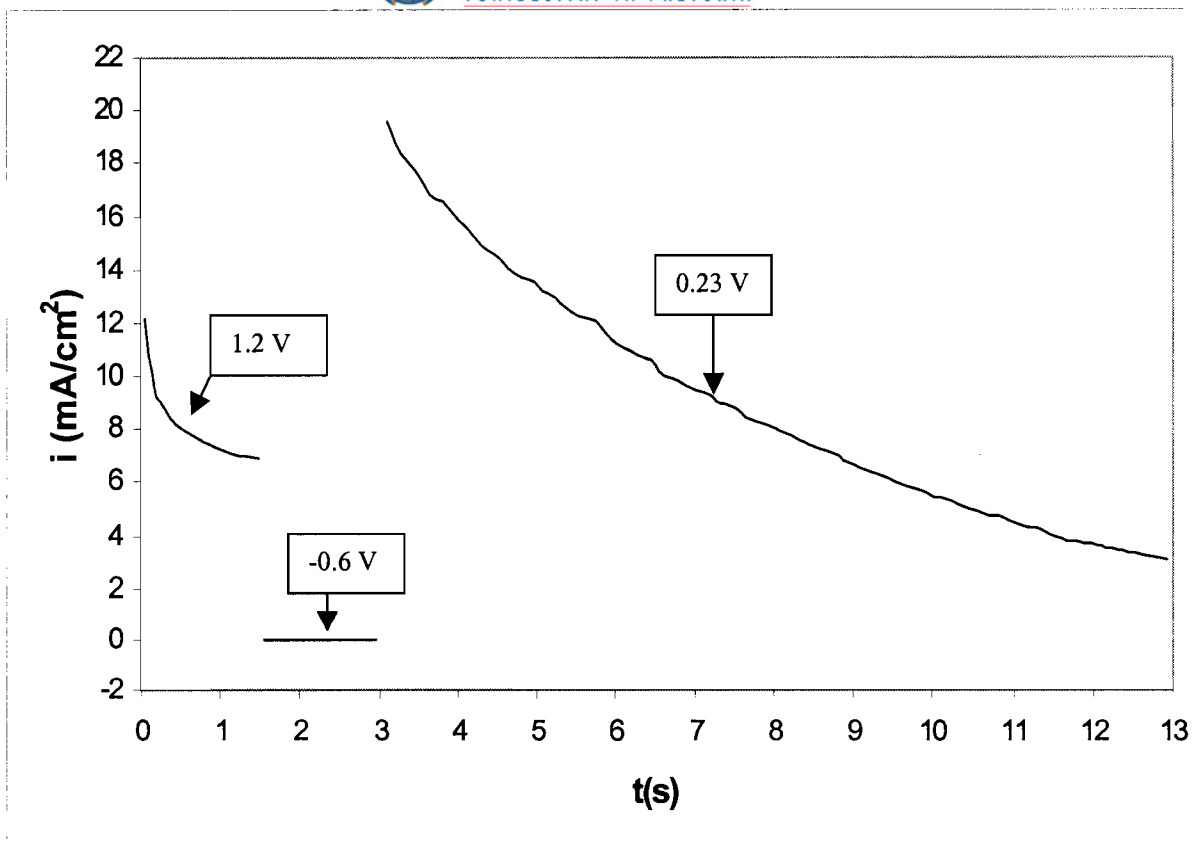
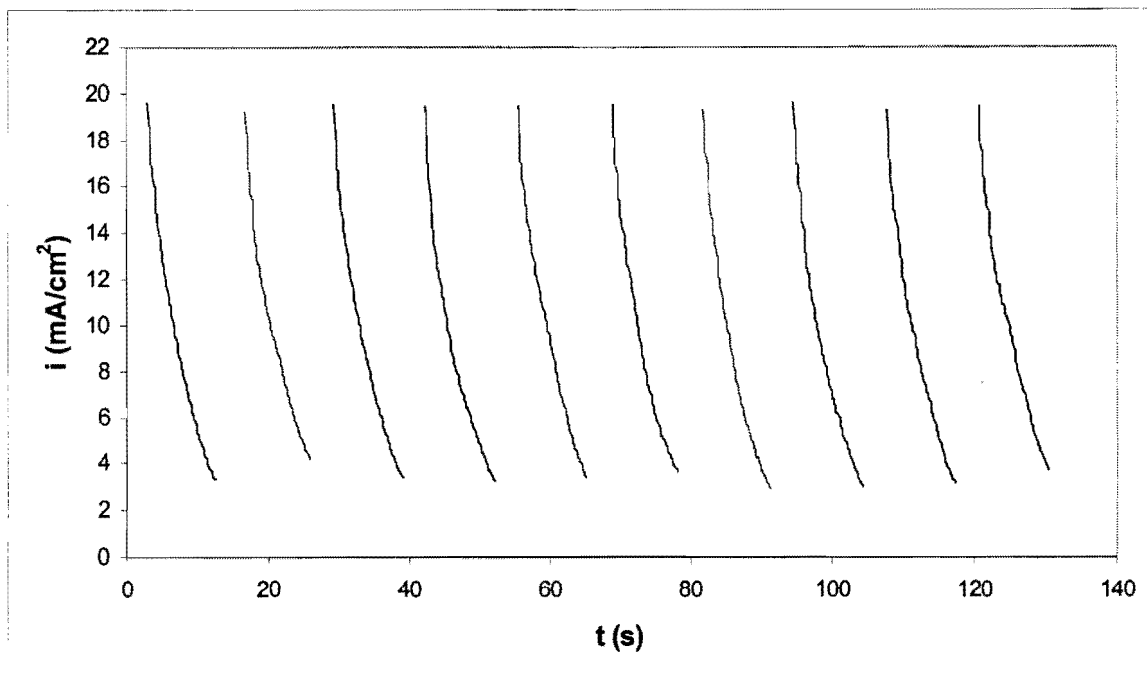
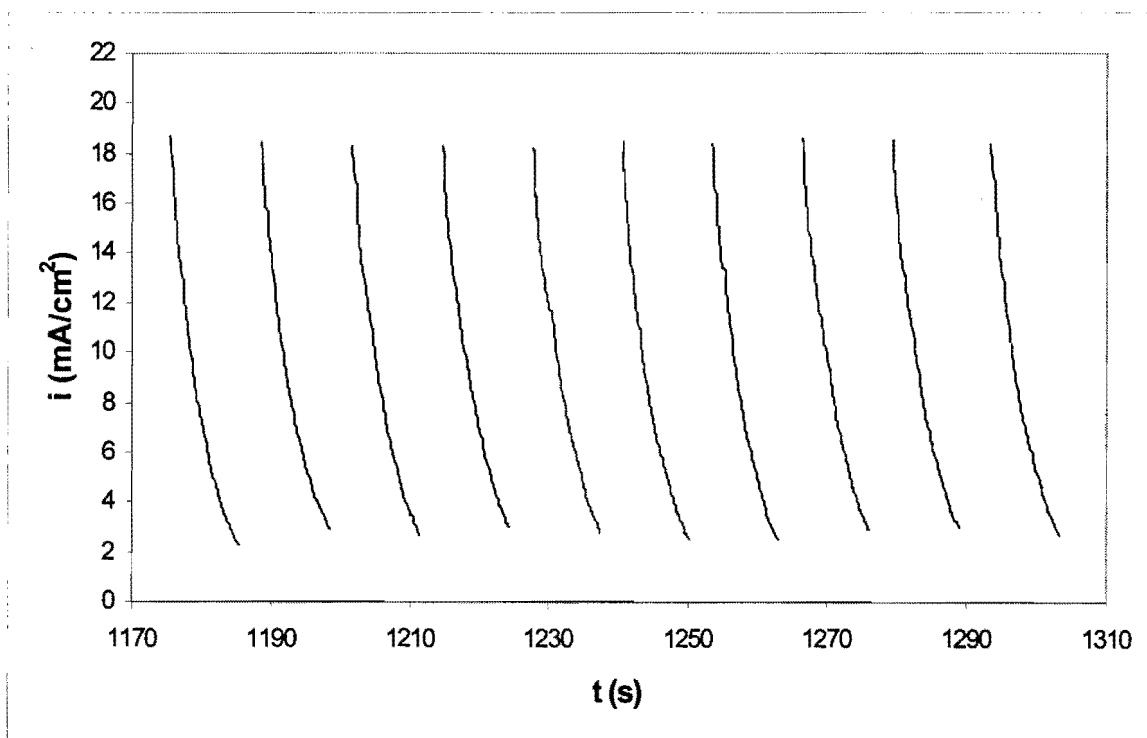


Figure 6. 21. The first cycle at a gold electrode during potential pulsing

The electrode was cleaned by the potential pulsing technique and it is seen that the 20 mA/cm² current density at the start of cycle 2 is once again achieved. The electrode poisons are therefore successfully removed by the potential pulsing technique. The current densities obtained during cycles 91 – 100 (Fig. 6.22(b)) are only slightly lower than those of cycles 1 – 10. Sustainable electrolysis of ethylene glycol at a gold electrode is therefore possible by potential pulsing. The initial current density for ethylene glycol oxidation obtained after each cleaning cycle is shown in Figure 6.23. This figure clearly illustrates how effective the potential pulsing technique is in cleaning the gold electrode of poisons to restore its activity.



(a)



(b)

Figure 6.22. Electrolysis of ethylene glycol by potential pulsing at a gold electrode; (a) Cycles 1-10; (b) Cycles 91-100 (Solution stirred during potential pulsing).

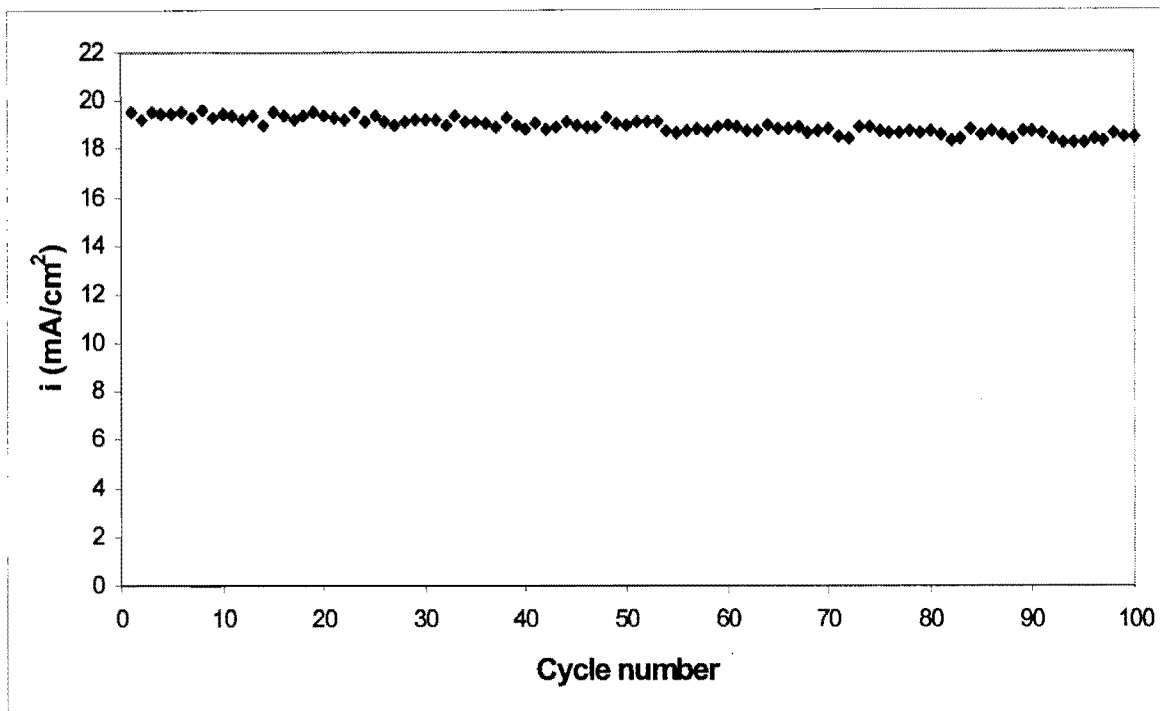


Figure 6.23. The initial current density for ethylene glycol oxidation at a gold electrode obtained after each cleaning cycle.

Numerical integration was used to calculate the charge passed during the electro-oxidation of ethylene glycol at the gold electrode over the time period of the 100 cycles. The results are summarised in Table 6.13.

Table 6.13. The charge passed during oxidation of ethylene glycol at a gold electrode during cycles 1-10, 91-100 and 1-100

Cycles 1-10	Cycles 91-100	Cycles 1-100
0.242 C	0.225 C	2.37 C

When ethylene glycol is oxidised up to oxalate, 8 electrons per molecule are delivered within the overall process (Hauffe and Heitbaum, 1978). The charge of 1 mol of electrons is 96472 C/mol (Faraday's constant) (Fishbane et al., 1996). The quantity of electrons for the oxidation of ethylene glycol at gold over 100 cycles equal $(2.37)/(96472) = 2.46 \times 10^{-5}$ mol electrons. The quantity of ethylene glycol molecules oxidised is $(2.46 \times 10^{-5})/8 = 3.07 \times 10^{-6}$ mol.

The original quantity of ethylene glycol prior to the hundred cycles was $(0.4)(0.1) = 0.04$ mol, where the volume of the solution was 0.4 dm^3 and the concentration of ethylene glycol was 0.1 mol/dm^3 .

Only $(3.07 \times 10^{-6})/0.04) = 0.008 \%$ of the original ethylene glycol content was oxidised during the hundred cycles at gold. The above calculations are summarised in Table 6.14.

Table 6.14. The estimated amount of ethylene glycol oxidised at gold during the hundred cycles.

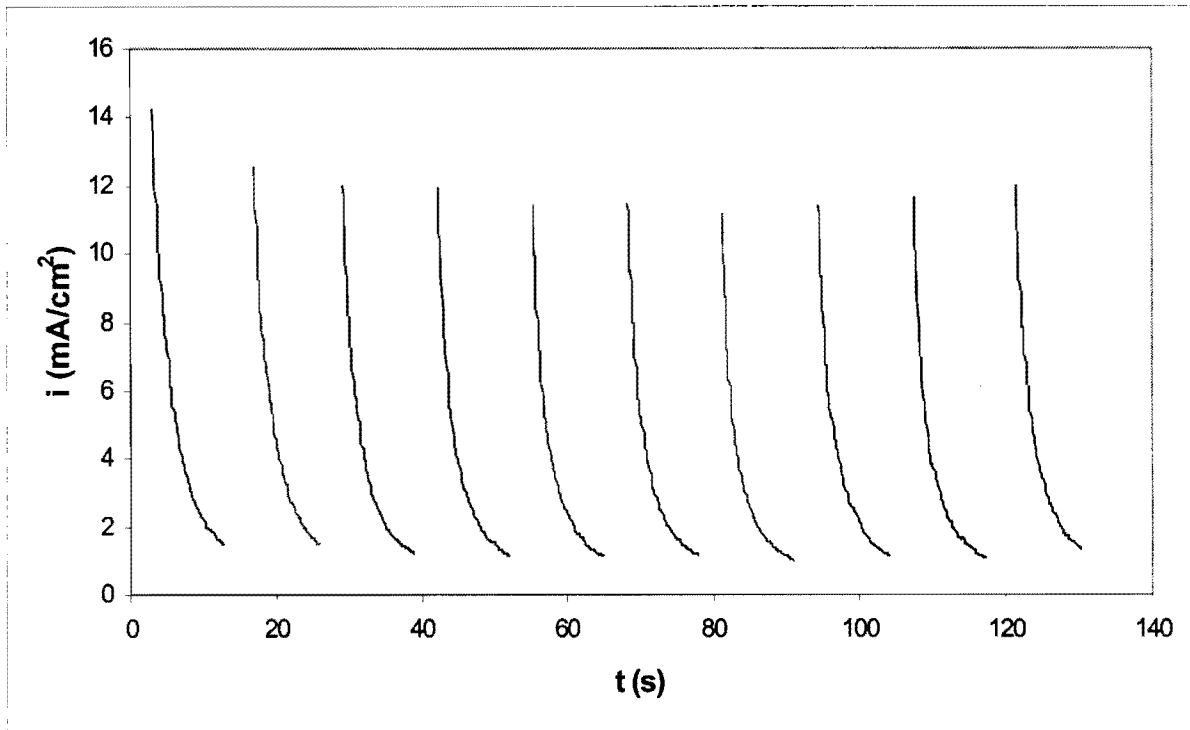
Original number of moles ethylene glycol	Number of moles oxidised	% ethylene glycol oxidised
0.04	3.07×10^{-6}	0.008

Even though the percentage of ethylene glycol that was oxidised is only an estimate, it still shows that its concentration did not change much during the hundred cycles. This is also true even if partial oxidation (less than 8 electrons/molecule) is assumed. Despite this, the charge passed during the final ten cycles is slightly lower than the first ten cycles (Table 6.13). The poisons are possibly more difficult to remove during the final cycles resulting in slightly less ethylene oxidation.

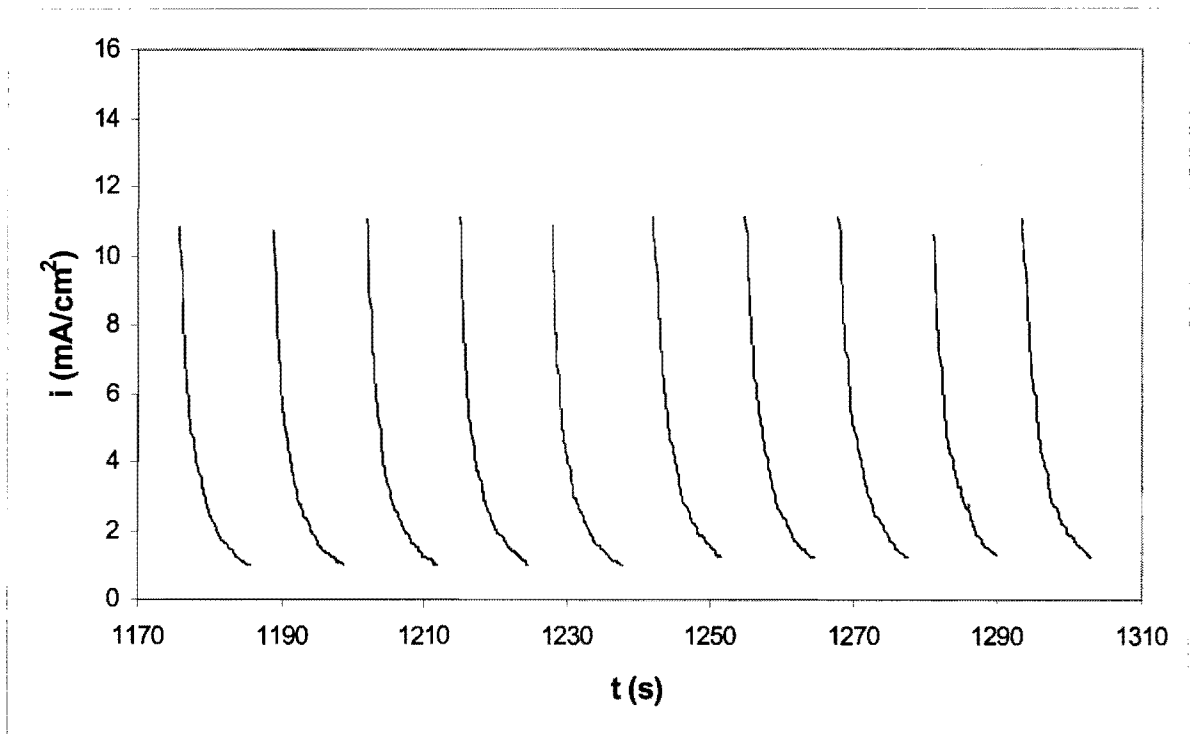
6.3.7.2. Platinum

The electrolysis of ethylene glycol was performed at $-0.20 \text{ V}_{\text{SSC}}$. In Figure 6.24 (a), the current densities obtained during cycles 1 – 10 are shown. Figure 6.24(b) shows the current densities for cycles 91 – 100. The current densities for the electro-oxidation of ethylene glycol are lower than at gold (Fig. 6.22). The time needed to decrease the initial current density of the first cycle by 50% is 2.5 seconds (also see Table 6.12).

The electrode poisons are successfully removed by the potential pulsing technique at platinum. The current densities obtained during cycles 91 – 100 (Fig. 6.24(b)) are only slightly lower than those of cycles 1 – 10.



(a)



(b)

Figure 6.24. Electrolysis of ethylene glycol by potential pulsing at a platinum electrode; (a) Cycles 1-10; (b) Cycles 91-100 (Solution stirred during potential pulsing)

The initial current density for ethylene glycol oxidation obtained after each cleaning cycle is shown in Figure 6.25. This figure illustrates that the potential pulsing technique cleans the platinum electrode of poisons and restores its activity.

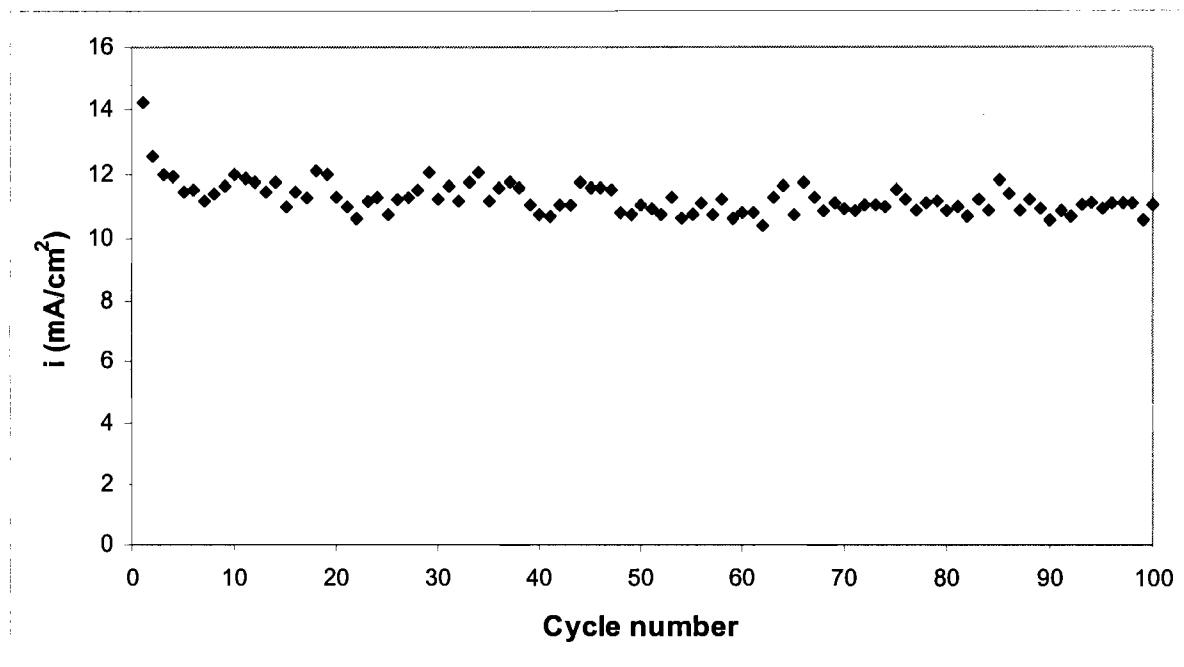


Figure 6.25. The initial current density for ethylene glycol oxidation at a platinum electrode obtained after each cleaning cycle.

Numerical integration was also used to calculate the charge passed during the electro-oxidation of ethylene glycol at the platinum electrode over the time period of the 100 cycles. The results are summarised in Table 6.15.

Table 6.15. The charge passed during oxidation of ethylene glycol at a platinum electrode during cycles 1-10, 91-100 and 1-100

Cycles 1-10	Cycles 91-100	Cycles 1-100
0.095 C	0.089 C	0.902 C

The same procedure to calculate the amount of ethylene glycol oxidised during the hundred cycles at gold was followed for platinum. The calculations are summarised in Table 6.16.

Table 6.16. The estimated amount of ethylene glycol oxidised at platinum during the hundred cycles.

Original number of moles ethylene glycol	Number of moles oxidised	% ethylene glycol oxidised
0.04	1.17×10^{-6}	0.003

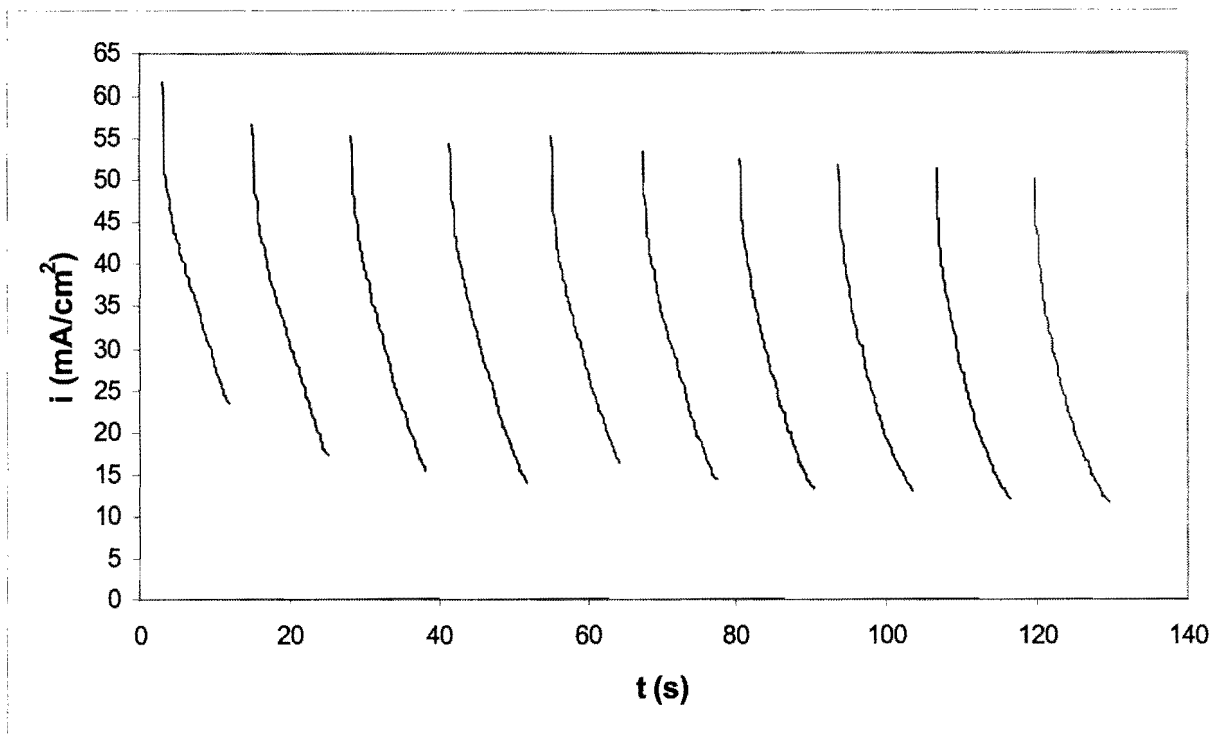
Approximately 2.5 times more ethylene glycol was oxidised during the hundred cycles at gold than at platinum (Tables 6.14 and 6.16).

For platinum, the charge passed during the final ten cycles is also slightly lower than for the first ten cycles (Table 6.15). This cannot be due to a drop in ethylene glycol concentration (Table 6.16). As with gold, the poisons are possibly more difficult to remove during the final cycles resulting in slightly less ethylene oxidation.

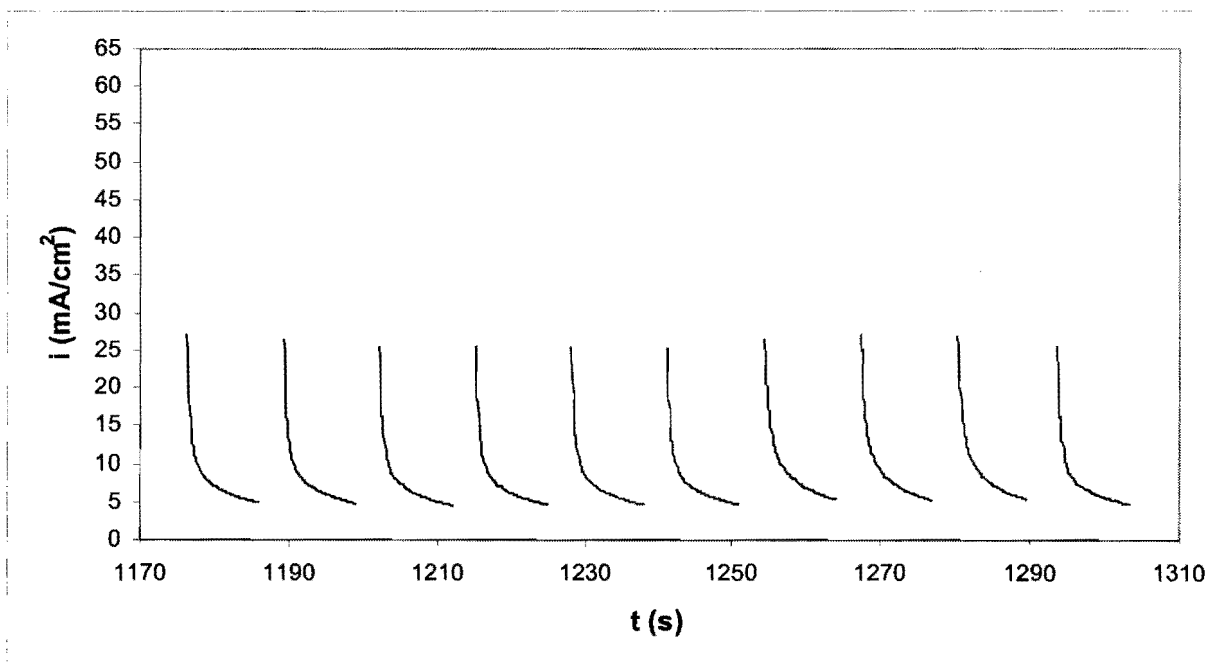
6.3.7.3. The 60Au-40Pt alloy electrode in the 1200°C-24h condition

The electrolysis of ethylene glycol was performed at $-0.05 V_{SSC}$. In Figure 6.26 (a), the current densities during cycles 1 – 10 are shown. Figure 6.26(b) shows the current densities for cycles 91 – 100. The time needed to decrease the initial current density of the first cycle by 50% is 5.5 seconds (also see Table 6.12).

The initial apparent current density for first cycle is very high. However, the current density of each subsequent cycle is lower than that of the previous cycle. The current densities during cycles 91 – 100 (Fig. 6.26(b)) are much lower than those of cycles 1 – 10.



(a)



(b)

Figure 6.26. Electrolysis of ethylene glycol by potential pulsing at the 1200°C-24h (60Au-40Pt) electrode; (a) Cycles 1-10; (b) Cycles 91-100 (Solution stirred during potential pulsing)

The initial current density for ethylene glycol oxidation obtained after each cleaning cycle is shown in Figure 6.27. This figure illustrates that the potential pulsing technique is not able to restore the activity of the alloy completely. The very high current densities obtained during the first cycles presumably lead to the formation of more poisoning species than at both pure gold and platinum. It appears that the cleaning cycles are too short (or not aggressive enough) to remove all the poisons and the current densities decline.

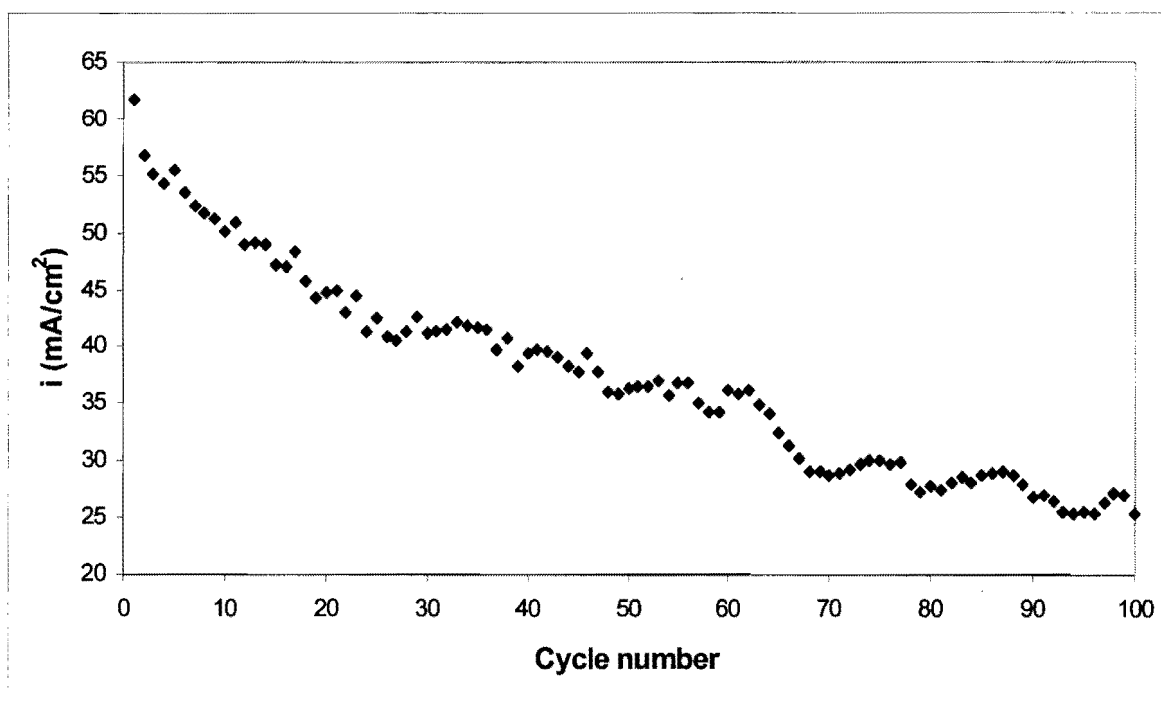


Figure 6.27. The initial current density for ethylene glycol oxidation at the 1200°C-24h (60Au-40Pt) electrode obtained after each cleaning cycle.

Numerical integration was also used to calculate the charge passed during the electro-oxidation of ethylene glycol at the 1200°C-24h (60Au-40Pt) electrode over the time period of the 100 cycles. The results are summarised in Table 6.17.

Table 6.17. The charge passed during oxidation of ethylene glycol at the porous 1200°C-24h electrode during cycles 1-10, 91-100 and 1-100

Cycles 1-10	Cycles 91-100	Cycles 1-100
0.768 C	0.220 C	3.67 C

Approximately three times more ethylene glycol is oxidised during the first ten cycles at the alloy electrode than at gold. Almost the same amount of ethylene glycol is oxidised during the final ten cycles. Over the period of the whole hundred cycles, only 1.5 times more ethylene glycol is oxidised at the alloy electrode than at gold (Tables 6.13 and 6.17).

The estimated amount of ethylene glycol oxidised during the hundred cycles at the 1200°C-24h electrode is shown in Table 6.18.

Table 6.18. The amount of ethylene glycol oxidised at the 1200°C-24h electrode during the hundred cycles.

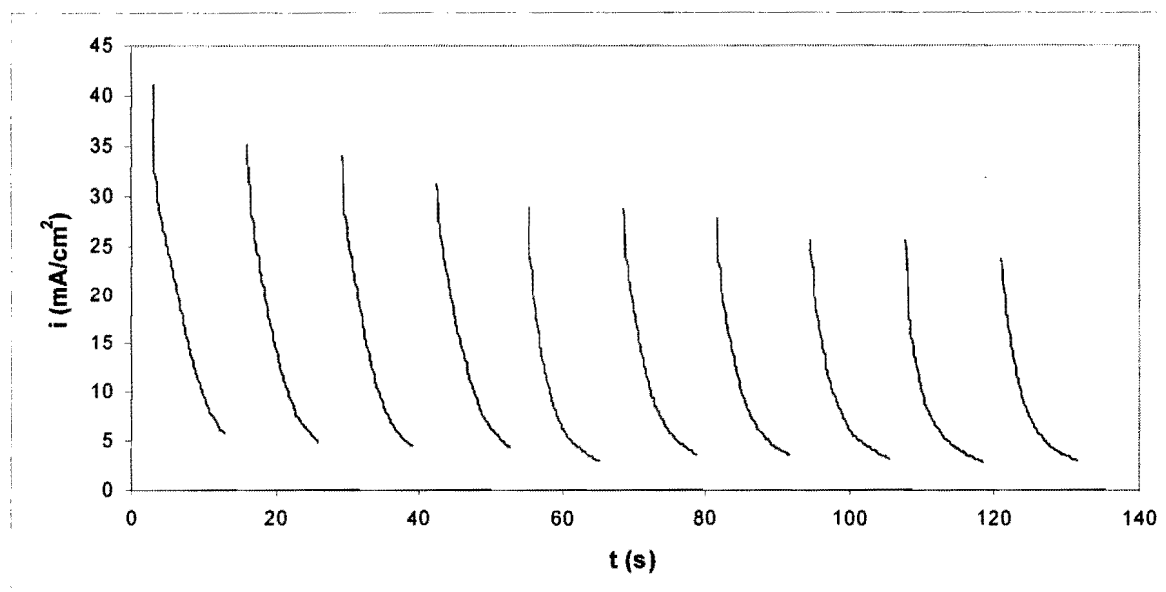
Original number of moles ethylene glycol	Number of moles oxidised	% ethylene glycol oxidised
0.04	4.76×10^{-6}	0.012

Table 6.18 confirms that the decline in current densities cannot be due to a decrease in ethylene glycol concentration, but is rather a poisoning effect.

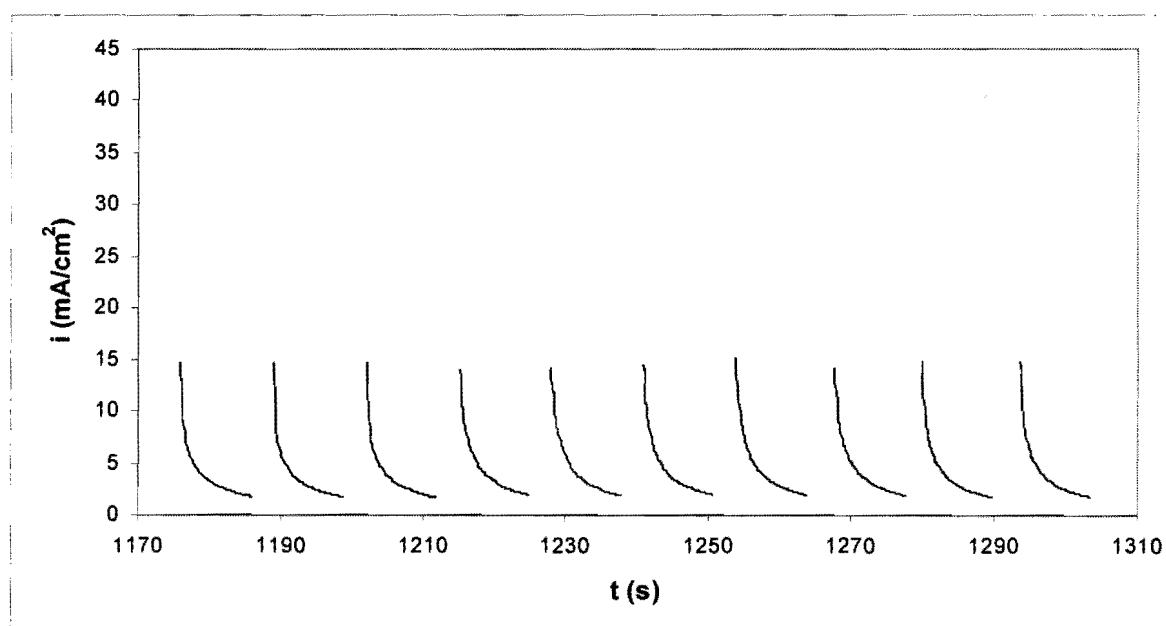
6.3.7.4. The 50Au-50Pt alloy electrode in the “ductile” condition

The electrolysis of ethylene glycol was performed at $-0.05 V_{SSC}$. In Figure 6.28 (a), the current densities during cycles 1 – 10 are shown. Figure 6.28(b) shows the current densities for cycles 91 – 100. The time needed to decrease the initial current density of the first cycle by 50% is 3 seconds (also see Table 6.12).

The apparent current densities for the first cycles are lower than for the porous 1200°C-24h electrode (60Au-40Pt) (Fig.6.26). The current densities decline more rapidly with each cycle than the 1200°C-24h electrode. The current densities during cycles 91 – 100 (Fig. 6.28(b)) are much lower than those of cycles 1 – 10.



(a)



(b)

Figure 6.28. Electrolysis of ethylene glycol by potential pulsing at the “ductile” (50Au-50Pt) electrode; (a) Cycles 1-10; (b) Cycles 91-100 (Solution stirred during potential pulsing)

The initial current density for ethylene glycol oxidation obtained after each cleaning cycle is shown in Figure 6.29. This figure confirms that the potential pulsing technique is also not able to restore the activity of this alloy completely.

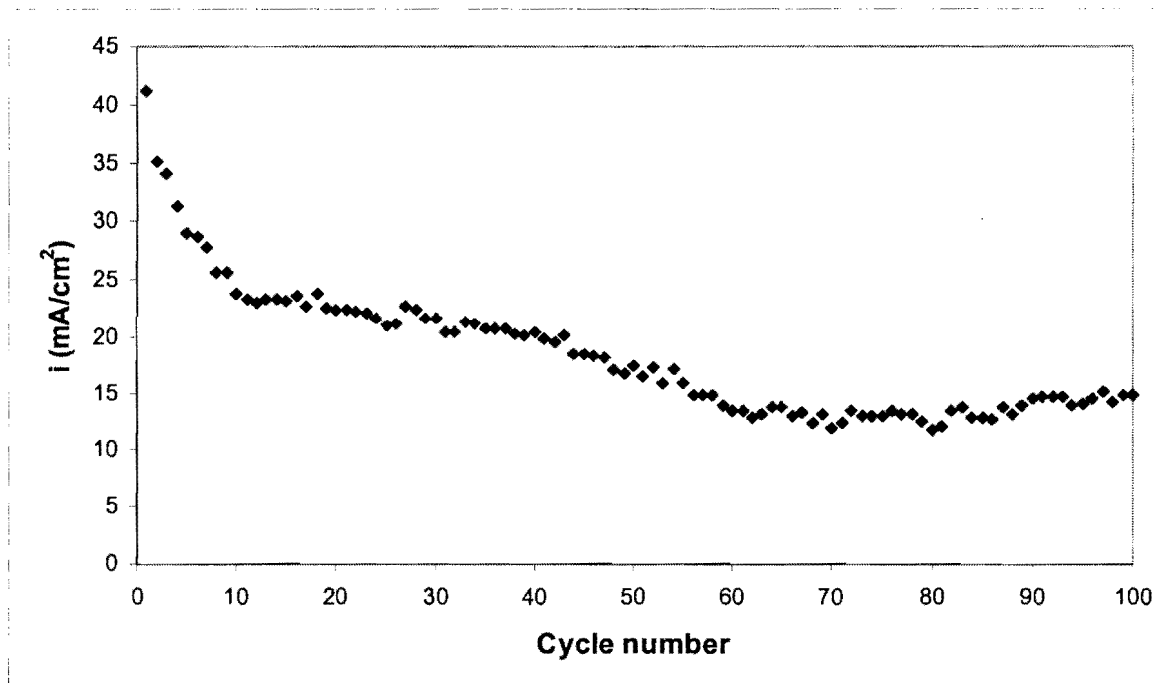


Figure 6.29. The initial current density for ethylene glycol oxidation at the “ductile” (50Au-50Pt) electrode obtained after each cleaning cycle.

Numerical integration was again used to calculate the charge passed during the electro-oxidation of ethylene glycol at the “Ductile” (50Au-50Pt) electrode over the time period of the 100 cycles. The results are summarised in Table 6.19.

Table 6.19. The charge passed during oxidation of ethylene glycol at the “ductile” electrode during cycles 1-10, 91-100 and 1-100

Cycles 1-10	Cycles 91-100	Cycles 1-100
0.306 C	0.109 C	1.52 C

Approximately 1.3 times more ethylene glycol is oxidised during the first ten cycles at this alloy electrode than at gold. Only half the amount of ethylene glycol is oxidised

during the final ten cycles Over the period of the whole hundred cycles, less ethylene glycol (1.5 times) is oxidised at the alloy electrode than at gold (Tables 6.13 and 6.19).

The estimated amount of ethylene glycol oxidised during the hundred cycles at the “ductile” electrode is shown in Table 6.20.

Table 6.20. The estimated amount of ethylene glycol oxidised at the “ductile” electrode during the hundred cycles.

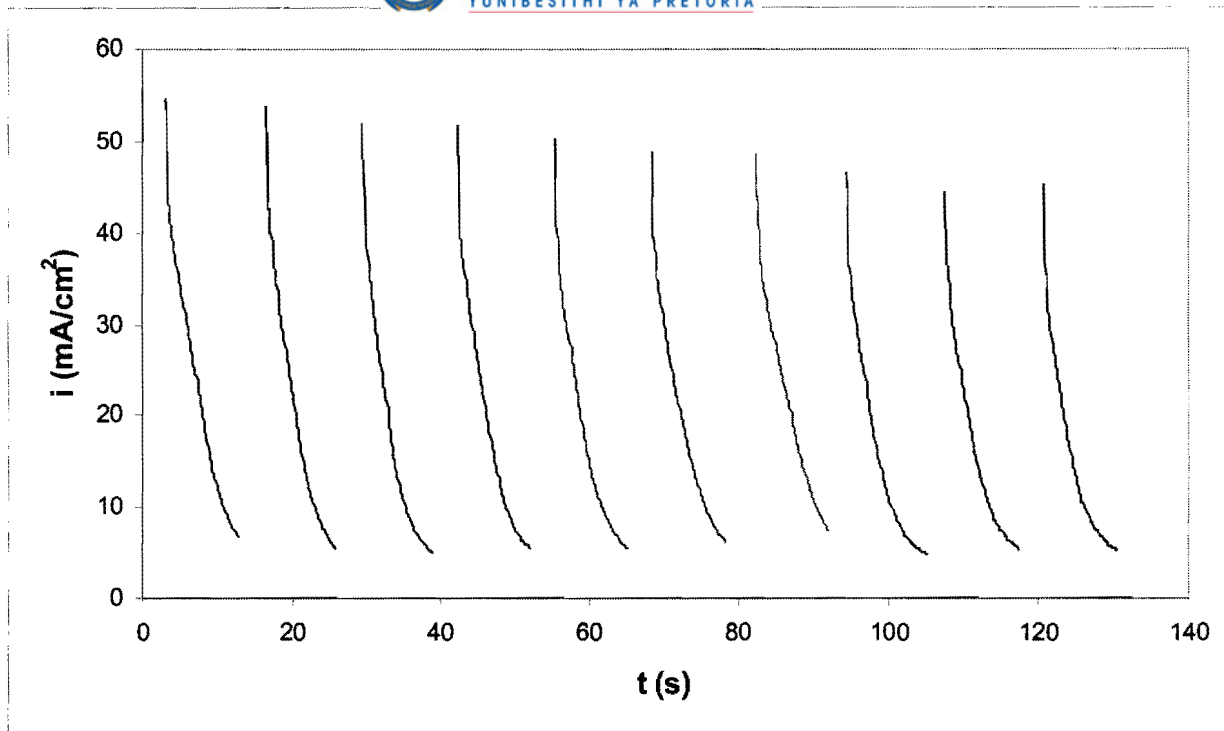
Original number of moles ethylene glycol	Number of moles oxidised	% ethylene glycol oxidised
0.04	1.98×10^{-6}	0.0049

6.3.7.5. The 50Au-50Pt alloy electrode in the solid solution condition

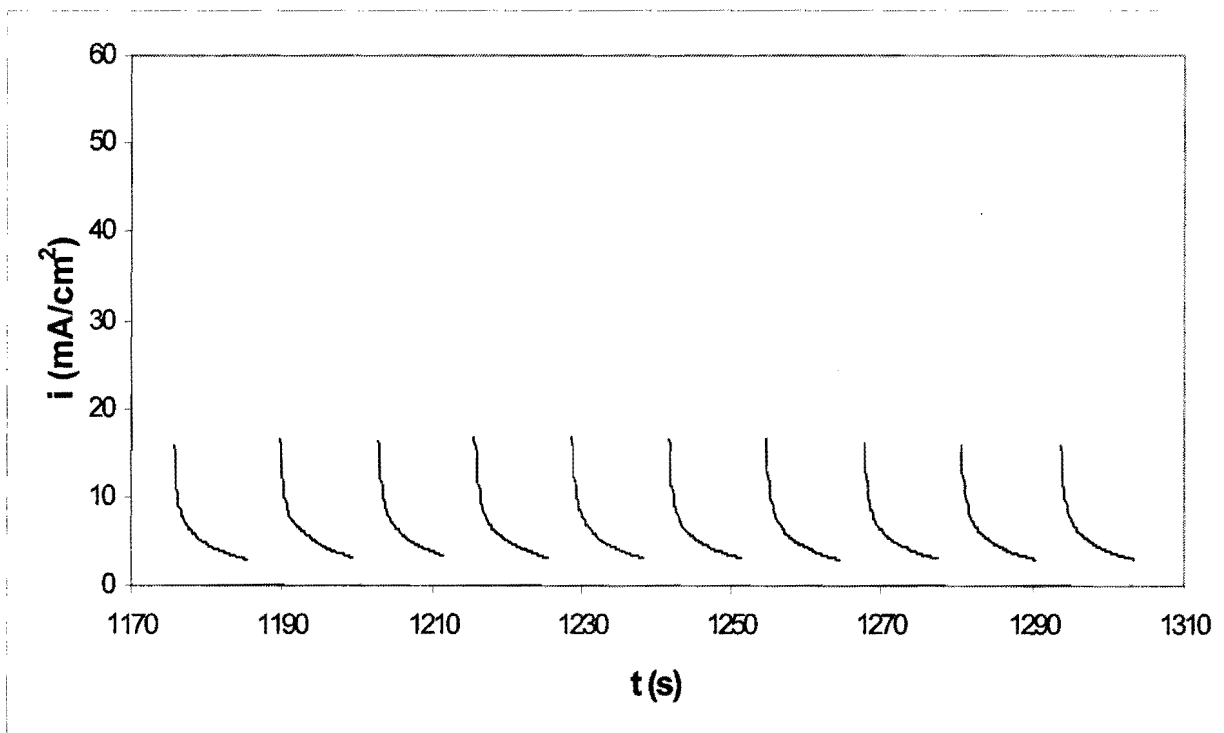
The electrolysis of ethylene glycol was performed at $-0.05 V_{SSC}$. In Figure 6.30 (a), the current densities during cycles 1 – 10 are shown. Figure 6.30(b) shows the current densities for cycles 91 – 100. The time needed to decrease the initial current density of the first cycle by 50% is 3 seconds (also see Table 6.12).

The initial apparent current densities for the first cycles are higher than for the “ductile” electrode (Fig. 6.28). Unfortunately, the current densities also decline with each cycle. The current densities during cycles 91 – 100 (Fig. 6.30(b)) are much lower than those of cycles 1 – 10.

The initial current density for ethylene glycol oxidation obtained after each cleaning cycle is shown in Figure 6.31. This figure confirms that the potential pulsing technique is also not able to restore the activity of this alloy completely.



(a)



(b)

Figure 6.30. Electrolysis of ethylene glycol by potential pulsing at the solid solution (50Au-50Pt) electrode; (a) Cycles 1-10; (b) Cycles 91-100 (Solution stirred during potential pulsing).

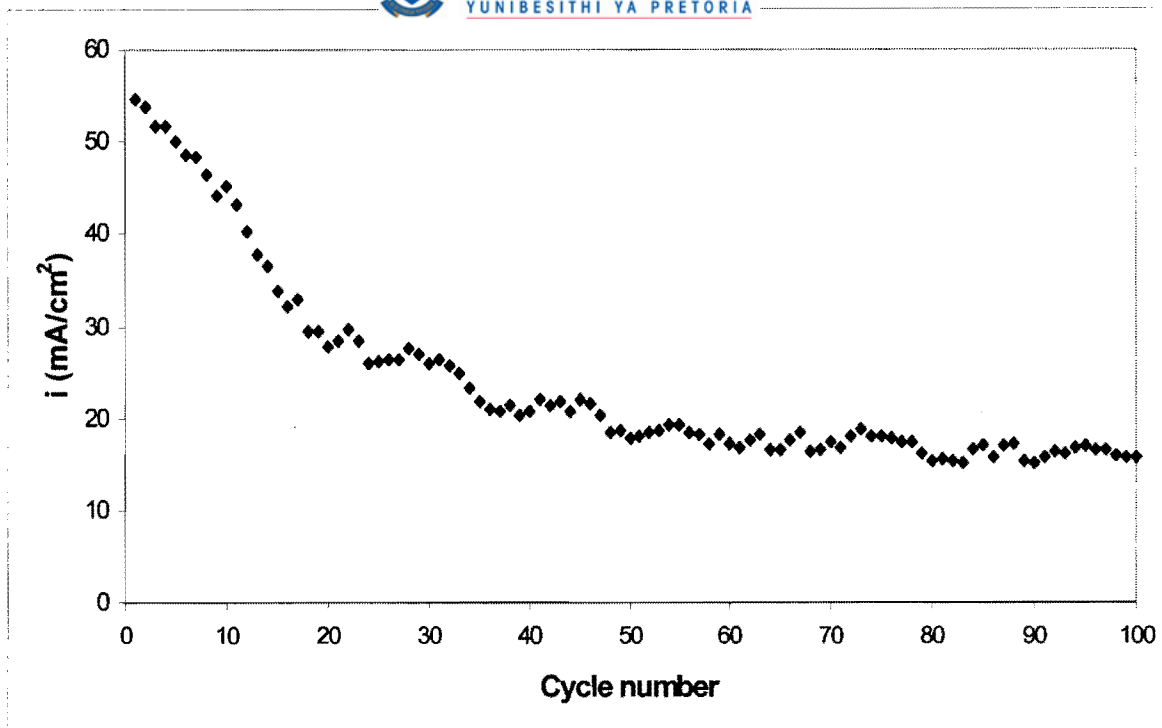


Figure 6.31. The initial current density for ethylene glycol oxidation at the solid solution (50Au-50Pt) electrode obtained after each cleaning cycle.

Numerical integration was again used to calculate the charge passed during the electro-oxidation of ethylene glycol at the solid solution (50Au-50Pt) electrode over the time period of the 100 cycles. The results are summarised in Table 6.21.

Table 6.21. The charge passed during oxidation of ethylene glycol at the solid solution 50Au-50Pt electrode during cycles 1-10, 91-100 and 1-100

Cycles 1-10	Cycles 91-100	Cycles 1-100
0.492 C	0.149 C	2.21 C

Approximately two times more ethylene glycol is oxidised during the first ten cycles at this alloy electrode than at gold. Less ethylene glycol is oxidised during the final ten cycles. Over the period of the whole hundred cycles, slightly less ethylene glycol is oxidised at the alloy electrode than at gold (Tables 6.13 and 6.21).

The estimated amount of ethylene glycol oxidised during the hundred cycles at the solid solution electrode is shown in Table 6.22.

Table 6.22. The estimated amount of ethylene glycol oxidised at the solid solution electrode during the hundred cycles.

Original number of moles ethylene glycol	Number of moles oxidised	% ethylene glycol oxidised
0.04	2.87×10^{-6}	0.0072

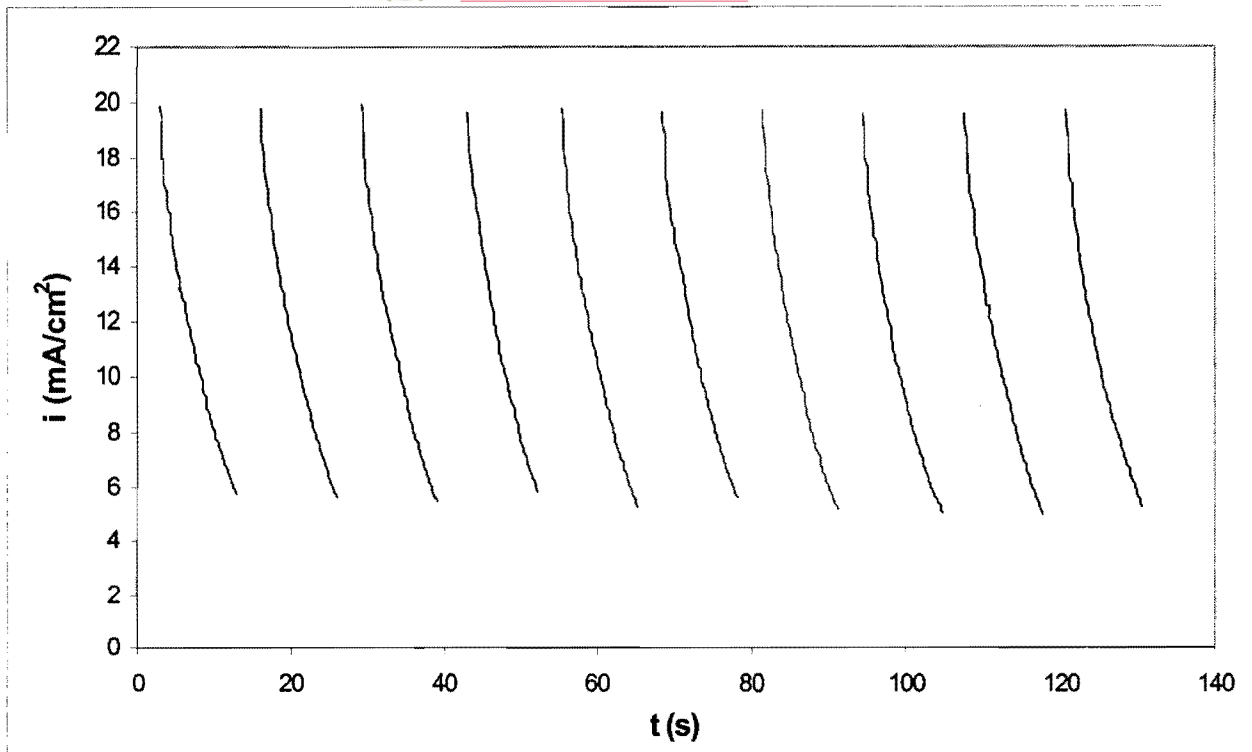
6.3.7.6. The Gold 990 alloy in the solid solution condition

The electrolysis of ethylene glycol was performed at 0.23 V_{SSC}. In Figure 6.32(a), the current densities during cycles 1 – 10 are shown. Figure 6.32(b) shows the current densities for cycles 91 – 100. The time needed to decrease the initial current density of the first cycle by 50% is 5 seconds (also see Table 6.12).

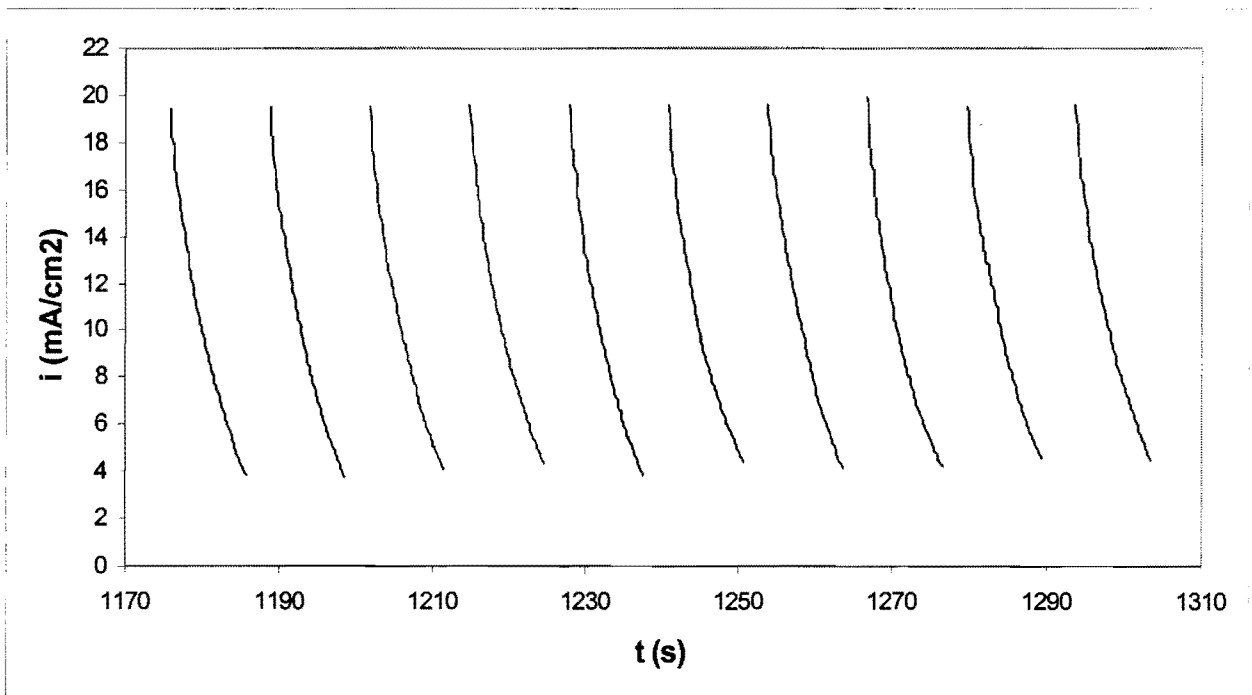
From Figure 6.32(a) it is seen the initial current density after potential pulsing (cycle 1) was approximately 20 mA/cm², falling to 5.5 mA/cm² after 10 seconds. The corresponding values for pure gold are 20 mA/cm² and 3.5 mA/cm² (Fig. 6.22). The decline in current density over the 10 seconds at the Gold 990 electrode is therefore slightly less than at pure gold.

The electrode poisons are successfully removed by the potential pulsing technique. The current densities during cycles 91 – 100 (Fig. 6.32(b)) are only slightly lower than those of cycles 1 – 10. Sustainable electrolysis of ethylene glycol at this electrode will therefore be possible by potential pulsing. The initial current density for ethylene glycol oxidation obtained after each cleaning cycle is shown in Figure 6.33. This figure illustrates how effective of the potential pulsing technique is to restore the activity of this electrode.

Numerical integration was used to calculate the charge passed during the electro-oxidation of ethylene glycol at the solid solution Gold 990 electrode over the time period of the 100 cycles. The results are summarised in Table 6.23.



(a)



(b)

Figure 6.32. Electrolysis of ethylene glycol by potential pulsing at the solid solution Gold 990 electrode; (a) Cycles 1-10; (b) Cycles 91-100 (Solution stirred during potential pulsing).

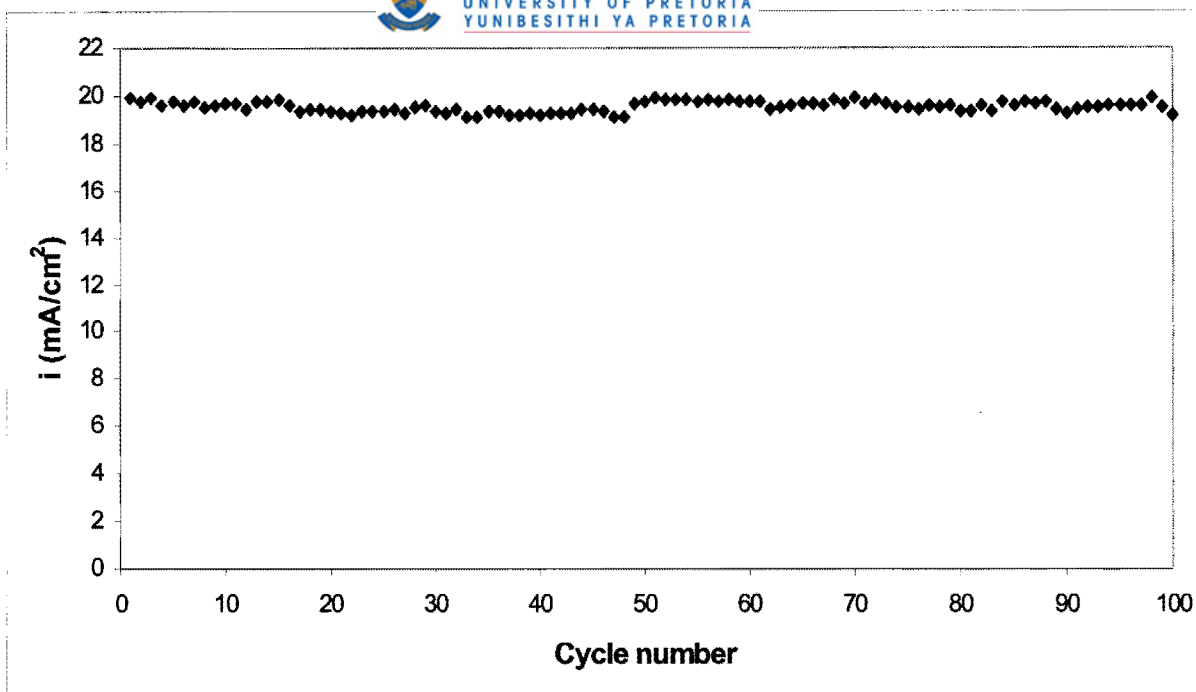


Figure 6.33. The initial current density for ethylene glycol oxidation at the solid solution Gold 990 electrode obtained after each cleaning cycle.

Table 6.23. The charge passed during oxidation of ethylene glycol at the solid solution Gold 990 electrode during cycles 1-10, 91-100 and 1-100

Cycles 1-10	Cycles 91-100	Cycles 1-100
0.293 C	0.268 C	2.76 C

Slightly more ethylene glycol is oxidised at this alloy electrode than at pure gold (Tables 6.13 and 6.23). This is probably due to the higher current densities obtained at the Gold 990 electrode at the end of the cycle prior to the cleaning procedure. Gold-titanium electrodes with a higher titanium content than Gold 990 have to be studied to indicate whether this observation is significant or not.

The estimated amount of ethylene glycol oxidised during the hundred cycles at the Gold 990 solid solution electrode is shown in Table 6.24.

Table 6.24. The estimated amount of ethylene glycol oxidised at the solid solution Gold 990 electrode during the hundred cycles

Original number of moles ethylene glycol	Number of moles oxidised	% ethylene glycol oxidised
0.04	3.59×10^{-6}	0.0089

The initial current densities for ethylene glycol oxidation at the different electrodes after each cleaning cycle are compared in Figure 6.34. This figure clearly illustrates that the initial current densities after each cleaning cycle remain fairly constant for gold and platinum (Gold 990 is similar to gold). The initial current densities for the Au-Pt alloy electrodes are high after the first few cycles, but then decline as the number of cycles increases.

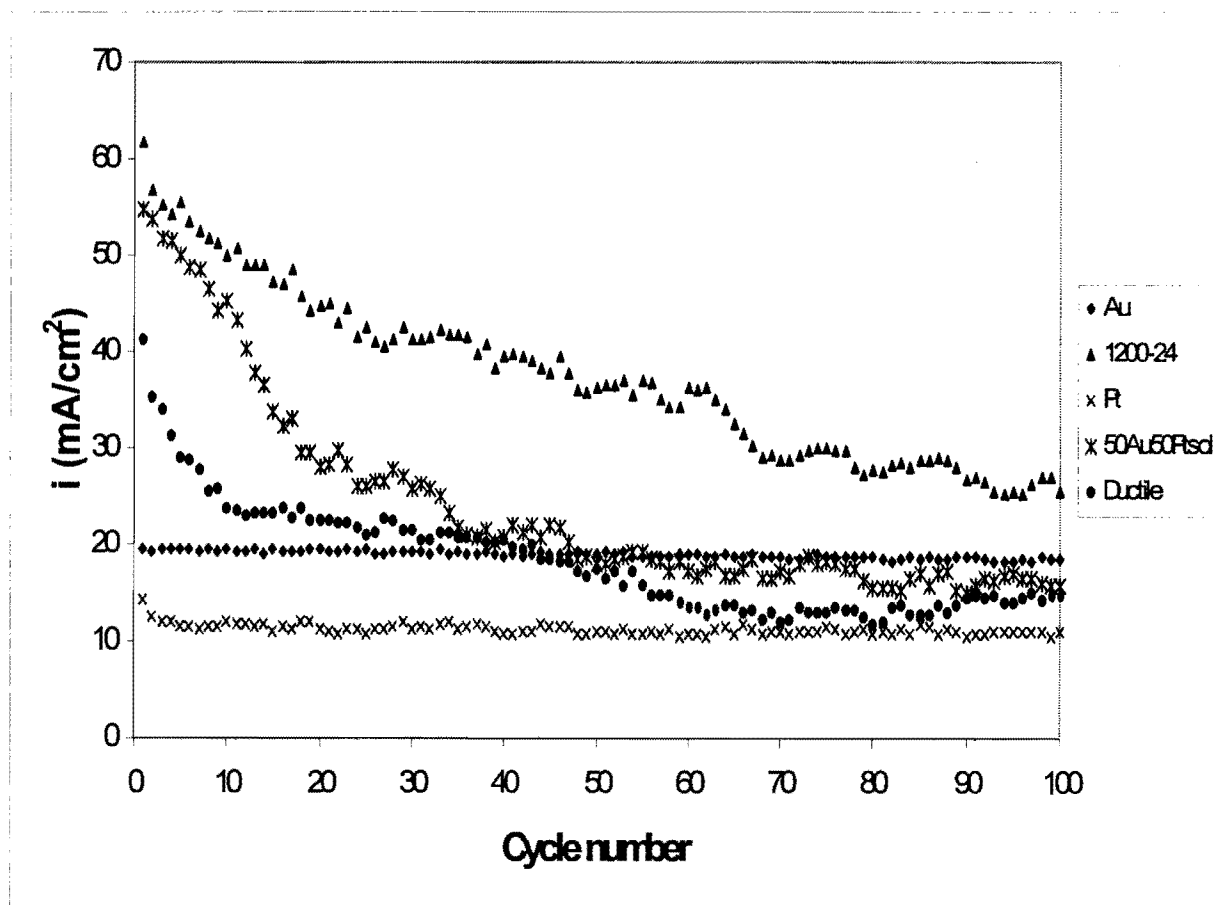


Figure 6.34. The initial current densities for ethylene glycol electro-oxidation at the different electrodes after each cleaning cycle.

This section is summarised by a graph of the charge density passed during electro-oxidation at the different electrodes against time (Fig. 6.35). The graphs of pure gold, pure platinum and the Gold 990 electrode are nearly linear, because the rate at which ethylene glycol is oxidised at these electrodes remained relatively constant over the 100 cycles period (Tables 6.13, 6.15 and 6.23). More ethylene glycol is oxidised during the first cycles at the Au-Pt alloys than during the final cycles (Tables 6.17, 6.19 and 6.21). The slopes of the graphs for these electrodes in Fig. 6.35 are therefore high at short times, but lower at longer times.

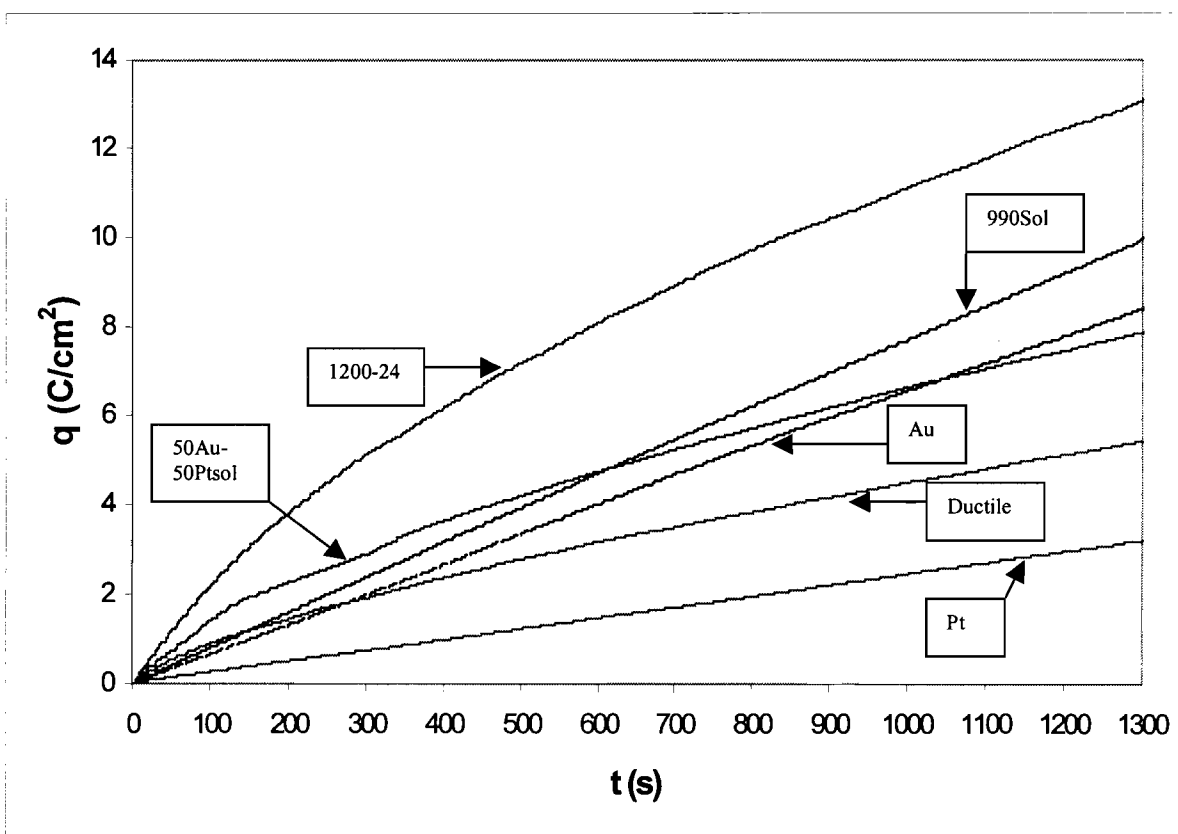


Figure 6.35. Charge density against time for the different electrodes

High apparent current densities are found during the first few cycles at the Au-Pt alloy electrodes (Fig. 6.34). Unfortunately, these high current densities lead to the formation of more poisoning species than at both pure gold and platinum. The cleaning cycles are too short (or not aggressive enough) to remove all the poisons and the current densities decline (Fig. 6.34). For this reason it was decided to increase the time of the cleaning

cycle for one of the Au-Pt alloys to see whether the poisoning species can be removed. The 50Au-50Pt alloy electrode was selected for this experiment (see paragraph 6.3.7.5.). The electrode was cycled for 100 cycles using the same procedure as before (1.5 s at 1.2 V_{SSC} , 1.5 s at $-0.6 V_{SSC}$, 10 seconds at $-0.05 V_{SSC}$). After the 100th cycle, the following procedure was used: 30 s at 1.2 V_{SSC} , 10 s at $-0.6 V_{SSC}$, 10 seconds at $-0.05 V_{SSC}$. The three cycles prior to the change in the cleaning procedure and the first three cycles after the change in the cleaning procedure are shown in Fig. 6.36 (The current densities for the cleaning cycles have been omitted). The longer cleaning procedure does indeed cause an increase in the current densities, because more of the poisoning species are removed from the surface of the electrode. The initial current densities of cycles 101-103 are much higher than those of cycles 98-100. Unfortunately, the current densities at the end of each cycle are not increased significantly by the longer cleaning procedure (Fig. 6.36).

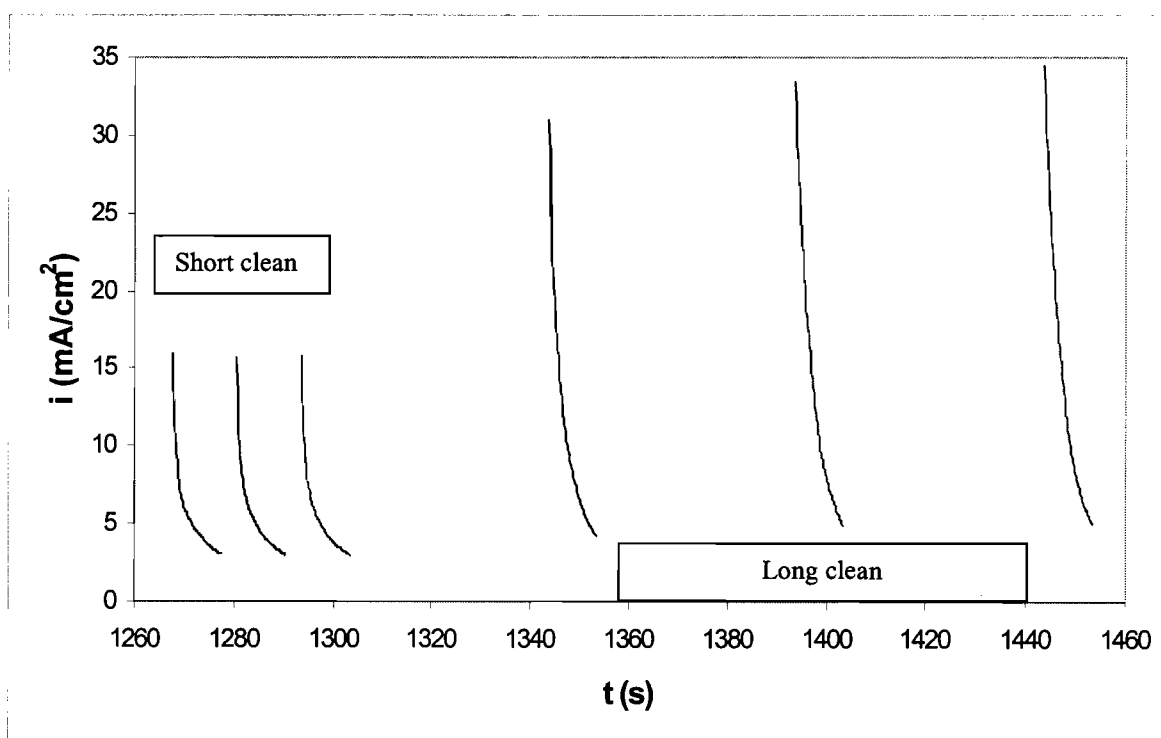


Figure 6.36. The three cycles prior to the change in the cleaning procedure and the first three cycles after the change in the cleaning procedure for the 50Au-50Pt electrode in the solid solution condition.

The initial current density after the longer cleaning procedure increases with each cycle. This effect is seen more clearly in Figure 6.37, where the initial current density for this electrode is shown after each cleaning cycle. The initial current densities after the longer cleaning cycles are still not as high as during the first few cycles with the short cleaning procedure (Fig. 6.31). This suggests that the poisoning species are not completely removed by the longer cleaning procedure.

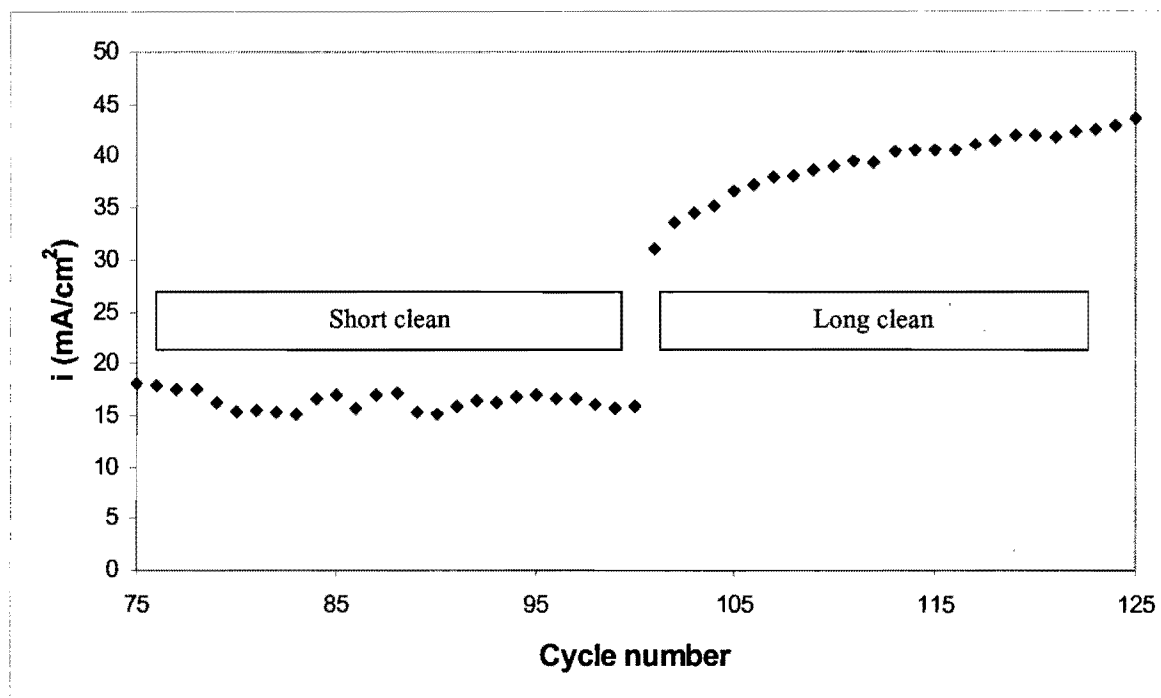


Figure 6.37. The initial current densities for ethylene glycol electro-oxidation at the 50Au-50Pt solid solution electrode.

6.4. Conclusions

The following conclusions on the electro-oxidation of ethylene glycol can be made based on the cyclic voltammetry experiments:

- The platinum region of the Au-Pt alloys is more active for ethylene glycol electro-oxidation than pure platinum after anodic activation. The gold region of the alloys is less active than pure gold after anodic activation.

- The solid solution Au-Pt electrodes are more active for the electro-oxidation of ethylene glycol than the two-phased electrodes. This can perhaps be explained by the “third-body effect”.
- Poisoning of all electrodes occurs. Poisoning is thought to occur by linearly bonded CO.
- The anodic treatment at 1.2 V_{SSC} after the 10th cycle (poisoned surface) reactivates the platinum region of the Au-Pt alloy electrodes, but deactivates the gold region. It therefore seems as if the activities of the two regions are linked – the activity of the one is high when the activity of the other is low and vice versa.
- Stirring of the solution reduces the current densities at non-porous electrodes. Stirring presumably causes an accelerated transportation of intermediates into the solution, resulting in lower current densities.
- Stirring does not have a great effect on the current densities at porous electrodes. The solution inside the pores is probably not affected much by stirring.
- The porosity does not increase the maximum apparent current densities. The advantage of the porosity is to maintain high current densities when the solution is stirred.
- The electro-oxidation of ethylene glycol at gold and the two Gold 990 electrodes is similar. The titanium content of 4 at% may be too low to have a significant influence on the electrochemical behaviour of gold. The titanium may be in the passive condition (Fig 2.21) or the titanium may have dissolved selectively from the Gold 990 alloy resulting in a pure gold surface.

The following conclusions on the electro-oxidation of ethylene glycol can be made based on the electrolysis of ethylene glycol at a fixed potential:

- Electrode poisoning occurs rapidly and the current densities drop to low values in a matter of seconds.
- The observation that Au-Pt electrodes in the solid solution condition are more effective for the electro-oxidation of ethylene glycol than the two-phased electrodes was confirmed.

- Stirring of the solution results in a faster decay of the current densities at all the electrodes. The effect is much less pronounced with porous electrodes.
- The observation that the electro-oxidation of ethylene glycol at gold and Gold 990 electrodes is similar was confirmed.

The following conclusions on the electro-oxidation of ethylene glycol can be made based on electrolysis using the potential pulsing technique:

- Potential pulsing is successful in removing the poisoning species formed at the pure gold and pure platinum electrodes. The activities of these two electrodes remain high over a period of 100 cycles.
- High apparent current densities are found during the first few cycles at the Au-Pt alloy electrodes. Unfortunately, these high current densities lead to the formation of more poisoning species than at both pure gold and platinum. The cleaning cycles are too short (or not aggressive enough) to remove all the poisons and the current densities decline. The activity of the Au-Pt electrodes can decline to levels lower than the pure metals within a hundred-cycle period. A longer cleaning cycle is able to remove most of the poisons at the electrode and the current densities increase.
- Slightly more ethylene glycol is oxidised at the Gold 990 electrode (solid solution) than at pure gold. This is probably due to the higher current densities obtained at the Gold 990 electrode at the end of the cycle prior to the cleaning procedure. Gold-titanium electrodes with a higher titanium content than Gold 990 have to be studied to indicate whether this observation is significant or not.

Chapter 7

CONCLUSIONS AND RECOMMENDATIONS

The electrochemistry of gold-based alloys in different heat treatment conditions were investigated in this study. Based on the heat treatment results (Chapter 3), the following conclusions can be made:

- The solid solution heat treatment of the two-phased 60Au-40Pt alloy leads to Kirkendall porosity. This porosity increases the surface area of the sample.
- Conventional nucleation and growth of the platinum-rich areas occurs when the 60Au-40Pt alloy samples are heat treated in the miscibility gap.
- Spinodal decomposition occurs when the 50Au-50Pt alloy samples are heat treated in the miscibility gap.
- The solid solution heat treatment of the two-phased 50Au-50Pt alloy does not lead to Kirkendall porosity.
- The Gold 990 sample in the solid solution condition has a Vickers hardness of $HV_5 = 50 \text{ kg/mm}^2$. It is possible to increase the hardness to 150 kg/mm^2 by a precipitation-hardening heat treatment.

The electrochemical properties of the gold-based alloys were determined in acid (Chapter 4) and alkaline (Chapter 5) solutions without an organic in the solution. The main conclusions from these experiments are:

- The cyclic voltammograms of the Au-Pt alloy electrodes have features corresponding to both pure gold and platinum.
- The extra surface area of the porous Au-Pt electrodes results in higher currents. Higher apparent current densities are therefore obtained with these electrodes.
- The electrochemical behaviour of gold and Gold 990 are similar.

The electro-oxidation of ethylene glycol in an alkaline solution at the gold-based electrodes were investigated in Chapter 6. The main conclusions of these experiments are:

- The platinum region of the Au-Pt alloys is more active for ethylene glycol electro-oxidation than pure platinum after anodic activation. The gold region of the alloys is less active than pure gold after anodic activation.
- The solid solution Au-Pt electrodes are more active for the electro-oxidation of ethylene glycol than the two-phased electrodes. This can perhaps be explained by the “third-body effect”.
- Poisoning of all electrodes occurs. Poisoning is thought to occur by linearly bonded CO.
- Stirring of the solution reduces the current densities at non-porous electrodes. Stirring presumably causes an accelerated transportation of intermediates into the solution, resulting in lower current densities.
- Stirring does not have a great effect on the current densities at porous electrodes. The solution inside the pores is probably not affected much by stirring.
- The porosity does not increase the maximum apparent current densities. The advantage of the porosity is to maintain high current densities when the solution is stirred.
- The electro-oxidation of ethylene glycol at gold and the two Gold 990 electrodes is similar. The titanium content of 4 at% may be too low to have a significant influence on the electrochemical behaviour of gold. The titanium may be in the passive condition (Fig 2.21) or the titanium may have dissolved selectively from the Gold 990 alloy resulting in a pure gold surface.
- Potential pulsing is successful in removing the poisoning species formed at the pure gold and pure platinum electrodes. The activities of these two electrodes remain high over a period of 100 cycles.
- High apparent current densities are found during the first few cycles at the Au-Pt alloy electrodes. Unfortunately, these high current densities apparently lead to the formation of more poisoning species than at both pure gold and platinum. The cleaning cycles are too short (or not aggressive enough) to remove all the poisons and the current densities decline. The activity of the Au-Pt electrodes can decline to levels lower than the pure metals within a hundred-cycle period. A longer cleaning cycle is able to remove most of the poisons at the electrode and the current densities increase.

The following recommendations are made based on the results obtained in this study:

- The 60Au-40Pt alloy in the "ductile" heat treatment condition needs to be studied. It will be interesting to see whether Kirkendall porosity is formed when such a sample is solutionised.
- The mechanism for oxide formation and oxide reduction at Au-Pt alloys in the solid solution condition has to be investigated. It is surprising that two oxide reduction peaks are observed at alloys in the solutionised condition.
- The poisoning phenomena at Au-Pt alloys during ethylene glycol oxidation have to be studied. The solid solution electrodes give higher current densities for ethylene glycol oxidation than the two-phased electrodes, presumably due to the "third-body effect". However, the solid solution electrodes also poison during electrolysis. The exact role of poisoning at Au-Pt alloys therefore has to be determined.
- The cleaning cycle (potential and time at potential) has to be optimised for electrolysis by potential pulsing.
- Gold-titanium alloys with a higher titanium content than Gold 990 have to be studied to determine how titanium will influence the electrochemical properties of pure gold. It is possible to have 10 at% titanium in solid solution with gold (see Fig. 3.20). A higher solutionising heat treatment temperature (approximately 1000°C) will be needed to obtain a Au-10at% Ti solid solution.

REFERENCES

Armstrong, N.R., 1977. Auger and x-ray photoelectron spectroscopic and electrochemical characterization of titanium thin film electrodes. *Surface Science*, 67: 451-468.

ASM Handbook Volume 3: Alloy Phase Diagrams. 1992. Materials Park, Ohio: ASM International.

Beden, B., Kadirgan, F., Kahyaogly, A. and Lamy, C., 1982. Electrocatalytic oxidation of ethylene glycol in alkaline medium on platinum-gold alloy electrodes modified by underpotential deposition of lead adatoms. *Journal of Electroanalytical Chemistry*, 135: 329-334.

Beden, B., Cetin, I., Kahyaoglu, A., Takky, D. and Lamy, C., 1987. Electrocatalytic oxidation of saturated oxygenated compounds on gold electrodes. *Journal of Catalysis*, 104: 37-46.

Beltowska-Brzezinska, M., 1979. Untersuchungen zur anodischen oxidation von alkoholen an gold-platin-legierungselektroden in alkalischer lösung. *Electrochimica Acta*, 24: 247-251.

Beltowska-Brzezinska, M. and Heitbaum, J., 1985. On the anodic oxidation of formaldehyde on Pt, Au and Pt/Au-alloy electrodes in alkaline solution. *Journal of Electroanalytical Chemistry*, 183: 167-181.

Birss, V.I., Chang, M. and Segal, J., 1993. Platinum oxide film formation-reduction: an in-situ mass measurement study. *Journal of Electroanalytical Chemistry*, 355: 181-191.

- Birss, V.I. and Xia, S.J., 2001. A multi-technique study of compact and hydrous Au-oxide growth in 0.1 M sulfuric acid solutions. *Journal of Electroanalytical Chemistry*, 500: 562-573.
- Bock, C. and MacDougall, B., 2000. The influence of metal oxide properties on the oxidation of organics. *Journal of Electroanalytical Chemistry*, 491: 48-54.
- Bolk, A., 1958. Kirkendall-effect in the gold-platinum system. *Acta Metallurgica*, 6: 59-63.
- Breiter, M.W., 1965. Electrochemical characterisation of the surface composition of heterogeneous Platinum-Gold alloys. *The Journal of Physical Chemistry*, 69: 901-904.
- Burke, L.D. and O'Leary, W.A., 1989. The importance of superficial (adatom) surface oxidation in the electrocatalytic behaviour of noble metals in aqueous media. *Journal of Applied Electrochemistry*, 19: 758-767.
- Burke, L.D. and Nugent, P.F., 1997. The electrochemistry of gold I: The redox behaviour of the metal in aqueous media. *Gold Bulletin*, 30(2): 43-53.
- Burke, L.D. and Nugent, P.F., 1998. The electrochemistry of gold II: The electrocatalytic behaviour of the metal in aqueous media. *Gold Bulletin*, 31(2): 39-50.
- Cahn, R.W., 1970. *Physical Metallurgy*. Amsterdam: North-Holland Publishing Company.
- Christensen, P.A. and Hamnett, A., 1989. The oxidation of ethylene glycol at a platinum electrode in acid and base: An in situ FTIR study. *Journal of Electroanalytical Chemistry*, 260: 347-359.

Comninellis, C., 1994. Electrocatalysis in the electrochemical conversion/combustion of organic pollutants for wastewater treatment. *Electrochimica Acta*, 39: 1857-1862.

Darling, A.S., 1962. Gold-Platinum alloys: A critical review of their constitution and properties. *Platinum Metals Review*, 6: 60-111.

Desilvestro, J. and Weaver, M.J., 1986. Surface structural changes during oxidation of gold electrodes in aqueous media as detected using surface-enhanced Raman spectroscopy. *Journal of Electroanalytical Chemistry*, 209: 377-386.

Enea, O. and Ango, J.P., 1989. Molecular structure effects in electrocatalysis – oxidation of polyols on Pt and Au electrodes. *Electrochimica Acta*, 34: 391-397.

Feinstein, L.G. and Bindell, J.B., 1979. The failure of aged Cu-Au thin films by Kirkendall porosity. *Thin Solid Films*, 62: 37-47.

Fishbane, P.M., Gasiorowicz, S. and Thornton, S.T., 1996. *Physics for scientists and engineers*. New Jersey: Prentice Hall Inc.

Gafner, G., 1989. The development of 990 gold-titanium: Its production, use and properties. *Gold Bulletin*, 22(4): 112-122.

Gordon, J.S. and Johnson, D.C., 1994. Application of an electrochemical quartz crystal microbalance to a study of water adsorption at gold surfaces in acidic media. *Journal of Electroanalytical Chemistry*, 365: 267-274.

Hahn, F., Beden, B., Kadirgan, F. and Lamy, C., 1987. Electrocatalytic oxidation of ethylene glycol. Part III: In-situ Infrared Reflectance Spectroscopic study of the strongly bound species resulting from its chemisorption at a platinum electrode in aqueous medium. *Journal of Electroanalytical Chemistry*, 216: 169-180.

Harrington, D.A., van der Geest, M.E. and Dangerfield, N.J., 1997. An ac voltammetry study of Pt oxide growth. *Journal of Electroanalytical Chemistry*, 420: 89-100.

Hauffe, W. and Heitbaum, J., 1978. The electrooxidation of ethylene glycol at gold in potassium hydroxide. *Berichte der bunsen-gesellschaft für physikalische chemie*, 82: 487-491.

Herranen, M. and Carlsson, J.O., 2001. An electrochemical quartz crystal microbalance and in situ SFM study of Ti in sulphuric acid. *Corrosion Science*, 43: 365-379.

Heyd, D.V. and Harrington, D.A., 1992. Platinum oxide growth kinetics for cyclic voltammetry. *Journal of Electroanalytical Chemistry*, 335: 19-31.

Hutton, R.S. and Williams, D.E., 1994. Photocurrent imaging of the layers formed during the electrooxidation of gold. *Journal of the American Chemical Society*, 116: 3453-3459

Kadirgan, F., Beden, B. and Lamy, C., 1983. Electrocatalytic oxidation of ethylene glycol. Part II: Behaviour of platinum-ad-atom electrodes in alkaline medium. *Journal of Electroanalytical Chemistry*, 143: 135-152.

Kadirgan, F., Bouhier-Charbonnier, E., Lamy, C., Leger, J.M. and Beden, B., 1990. Mechanistic study of the electrooxidation of ethylene glycol on gold and adatom-modified gold electrodes in alkaline medium. *Journal of Electroanalytical Chemistry*, 286: 41-61.

Kozłowska, H.A., Conway, B.E. and Sharp, W.B.A., 1973. The real condition of electrochemically oxidised platinum surfaces. *Journal of Electroanalytical Chemistry*, 43: 9-36.

Mho, S. and Johnson, D.C., 2001. Electrocatalytic response of carbohydrates at copper-alloy electrodes. *Journal of Electroanalytical Chemistry*, 500: 524-532.

Parsons, R. and VanderNoot, T., 1988. The oxidation of small organic molecules. *Journal of Electroanalytical Chemistry*, 257: 9-45.

Popovic, N.D., Cox, J.A and Johnson, D.C., 1998. A mathematical model for anodic oxygen-transfer reactions at Bi(V)-doped PbO₂-film electrodes. *Journal of Electroanalytical Chemistry*, 456: 203-209.

Pourbaix, M., 1974. *Atlas of electrochemical equilibria in aqueous solutions*. Houston: National Association of Corrosion Engineers.

Rach, E. and Heitbaum, J., 1987. Electrochemically induced surface modifications of Pt-Au alloys. *Electrochimica Acta*, 32: 1173-1180.

Rammelt, R. and Reinhard, G., 1990. On the applicability of a constant phase element (CPE) to the estimation of roughness of solid metal electrodes. *Electrochimica Acta*, 35: 1045-1049.

Reed-Hill, R.E. and Abbaschian, R., 1994. *Physical metallurgy principles*. Boston: PWS publishing company.

Shibata, T. and Zhu, Y., 1995. The effect of temperature on the growth of anodic oxide film on titanium. *Corrosion Science*, 37(1): 133-144.

Song, H., Hwang, H., Lee, K. and Dao, L.H., 2000. The effect of pore size distribution on the frequency dispersion of porous electrodes. *Electrochimica Acta*, 45: 2241-2257.

Stelmach, J., Holze, R. and Beltowska-Brzezinska, M., 1994. Electrocatalysis of the formaldehyde oxidation at alloys of platinum with sp metals II. *Journal of Electroanalytical Chemistry*, 377: 241-247.

Vitt, J.E., Larew, L.A. and Johnson, D.C., 1990. The importance of adsorption in anodic surface-catalyzed oxygen-transfer reactions at gold electrodes. *Electroanalysis*, 2: 21-30.

Vitt, J.E. and Johnson, D.C., 1992. The importance of anodic discharge of H₂O in anodic oxygen-transfer reactions. *Journal of the Electrochemical Society*, 139: 774-778.

Watanabe, T. and Gerischer, H., 1981. Photoelectrochemical studies on gold electrodes with surface oxide layers. *Journal of Electroanalytical Chemistry*, 122: 185-200.

Wen, T. and Li, Y., 1997. Electrochemical behaviour of gold electrodeposits with and without organic compounds in KOH. *Materials Chemistry and Physics*, 48: 191-198.

Woods, R., 1971. The surface composition of Platinum-Gold alloys. *Electrochimica Acta*, 16: 655-659.

Xia, S.J. and Birss, V.I., 2000. In situ mass and ellipsometric study of hydrous oxide film growth on Pt in alkaline solutions. *Electrochimica Acta*, 45: 3659-3673.

Zolfaghari, A., Conway, B.E. and Jerkiewicz G., 2002. Elucidation of the effects of competitive adsorption of Cl⁻ and Br⁻ ions on the initial stages of Pt surface oxidation by means of electrochemical nanogravimetry. *Electrochimica Acta*, 47: 1173-1187.